SACLANTCEN Conference Proceedings No. 5

SACLANTCEN
Conference Proceedings No. 5

PART I

SESSIONS 1 – 3

SACLANT ASW
RESEARCH CENTRE

GEOMETRICAL ACOUSTICS (RAY TRACING)

Proceedings of a Conference held at SACLANTCEN
on 27–30 September 1971

Organized by

BRIAN W. CONOLLY and RICHARD H. CLARKE

15 DECEMBER 1971

NORTH
ATLANTIC
TREATY
ORGANIZATION

VIALE SAN BARTOLOMEO 400
I – 19026 – LA SPEZIA, ITALY

SACLANTCEN
CONFERENCE PROCEEDINGS NO. 5

NORTH ATLANTIC TREATY ORGANIZATION
SACLANT ASW RESEARCH CENTRE
Viale San Bartolomeo 400
I 19026 - La Spezia, Italy

GEOMETRICAL ACOUSTICS (RAY TRACING)

Proceedings of a Conference held at SACLANTCEN
on 27-30 September 1971

PART I
Sessions 1-3

Organized by
Brian W. Conolly and Richard H. Clarke

15 December 1971

ATTENDEES — AUTHOR INDEX (page numbers in parentheses)

L.B. Palmer	(307)	NRL, Washington, U.S.
G. Pazienza		USEA, San Terenzo, La Spezia, Italy
E. Pichon	(49)	LDSM, Le Brusc, France
R.H. Prager		SACLANTCEN
R.L. Reeves	(114) & (323)	NSSC, Washington D.C., U.S.
J.G. Schothorst		NDRO, TNO, The Hague, Netherlands
L.P. Solomon	(114)	Tetra Techn. Inc., Arlington, Va., U.S.
C.W. Spofford	(228)	Bell Telephone Labs., Whippany N.J., U.S.
J.H. Stockhausen		SACLANTCEN
T. Strarup	(108)	DDRE, Copenhagen, Denmark
G. Tacconi		MARIPERMAN, La Spezia, Italy
P.R. Tatro		ONR, Washington D.C., U.S.
R. Thiele		Forschungsanstalt der Bundeswehr für Wasserschall und Geophysik, Kiel, Germany
M. Thompson	(37)	SACLANTCEN
S. Toft		DDRE, Copenhagen, Denmark
M.J. van der Scheur	(345)	NDRO, TNO, The Hague, Netherlands
W.S. van Langeweyde	(302)	Forschungsanstalt der Bundeswehr für Wasserschall und Geophysik, Kiel, Germany
G.C. Vettori	(150)	SACLANTCEN
H. Weinberg	(77)	NUSC, New London, Conn., U.S.
T.D. Westrup		SACLANTCEN
W. Wijmans	(37)	SACLANTCEN

AUTHORS NOT ATTENDING

I.M. Blatstein	(210)	NOL, Silver Spring, Md., U.S.
I. Roebuch	(243)	AUWE, Portland, Dorset, U.K.

TABLE OF CONTENTS

TABLE OF CONTENTS (Cont'd)

PART II

TABLE OF CONTENTS (Cont'd)

SESSION 1

THE MEDIUM

Session Chairman : B.W. Conolly
Session Secretary : R.H. Clarke

1.1 Oceanic Layered Microstructure and Fronts
by O.M. Johannessen

1.2 Considerations Relating to the Calculation of Sound Velocity
by C.C. Leroy

OCEANIC LAYERED MICROSTRUCTURE AND FRONTS

by

O.M. Johannassen
SACLANT ASW Research Centre
La Spezia, Italy

INTRODUCTION

This talk is divided into two parts: one deals with oceanic microstructure, with particular attention to the so-called "layered microstructure"; the other part is concerned with oceanic fronts. As an example of the latter I am going to describe in some detail a front east of Malta, which the Oceanography Group of this Centre is studying.

The intention of giving this paper in this Ray Tracing Conference is to remind you that the vertical profiles of temperature and salinity, and hence speed of sound, are not a continuous and smooth curve as a function of depth, but rather consist of a large number of nearly homogeneous layers separated with interfacial regions where strong gradients with values as high as 0.5°C/10 cm are present. The reported work on the front east of Malta will show you that very high horizontal gradients of the oceanographical parameters, and hence sound speed, are established, with values as high as 6 m/s over a horizontal distance of 1 km, when passing through the frontal region.

OCEANIC LAYERED MICROSTRUCTURE

The acousticians have been aware of thermal microstructure for about 20 years [see, for example, Refs. 1 & 2]. A recent review

by Gostev and Shvachko [Ref. 3] on "random inhomogeneities of microstructure of temperature and sound velocity profiles" summarized the results of Russian investigations as well as mentioning some of the more important contributions from "western scientists". However the acousticians have paid more attention to the so-called "patch size" microstructure of temperature and speed of sound fields [see, for example, Refs. 2, 4, 5, 6, 7, 8] than to the layered microstructure. Indication of the layered microstructure, however, was reported by Piip [Ref. 9], who measured some detailed vertical speed-of-sound profiles in the Bermuda area. Figure 1 shows an example of one of these profiles. Actually two velocity meters are shown, one displaced 25 cm/s to the left. Thin layers, a few metres thick, of lower speed are seen in the main thermocline. Piip referred to these layers as "strange layers of water" and we shall see that this is what we today call layered microstructure.

The study of layered microstructure has only recently attracted the attention of physical oceanographers. Such investigations have been possible due to the invention of the STDV system, which continuously records temperature, salinity and speed of sound versus pressure, and to the specially designed free-falling microstructure probes. Observations with these instruments have shown that the vertical profiles of the oceanographical parameters are not smooth curves, as normally seen by traditional Nansen cast technique, but rather exhibit a number of both regular and irregular homogeneous layers with typical thickness of metres or less, separated by interfacial regions or transition zones where large gradients are present.

Figure 2 shows a typical example of layered microstructure in the thermocline observed east of Malta by Woods [Ref. 10] with a free-falling microstructure probe. Both temperature and the gradient between two thermistors separated by 25 cm in the vertical are recorded. The layering effect is clearly established in the thermocline. Separating the nearly isothermal layers, which are of the order of 2 m - 4 m thick, are interfacial region, or as Woods calls them "thermocline sheets", only 20 cm - 50 cm thick where changes of 0.2°C - 0.4°C occur.

The investigators who are studying microstructure experimentally can be divided into two main groups; one which is using commercially available STDV systems which have a vertical resolution of about 0.5 m - 1 m depending on the sea state, and the other using prototype free-falling microstructure probes, not available on the commercial market, with vertical resolution of a cm or less. This vertical resolution enables one to study the finest structure in the temperature field. In the "western world" the latter group is, for example, presented by Woods [Refs. 10 & 11], Woods and Wiley [Ref. 12], Cox et al [Ref. 13], Grant et al [Ref. 14] and Nasmyth [Ref. 15]. The papers by Stommel and Fedorov [Ref. 16], Cooper and Stommel [Ref. 17], Grafe and Gallagher [Ref. 18], Siedler [Ref. 19], Tait and Howe [Ref. 20], Howe and Tait [Ref. 21] are examples of the STDV group. A modified XBT system has also been used by Neal et al [Ref. 22] in studying microstructure in the Arctic ocean. However, in the light of the results from the first group it becomes clear that the STDV group only shows the larger scale layered microstructure, because of the limited vertical resolution of this type of measurement.

I am now going to show you some typical observations of layered microstructure from different ocean regions. Figure 3 shows a recent profile after Woods and Wiley [Ref. 12] east of Malta, however with increased vertical resolution when compared with the profile in Fig. 2. The gradient is now measured 10 cm apart, and we see that both the temperature trace and the gradient are somewhat more irregular than the previous figure. The interfacial region between the isothermal layers which was thought previously to consist of one "thermocline sheet" [Ref. 10], now appears to consist of several sheets, and the thickness of the nearly isothermal layers are of the order of 1 m - 2 m or less. Figure 4 shows a temperature and speed of sound profile for the same area obtained by an STDV instrument suspended from a ship (SACLANTCEN, unpublished observations) and the finer detail shown on Fig. 3 is not resolved. However, the layering effect is clearly established in the thermocline region, decreasing with increasing depth. It should again be emphasized that finer structure is present, but not resolved with this instrument.

The last three figures were all from the Mediterranean. Figure 5 shows some successive STD analogue traces in the upper part of the main thermocline from an area south of Bermuda in the Atlantic Ocean [Ref. 17]. The arrows indicate the direction of the probe, and it is seen that some details are lost when the probe is on its way up, caused by unequal exposure of the sensors in opposite directions. Rather regular, homogeneous layers about 5 m thick separated by transition regions of 10 m - 15 m where temperature and salinity (not shown) change by 0.3°C - 0.5°C and 0.04‰ - 0.10‰ respectively. From several STDV dips in the area it was generally found that about one hundred of these layers were "filling up" the main thermocline.

Observations from the Pacific [for example, Refs. 16, 18, 13, 15] show the existence of layered microstructure. Furthermore, large numbers of unpublished STDV observations held by different laboratories around the world show that the layered microstructure is a common phenomenon in the thermocline region.

However, rather few investigations deal in detail with the horizontal extent, variability and generation of layered microstructure. Some preliminary results show that the same layers can extend from a few hundred metres to tens of kilometres in the horizontal. Furthermore the layers move up and down with the internal waves which are always present in the thermocline region. Several mechanisms for the generation of layered microstructure have been proposed such as breaking internal waves, formation of layers at boundaries (such as an oceanic front) followed by spreading along density surfaces and a double diffusion process, also referred to as the "salt fingering" process. At present, however, the generation mechanism(s) is not fully understood.

So far I have been talking about the layered microstructure in the thermocline region (seasonal and permanent). However, even more regular and pronounced stepped structure has been established in the deep part of the ocean, well below the thermocline region.

Figure 6 shows such stepped structure in an area between Gibraltar and Madeira in the north east Atlantic [Ref. 20], located just below the intrusion of the high saline Mediterranean water. The thickness of the layers was of the order of 15 m - 30 m and changes across the interfaces between the layers were of the order of 0.25 °C and 0.044‰, respectively, for the temperature and salinity. Unfortunately no observations were made below 1500 m, but probably the layering will extend to larger depths. A more detailed study of the variability of the layers was performed in the same area by Howe and Tait [Ref. 21]. The upper part of Fig. 7 gives some results of the average thickness of the layers and the interfaces and also the changes in oceanographic parameters across the interfaces. The lower part of Fig. 7 shows the time variability at one location over a 33-hour period. It is clearly seen that the layers are taking part in the internal-wave oscillation. Spatial investigation showed that the layers extended for about 20 n.mi in the horizontal.

Similar deep stepped structure has been observed in the Tyrrhenian Sea by Owen S. Lee from NUC, San Diego (unpublished data). Figure 8 shows one of the STDV stations and the stepped structure starting to form just below the high saline Levantine water. In the upper part the layers are of the order of 15 m - 20 m thick, but increasing their thickness with increasing depth, to as much as 200 m between 1100 m and 1300 m. Below 1600 m - 2000 m the stepped structure is not clearly seen. Figure 9 shows a magnification of the profiles and the change, for example, in the speed of sound across the interfaces is of the order of 0.2 m/s to 0.4 m/s. (The profiles in Fig. 9 are slightly displaced vertically with respect to each other due to the crossing of the three pens on the recorder). Deep stepped structure has also been established west of the Strait of Sicily (Johannessen, unpublished data) as shown in Fig. 10, however, the structure is not as pronounced when compared with the two previous mentioned cases. All these profiles show that the stepped structure started to form below the region in the profile

where maximum salinity occurred and where the temperature was decreasing, an oceanographic condition which favours the so-called "salt finger mechanism" which may be the reason for formation of the layers [Ref. 23]. Stepped structure of a similar kind has also been established in the Arctic Ocean [see Fig. 11 after Neal et al (Ref. 22)].

In summary one can say that this deep stepped structure has so far been established only in special areas, and it is by no means as common as the smaller scale layered microstructure in the thermocline region.

One can now ask the question: what is the acoustical effect when sound is propagated through the layered microstructure in the thermocline region? In order to get some qualitative understanding of this effect we (Johannessen and Mellberg, unpublished work) carried out a very simple-minded simulation experiment using ray tracing on profiles with and without microstructure and compared the results. Using the results from Cooper and Stommel [Ref. 17, Fig. 5], from the Bermuda area, we simplified a Bermuda profile as shown in Fig. 12. Layered microstructure was inserted in the main thermocline, using layer thickness of 5 m and transition zone of 10 m where the temperature changed by 0.3°C. For simplicity the salinity was held constant, which, however, is not the case in nature because similar steps also occur in the salinity profile. The ray tracing was carried out for source depths of 5 m, 125 m, 890 m and 1200 m. Comparing the results from the two profiles, no significant changes in the intensity contours (for example the 75 dB one) for the 5 m and 125 m source was established. However, for the source located in the microstructure region, significant changes occurred. Figure 13 shows that for the linear profile the 75 dB contours are smooth for all the ray families, but when microstructure is inserted [Fig. 14], no smooth intensity contour can be drawn for the vertexing rays. Similar results were obtained for the source at 1200 m, below the microstructure. We also performed a similar simulation experiment on some real observed

microstructure profile in the Mediterranean and compared it with the result when smoothing on the same profile was done. Again only the vertexing rays were significantly affected. Thus it seems that the layered microstructure has the effect of "scattering" the sound in the vertexing regions.

OCEANIC FRONTS

Oceanic fronts in general develop in areas where two or more water masses meet. When passing through a frontal zone one will observe a strong horizontal discontinuity in the oceanographic parameters. Typical horizontal changes in the few upper metres of the ocean are of the order of $0.5^{\circ}C - 1.5^{\circ}C$ in temperature, 0.5‰ - 1‰ in salinity and 1 m/s - 2 m/s in the speed of sound over 1 n.mi - 2 n.mi distance. However, at the deep level in the thermocline region, the horizontal changes are much larger when crossing a frontal region.

Oceanic fronts have, for example, been studied in the Atlantic by Voorhis and Hersey [Ref. 24], Voorhis [Ref. 25] and Katz [Ref. 26], by Cromwell and Reid [Ref. 27], Knauss [Ref. 28], Wooster [Ref.29], LaFond and LaFond [Ref. 30] in the Pacific and by Woods and Watson [Ref. 31] in the Mediterranean. Laevastu and LaFond [Ref. 32] studied the surface location of the frontal areas for the northern hemisphere and Fig. 15 (after Laevastu and LaFond) shows that large areas, say 25%-30% of the ocean are covered with frontal regions.

Woods and Watson [Ref. 31] had previously reported on a frontal study east of Malta in shallow water during the summer, however, our first study [Johannessen, Good and Smallenberger, (unpublished work)] was carried out in deep water in the Ionian Sea during December 1970 jointly with the Oceanography Group of NUC, San Diego. Figure 16 shows the cruise track of the US SP LEE and the shaded line indicates the location of the front. The NUC thermistor chain was used, sampling temperature at 45 levels down to 230 m for every 37 m in the horizontal. Figure 17, which is a copy of the analogue output of the recording unit of the thermistor

chain, shows the depth variation of each degree isotherm for a section perpendicular to the front. The thermocline is dramatically affected and entirely folded in the frontal region. The temperature structure is at least influenced by the front in the upper 230 m and it is seen that warmer water is located on the western side of the front. Figure 18 shows a section through the same area a few days later. The western edge of the front where the folding of the isotherms occurs has not moved more than 1 n.mi - 2 n.mi, however, the internal structure of the front has changed dramatically. In addition to the folding of the isotherms in the western part, the thermocline shows a "spiking" feature further east indicating upwelling. The thermocline is furthermore distorted for about 20 n.mi - 25 n.mi in the horizontal. Figure 19 presents the vertical profile for the same section as Fig. 18. The profiles are plotted for every 2/3 of a nautical mile. The lower part of the figure shows a magnification of the central part of the section with profiles given every 270 m. A large number of the vertical profiles show strong inversion, which is one of the typical characteristics of a frontal region. Figure 20 gives the horizontal temperature variation at three typical levels. As pointed out earlier, the largest variations or the strongest discontinuity is found at sub-surface levels, clearly illustrated in the figure. The calculated speed of sound field is shown in Fig. 21. Studying the figure in detail, horizontal changes can be seen to amount to as much as 6 m/s over less than 1 n.mi in the thermocline region.

In a recent study during the summer, Johannessen et al [Ref. 33] found that the frontal system had propagated from the deep water into the shallow water. Figure 22 shows the surface salinity, and that north of 35°30' the salinity changes rapidly from 37.40‰ to more than 38.0‰ along longitude 15°20' east, clearly indicating the frontal surface boundary. It appears that the front has been broken up by the east flowing surface Atlantic water, indicated by a region of low salinity water. Typical horizontal variation of

the surface temperature is shown on Fig. 23 when passing through the front (perpendicular) along latitude 36° north. The slight minimum temperature region located just west of the strong temperature discontinuity, indicates that upwelling is present. A typical STDV station for the same area is shown in Fig. 24. The inversion is located at 40 m depth with more than 1°C in temperature and about 5 m/s for the speed of sound. The two principal water masses also stand out clearly from the salinity profile.

In summary, oceanic fronts cover a large area of the world's oceans, and in general the features shown in Figs. 23 and 24 with, respectively, a strong horizontal discontinuity in the surface layer and inversions in the thermocline region are characteristic of a frontal zone.

REFERENCES

1. R.J. Urick and C.W. Searfoss, "The Microthermal Structure of the Ocean near Key West, Florida; Part 1: Description, Part 2: Analysis", U.S. Naval Research Lab. Repts. S-3392, 1948, and S-3444, 1949.

2. L. Liebermann, "Effect of Temperature Inhomogeneities in the Ocean on the Propagation of the Sound", J. Acoust. Soc. Am., Vol. 23, p. 563, 1951.

3. V.S. Gostev and R.F. Shvachko, "The Microstructure of the Temperature Field in the Ocean", Izv. Atmos. and Oceanic Phys., Vol. 5, No. 10, pp. 1066-1074, 1969.

4. D.C. Whitmarsh, E. Skudryzk and R.J. Urick, "Forward Scattering of Sound in the Sea and its Correlation with the Temperature Microstructure", J. Acoust. Soc. Am., Vol. 29, p. 1124, 1957.

5. M.J. Bowman, "Temperature Microstructure in the Sea and its Influence upon Acoustic Scattering", M.Sc. Thesis, University of Auckland, 1966.

6. R.J. Urick, "Principles of Underwater Sound for Engineers", McGraw-Hill Book Co., New York, 1966.

7. S.R. Murphy and W.E. Nodland, "An Unmanned Research Vehicle for use down to Mid-ocean Depths", Ocean Sciences and Engineering, Vol. 2, MTS, 1965.

8. S.R. Murphy and G.E. Lord, "Thermal and Sound Velocity Microstructure Data taken with an Unmanned Research Vehicle", Proceedings of the Second U.S. Navy Symposium on Military Oceanography, 5-7 May 1965.

9. A.T. Piip, "Structure and Stability of the Sound Channel in the Ocean", J. Acoust. Soc. Am., Vol.36, No. 10, October 1964.

10. J.D. Woods, "Diurnal Behaviour of the Summer Thermocline off Malta", Deutschen Hydrographischen Zeitschrift Vol. 21, No. 3, 1968.

11. J.D. Woods, "Wave-induced Shear Instability in the Summer Thermocline", J. Fluid Mech., Vol. 32, Pt. 4, pp. 791-800, 1968.

12. J.D. Woods and R.L. Wiley, "Billow Turbulence and Ocean Microstructure", Deep Sea Res., (in press, 1971).

13. C. Cox, Y. Nagata and T. Osborn, "Oceanic Fine Structure and Internal Waves", Bulletin of the Japanese Society of Fisheries Oceanography. Papers in dedication to Prof. Michitake Uda, November 1969.

14. H.L. Grant, A. Moilliet and W.M. Vogel, "Some Observations of the Occurrence of Turbulence in and Above the Thermocline", J. Fluid Mech., Vol. 34, Pt. 3, pp. 443-448, 1968.

15. P.W. Nasmyth, "Oceanic Turbulence", The University of British Columbia, 1970. (Ph.D. Thesis)

16. H. Stommel and K.N. Fedorov, "Small Scale Structure in the Temperature and Salinity near Timor and Mindanao", Tellus, Vol. XIX, No. 2, 1967.

17. J.W. Cooper and H. Stommel, "Regularly Spaced Steps in the Main Thermocline near Bermuda", J.G.R., Vol. 73, No. 18, September 1968.

18. V. Grafe and B. Gallagher, "Oceanographic Profiling with Improved Vertical Resolution", J.G.R., Vol. 74, No. 23, October 1969.

19. G. Siedler, "On the Fine Structure of Density and Current Distribution and its Short-time Variations in the Different Areas", Progress in Oceanography, Vol. 5, Pergamon Press, 1969.

20. R.I. Tait and M.R. Howe, "Some Observations of the Thermo-haline Stratification in the Deep Ocean", Deep Sea Res., Vol. 15, June 1968.

21. M.R. Howe and R.I. Tait, "Further Observations of the Thermo-haline Stratification in the Deep Ocean", Deep Sea Res., Vol. 17, 1970.

22. V.T. Neal and W. Denner, "Thermal Stratification in the Arctic Ocean", Science, October 17, 1969.

23. J.S. Turner, "Salt Fingers across a Density Interface", Deep Sea Res., Vol. 14, October 1967.

24. A.D. Voorhis and J.B. Hersey, "Oceanic Thermal Fronts in the Sargasso Sea", J.G.R., Vol. 69, No. 18, 1964.

25. A.D. Voorhis, "The Horizontal Extent and Persistence of the Thermal Fronts in the Sargasso Sea", Deep Sea Res., Vol. 16, 1969.

26. E.J. Katz, "Further Study of a Front in the Sargasso Sea", Tellus, Vol. XXI, No. 2, 1969.

27. T. Cromwell and J.L. Reid, "A Study of Oceanic Fronts", Tellus, Vol. VIII, 1956.

28. J.A. Knauss, "An Observation of an Oceanic Front", Tellus, Vol. IX, No. 2, 1957.

29. W.S. Wooster, "Equatorial Front between Peru and Galapagos", Deep Sea Res., Supplement to Vol. 16, 1969.

30. E.C. LaFond and K.G. LaFond, "Thermal Structure through the California Front", NUC TP 224, San Diego, July 1971.

31. J.D. Woods and N.R. Watson, "Measurement of Thermocline Fronts from Air", Underwater Science and Technology Journal, June 1970.

32. T. Laevastu and E.C. LaFond, "Oceanic Fronts and their Seasonal Positions on the Surface", NUC TP 204, San Diego, 1970.

33. O.M. Johannessen, F. De Strobel and C. Gehin "Observations of an Oceanic Frontal System east of Malta in May 1971 (MAY FROST)", SACLANTCEN Technical Memorandum No. 169, August 1971.

DISCUSSION

In response to a question the author said that ray tracing had been performed through fronts, by Allan and Gerrebout of SACLANTCEN using the range-dependent ray-tracing facility at the Fleet Numerical Weather Central, Monterey, California.

Some discussion ensued concerning the use of ray tracing through fronts, when the results are available only well after the event. However, most people seemed to feel that such tracings were useful in anticipating the effect of similar events, and indeed were of operational significance.

It was noted that there were many examples in the past of oceanographers rejecting the evidence of layered micro-structure as an artifact.

Asked about the scale size of the fronts, the author described them as being of the order of 20 n.mi across and hundreds of n.mi long; though further investigation was needed to reveal their true extent.

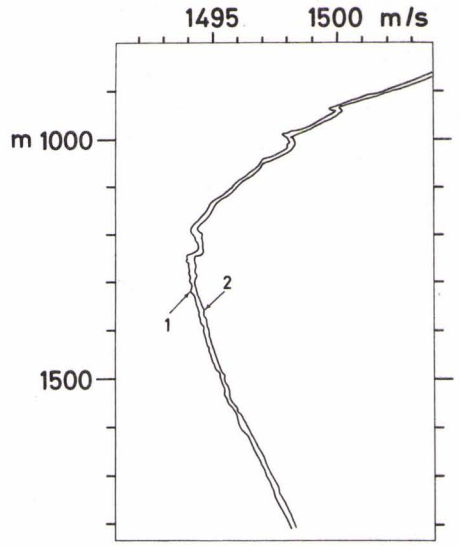

FIG. 1

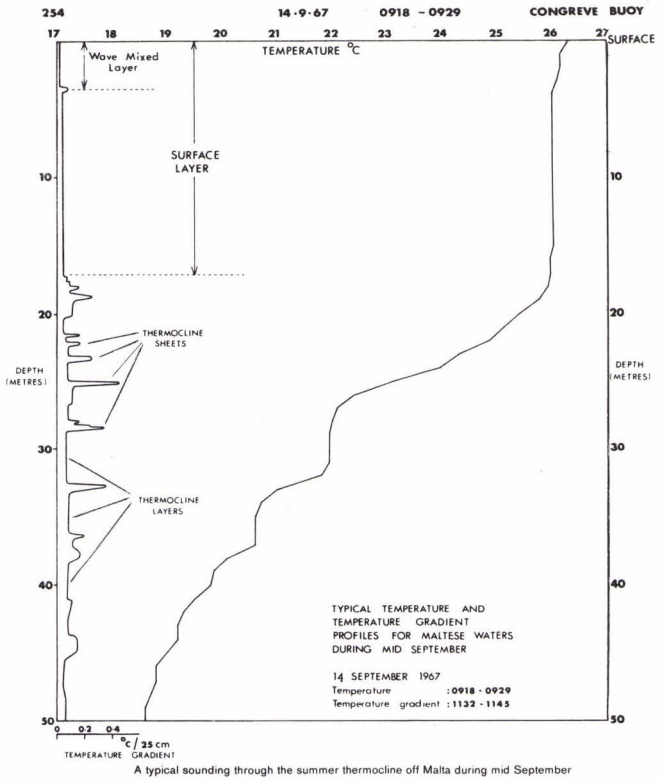

A typical sounding through the summer thermocline off Malta during mid September

FIG. 2

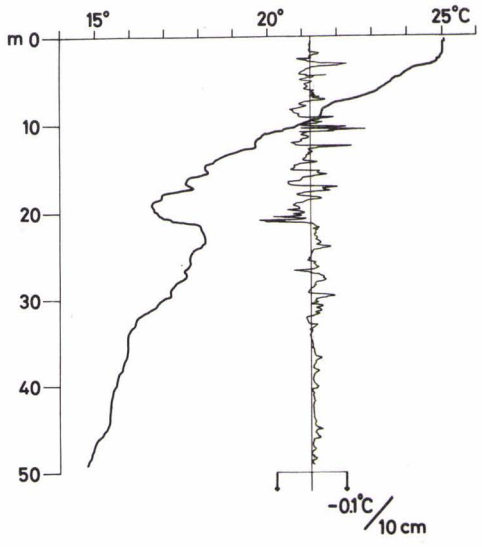

FIG. 3

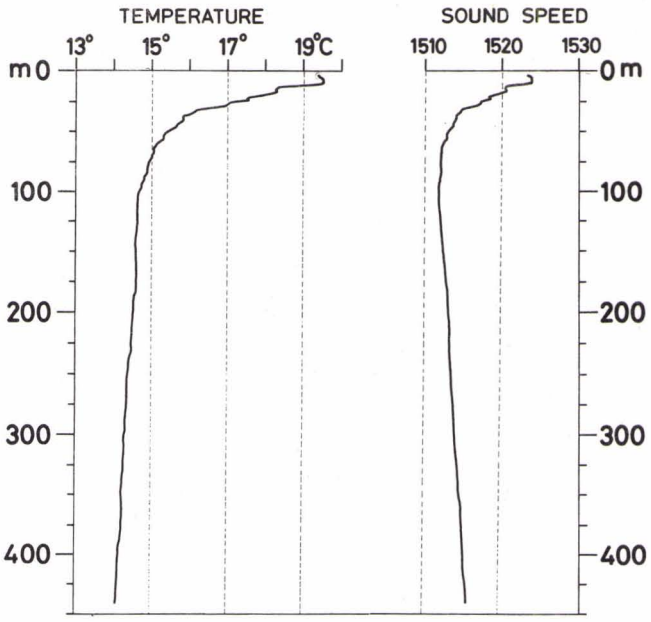

FIG. 4

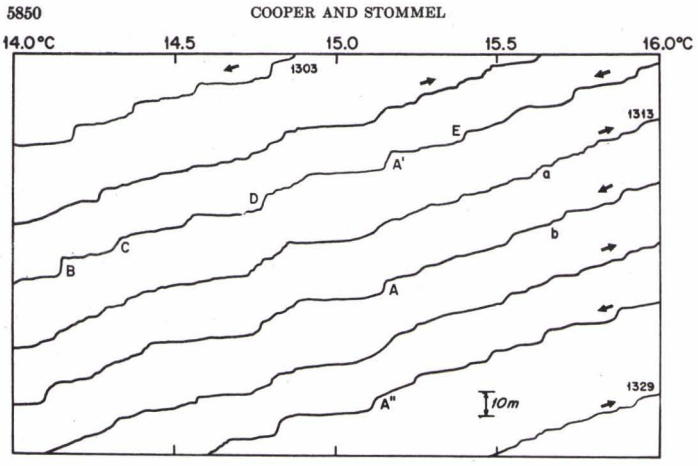

FIG. 5

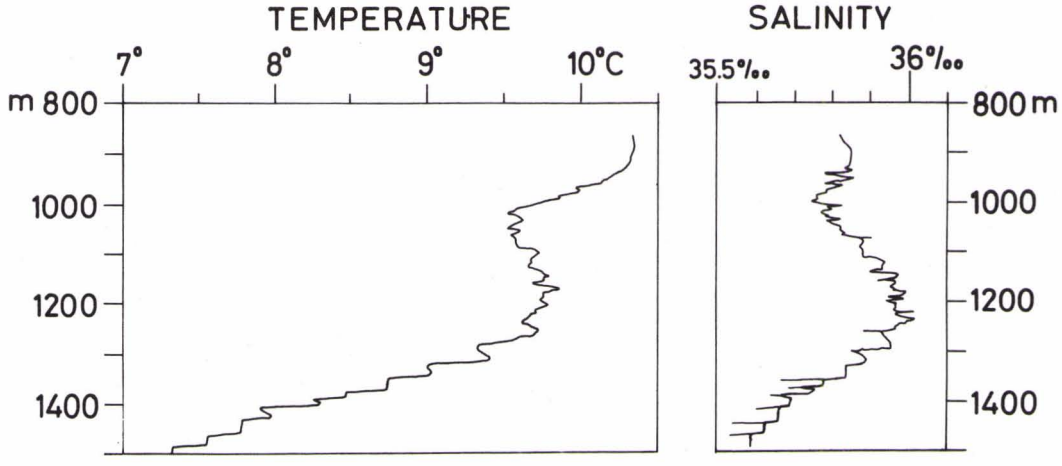

FIG. 6

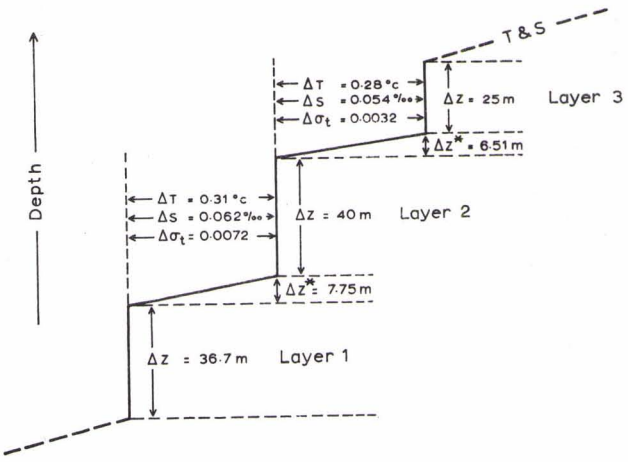

FIG. 7

Average parameters for the 3 layers considered in the analysis, computed from 33-hr of observation at a single station.

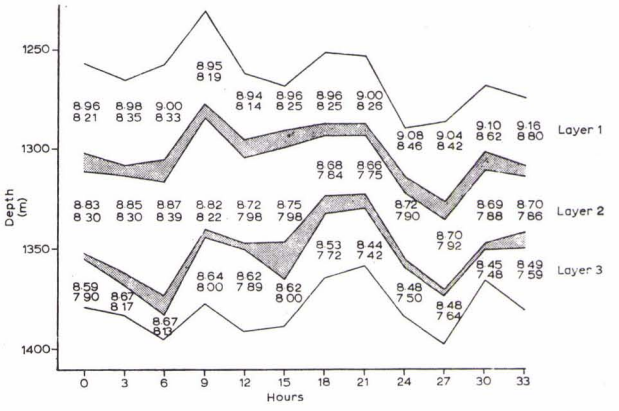

Depth variations of the layer system for Series A. Shading denotes interfaces and mean values of T and S within each layer also shown (S to three decimals after 35‰).

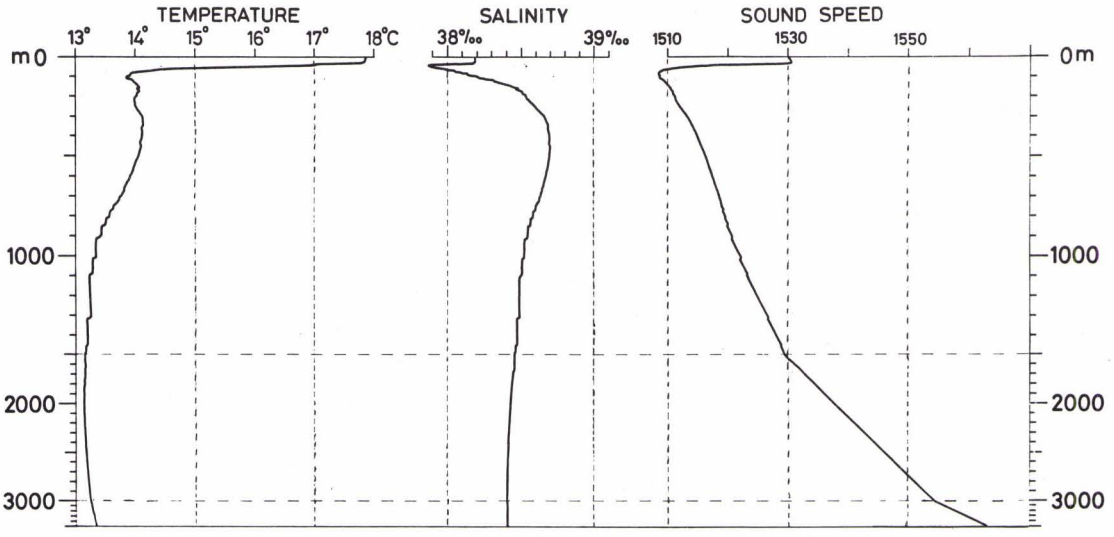

FIG. 8

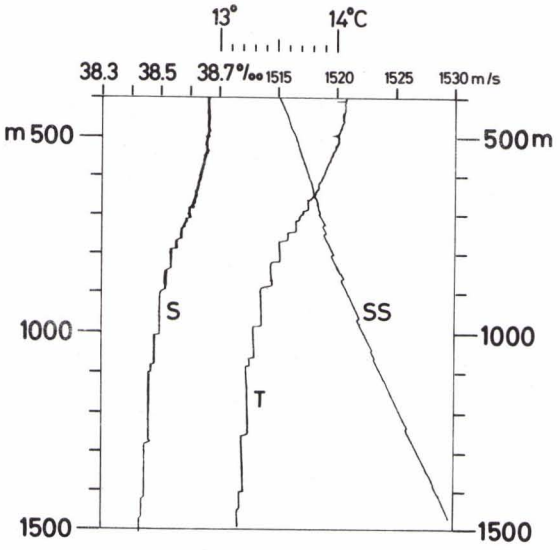

FIG. 9

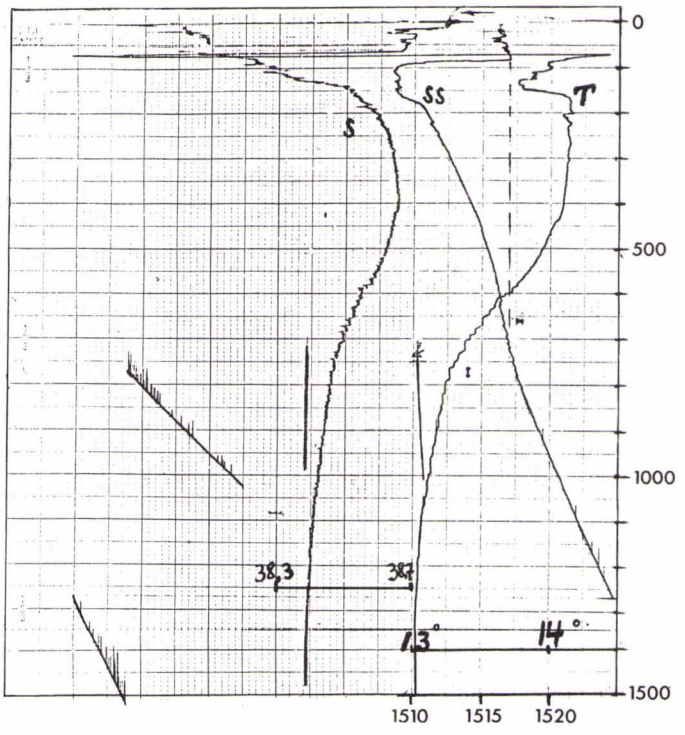

FIG. 10

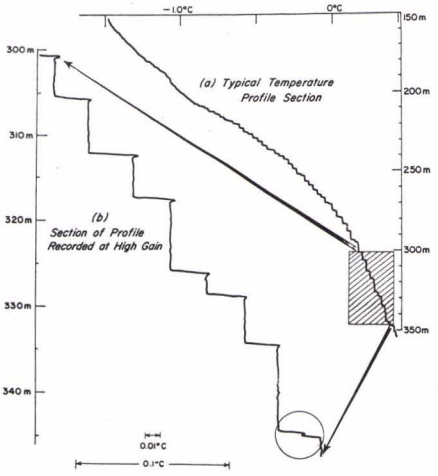

Vertical profile of temperature under T-3 (84°38'N, 128°21.6'W, 19 March 1969). Shaded section of profile (a) shown as observed in profile (b) to left.

FIG. 11

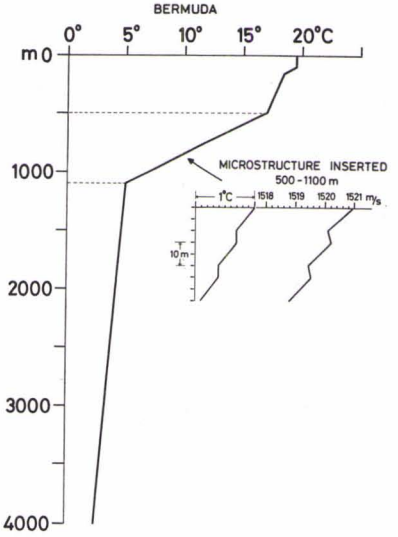

FIG. 12

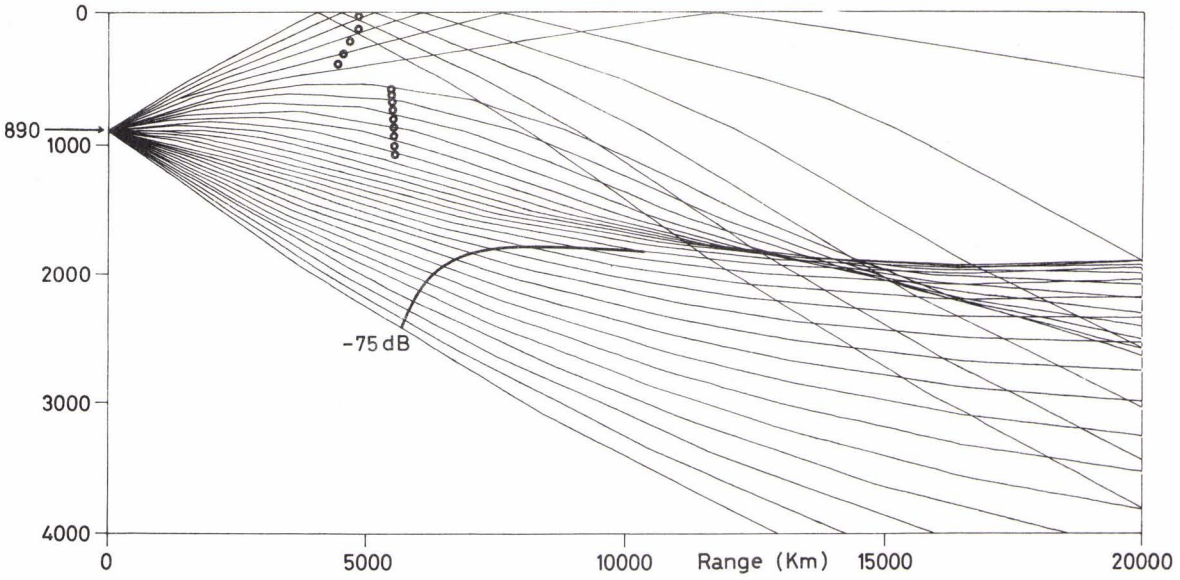

FIG. 13

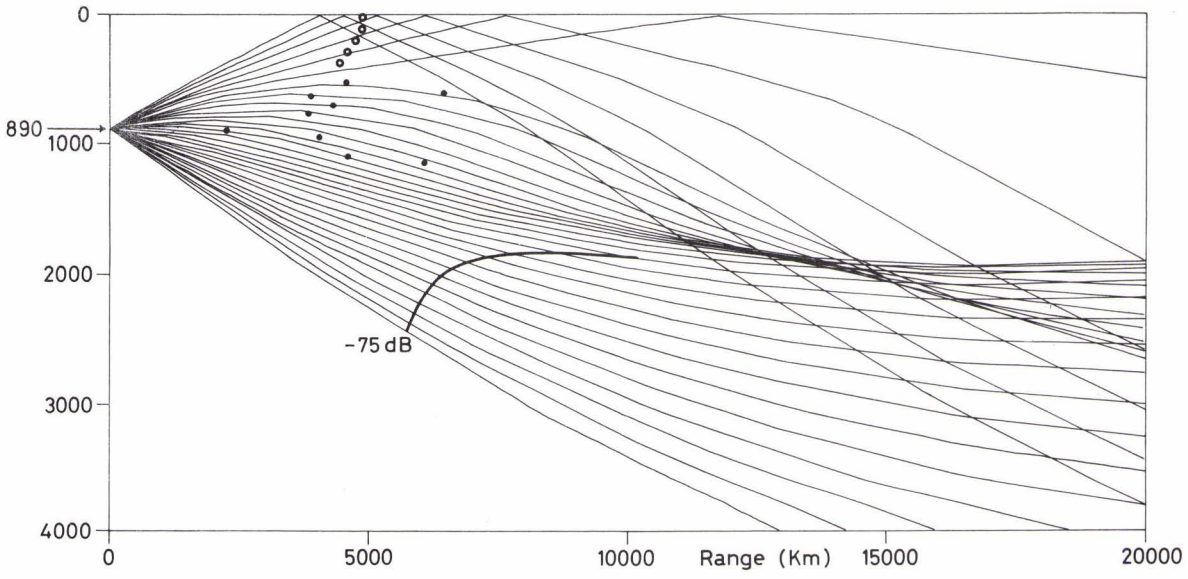

FIG. 14

FIG. 15

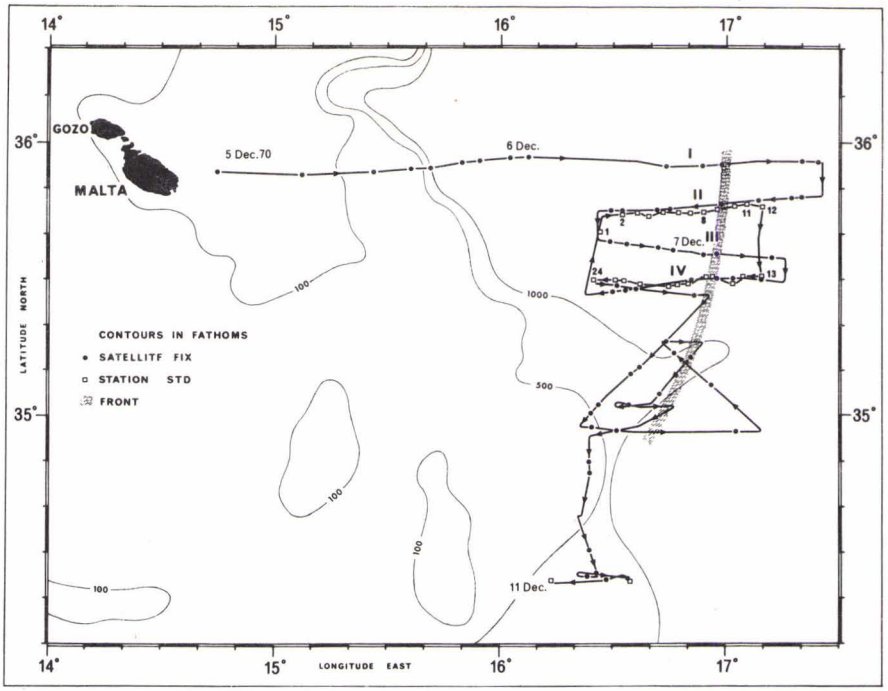

FIG. 16

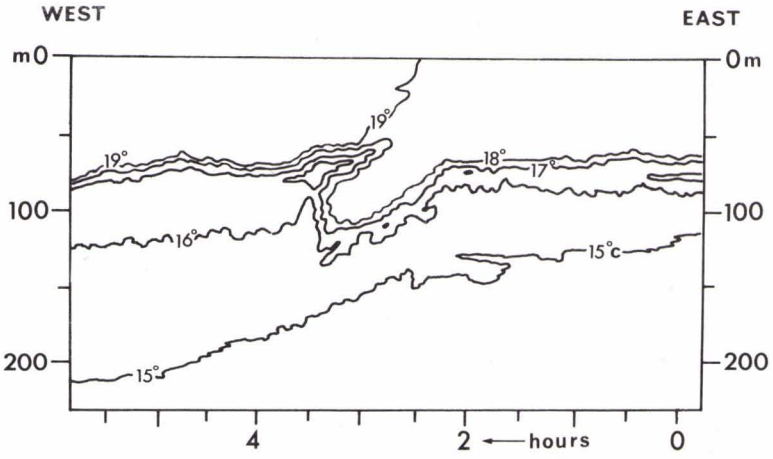

FIG. 17

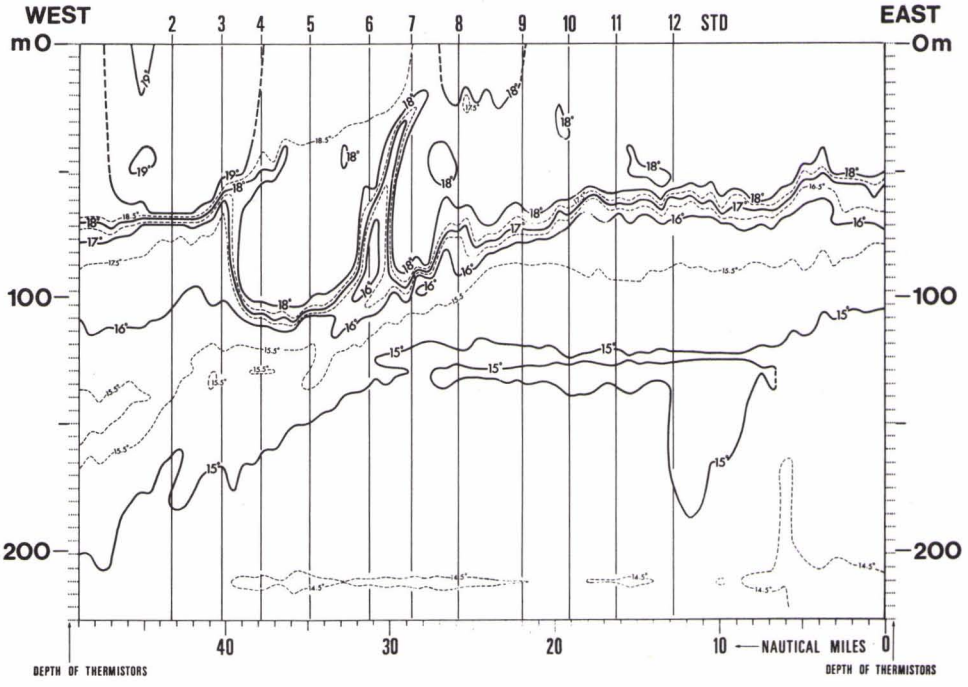

FIG. 18

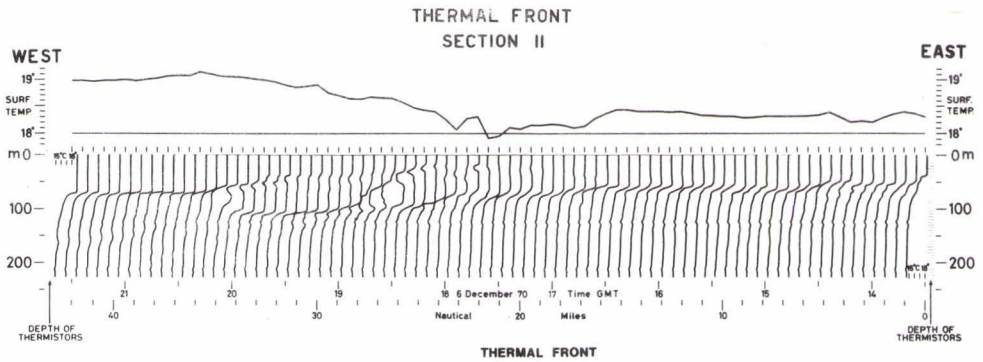

FIG. 19

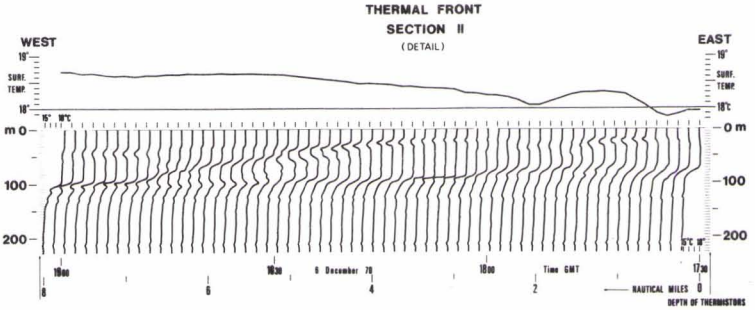

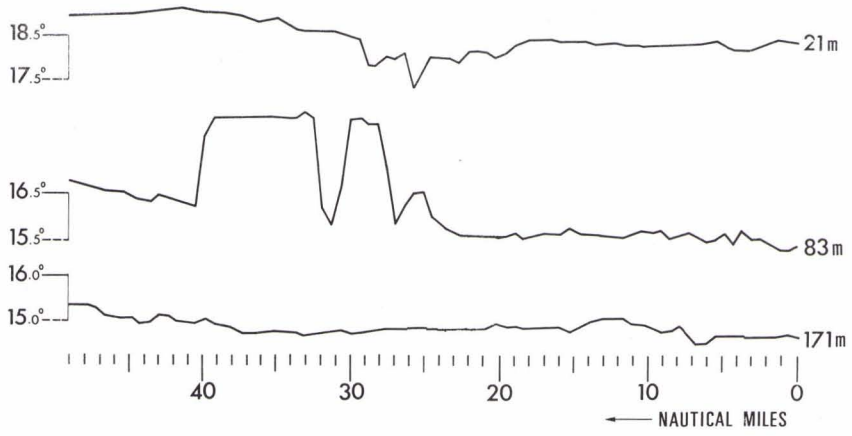

FIG. 20

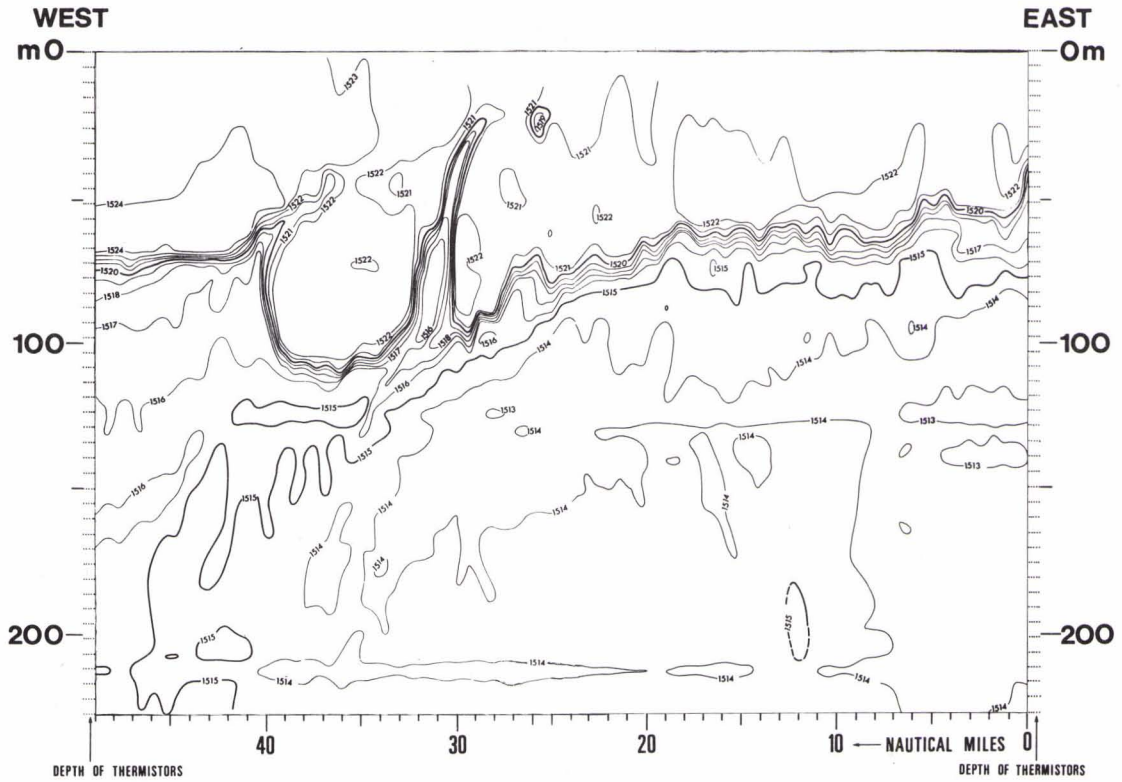

FIG. 21

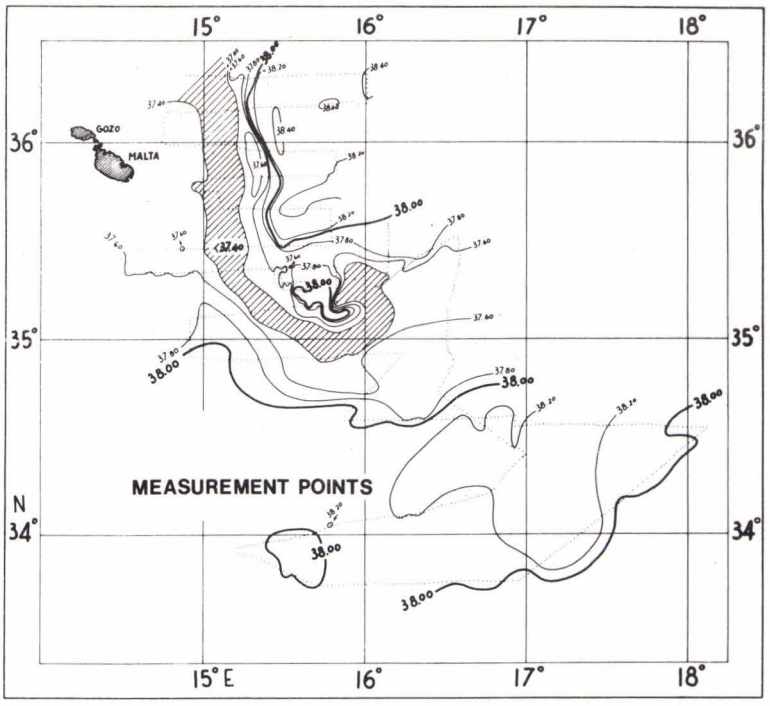

FIG. 22

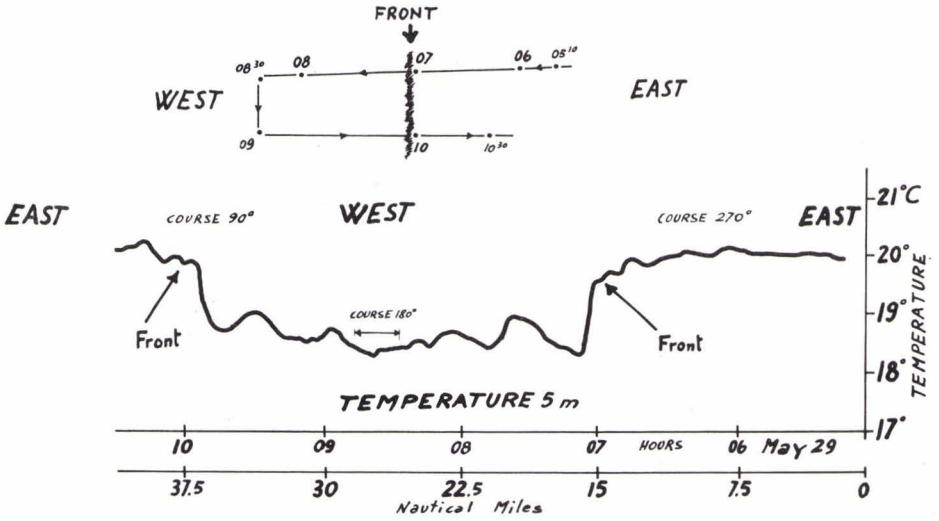

FIG. 23

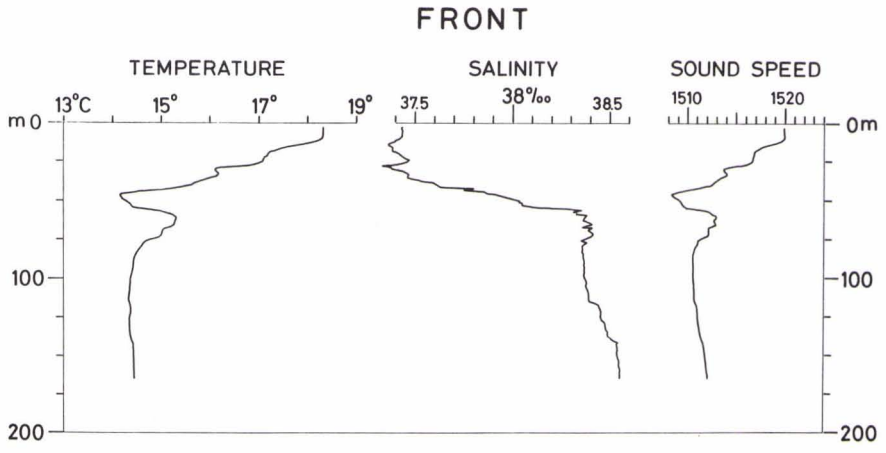

FIG. 24

CONSIDERATIONS RELATING TO THE CALCULATION OF SOUND VELOCITY

by

C.C. Leroy
Laboratoire Marine d'Acoustique
Arcueil, Paris, France

The various equations for the calculation of the speed of sound in sea water that can be found in the literature may be grouped into three main categories:

(a) Equations of the first investigators (see, for example, Wood [Ref. 1]). These were simple but are now too inaccurate.

(b) Equations to fit the tables of Kuwahara [Ref. 2] and Matthews [Ref.3]. The tables came from computations based on physical formulae and data. The equations that were developed in the early stages of electronic computers were already complex. The pressure effect was taken into account. We can mention Mackenzie's equation [Ref. 4].

(c) Equations to fit directly measured values of sound velocities.

The equations appeared progressively with the measurements and were made possible by the development of sound velocimeters.

One finds the following equations:

1. By Del Grosso [Ref. 5] for sea water at atmospheric pressure. Simple but now inaccurate.

2. By Greenspan and Tschiegg [Ref. 6] for fresh water from 0^{o} to 100^{o} C. Few terms of some complexity and excellent agreement between formula and data points (but there is only one parameter: temperature).

3. The various Wilson equations [Ref. 7]. For fresh water under pressure up to 14 000 lb/in^2: 20 terms, 7 significant figures in each coefficient. For sea water, up to 14 000 lb/in^2 pressure, June 1960. Fits data points of limited salinity: 21 terms, 4 to 6 significant figures. This equation is not applicable outside the investigated domain of salinity [see below Fig. 7].

4. Another equation by Wilson [Ref. 7] of October 1960, for sea water. It fits previous data points + fresh water data points, + new data points at 10, 20, 30‰ salinity. Again complex equations (22 terms, 4 to 6 significant figures).

Wilson's second equation [Ref. 7] was the last to have been published when the present author, trying to develop a simple equation for use in the limited oceanographic conditions encountered in the Red Sea, realised how easy it was to make a simple formula once the data points to be fitted were reduced.

At the same time, the author started to investigate simple ways of computing the pressure at depth, in order to apply Wilson's equation [Ref. 7] easily and his own (unpublished) equation for the Red Sea. It turned out that pressure could be computed from depth and latitude only, without having to consider temperature or salinity. One universal equation was developed which only needed to be replaced by other ones for the Black Sea and the Baltic. This work has been published in Ref. 8.

The possibility then appeared of developing a universal equation for sea water using depth as a parameter.

An investigation of the existing water masses of the world demonstrated that Wilson [Ref. 7] had used, to establish his formula, data points that were made outside realistic values [Figs. 1 and 2]. By limiting the domain of validity to existing waters, a much simpler formula than Wilson's could be developed [Fig. 3] that could approximate his second equation to within $\pm$ 0.1 to $\pm$ 0.2 m/s [Fig. 4]. This equation is built up with progressive terms that have either to

be omitted or taken into account, according to the ranges of temperatures and salinities involved.

A further step was to try using the original data points, belonging to the realistic domain, for making a new equation. This equation differs only slightly from the previous one. Both have been published in Ref. 9.

The data taken into account were all data points from Wilson [Ref.7] inside the defined domain except those for fresh water at atmospheric pressure, which were replaced by Greenspan & Tschiegg's [Ref. 6]. The last data of Wilson [Ref. 7] (high salinity and high temperature) were also considered.

Again the formula was dictated by the following considerations (besides the choice of the data):

(a) Make it simple so that it could be programmed on desk computers or even by hand.

(b) Make it susceptible to simplification in certain cases (progressive terms for high temperature, unusual depths or salinities, etc.)

(c) Use depth instead of pressure.

The equation published proved to fit Wilson's data better [Ref. 7] in the useful domain [Fig. 5]. An example of comparison between various equations is given in Fig. 6, the author's second equation being taken as the reference.

Since the time of its publication no other equation has been proposed but a number of new data appeared:

(a) It was agreed generally that Greenspan & Tschiegg [Ref.6] were too high by 0.35 m/s in the entire range of temperature (instrumental error).

(b) Extremely precise measurements of sound speed were performed by Vincent Del Grosso [Ref. 5] who kindly sent his results to the author.

For the moment only data at atmospheric pressure are available, but further values at pressure should be published.

In view of this, the author tried to compare the value given by his equation simply corrected by -0.35 m/s (the instrumental error of Greenspan & Tschiegg [Ref. 6]) with the new data of Del Grosso. The comparison was made with tabulated values of Del Grosso (that agree within 2 or 3 cm/s with the data points) and with the data of Greenspan & Tschiegg [Ref. 6] corrected by -0.35 m/s.

The comparison with Del Grosso's new data was made at 35‰, and at the extreme ranges of salinity investigated, viz. 31‰ and 39‰. The overall results are quite encouraging.

Figure 7 (taken from Del Grosso) shows the difference between his new data and equation and the previous equations of Del Grosso and Wilson [Ref. 7]. If plotted on that curve, the values of sound speed from the author's corrected second formula would stay within -0.045 and + 0.11 m/s of Del Grosso's results in the entire range of temperature from 0 to 35°C, which is perfectly acceptable and much better than any other formula valid also at depth.

At 31‰ the difference with Del Grosso [Ref. 5] was found to be between - 0.10 and - 0.20 m/s from 0 to 30°C, and at 39‰ this difference varied from + 0.17 to + 0.32 (the maximum being at 10°C). This less good agreement at 39‰ comes from the paucity of high salinity data that could be used for the author's equation.

At zero per unit salinity (fresh water) the agreement with Greenspan & Tschiegg [Ref. 6] lies between - 0.18 m/s and + 0.30 m/s in the useful range of temperature.

In all it appears that the author's second equation simply corrected by the constant figure of - 0.35m/s, is appropriate to approximate the latest accurate figures. This does not mean that some effort should not still be made, but in my view it would be better to wait until new data are published concerning the speed of sound at various hydrostatic pressures.

An interesting result may also be drawn from the above. Most often the comparisons of sound speed values have been made from the results of the equations. One of the discrepancies illustrated in Fig. 7 is between the new Del Grosso equation (very accurate) and Wilson's equations [Ref. 7] (not too accurate). As the author's formula was approximating Wilson's data, and as it fits well with Del Grosso's this means that, in the end, Wilson's data points were not as far from Del Grosso's as one would think. This is also a good reason for having confidence for the moment in the pressure effect unless there should be some inaccuracy in the measurements of pressure itself.

To conclude, the author wishes to stress the importance for the next equations to appear, that they should be

(a) more concerned with realistic values of temperature, salinity and depth;

(b) as simple as possible with not too complicated coefficients although this is less critical now;

(c) capable of simplifications by the removal of well-defined terms in the polynomial development;

(d) using depth directly instead of pressure.

REFERENCES

1. A.B. Wood, "A Textbook of Sound". Bell, London, (First Edition, 1930) Third Edition, 1955, p. 261.

2. Susumu Kuwahara, "The Velocity of Sound in Sea Water and Calculation of the Velocity for Use in Sonic Sounding". The Hydrographic Review, Monaco, Vol. 16, No. 2, November 1939.

3. D.J. Matthews, "Tables of the Velocity of Sound in Pure Water and Sea Water". 2nd Edition, London, British Admiralty, Hydrographic Department, 1939.

4. K.V. Mackenzie, "Formulas for the Computation of Sound Speed in Sea Water". J. Acoust. Soc. Am., Vol. 32, No. 1, January 1960, p. 100.

5. V.A. Del Grosso,"The Velocity of Sound in Sea Water at Zero Depth." Naval Research Laboratory, NRL Report 4002 - June 1962.

6. M Greenspan & C.E. Tschiegg,"Tables of the Speed of Sound in Water." J. Acoust. Soc. Am., Vol. 31, No. 1, January 1959,p. 75.

7. W.D. Wilson,"Speed of Sound in Distilled Water as a Function of Temperature and Pressure." J. Acoust. Soc. Am., Vol. 31, No. 8, August 1959, p. 1067.

W.D. Wilson,"Ultrasonic Measurement of the Velocity of Sound in Distilled Water and Sea Water." U.S. Naval Ordnance Laboratory, NAVORD Report 6746, January 1960.

W.D. Wilson,"Speed of Sound in Sea Water as a Function of Temperature, Pressure and Salinity." J. Acoust. Soc. Am., Vol. 32, No. 6, June 1960, p. 641.

W.D. Wilson,"Equations for the Computation of the Speed of Sound in Sea Water." U.S. Naval Ordnance Laboratory, NAVORD Report 6906.

W.D. Wilson,"Equation for the Speed of Sound in Sea Water." J. Acoust. Soc. Am., Vol. 32, No. 10, October 1960, p. 1357.

W.D. Wilson,"Extrapolation of the Equation for the Speed of Sound in Sea Water." J. Acoust. Soc. Am., Vol. 34, No. 6, June 1962, p. 866.

8. C.C. Leroy,"Formulas for the Calculation of Underwater Pressure in Acoustics." J. Acoust. Soc. Am., Vol. 44, 1968, pp. 651-653.

9. C.C. Leroy,"Development of Simple Equations for Accurate and more Realistic Calculations of the Speed of Sound in Sea Water." J. Acoust. Soc. Am., Vol. 46, 1969, pp. 216-226.

DISCUSSION

The author was asked whether the low-salinity correction, recommended for salinities below 30‰ but having an (S-35) dependence, could be used without too much error from salinities of 35‰ on down; the advantage being that no discontinuity at S=30 is thus introduced. The answer was affirmative, but with the warning that for salinities above 35‰ the error so introduced might become unacceptable.

A discussion followed concerning the importance of the effect of pressure on sound speed. There were certain experimental anomalies which indicated the need for more extensive information at depth. In fact, because some commonly used STD systems use pressure as a measure of depth, it might be advisable to develop both depth and pressure sound-speed formulae.

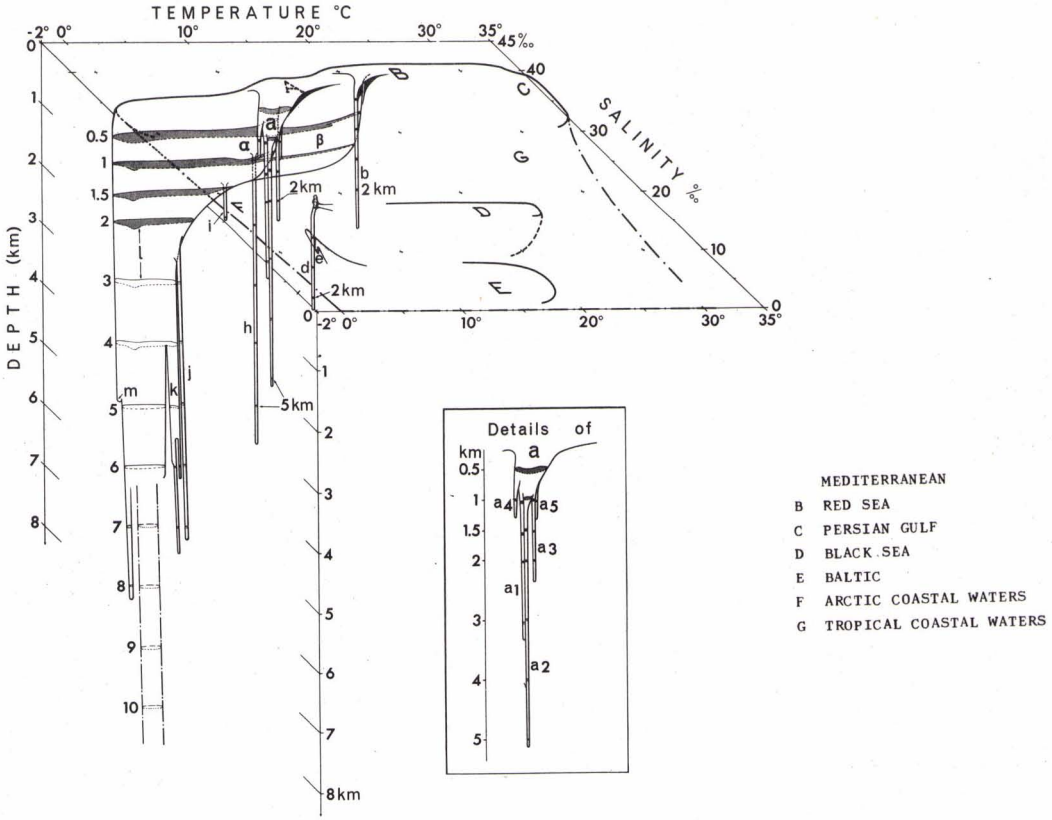

THREE-DIMENSIONAL REPRESENTATION OF THE TEMPERATURE-SALINITY-DEPTH VOLUME ENCLOSED BY REAL WATERS

FIG. 1

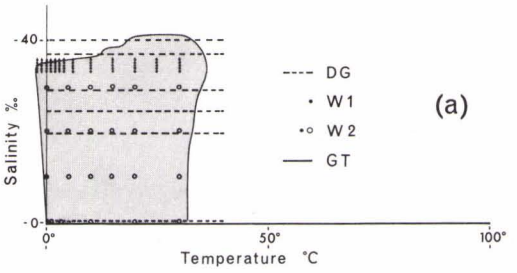

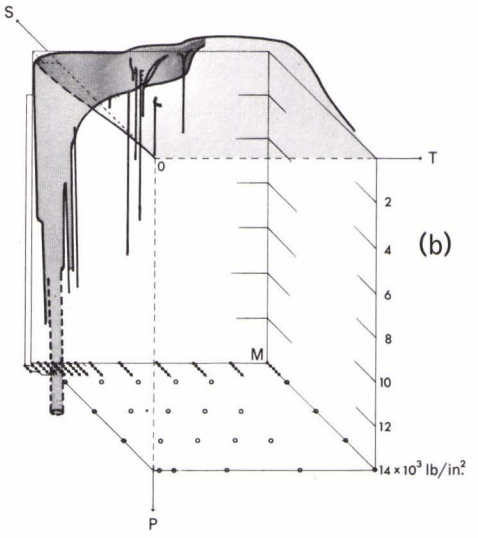

FIG. 2

COMPARISON OF REAL TEMPERATURE-SALINITY-PRESSURE COMBINATIONS WITH THOSE FOR WHICH SOUND SPEED MEASUREMENTS HAVE BEEN MADE

(a) AT SURFACE PRESSURE
(b) AT DEPTH

FORMULA FOR THE CALCULATION OF SOUND VELOCITY IN SEA WATER

COMPLETE	$V = V_o + V_a + V_b + V_c + V_d$
BASIC	$V = V_o + V_a + V_b$
SIMPLIFIED	$V = V_o$

in which

$$V_o = 1492.9 + 3(T-10) - 6\times10^{-3}(T-10)^2 - 4\times10^{-2}(T-18)^2 + 1.2(S-35) - 10^{-2}(T-18)(S-35) + Z/61$$

$$V_a = +10^{-1}\zeta^2 + 2\times10^{-4}(T-18)^2 + 10^{-1}\zeta\,\phi/90$$

$$V_b = +2\times10^{-7}T(T-10)^4$$

$$V_c = -5\times10^{-4}\zeta^2(\zeta-6)^2$$

$$V_d = +1.5\times10^{-3}(S-35)^2(1-\zeta)$$

Where
- V is the sound velocity in m/s
- T is the temperature in °C
- S is the salinity in ‰
- Z is the depth in m, and $\zeta = Z/1000$, the depth in km
- ϕ is the latitude in degrees

Note: V_o can also be written:

$$V_o = 1449.34 + 4.56T - 0.046T^2 + 1.2(S-35) - 10^{-2}(T-18)(S-35) + Z/61$$

FIG. 3

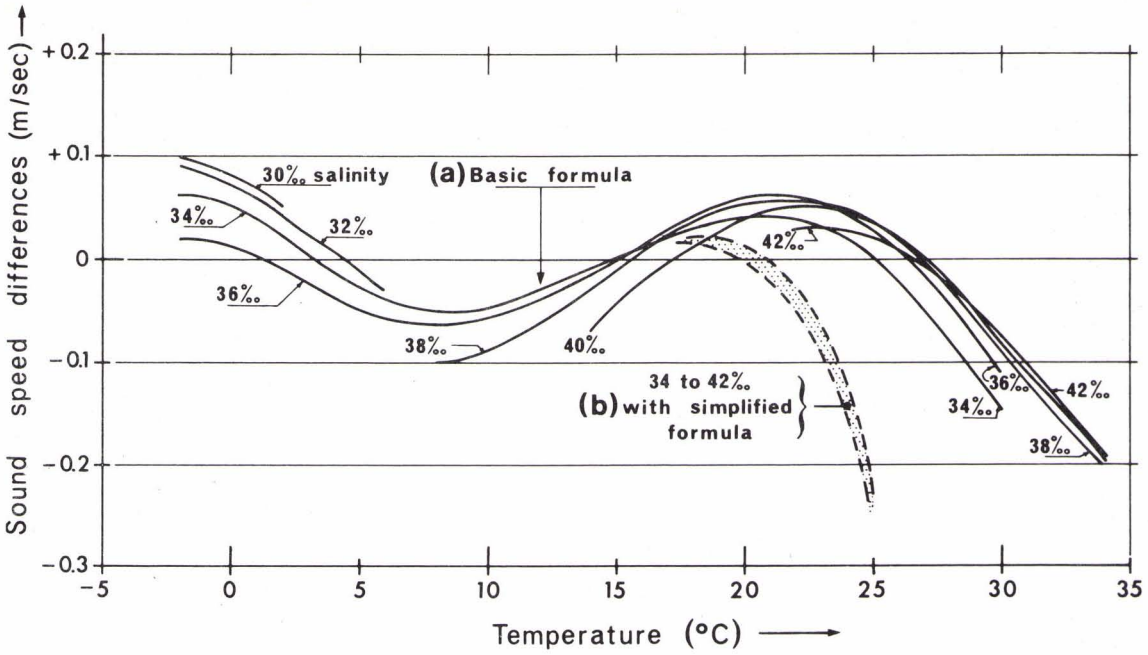

DIFFERENCES IN SOUND VELOCITY AT SEA LEVEL BETWEEN RESULTS OF

(a) Basic and Wilson's formulae ———

(b) Simplified and Wilson's formulae – – – –

AS FUNCTIONS OF TEMPERATURE AND AT DIFFERENT SALINITIES

FIG. 4

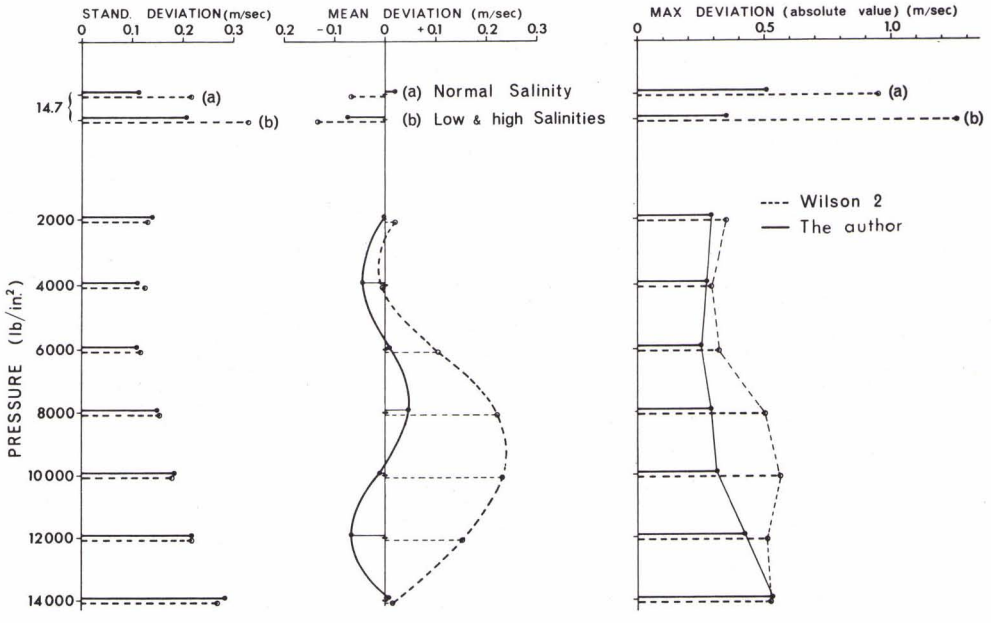

COMPARISON OF THE STANDARD, MEAN AND MAXIMUM DEVIATIONS OF WILSON'S SECOND EQUATION FOR SEA WATER AND THOSE OF THE AUTHOR

FIG. 5

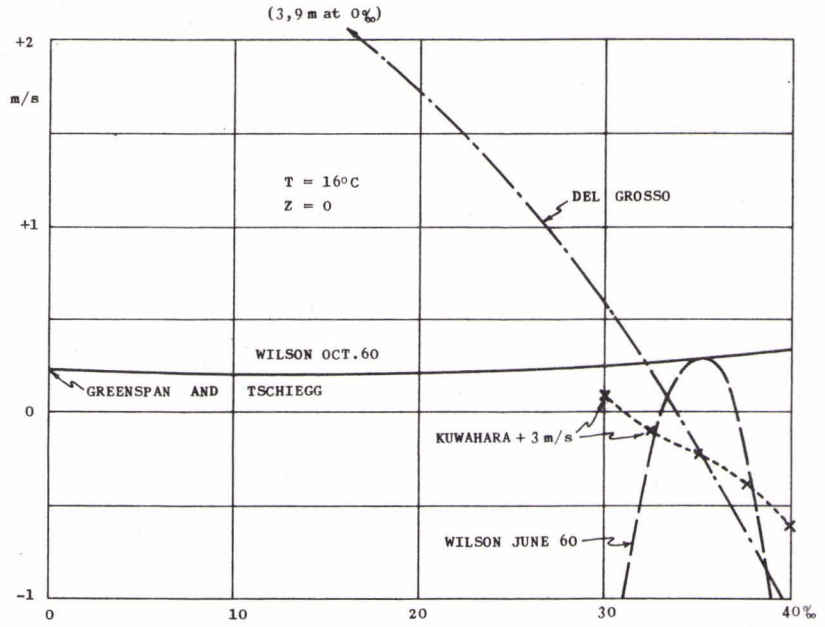
(3,9 m at 0‰)
+2
m/s
+1
0
-1
T = 16°C
Z = 0
DEL GROSSO
WILSON OCT.60
GREENSPAN AND TSCHIEGG
KUWAHARA + 3 m/s
WILSON JUNE 60
0
10
20
30
40‰

FIG. 6

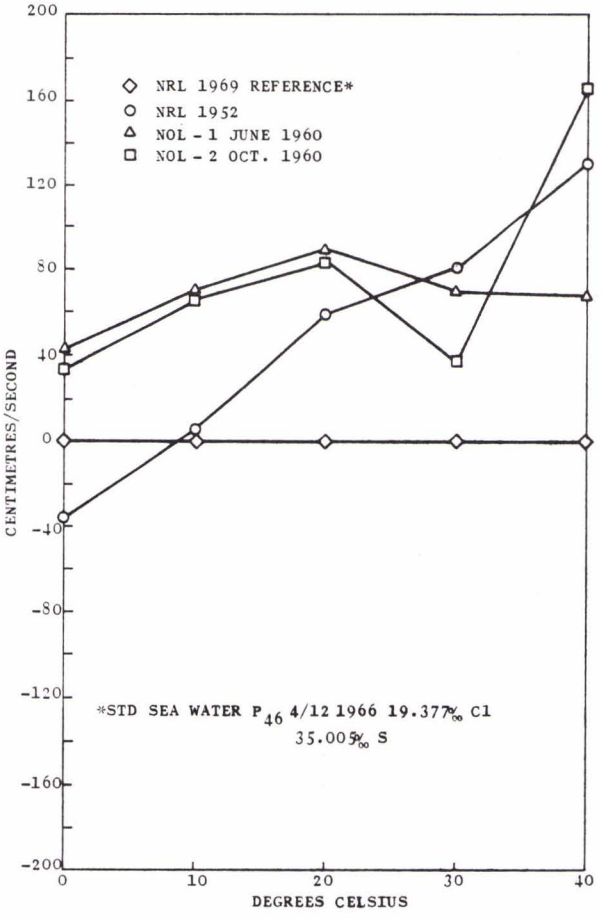
200
160
120
80
40
0
-40
-80
-120
-160
-200
NRL 1969 REFERENCE*
NRL 1952
NOL - 1 JUNE 1960
NOL - 2 OCT. 1960
*STD SEA WATER P46 4/12 1966 19.377‰ Cl
35.005‰ S
CENTIMETRES/SECOND
0
10
20
30
40
DEGREES CELSIUS

FIG. 7

SESSION 2

RAY TRACING COMPUTATION

Session Chairman : P.R. Tatro

Session Secretary : T.D. Westrup

SOME COMMENTS ON RAY THEORY WITH EXAMPLES FROM CURRENT NUC RAY TRACE MODELS

by

H.P. Bucker
Naval Undersea Research and Development Center
San Diego, California, U.S.

Three topics were covered in this paper:

1. Ray Sweep-out Method — a technique for calculating sound intensities at a large number of receiver points in range and depth.

2. Bi-static Reverberation Model — a technique based on the superposition principle for relatively quick reverberation calculations.

3. Ray/Wave Method — a technique for combining ray and wave methods in long range propagation calculations.

Because material on the first two topics will be available in a review article by Bucker and Cybulski in the Journal of Underwater Acoustics, September 1971, only the third subject will be repeated in this summary.

THE RAVE (Ray/Wave) METHOD

In long-range sound propagation in the ocean, account must be made for the horizontal changes in the sound velocity profile and for major bathymetry features. In this talk a method will be presented that satisfies the following requirements:

1. Account for large scale profile and bathymetric features.
2. Use a minimum number of rays.
3. Eliminate caustics and fill in shadow zones.
4. Account for boundary and volume scattering.

The proposed method for calculating the sound field is a combination of ray theory and wave theory; hence, the acronym RAVE method.

The first step in the calculation is to separate the ocean into triangles as shown in Fig. 1. By suitable choice of the range increments we can make the ocean bottom be the lower side of the bottom triangle.

Within a triangle we can choose either the sound speed or one over the square of the sound speed as a linear function of range and depth as shown in Fig. 2. In the first case, the ray paths are arcs of circles while in the second case the ray paths are segments of parabolas.

For the intensity calculation we will associate a wave function with each ray path as shown in Fig. 3. The spread of the wave functions will be a function of frequency while the height of the functions will be determined by the vertical beam pattern at the source and the spacing between adjacent rays at the source.

Next we trace the rays out to a specified range as shown in Fig. 4. The wave functions are now summed at the depths where there are rays. The value of this field is called Σf_j^*. If sufficient rays have been traced the depth dependence of Σf_j^* should be a good measure.

The final steps is to normalize Σf_j^* so that it represents the proper rate of flow of acoustic energy. These steps are as follows:

At 1 unit length:

$$E_o = 2\pi \int_{-\gamma_u}^{\gamma_d} R(\gamma_s) \cos\gamma_s \, d\gamma_s = 2\pi \sum_{n=1}^{N} R_n \cos\gamma_{sn} \, \delta\gamma_n$$

At range r:

$$E_r = 2\pi \Sigma R_n g_n \cos\gamma_{sn} \gamma_n$$

where g_n accounts for boundary losses and volume attenuation ($g_n < 1$)

Let $\sum f_i(z)$ be the sound field at (r,z). We have a function $\sum f_j^*(z)$ that is an approximation to the sound field.

Let $N \sum f_j^* = \sum f_i(z)$

we have,

$$E_r = 2\pi r S(\underbrace{\sum f_i^* \cos \gamma_i}_{\text{SS}}) \delta z = 2\pi \sum R_n g_n \cos \gamma_{sn} \gamma_n$$

$$\text{SS} = N \sum f_j^* \cos \gamma_j$$

DISCUSSION

Following the description of the Ray Sweep-out Method, several queries were raised regarding the validity of the method, particularly in the case of limiting rays, and multi-ray path structure if and as intensity losses were taken into account at reflective boundaries. The author replied that by computing for a sufficiently close interval between adjacent rays, that is, between $1/100^\circ$ and $1/1000^\circ$, such problems could be largely avoided. In reply to another question he confirmed that the source beam pattern could be specified and taken into account.

Regarding bi-static reverberation, the author stated that the method had not yet fully been tested as a predictive model. In reply to a question regarding the effect of thick scattering layers on volume reverberation, he said that these would normally be approximated by multi-layer thin layers, and agreed that the effectiveness of such an approximation would depend on the position and distribution of such layers. Reverberation calculations were, in the author's opinion, more applicable to long pulses. The program takes account of the effect on surface reflection of the angle of incidence.
A questioner was assured that ray paths were not duplicated, although this superficially appeared to be so. Energy is normally summed over about 10 000 elements of area.

The discussion following the presentation on the combined use of ray/wave theory centred on what assumptions were made regarding phase. Random phase is assumed, and phase shift and surface losses are computed at reflective surfaces. No conclusive experimental verification had yet been obtained for this method.

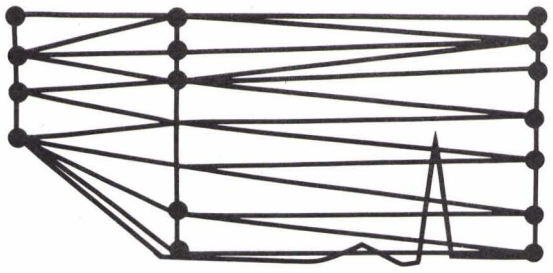

FIG. 1

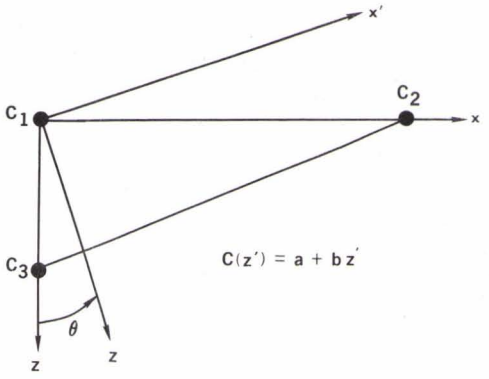

a, b, AND θ ARE DEFINED BY THE THREE SOUND SPEEDS C_1, C_2, C_3

FIG. 2

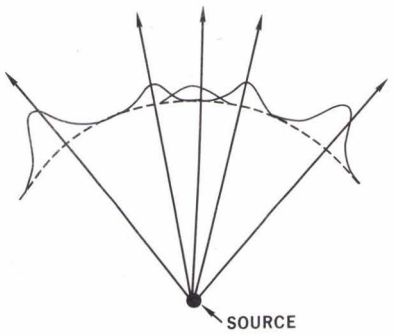

FIG. 3

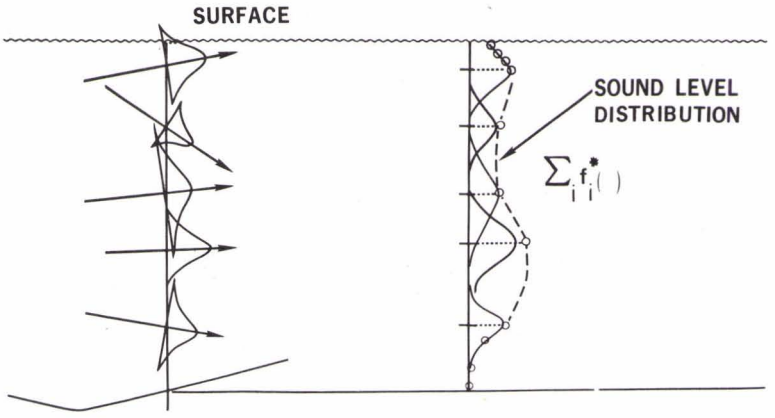

FIG. 4

RAY TRACING ON A MINI-COMPUTER

by

M. Thompson and W. Wijmans
SACLANT ASW Research Centre
La Spezia, Italy

INTRODUCTION

It would appear that most people engaged in solving problems in ray-tracing, use programs written for large computers. These machines commonly have large memory sizes, fast cycle times and large word length. This paper describes how SACLANTCEN has provided a ray-tracing capability on a mini-computer.

Let us firstly define what we mean by a mini-computer. It is typically a machine with a memory size of between 1K and 32K words, each word being of between 12 and 18 bits in length. Cycle times of between 1 and 2 μs are the norm for this type of computer. Standard peripherals are a system Teletype, photo-reader and paper tape punch. Extra peripherals can be added easily by using plug-in card interfaces; memory expansion is often available so that a user can build up a system to his own requirements.

Reasons for Using Mini-Computer

Now let us consider why we should wish to use a mini-computer instead of a larger, often faster, system.

Firstly, most large ray-tracing programs are very inflexible. Particularly, if the program is of monolithic structure and if a user requires any additions to the program, then major modifications are normally required.

Secondly, complicated data tapes must be produced by the user, [Ref. 1], and if a mistake is made then the error is not found until the job has been run, which, depending on the workload of the particular computer, may take several hours.

We have tried to eliminate both these points, as I will describe later.

The third, and possibly most important reason for using a mini-computer is the need to have a ray-tracing capability on board ship during propagation experiments at sea. With this capability available, a scientist on board will be in a better position to decide whether an experiment should continue as planned or be modified because of the prevailing propagation properties of the medium.

Ray Tracing on Board Ship

This latter point was first implemented on an Olivetti 101 desk-top calculator, [Ref. 2], which has a very limited memory size and register length. It was therefore necessary to have the program split into several parts so that memory restrictions were overcome, and to simplify some of the formulae, especially those containing the sines of small angles, to overcome accuracy problems.

Each part of the program was stored on magnetic cards and the output of one program had to be manually input into the next part of the program. Three typical parts of the program could be:

(1) Conversion of depth, temperature, salinity values to a sound speed profile.

(2) Calculation of Snell's constant for a given source depth and initial angle.

(3) Computation of the coordinates of the ray path.

Other cards for the calculation of travel time, path length and intensity made this a comprehensive program but necessitated many hours and much patience to get the desired results.

Last year, however, a number of Hewlett-Packard 2116B mini-computers were purchased by SACLANTCEN. One of these computers is available for shipborne use, and is loaded on board ship as required. This machine has a cycle time of 1.6 μs and a memory size of 32 000 16-bit words. Apart from the standard peripherals we also have a fixed head disc, magnetic tape, Calcomp incremental plotter and a Tektronix 4002 (visual display device), which is used as the machine-operator interface and fast plotting device.

Its physical size is such that it can easily be transported and loaded on board ship. It is $31\frac{1}{2}$" high, $19\frac{3}{8}$" deep and is mounted in a standard 19" rack. All of its peripherals can also be rack mounted.

We have at present two programs for ray-tracing on this machine. Both are written in Fortran II, which should facilitate easy conversion to most other machines.

The first program is designed to give the scientist on board ship a quick plot of the ray diagram. It has a memory size of 3500 locations and therefore can be run on a basic 4K mini-computer which is fitted with some plot device. It simply calculates the ray paths from a source at a given depth to a given range in constant increment steps of angle, using a sound speed profile divided into layers of constant gradient input on the photo-reader.

The ray diagram is displayed, in our case, on the Tektronix terminal. Using the cursor provided with this terminal, a user can quickly indicate a new source depth on the sound speed profile and obtain a new ray diagram, thus seeing quickly the effect of moving the source on the ray diagram.

The computation time for this program is approximately 60 ms per layer crossing. Using an Epstein profile, as described in Ref. 3, divided into 75 layers, 45 rays from the source and a range of 2500 m, took 4 min 10 s for computation and plotting.

This program is analogous to some hardware machines which are commercially available solely for ray tracing purposes. The physical dimensions of the equipment necessary, and the time of computation and display, compare favourably with these machines, with the added advantage that the equipment is available for other jobs when ray tracing is not required.

Modular Ray Tracing

The second program being implemented is a comprehensive ray-tracing program which we feel will be easy to modify in the future and easy to run.

It is partly based on the philosophy of the program for the Olivetti machine in that it is of modular structure, each module being a completely self-contained sub-program. We can make an analogy to a loose-leaf book system as shown in Fig. 1, where each 'page' is a separate 'chapter' of the book and all the relevant 'chapters' can be found in the index. For instance, page 1 of Fig. 1 is called "Fixed RT" and after choosing this option in the Index, the fast program described earlier would be called into the memory of the computer ready for execution.

Pages 2 onward are part of the comprehensive program; a user can start from a depth, temperature, salinity profile and calculate a sound speed profile, or alternatively directly input a sound speed profile into the ray calculation page. These profiles can be produced off-line from previous data or on-line from the sensor instruments which are interfaced to the computer.

Other necessary inputs are source depth, bottom depth (a flat bottom is assumed), maximum range and ray information. Rays can either be specified by the user as a set of constant increment angles from the source, or found automatically as the rays from the source which have a vertex at a layer depth in the velocity profile [Fig. 2]. We have termed these rays the 'characteristic'

rays, and the user may specify the number of rays to be interpolated between two 'characteristic' rays.

Page 3, the ray calculation page, computes ray coordinates, travel time, path length and intensity at each layer crossing and stores all the information on the disc storage device.

From here, depending on what the user chose from the index (Page 1), the data can be

(a) stored permanently on magnetic tape

(b) ray diagram plotted

(c) printed out on line printer

(d) special plots i.e. plots of travel time, intensity, start angle, emergent angle versus range for a given depth, and constant increment intensity contours.

Figure 3 shows the general layout of the system. With this form of system it is hoped that additions and/or modifications to the program should be a simple matter. For instance, Fig. 1 indicates blank pages which we envisage as being addition of continuous gradient sound speed profiles, range dependent ray tracing etc. The flexibility inherent in this system means a user may make his own modifications or replacements and each user can pick a system best suited to his needs.

To ensure that the program is easy to operate by people without experience of either computers or ray tracing, a conversational mode has been employed, [Fig. 4]; all data are entered through simple self explanatory questions and each step in the running of the program is preceded by a set of clear instructions on how to do it.

Figures 5 to 8 show some examples of the output produced by this program.

Using the same Epstein profile as described previously, and all the other data remaining the same, the modular ray tracing took 13 min for calculation and display. The greater time as compared to the previous program is due to the greater amount of information that is computed and the file management on the mass storage device that is required.

The size of this program, if considered as a whole, is of the order of 16 000 memory words. However, as it consists of a number of self-contained sub-programs, it is an easy matter to have the program in, say, two or three small parts, where one part automatically calls the next part into the computer memory when necessary. In this way we never use more than 7000 words of memory. This program can therefore be successfully used on a moderate sized mini-computer.

CONCLUSION

Ray tracing is easily implemented on a mini-computer, and can be extended to be a comprehensive program.

For laboratories with only limited computing facilities, and for shipborne use where it is only possible to have a computer installed of small physical dimensions, the programs described provide a powerful tool for the investigation of the propagation properties of the ocean which will satisfy the requirements of most users.

Because of the limited word length available on most mini-computers, an accuracy of more than 6 decimal places cannot be expected. Also, computation times are by no means fast when compared to that obtainable with large modern computer systems. If, therefore, we require extra speed and accuracy, we envisage that a modular program like the one described here, with its advantages of flexibility and conversational mode, would be an excellent method of applying ray tracing to a large multi-access machine.

REFERENCES

1. I. Verdoni, "Acoustic Ray Tracing at SACLANTCEN on the Elliott 503 Computer", SACLANTCEN Internal Note No. 260, 1 December 1970.

2. A. Skretting, "Sound Field Computation by Means of Desk Top Computers", SACLANTCEN Technical Report No. 141, 15 March 1969.

3. C.B. Moler and L.P. Solomon, "Use of Splines and Numerical Integration in Geometrical Acoustics", J. Acoust. Soc. Am., Vol. 48, p.739, 1970.

DEMONSTRATION AND DISCUSSION

A short demonstration of the ray tracing facilities on SACLANTCEN's Hewlett Packard computers followed the presentation. Both the fast ray tracing program and the modular system were shown. Delegates had the opportunity to operate the systems themselves and were invited to suggest any improvements that they thought necessary. One such suggestion was that the representation of the rays would look more 'natural' if the rays were drawn as continuous curves instead of straight line segments. In reply it was stated that a routine for such a plot had been written and tried but the increase in running time became unacceptably high.

The demonstration clearly showed the usefulness of the mini-computer as a ray tracing device; remarks such as the favourable speed of obtaining results, and the advantage of man-machine interfacing through the conversational mode were typical. It was also considered by many that laboratories with large computer systems and a large workload could use a mini-computer ray tracing capability to great advantage.

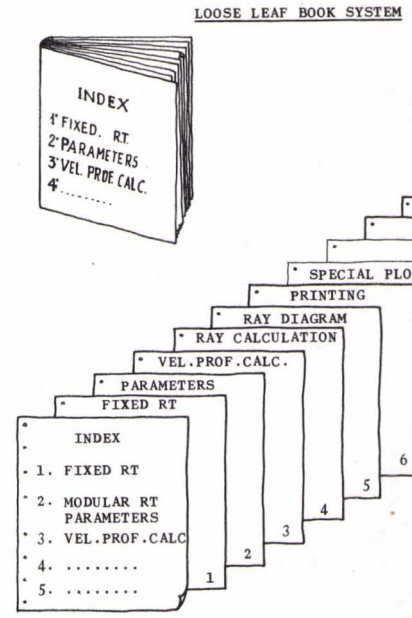

FIG. 1

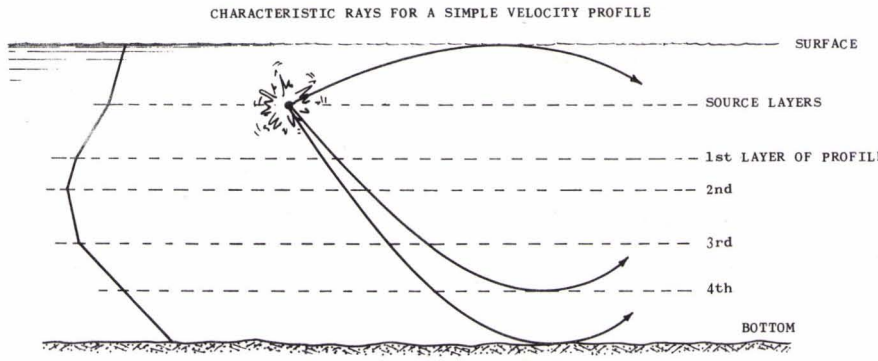

FIG. 2

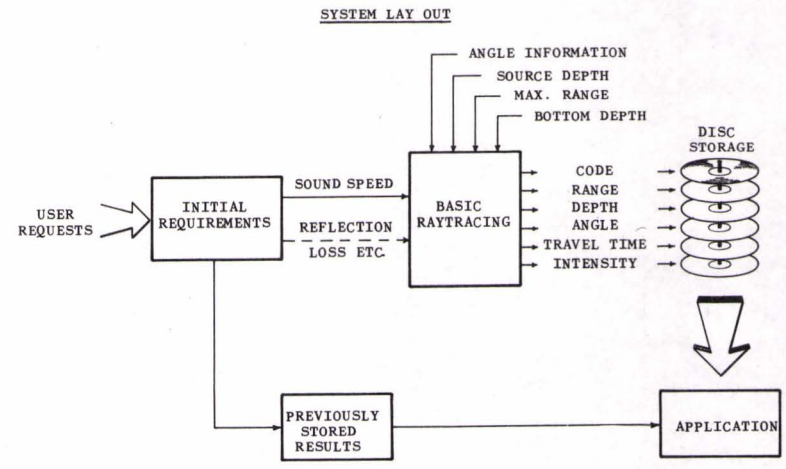

FIG. 3

RAYTRACING

INITIAL QUESTIONS TO DETERMINE INPUT AND OUTPUT REQUIREMENTS
IN ALL THE FOLLOWING QUESTIONS TYPE Ø‹=NO› OR 1‹=YES› CR.LF
IS A SOUND SPEED PROFILE TO BE INPUT? 1
IS A RAY DIAGRAM TO BE PLOTTED? 1
ARE ANY SPECIAL PLOTS REQUIRED? Ø
IS PRINT OUT ON LINE PRINTER REQUIRED? 1
ARE RESULTS TO BE STORED ON MAG. TAPE? Ø

FIG. 4

INITIAL PARAMETERS FOR
RAYTRACING CALCULATIONS

MAKE SURE SOUND SPEED OR TEMPERATURE/SALINITY PROFILE IS IN PHOTOREADER
PROBLEM NUMBER ‹MUST BE ›Ø› = 1
SOURCE DEPTH IN MTS.= 1Ø8
DEPTH OF BOTTOM IN MTS.= 15Ø
MAX. RANGE IN MTS.= 25ØØ
INITIAL ANGLE FROM SOURCE IN DEGREES = -11
INCREMENT ANGLE IN DEGREES = 1
MAX. ANGLE FROM SOURCE IN DEGREES = Ø

RAY DIAGRAM (SOURCE AT 45 m; SURFACE AND BOTTOM REFLECTIONS SUPPRESSED)

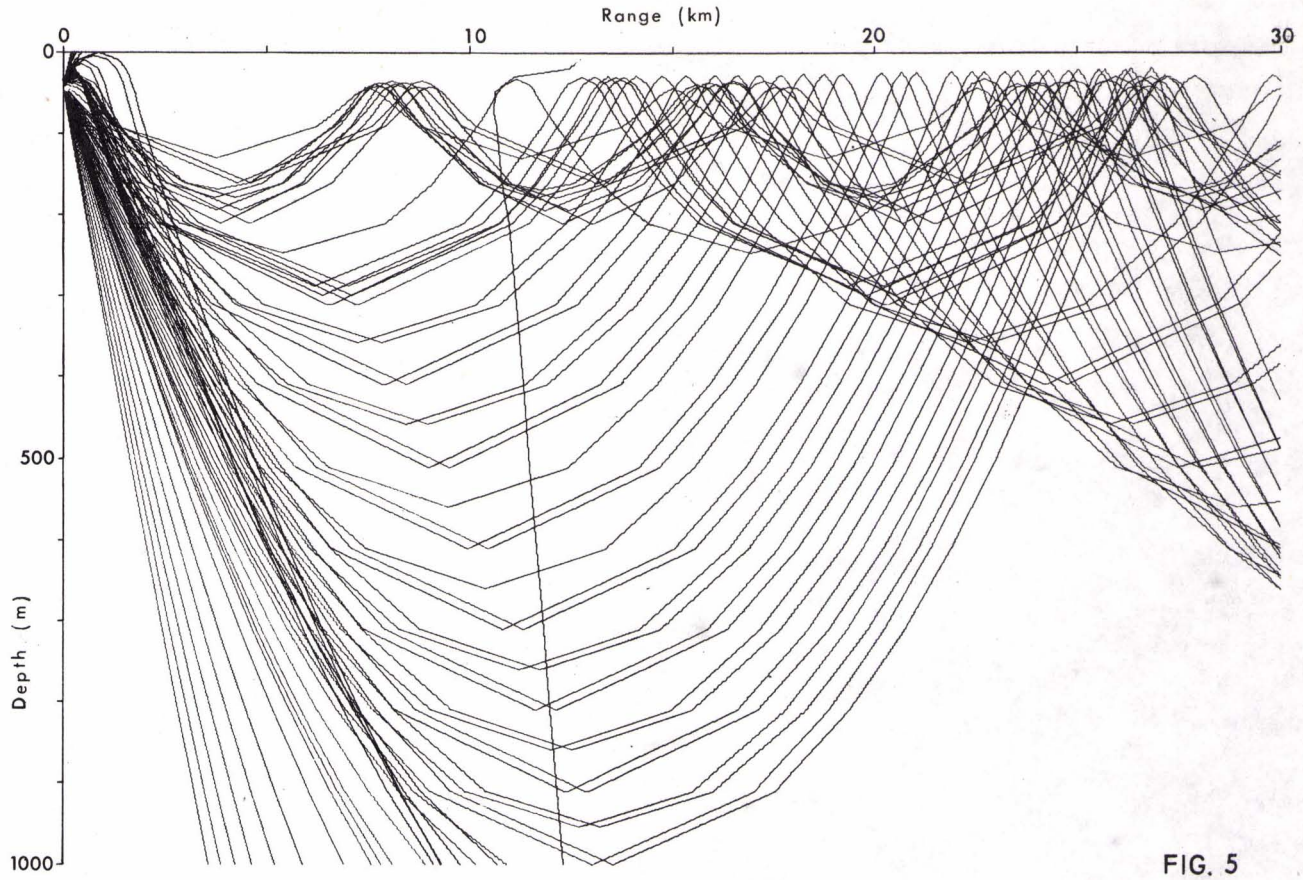

FIG. 5

ANGLE FROM SOURCE vs RANGE
LAYER DEPTH 310 m

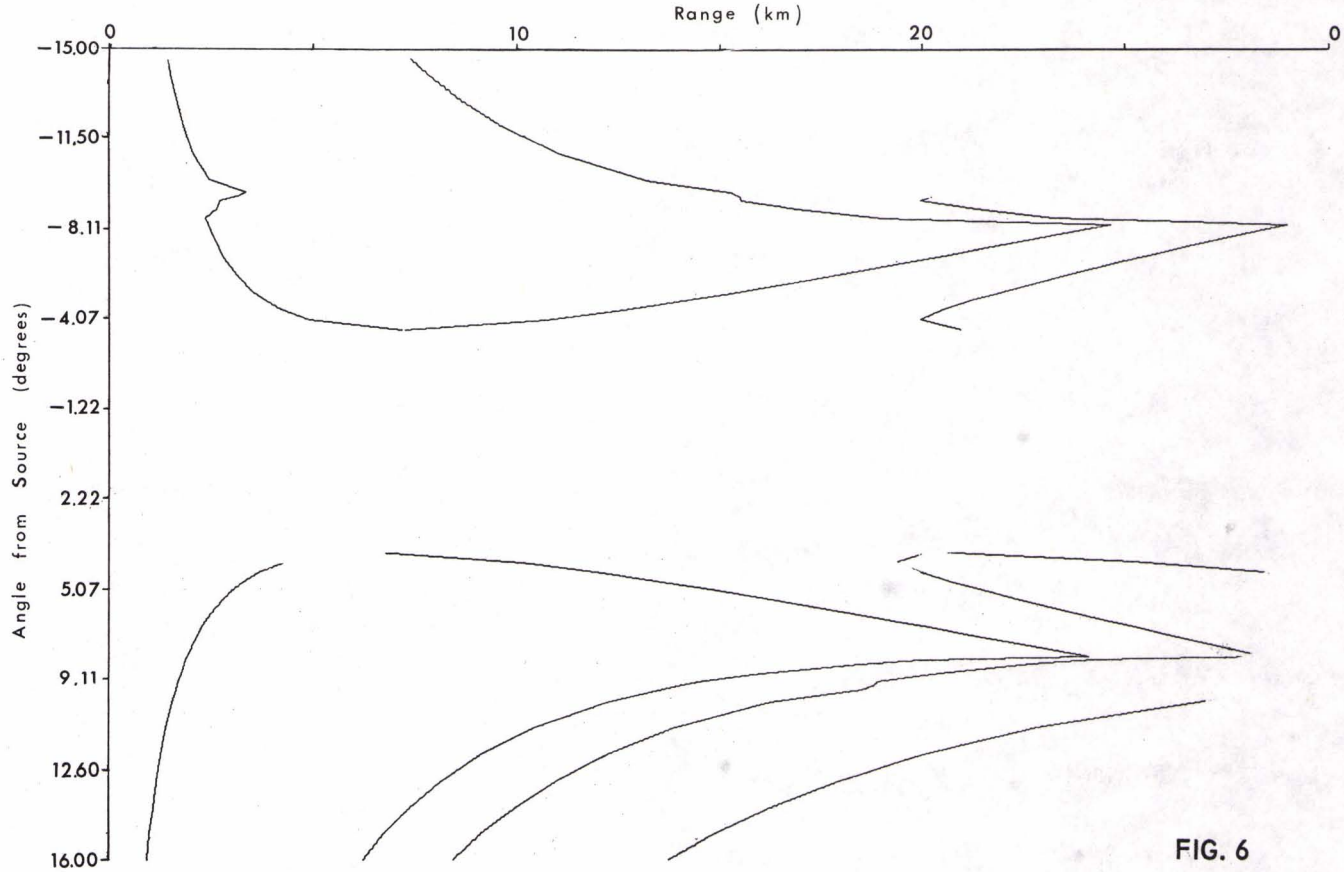

FIG. 6

EMERGENT ANGLE FROM LAYER vs RANGE

LAYER DEPTH 310 m

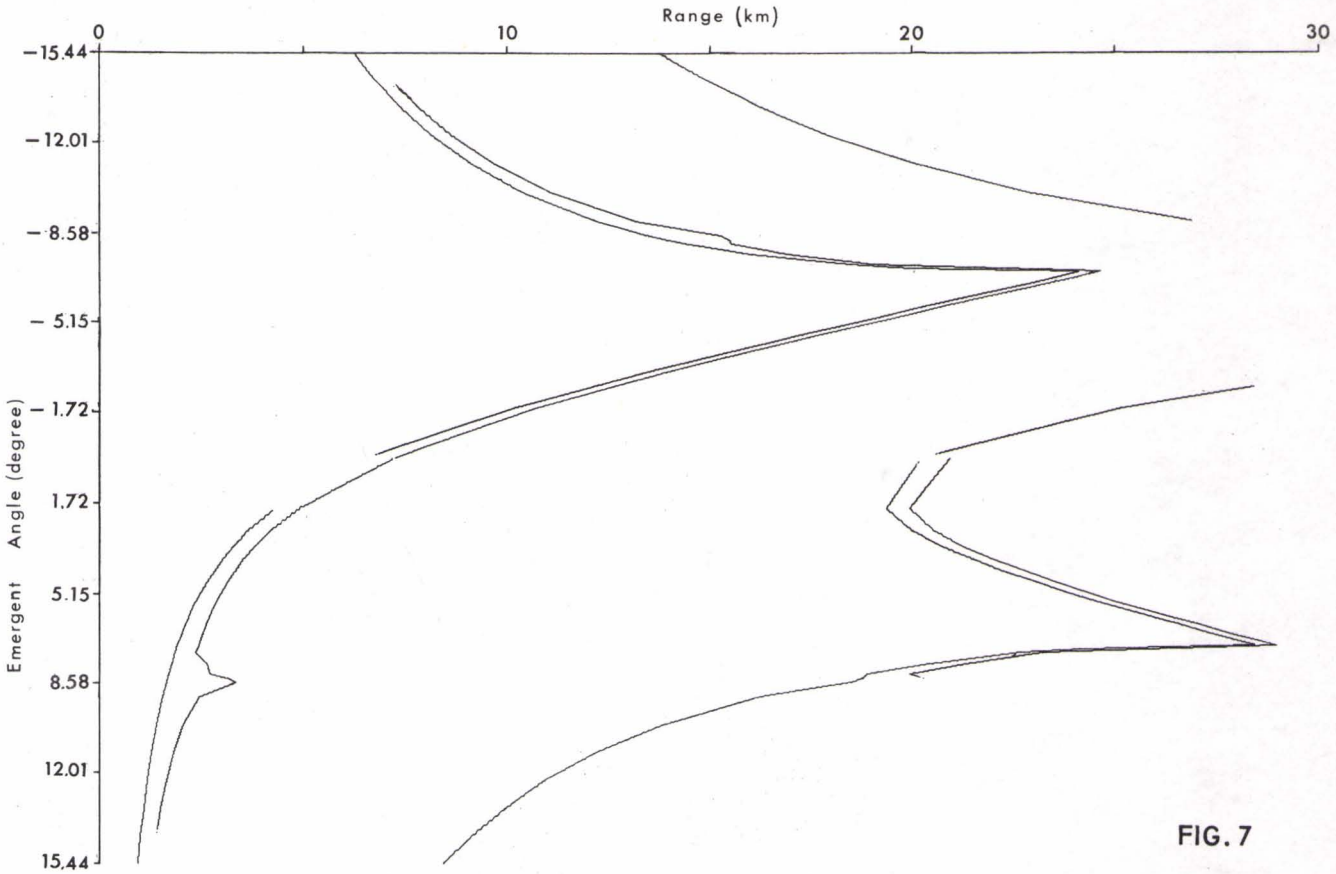

FIG. 7

TRAVEL TIME vs RANGE

LAYER DEPTH 310 m

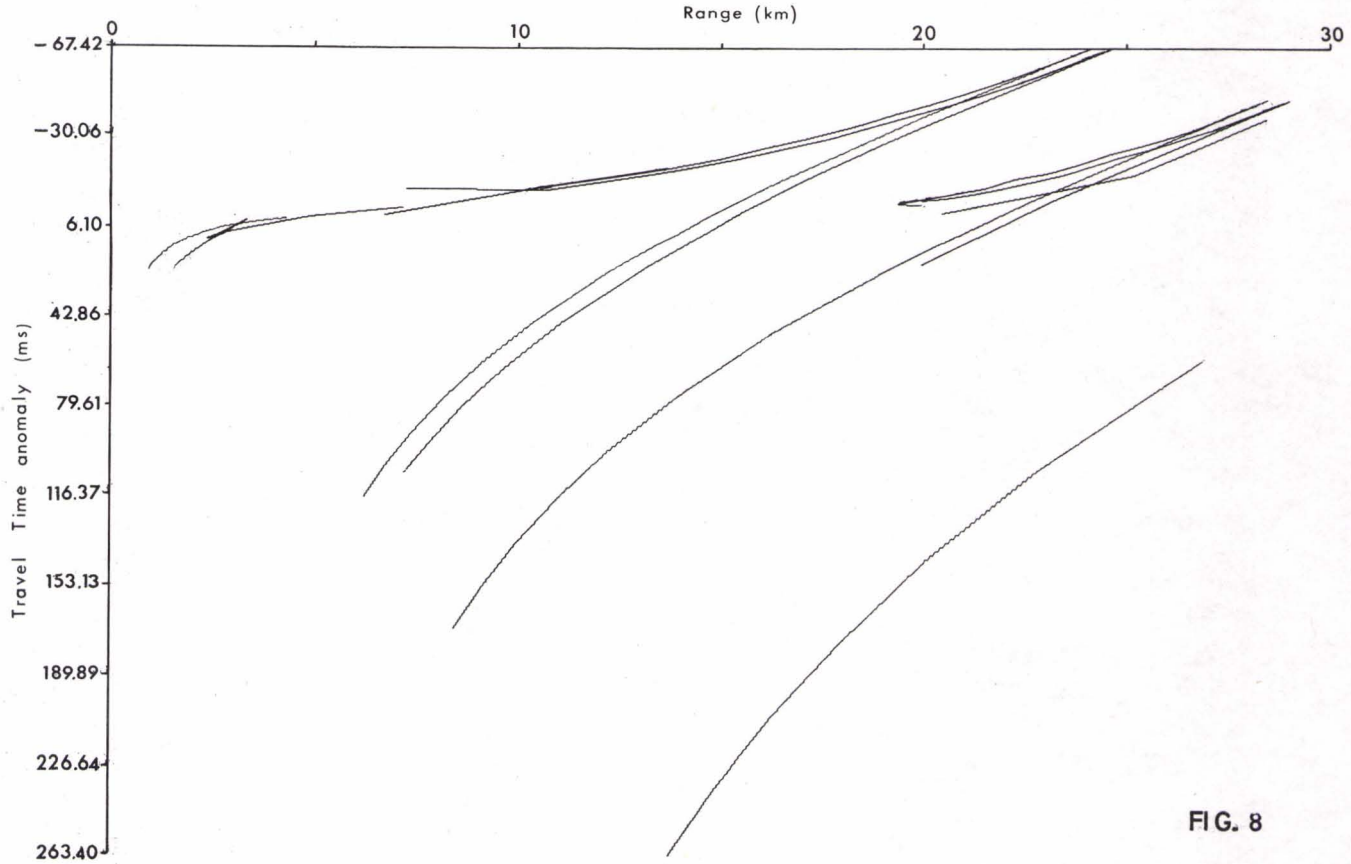

FIG. 8

COMMENTS ON THE RAY THEORY APPROXIMATION

by

B. Grandvaux
Laboratoire de Détection Sous-Marine
Le Brusc, France

The eikonal equation from which one deduces Fermat's principle, Snell's law ... is an approximation of the wave equation. For this approximation to be valid a condition arises which is:

$$\left|\frac{\Delta A}{k^2 A}\right| \ll 1 \qquad \text{[Eq. 1]}$$

with

$$\varphi = Ae^{is} \qquad \text{[Eq. 2]}$$

being a solution of the harmonic wave equation:

$$\Delta\varphi + k^2\varphi = 0 \ . \qquad \text{[Eq. 3]}$$

Let us consider a one-dimensional (z) problem to discuss the physical aspects of this condition and give some orders of magnitude. Noting by subscripts z and zz the first and second space derivatives, the condition becomes:

$$\left|\frac{3}{4}\, k^{-4}\, k_z^2 - \frac{1}{2}\, k^{-3}\, k_{zz}\right| \ll 1 \qquad \text{[Eq. 4]}$$

or

$$\left|\frac{1}{2\omega^2}\left(cc_{zz} - \frac{1}{2}\, c_z^2\right)\right| \ll 1 \qquad \text{[Eq. 5]}$$

conditions which can be satisfied in two different ways:

1) ω high, c_z and c_{zz} low

For instance, assuming that the maximum values of c_z and c_{zz} in the open ocean are respectively 2 m/s/m and 4 $m/s/m^2$, Eq. 5 is just satisfied when the frequency $f \geq 9$ Hz, within 10% when $f \geq 28$ Hz and within 1% when $f \geq 90$ Hz

2) c(z) solution of the differential equation:

$$cc_{zz} - \frac{1}{2} c_z^2 = 0 \qquad \text{[Eq. 6]}$$

that is

$$c(z) = (a + bz)^2 \qquad a \text{ and } b \text{ constants.} \qquad \text{[Eq. 7]}$$

When c(z) follows such a quadratic form, ray theory is valid whatever the frequency.

Looking at the case where the direction of propagation (vector $\vec{k}$) makes an angle θ with the direction of variation of c(z), Eq. 4 remains valid, k being replaced by

$$\gamma = k \cos \theta \ . \qquad \text{[Eq. 8]}$$

It is then evident that the condition is not satisfied when $\theta = \frac{\pi}{2}$ (turning point).

DISCUSSION

Subsequent discussion revolved around the inequalities developed by the author under which ray tracing theory could be shown to be valid.

METHODS USED IN FRANCE FOR THE CALCULATION OF SOUND FIELDS

by

E. Pichon
Laboratoire de Détection Sous-Marine
Le Brusc, France

METHOD OF CONSTANT GRADIENTS

The advantage of this very well-known method is its fast and simple implementation. It gives the possibility of numerous forms of presentation:

Tracing of the field, flat bottom [Fig. 1].

Tracing of the field, variable bottom [Fig. 2].

Curves made by horizontal sections and used to characterize the sound field.

(a) Angle at source (receiver) as a function of range [Fig. 3].

(b) Derivative of range with respect to angle of transmission as a function of range [Fig. 4].

(c) Travel time as a function of range [Fig. 5].

(d) Loss as a function of range [Fig. 6].

Enlarged tracing of a part of the field [Fig. 7].

Tracing of the field with graphic indication of loss [Fig. 8].

Contours of constant loss superposed on the ray tracing [Fig. 9].

Other possibilities exist.

The discontinuities introduced by the constant gradient approximation lead to large errors in the calculation of loss [Figs. 10 & 11].

There are two methods of smoothing intermediate initial angle vs range results which give the possibility of overcoming the difficulty:

(1) Smoothing by Tchebycheff polynomials [Figs. 12 & 13].

(2) Smoothing by splines [Figs. 14 & 15].

The realization and effect of these two methods are equivalent, with possibly an advantage for splines (better approximation of the initial angle vs range curve).

Implementation on a computer is being programmed.

METHOD OF VARIABLE PROFILE

This method consists in choosing a (cubic) interpolation function for each ray, refining the interpolation in the regions where the ray has a turning point. It is necessary to provide a complete tabulation of sound velocity and its first derivative.

The sound rays retain their usual symmetry but are deformed when passage to the cubic is made. The loss-range curve has very many oscillations due to the method itself since for each ray the interpolation and the degree of fit are different.

METHOD OF 3 RAYS

This method requires no search for layers with which to approximate the profile, globally or locally. The velocity depth profile is given numerically and one determines the depth as a function of range at all points of a ray by numerical integration of the equation

$$dz = dx \sqrt{\left(\frac{\gamma^2}{c^2} - 1\right)} .$$

To calculate the loss from geometrical spreading

$$D = - \frac{c(z)}{c_o} \frac{\partial z}{\partial \theta_o} x$$

one replaces the derivative $\partial z / \partial \theta_o$ by the difference approximation

$$\frac{\Delta z}{\Delta \theta_o} = \frac{z(\theta_o + \Delta\theta_o) - z(\theta_o - \Delta\theta_o)}{2\Delta\theta_o}$$

using calculation of z made for the two rays which are neighbours ($\pm \Delta\theta_o$) of the ray under consideration. This method is simple to implement but requires a computer with a rather large memory [Fig. 16].

DISCUSSION

It was suggested that interpolation techniques could yield eigenrays more readily than the use of very fine ray bundles. The author agreed, but thought troubles could then be encountered at caustics. There might also be difficulties with a discontinuous sloping bottom.

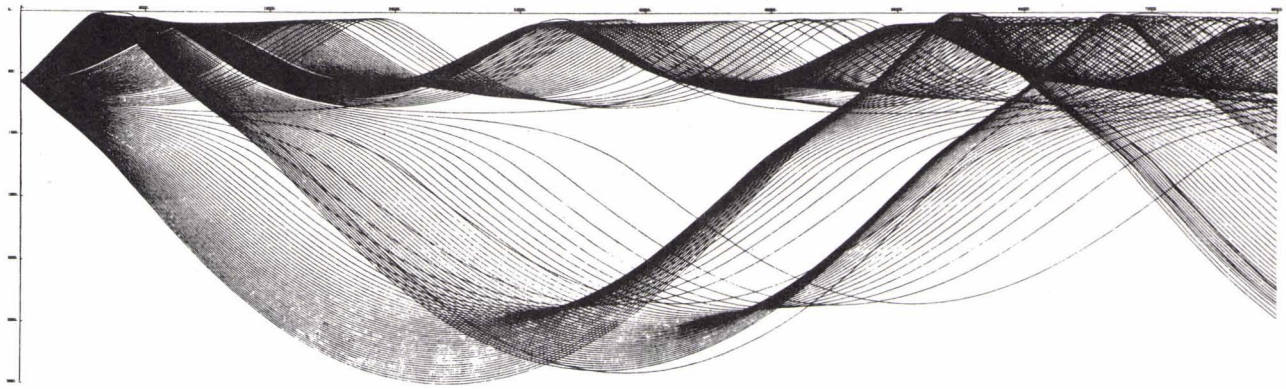

TRACE DE CHAMP SONORE

FIG. 1

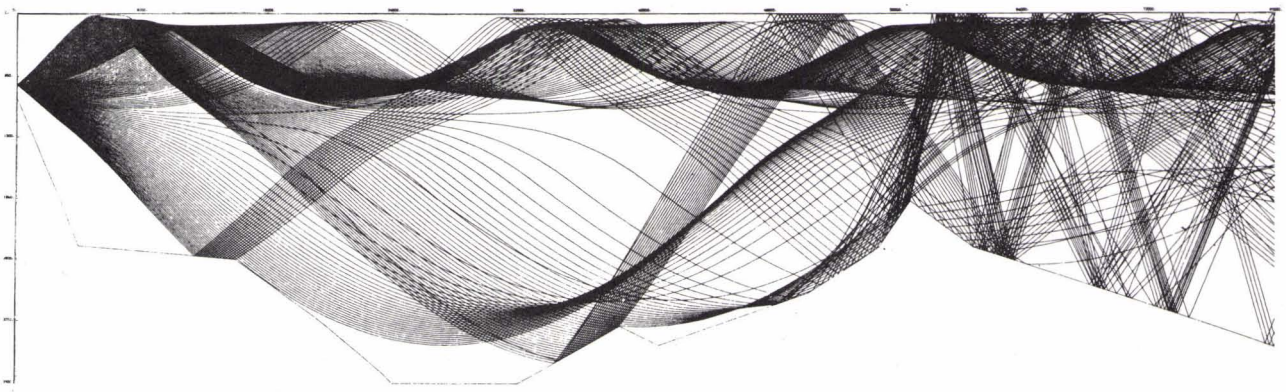

TRACE DE CHAMP SONORE A FOND VARIABLE

FIG. 2

FIG. 3

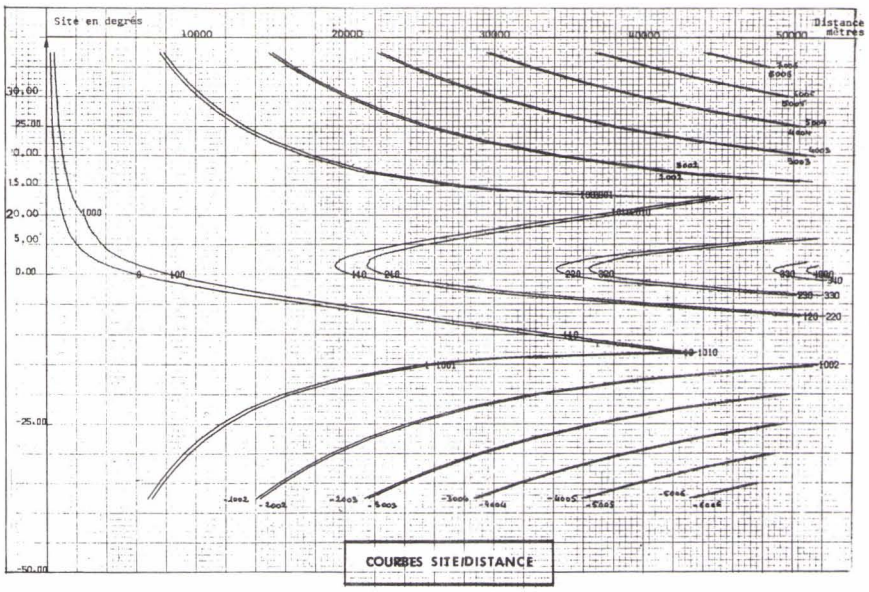

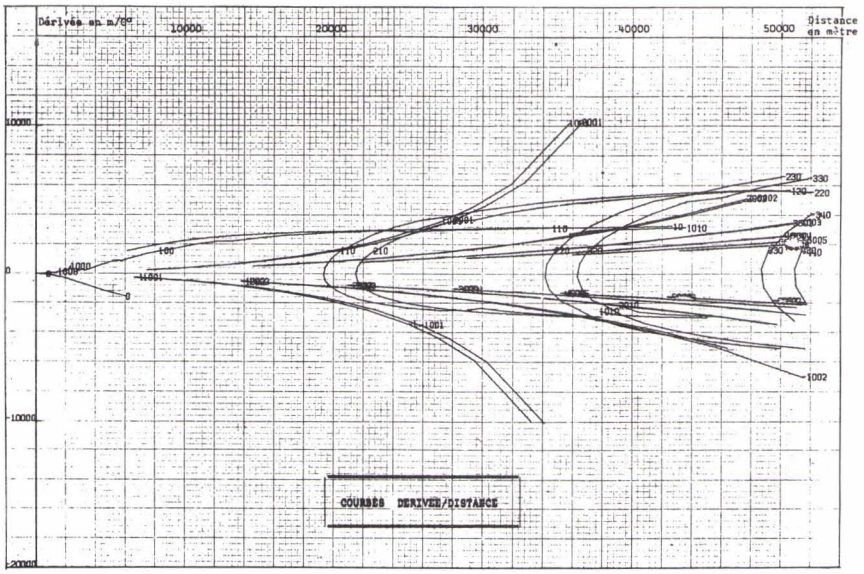

FIG. 4

FIG. 5

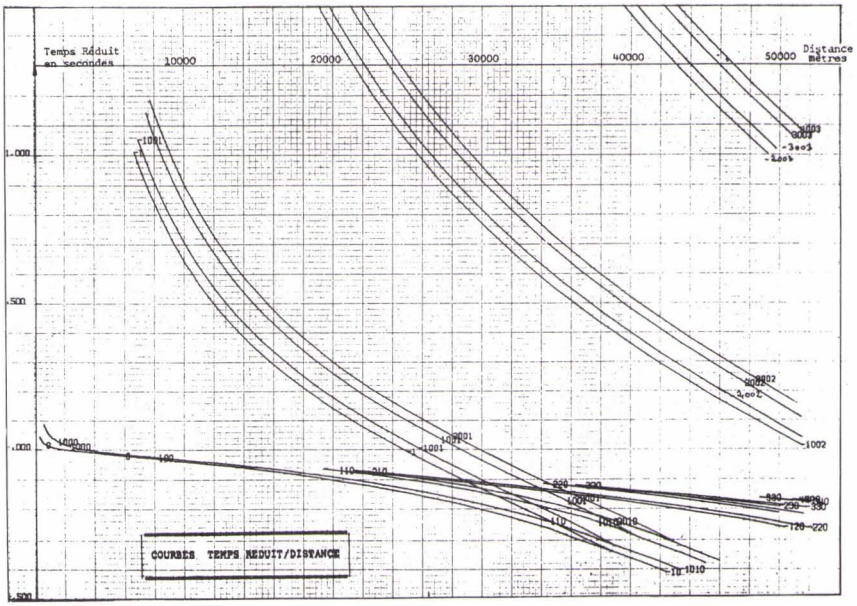

FIG. 6

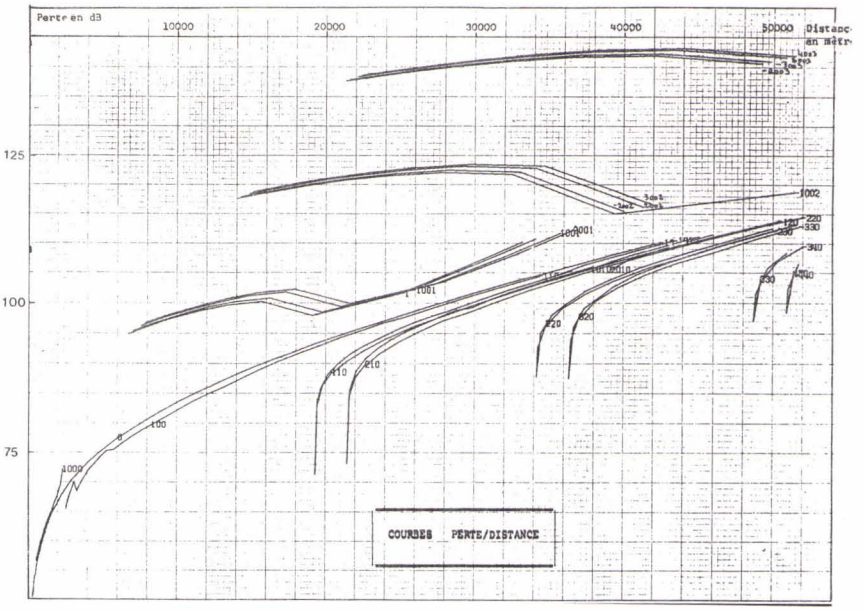

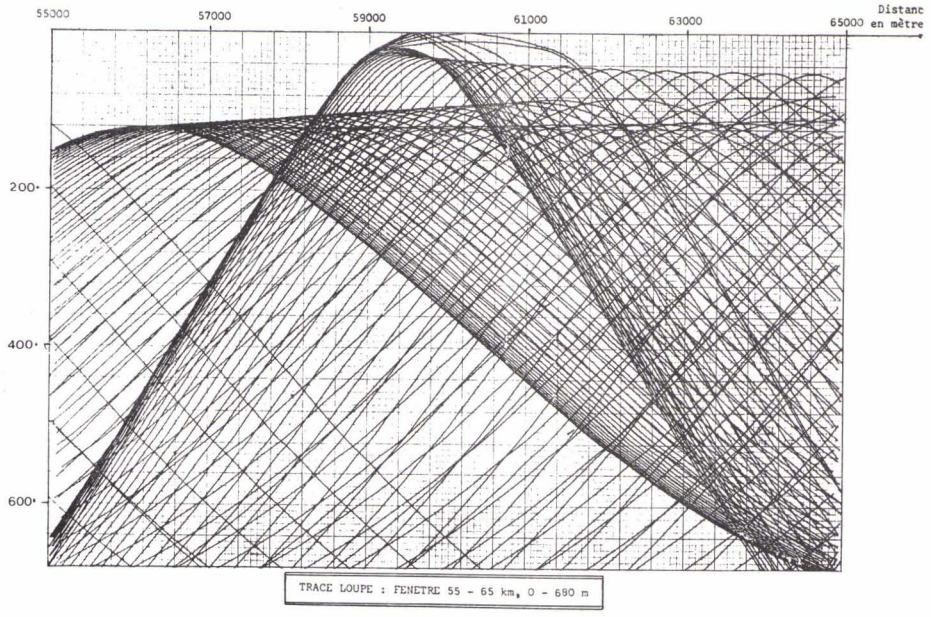

FIG. 7

FIG. 8

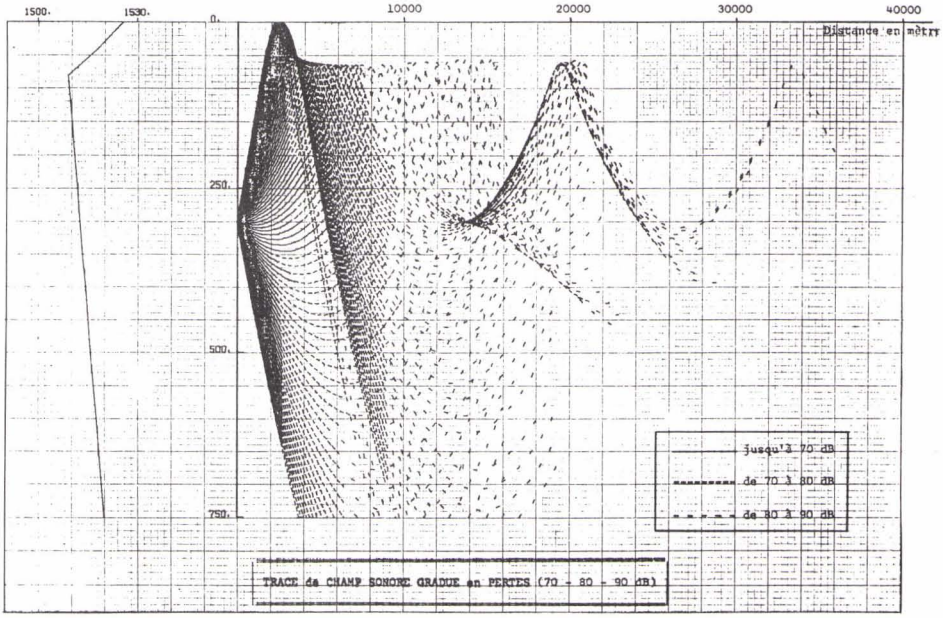

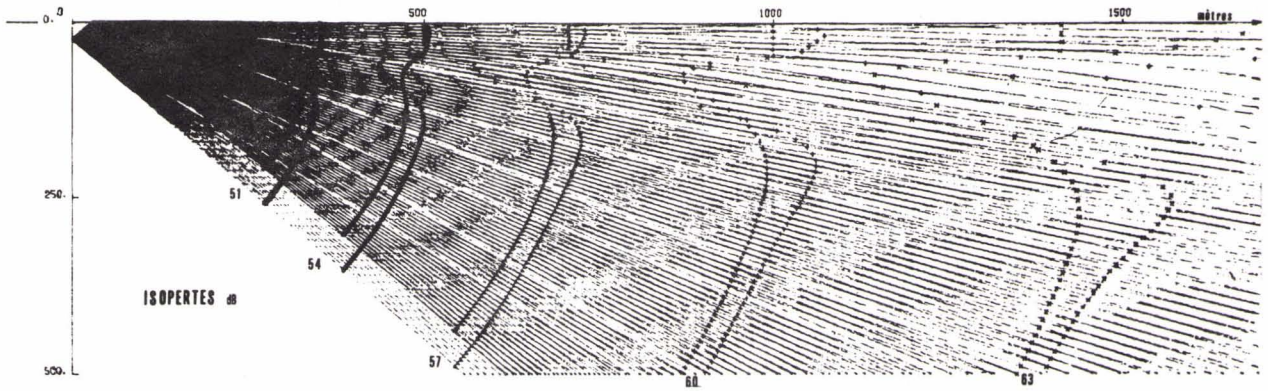

FIG. 9

FIG. 10

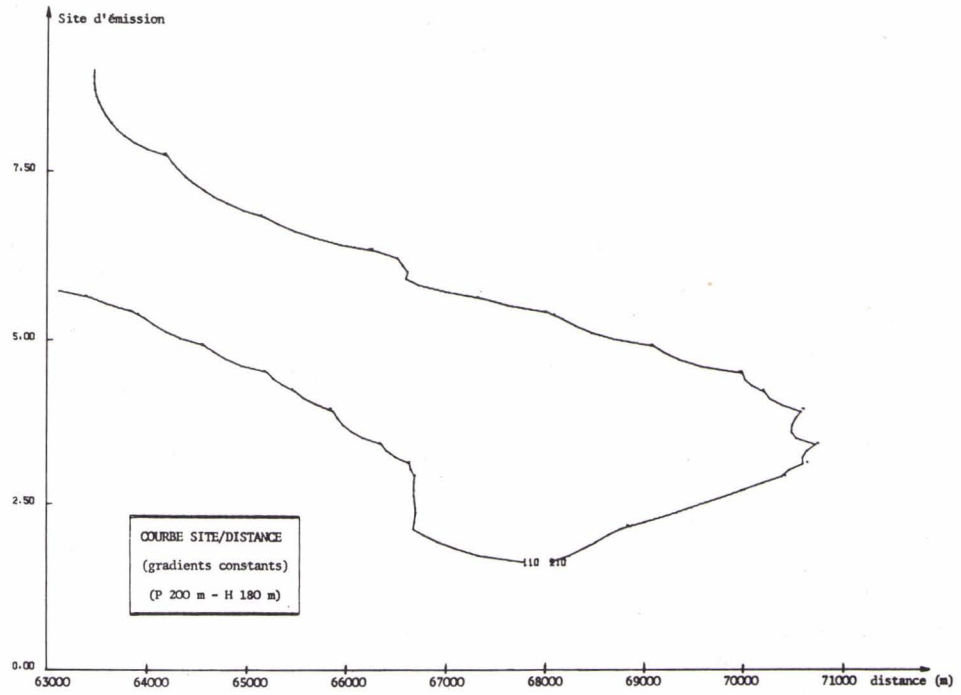

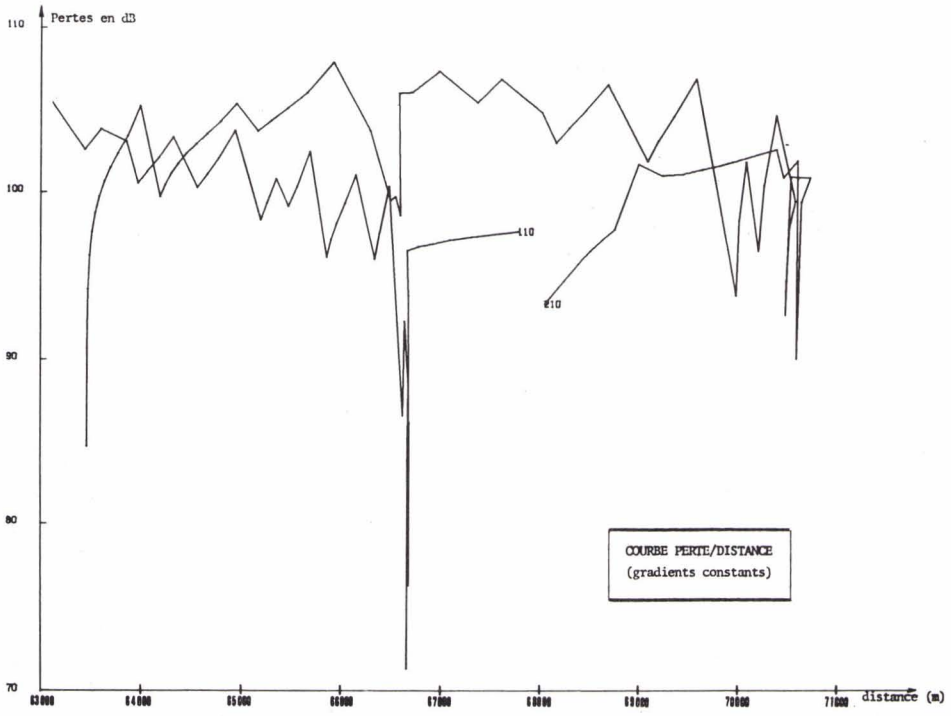

FIG. 11

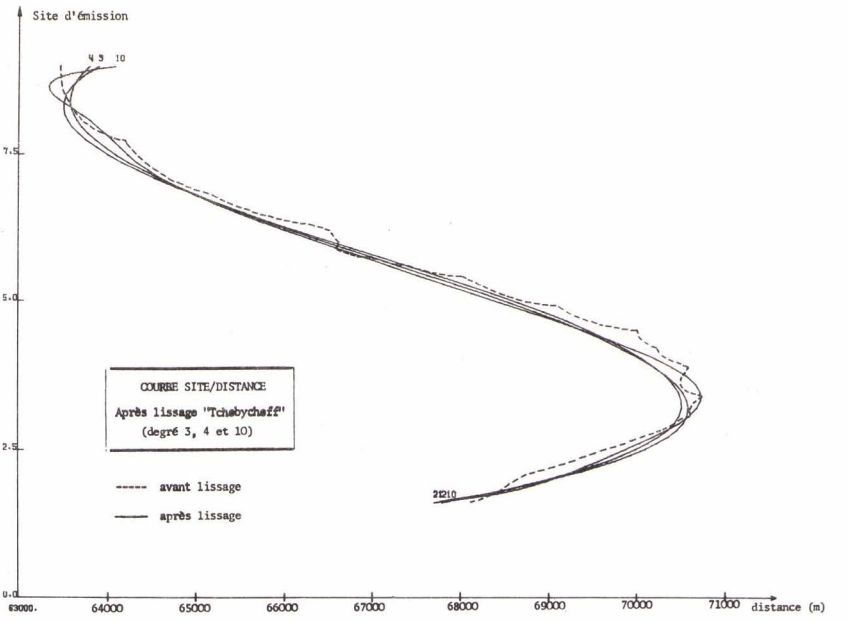

FIG. 12

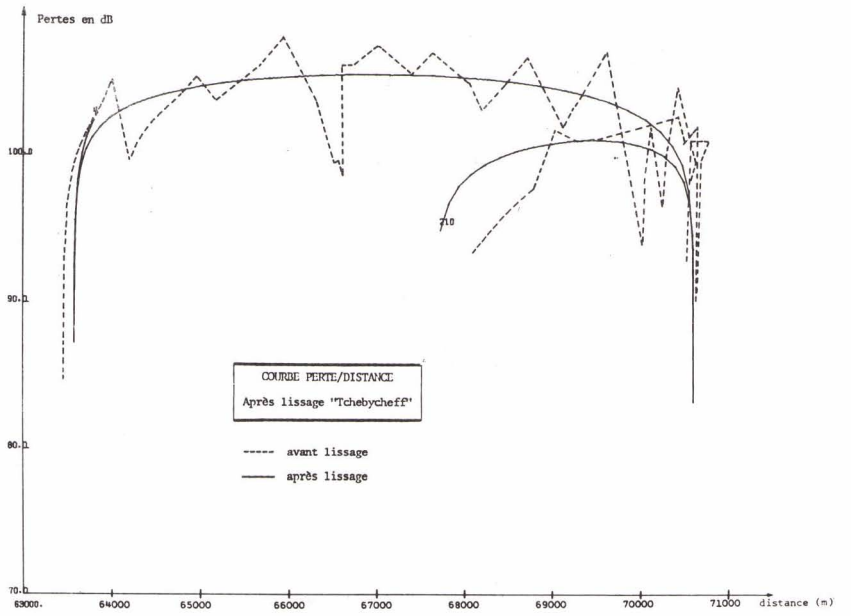

FIG. 13

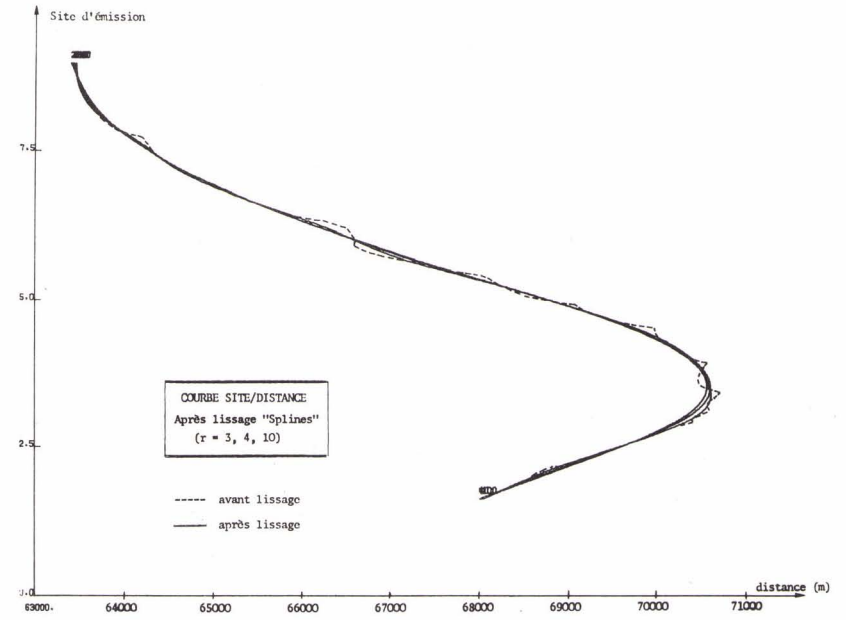

FIG. 14

A REVIEW OF SOME DEVELOPMENTS IN RAY TRACING AT THE NAVAL AIR DEVELOPMENT CENTER

by

C.L. Bartberger
Naval Air Development Center
Johnsville, Pa., U.S.

INTRODUCTION

The Naval Air Development Center has a comprehensive ray-tracing program which has been extensively used for a number of years not only by our own laboratory, but also by other naval activities and private contractors. In this paper I shall present a brief overall description of the program and shall then describe in somewhat more detail the so-called Target Ray Routine, which searches for and computes the various rays which propagate from a specified source location to a specified receiver location, and combines the rays to compute an effective resultant propagation loss. This will be followed by a few comparisons of ray theory with normal mode theory and with experimental data. The paper will conclude with a few remarks about a suggested technique for ray computation based on a more general type of velocity profile than is currently being used.

GENERAL DESCRIPTION

The NAVAIRDEVCEN ray-tracing program [Ref. 1] is based on a horizontally stratified ocean model consisting of a flat horizontal bottom and a single velocity profile. The velocity profile may be read into the program either as a table of sound speed versus depth

or temperature and salinity versus depth. In the latter case, the sound speed is computed from Wilson's equations [Ref. 2]. The data may be expressed in either English or metric units. Two options are available for curve-fitting, either straight lines or curvilinear segments [Fig. 1]. The straight-line fit, of course, is the old-fashioned method of constant gradients. Although the limitations of this approach are well known, it is still occasionally useful and has been retained as an option. The curvilinear segments are of the same form as those employed by Pedersen and Gordon [Ref. 3], in which the reciprocal of c^2 is quadratic in depth. The curve-fitting technique is completely automatic. It is basically similar to that of Gordon [Ref. 4], though it differs considerably in detail.

In addition to the profile layer depths, a set of special receiver depths may be read into the program, and a composite table of up to 100 depths and sound speeds is formed.

Each individual ray is specified by its source angle, from which the ray vertex velocity is computed. As a consequence of the assumption of horizontal stratification, the vertex velocity of each ray is constant, and the ray travels in a set of repetitive cycles between its upper and lower vertices. As a result, it is possible to pre-compute the increments of range, travel time, etc., in each layer. The tracing of the ray then consists simply of adding up the increments and computing the propagation loss as the ray proceeds outward in range.

The ray output data consist of the following: depth, range, ray angle, travel time, spreading loss, and propagation loss at up to six frequencies.

The actual tracing of rays is a relatively minor part of the NAVAIRDEVCEN ray-tracing program. The bulk of the program consists of four executive routines and their associated subroutines, which

contain the logic for determining what rays should be computed. The four executive routines are: (a) limiting rays, (b) ray families, (c) target rays (from source to specified receiver location, and (d) constant loss contours (used chiefly for multipath propagation loss versus range).

The first two routines are more or less straightforward items which, I suppose, are common to all ray-tracing programs. The limiting ray routine may be used to compute limiting rays to any desired local maximum of the velocity profile. It may also be used to compute families of rays in the vicinity of limiting rays. The only unusual feature of the ray family routine is the method of specifying the ray source angles. The data input format is extremely flexible, allowing any desired combination of individual rays and incremental sets of rays to be specified.

The target ray routine is designed to provide complete detailed information regarding multipath propagation between a specified source and a specified receiver location. It contains a search and iteration procedure which computes the source angle of each ray. After all the target rays have been computed, it then combines the rays in three different ways to obtain a resultant effective propagation loss:

(a) Strongest ray only.

(b) Intensities added (random phase).

(c) Amplitudes added (including phase interference computed from ray travel times).

The first is not really a combination, but merely gives the loss corresponding to the single strongest ray. The second method of combination consists of adding ray intensities, assuming random phase. The third method computes the relative phases, based on the ray travel times, and computes a loss based on pressure addition, phase included.

The constant loss contour routine has turned out in practice to be a misnomer since the contour portion of it is seldom used. This routine is a sort of "quick and dirty" target ray routine, designed to handle thousands of receiver locations instead of one. First of all, it computes a large family of rays and then interpolates between pairs of adjacent rays to determine the ray intensities at each of the specified receiver locations. It then adds the intensities of all the rays which reach each receiver location and computes the resultant propagation loss. The user has also the option of selecting the strongest ray only, but the pressure addition option is not available in this routine.

An optional second stage of this routine provides for a second interpolation to compute the ranges at each receiver depth at which the propagation loss is equal to a set of specified contour values, thus providing data for drawing contours of constant propagation loss.

We also have a modified version of the constant loss contour routine in which the printer prints a symbol at each point in a grid of 200 ranges and 40 depths. A different symbol is used for each 3 dB interval of propagation loss from 59 dB to 110 dB. After the array has been printed, it is a simple matter to draw contour lines manually.

TARGET RAYS

After this rather sketchy description of the program, I should like now to discuss the target ray procedure in somewhat more detail. The basic problem here is to find the source angles of the rays which propagate from a given source location to a given receiver location.

A simple graphical solution to the problem may be obtained by computing a large number of rays and plotting the ranges at the target

depth against the ray source angles. Consider the sample velocity profile shown in Fig. 2. Let the source be at the depth S within the deep sound channel, and let the target be at the depth T, slightly above the source. Before proceeding to the graph of range versus source angle, let us note some of the salient features of the propagation in this example. First, there will be a sector of rays, with source angles near the horizontal, which are trapped in the deep sound channel and do not reach the target depth. Secondly, as the source angle increases, both above and below the horizontal, there will be sectors of rays which penetrate above the target depth, but remain within the channel. These sectors are bounded by the limiting ray to the bottom of the surface duct. Thirdly, as the source angle increases further, there will be rays which reach the surface but are refracted before reaching the bottom. These rays represent RSR propagation. Finally, beyond the limiting ray to the bottom, and extending to $\pm 90^{\circ}$, there are the outermost sectors containing the rays which strike both the surface and the bottom.

If we now trace a large number of rays and plot the range at the target depth as a function of ray source angle, we get the rather strange-looking family of curves shown in Fig. 3. The different curves of the family correspond to successive crossings of the target depth as the rays move outward in range. Thus, each curve can be identified by the number of vertices through which the rays have passed. The innermost vertical dashed lines represent the rays tangent to the target depth. The central sector between these lines is a blank sector. It contains no rays which reach the target. Proceeding outward, the next pair of vertical lines, one on either side, correspond to the limiting rays to the bottom of the surface duct, while the outermost vertical lines correspond to the limiting rays to the bottom of the ocean. These limiting rays divide the angular region into sectors within which the various types of propagation occur — SOFAR channel, RSR, and bottom-surface bounce.

The graphical solution for a target at 50 kyd is indicated by the horizontal line drawn across the graph at that range. Each intersection of this line with one of the curves yields the source angle of a target ray.

The question now arises, how does one implement such a solution on a digital computer? Since an analytic solution is impossible, the most obvious approach is to use an iteration procedure, but there still remains the problem of making suitable initial estimates. This is where the concept of limiting rays and sectors is useful, since it is clearly not permissible to iterate across a sector boundary. Once the sectors have been defined, a search and iteration procedure is carried out separately in each sector.

Time will permit only a few brief comments about the procedures used in the program. First of all, we distinguish between the outer sector rays, i.e., those rays which bounce off both the surface and bottom, and the inner sector rays, i.e., those rays which experience refractive vertices, either upper or lower, or both.

As may be seen in Fig. 3, the range curves have no maxima or minima in the outer sectors. They are monotonic functions of the source angle. To see why, let us "unfold" the ocean, as indicated in Fig. 4. If we consider the extensions of two adjacent rays into the "unfolded" regions, as indicated by the dashed lines, we see that the rays continue to spread out and never cross one another. This behaviour permits an extremely simple search and iteration procedure. We start with a source angle slightly beyond the sector boundary and employ Newtonian iteration to find the first ray which reaches the target. We count the total number of vertices passed. To find the next ray, we use the preceding target ray as an initial estimate and iterate again, requiring this time that the ray pass through one more vertex. The process is continued in this manner until the desired number of outer sector rays have been found.

The problem of finding rays in the inner sectors is more complicated, and I must restrict the discussion to a brief statement of the basic concept. Each sector is divided into four equal intervals, and a separate search is conducted in each interval. The concept is illustrated in Fig. 5. Let θ_1 and θ_2 be the bounding source angles of the interval. As each of these rays is traced, the range is noted each time the ray crosses the target depth. Also, the number of ray vertices is counted. As soon as the target range has been exceeded, the number of vertices is recorded. Let the respective numbers be N_{V1} and N_{V2}. If N_{V1} and N_{V2} are the same, as indicated by the left-hand diagram, there is no target ray in the interval. If N_{V1} and N_{V2} differ by 1, as indicated in the centre diagram, there is one ray, and it is found by an iteration procedure based on interpolation. If N_{V1} and N_{V2} differ by more than 1, the interval is divided by 2 and the process is repeated.

The target ray routine in our ray-tracing program has proved very successful and has been used extensively in studying multipath propagation. Because of the accuracy with which travel times can be computed, it is particularly useful for investigating the effects of phase interference.

COMPARISON WITH NORMAL MODE THEORY

In presenting a few results obtained with our ray-tracing program, I shall concentrate on the phenomenon of phase interference. Consider first of all a comparison with normal mode theory. We have developed a number of normal mode programs, one of which is based on a three-layer model in which $1/c^2$ varies linearly with depth in each layer. With a three-layer model it is possible to approximate a typical deep-ocean velocity profile containing a surface duct. The upper graph of Fig. 6 is a plot of propagation loss versus range for a three-layer profile without a surface duct, i.e.,

the surface layer has a negative gradient. At the bottom of Fig. 6 is a comparison run made with the ray-tracing program, using the same bottom parameters and approximately the same velocity profile.

Except for the convergence zone, the agreement between the two curves is quite remarkable, even down to the short-period oscillations. The most puzzling feature, however, is the convergence zone. Although it is to be expected that the detailed structure of the zone as predicted by ray theory should be inaccurate, it is quite surprising to find that the entire outer portion of the ray theory zone is missing from the normal mode curve. Investigation of this problem has revealed that the entire outer portion of the zone predicted by ray theory is formed by a small bundle of rays leaving the source within $\pm 2^\circ$ of the horizontal. According to ray theory, the energy radiated into this small bundle should stay intact as the rays propagate and should become concentrated in a small region at the convergence zone. Apparently, however, diffraction effects are sufficiently important to cause the energy to spread out beyond the geometric confines of the ray bundle and to become widely diffused before it reaches the range of the convergence zone. It appears that one must be very cautious about using simple ray theory to make predictions of this sort.

The dashed curve in the lower figure shows the propagation loss computed on the basis of random-phase intensity addition.

COMPARISON WITH EXPERIMENT

It is commonly assumed that phase coherence is lost in bottom-bounce propagation in the deep ocean. However, this is not necessarily the case. The large fluctuations which are observed in propagation loss are evidence of phase interference effects, and in some instances these fluctuations show some correlation with ray-theory predictions. Figure 7 shows some results of an experiment conducted near the Bahamas a few years ago. Ten sonobuoys were dropped at various points

along a straight line, and a source ship, towing a CW projector, proceeded along the line. Values of propagation loss computed from the various hydrophone outputs were superimposed on the same range scale, resulting in the various "wiggly" segments shown in the figure. At any given range on the graph, the curves thus correspond to different ship locations for the different buoys. In spite of the spread of the results, it can be seen that certain distinct trends stand out. In particular, a large scallop may be seen, extending from 20 kyd to about 40 kyd. Beyond this is another broad scallop extending out to the convergence zone.

The heavy line on the graph shows the propagation loss predicted by the ray-tracing program, assuming phase coherence. Although there are slight discrepancies in the predicted ranges, the main features of the theoretical curve at ranges beyond 20 kyd are in sufficient agreement with the experimental data as to leave little doubt as to the existence of phase-coherent propagation. At ranges shorter than 20 kyd the scatter of the experimental data is too large to exhibit a consistent pattern. Also, at ranges beyond the first convergence zone the correlation between the experimental and theoretical propagation loss is poor, suggesting that phase coherence is lost after the second bounce.

A SUGGESTED RAY COMPUTATION PROCEDURE FOR GENERAL SOUND SPEED VERSUS DEPTH RELATION

The use of curvilinear segments permits the construction of a velocity profile curve in which the slope is everywhere continuous. This is obviously a great improvement over the use of straight line segments, where the discontinuities in slope at the layer boundaries give rise to false caustics and shadow zones. However, with the quadratic functions currently used in the ray-tracing program, it is impossible to avoid discontinuities in the second derivative at the points where adjacent segments are joined. Discontinuities in the second derivative, while not as serious as discontinuities in slope, are nevertheless capable of causing undesirable kinks in the curve of propagation loss versus range.

To treat the more general case in which functional forms are used which permit continuity of both first and second derivatives, consideration has been given to the use of numerical integration. The integrals involved in the computation of horizontal range, travel time, and spreading loss are:

Horizontal range

$$x = \sum \Delta x \qquad \Delta x = \int_{z_1}^{z_2} \frac{\cos\theta}{\sin\theta}\, dz$$

Travel time

$$t = \sum \Delta t \qquad \Delta t = \frac{1}{C_V} \int_{z_1}^{z_2} \frac{1}{\sin\theta \cos\theta}\, dz$$

Spreading loss

$$N_{spr} = 10 \lg \left| \frac{xu \sin\theta_o \sin\theta}{r_1^2 \cos^2\theta_o} \right|$$

$$u = \sum \Delta u \qquad \Delta u = \int_{z_1}^{z_2} \frac{\cos\theta}{\sin^3\theta}\, dz$$

where

z	=	depth
θ	=	$\theta(z)$ ray angle
θ_o	=	ray angle at source
C	=	$C(z)$ = sound speed
C_o	=	sound speed at source
C_V	=	$C_o/\cos\theta_o$ = vertex velocity
$\cos\theta$	=	C/C_V
r_1	=	1 yd

The spreading loss is usually expressed in terms of the range derivative $\partial x/\partial\theta_o$. If instead of this derivative, we use a related parameter u, as indicated above, the integrals for the increments Δx, Δt, and Δu in each layer all have a similar form.

In general, numerical integration appears to be an attractive method of evaluating these integrals. There is a problem, however, at a refractive vertex, where the ray becomes horizontal and hence the ray angle θ is zero. At such a point the integrands of both Δx and Δt blow up (although the integrals are finite), and the Δu integral itself blows up.

Let us now transform the integrals by expressing $1/C^2$ as a function $P(z)$, which might logically, though not necessarily, be chosen to be a polynomial in z. With this transformation, the integrals appear as follows. Let

$$P(z) = 1/C^2$$
$$P_V = 1/C_V^2$$
$$Q = P - P_V$$

then

$$\Delta x = \sqrt{P_V} \int_{z_1}^{z_2} \frac{dz}{\sqrt{Q}}$$

$$C_V \Delta t = \sqrt{P_V}\ \Delta x + \int_{z_1}^{z_2} \sqrt{Q}\ dz$$

$$\Delta u = \Delta x + P_V^{3/2} \int_{z_1}^{z_2} \frac{dz}{Q^{3/2}} \quad .$$

Note: At a refractive vertex,

$$C = C_V$$
$$P = P_V$$
$$Q = 0$$

The limits of integration z_1 and z_2 are the depths of the upper and lower boundaries of the layer. The travel time Δt is now well behaved, but problems still remain in Δx and Δu, since the function Q goes to zero at a refractive vertex.

The problem can be circumvented by removing Q from the denominator through integration by parts, once for Δx and twice for Δu. Let

$$P' = \frac{dP}{dz} = \frac{dQ}{dz} \quad \text{so that} \quad dz = \frac{dQ}{P'}$$

$$\Delta x = \sqrt{P_V} \int_{z_1}^{z_2} \frac{dQ}{P'\sqrt{Q}}$$

$$= 2\sqrt{P_V} \left[-\frac{\sqrt{Q}}{P'} \Bigg|_{z_1}^{z_2} + \int_{z_1}^{z_2} \frac{P''\sqrt{Q}}{P'^2} \right]$$

$$\Delta u = \Delta x + P_V^{3/2} \int_{z_1}^{z_2} \frac{dQ}{P'Q^{3/2}}$$

$$= \Delta x - 2P_V^{3/2} \left[\left(\frac{1}{P'\sqrt{Q}} + \frac{2P''\sqrt{Q}}{P'^3} \right) \Bigg|_{z_3}^{z_2} + 2 \int_{z_1}^{z_2} \left(\frac{3P''^2}{P'^4} - \frac{P'''}{P'^3} \right) \sqrt{Q}\, dz \right]$$

(Note: when $Q = 0$ omit term $\frac{1}{P'\sqrt{Q}}$).

Except for the term $1/P'\sqrt{Q}$ in the formula for Δu, the only function appearing in the denominators is the derivative P'. This function is zero only at a local extremum (i.e., maximum or minimum) of the velocity profile. Hence these formulae can be used for any profile segment which does not contain an extremum. In the special case where a vertex occurs within a segment containing an extremum, it is a simple matter to divide the segment into two parts, using the basic formulae in one part and the transformed formulae in the other.

A final comment is in order regarding the term $1/P'\sqrt{Q}$, which becomes infinite at the vertex. This is a problem which is common

to all spreading loss computations based on the range derivative. The value of u is infinite at a refractive vertex, and the spreading loss there must be computed by a special formula which does not involve u. However, values of u are required at points beyond the vertex. It will be noted that in passing through the vertex, the infinite term occurs twice — once in the interval immediately preceding the vertex, and again in the interval immediately following. It can be shown that the correct answer is obtained simply by ignoring this term altogether.

A small computer program was written to check out this approach. Two simplified types of curve-fitting were included, one based on segments in which $P(z)$ is quadratic in z, as in the NAVAIRDEVCEN ray-tracing program, and the other based on a spline fit of segments in which $P(z)$ is a cubic. Figure 8 shows a sample velocity profile consisting of four quadratic segments. At the right of the figure is an expanded-scale plot of the difference between the quadratic fit and the spline fit. Except for the first 100 ft at the top, which will not concern us, the profiles differ by less than 0.2 ft/s.

A source was placed near the bottom at a depth of 1170 ft, and a family of rays were traced up over the first vertex and down again until they reached the source depth. The effects of the discontinuities in the second derivative may be expected to show up in those rays which vertex in the vicinity of the layer boundaries A, B and C.

In Fig. 9 the spreading loss is plotted as a function of ray source angle for both the quadratic fit and the spline fit. The source angle scale has been chosen to show the effects of the two layer boundaries A and B. (The effect of boundary C would be off-scale at the right.) The effects of the discontinuities are indicated by the kinks in the solid curve at the points A and B. The spike immediately beyond A represents a focal point resulting from the nature of the velocity profile.

The spline fit is represented by the dashed curve, which does not exhibit the discontinuities in slope. The oscillatory nature of this curve to the left of the focal point is a result of the rather simple-minded technique of forcing the spline curve to pass rigorously through all the data points. With a little more care, it would be possible to obtain better results.

Figure 10 shows another sample velocity profile consisting of three layers and exhibiting a reverse curvature. The difference between the spline and quadratic fits is shown at the right. The accompanying plot of spreading loss versus source angle is shown in Fig. 11, where, as before, kinks occur in the quadratic-fit curve in the vicinity of the layer boundaries A and B.

In making these runs, it has been found that the special formulae based on integration by parts should be used not only in intervals where a refractive vertex actually occurs, but also where a vertex is merely approached, that is, where the ray angle approaches within a degree or so of the horizontal. The transformed integrals have proven to be exceedingly well behaved in all examples investigated.

It is doubtful whether the errors arising from discontinuities in the second derivative of the profile curve are serious enough to warrant the inclusion of this approach into general ray-tracing programs. However, if special situations arise in which continuity of the second derivative is important, the technique suggested above appears to be quite appropriate. Furthermore, because virtually no restrictions are placed on the mathematical form of the fitting function, it should be possible to fit most velocity profiles with a relatively small number of segments.

REFERENCES

1. C.L. Bartberger and T.L. Stover, "The NADC Ray-Tracing Program", Report No. NADC-SD-6833, 4 November 1968.

2. W.D. Wilson, "Equation for the Speed of Sound in Sea Water", J. Acoust. Soc. Am., Vol. 32, p. 1357, October 1960.

3. M.A. Pedersen, D.F. Gordon and Alice Joy Keith, "A New Ray Intensity Procedure for Underwater Sound Based on a Profile Consisting of Curvilinear Segments (U)", Navy Electronics Laboratory (Naval Undersea Research and Development Center) Report No. 1105, 30 March 1962, CONFIDENTIAL.

4. D.F. Gordon, "Extensions of the Ray Intensity Procedure for Underwater Sound Based on a Profile Consisting of Curvilinear Segments (U)", Navy Electronics Laboratory (Naval Undersea Research and Development Center) Report No. 1217, 3 April 1964, CONFIDENTIAL.

DISCUSSION

In reply to queries, Bartberger confirmed that only one ray was used for intensity calculations.

When comparing results between ray theory and normal mode calculations, a profile with C^{-2} linear in depth was assumed for the latter. This was approximated for the ray tracing by closely spaced segments in which C^{-2} was quadratic in depth.

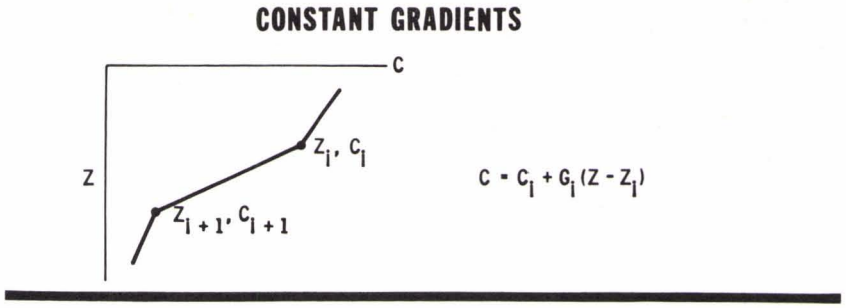

FIG. 1

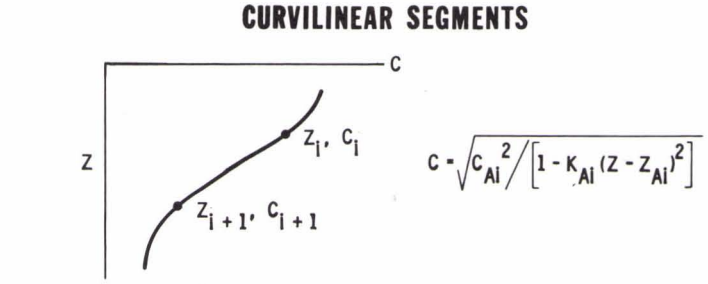

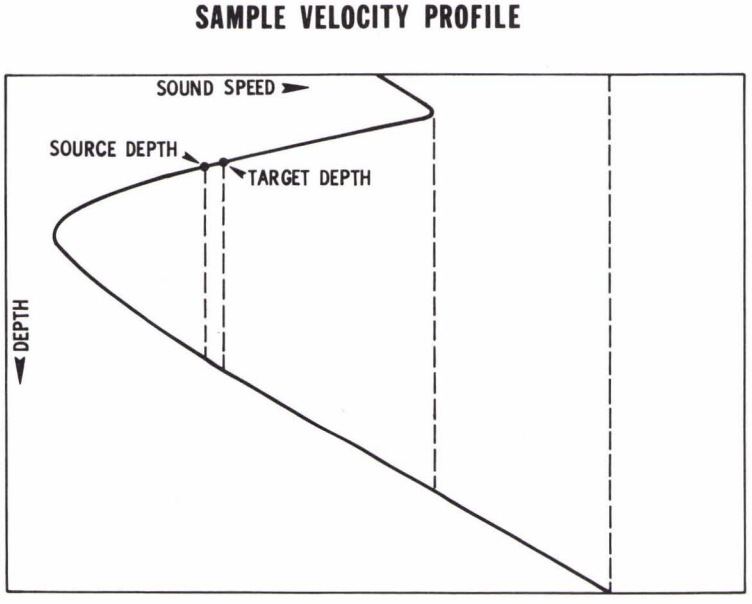

FIG. 2

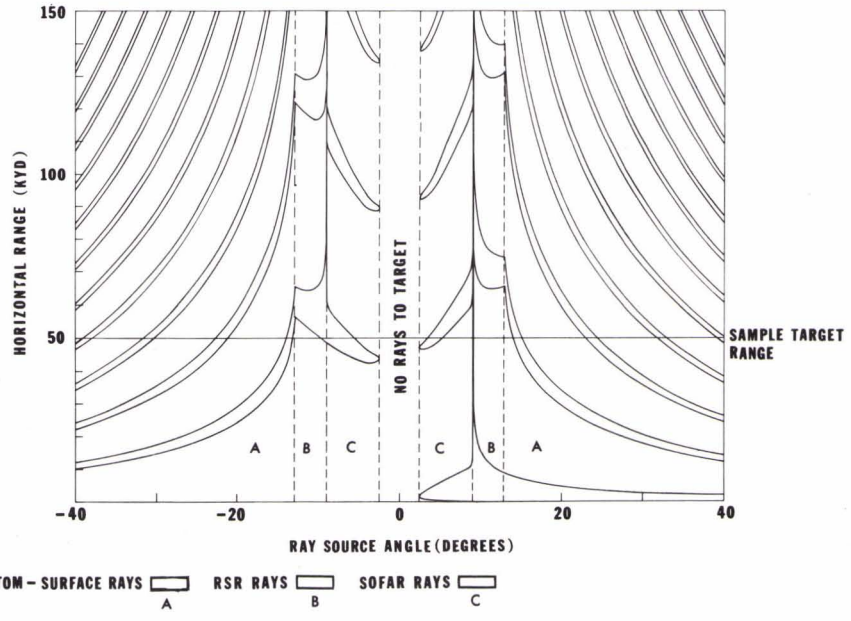

FIG. 3

BEHAVIOR OF OUTER SECTOR RAYS

(WHEN "UNFOLDED," THEY NEVER CROSS EACH OTHER)

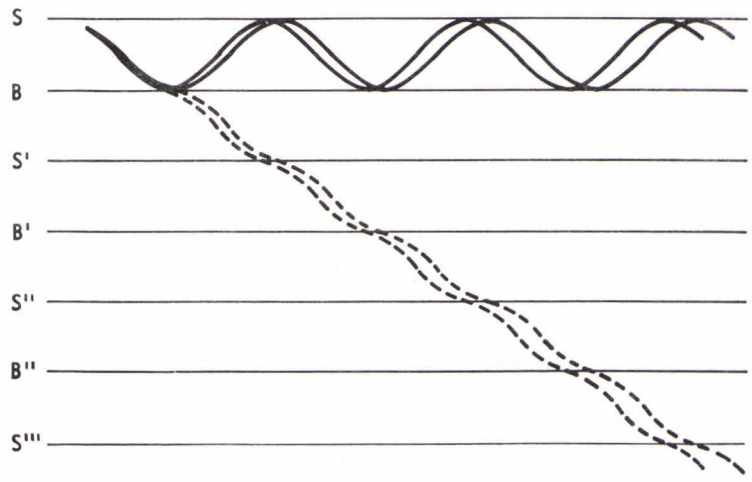

FIG. 4

INNER SECTOR TEST FOR TARGET RAYS

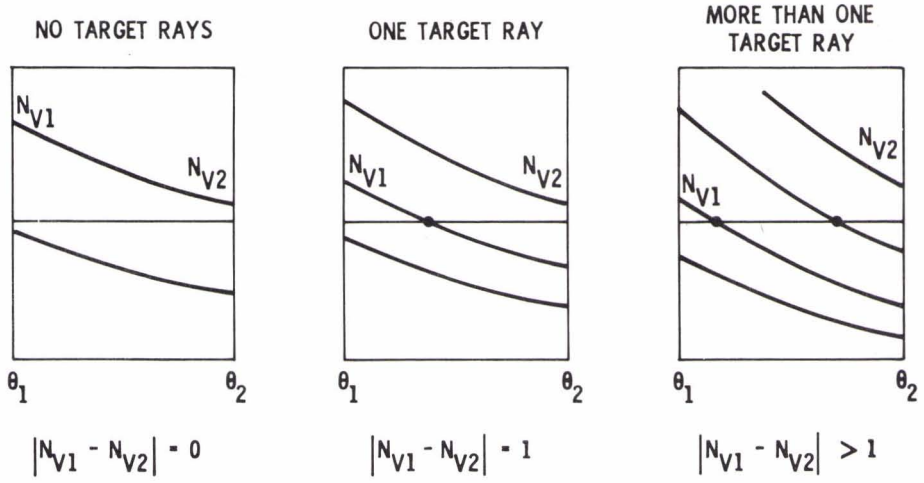

FIG. 5

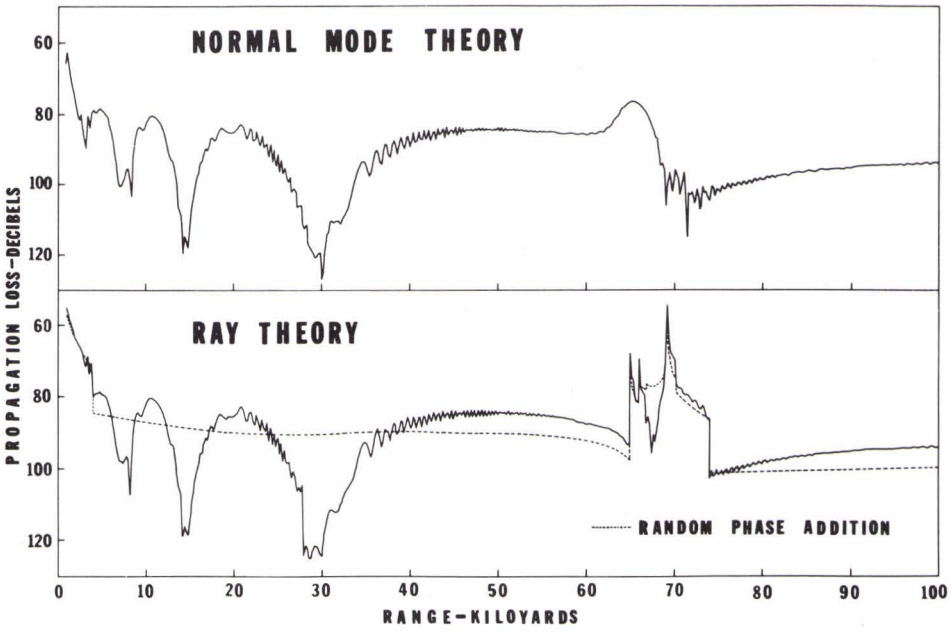

FIG. 6

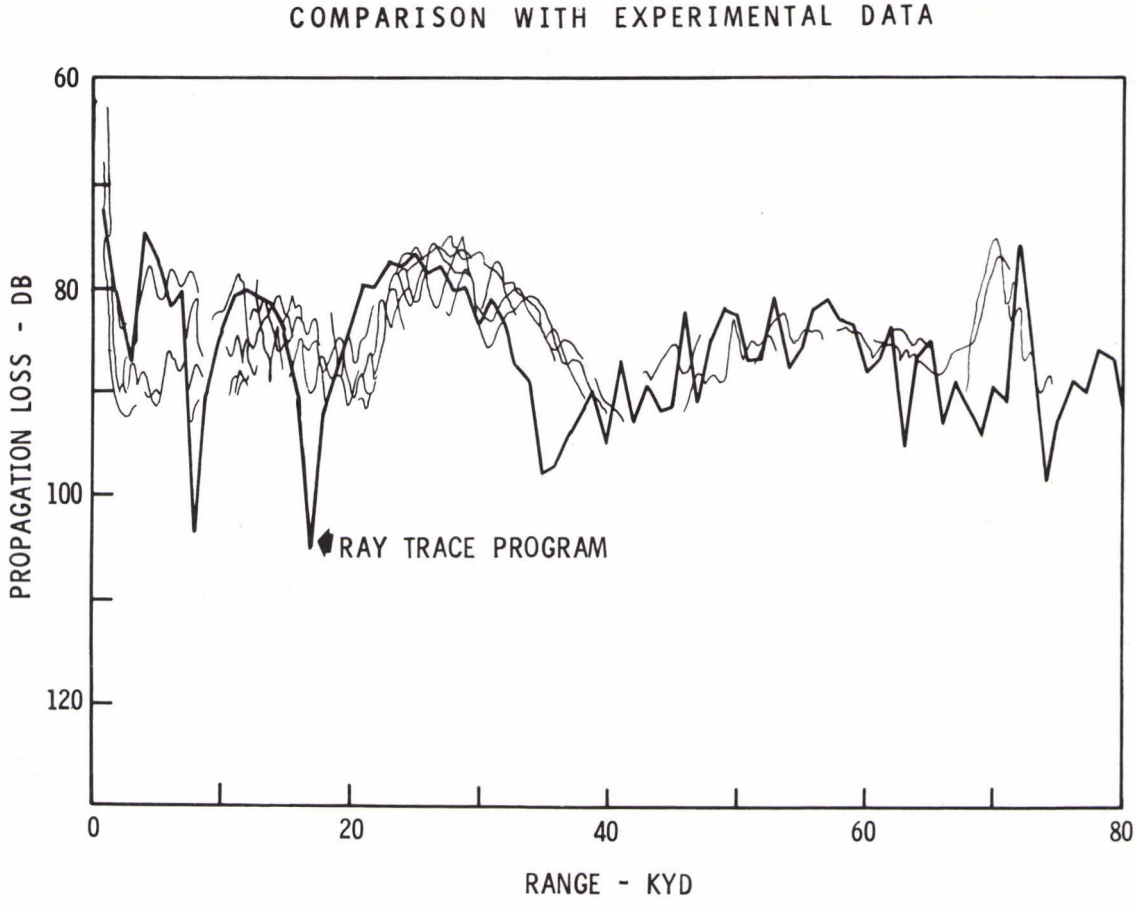
COMPARISON WITH EXPERIMENTAL DATA
PROPAGATION LOSS - DB
60
80
100
120
RAY TRACE PROGRAM
0
20
40
60
80
RANGE - KYD

FIG. 7

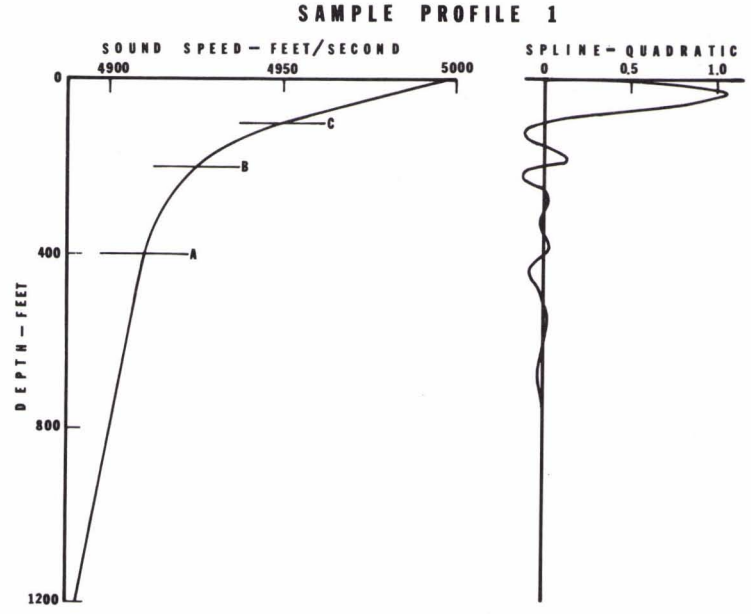
SAMPLE PROFILE 1
SOUND SPEED - FEET/SECOND
4900
4950
5000
SPLINE - QUADRATIC
0
0.5
1.0
0
400
800
1200
DEPTH - FEET
A
B
C

FIG. 8

SAMPLE PROFILE 1

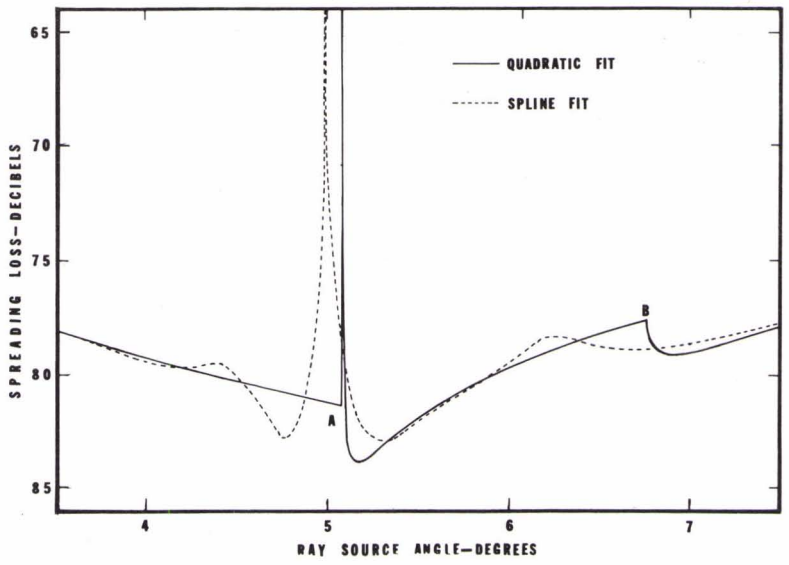

FIG. 9

SAMPLE PROFILE 2

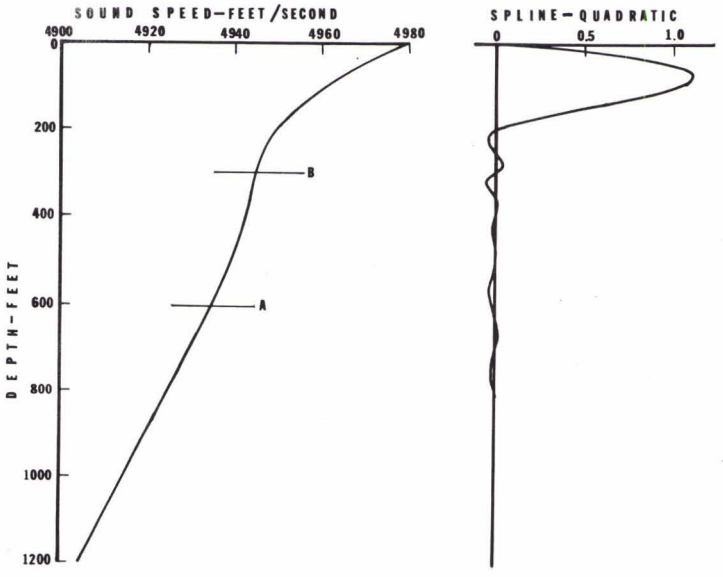

FIG. 11

SAMPLE PROFILE 2

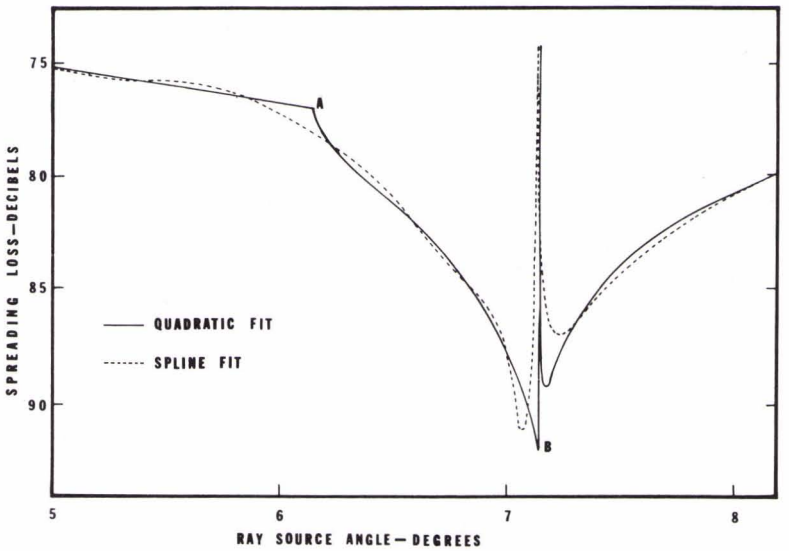

FIG. 10

THE CONTINUOUS GRADIENT RAY TRACING SYSTEM (CONGRATS)

by

H. Weinberg and J.S. Cohen
Naval Underwater System Centre
New London, Conn., U.S.

INTRODUCTION

CONGRATS, an acronym for the Continuous Gradient Ray Tracing System, is an integrated collection of ray tracing programs designed to model acoustic propagation and reverberation. The fundamental programs of the series, CONGRATS I, construct ray diagrams and generate eigenrays, that is, rays that join a given source to a given target [Ref. 1]. The most distinguishing feature of CONGRATS I is that the velocity of sound in the ocean is represented by a function of depth whose first derivative is continuous, and still permits one to integrate the resulting ray tracing equations in closed form.

CONGRATS II processes the eigenray information that was generated by CONGRATS I, and displays it in such useful forms as total propagation loss as a function of range, and pulse shape as a function of time [Ref. 2]. The various multipath arrivals can be summed using random phase or coherent phase addition.

The most recent contribution to the ray tracing series, CONGRATS III, is the main topic of discussion [Ref. 3]. Bottom, surface, and volume reverberation are computed as a function of time for a given set of environmental and sonar parameters. The total reverberation level is assumed to be the sum of the three components. Among the notable features of CONGRATS III is the large number of multipath arrivals that can be considered in the reverberation computation.

REVERBERATION THEORY

Let us review reverberation theory. Consider an acoustic signal which originates at a point source at a reference time equal to zero and is transmitted through the ocean [Fig. 1]. A portion of the signal is scattered back toward the source as the signal encounters scatterers on the ocean bottom or surface or within the ocean volume. When the rescattering of the scattered sound is neglected, a closed ray path from a source to a scatterer and back to the source can be constructed from an incident ray (a ray from the source at point 'a' to the scatterer at point 'b') and a backscattered ray (a ray from the scatterer back to the source). Let the incident ray enter the water at time t_0 and have travel time t_1 and let the backscattered ray have travel time t_2. Then the closed ray path will have round trip travel time

$$t = t_1 + t_2 \quad . \qquad \text{[Eq. 1]}$$

It will return to the source at time

$$T = t_0 + t \quad , \qquad \text{[Eq. 2]}$$

and have an intensity

$$I = I_s \, \eta_d \, \eta'_d \, \eta_w \, \eta'_w \, k \qquad \text{[Eq. 3]}$$

where

I_s is the reference intensity 1 yd from the source,
η_d is the transmitting response of the sonar,
η'_d is the receiving response of the sonar,
η_w is the propagation loss factor of the incident ray,
η'_w is the propagation loss factor of the backscattered ray, and
k is the backscattering coefficient expressing the ratio of reflected intensity to incident intensity per scatter.

If the acoustic signal has pulse length τ, it follows that

$$0 \leq t_0 \leq \tau \quad , \qquad \text{[Eq. 4]}$$

and the closed ray paths contributing to the reverberation intensity at time T are those with travel time satisfying

$$T - \tau \leq t \leq T \quad . \qquad \text{[Eq. 5]}$$

The corresponding scatterers will be contained in a region R. Let this region be partitioned into numerous subregions ΔR_i in each of which $\eta_d\ \eta'_d\ \eta_w\ \eta'_w$ and k are representative values, and let there be N scatterers per unit region. Then if the reverberation intensity I_{rev} is the sum of the intensities of the individual contributors

$$I_{rev} = I_s \sum_R \eta_d\ \eta'_d\ \eta_w\ \eta'_w\ kN\Delta R_i \qquad \text{[Eq. 6]}$$

In the limit as ΔR_i approaches zero,

$$I_{rev} = I_s \int_R \eta_d\ \eta'_d\ \eta_w\ \eta'_w\ m dR \quad , \qquad \text{[Eq. 7]}$$

where

$$m = kN \qquad \text{[Eq. 8]}$$

is the backscattering strength.

NUMERICAL INTEGRATION OF THE REVERBERATION INTEGRALS

When the scatterers are confined to the ocean volume, the corresponding reverberation is called volume reverberation and Eq. 7 becomes

$$I_{rev} = I_s \int_{\Delta\Phi} \int_{A(\Phi)} \eta_d\ \eta'_d\ \eta_w\ \eta'_w\ mrdAd\Phi \quad , \qquad \text{[Eq. 9]}$$

where

r is the horizontal range,

$\Delta\Phi$ is the change in azimuthal angle, and

$\Delta(\Phi)$ is the intersection of the insonified region R with the half-plane Φ = constant.

In order to accomplish this integration numerically, the ocean is partitioned by vertical half-planes $\Phi = \Phi_k$ and each vertical plane is further partitioned by a range-depth grid. The eigenrays to each point in the grid are computed and combined according to the summation

$$I_{rev} = I_s \sum_k \sum_{i,j} (\eta_d \, \eta'_d \, \eta_w \, \eta'_w \, m) \, r_i \, A_{ij} \, \Delta\Phi_k \qquad \text{[Eq. 10]}$$

where A_{ij} is an area insonified around the (r_i, z_j)-th grid point.

A similar analysis results in the boundary reverberation summation

$$I_{rev} = I_s \sum_k \sum_i (\eta_d \, \eta'_d \, \eta_w \, \eta'_w \, m) \frac{r_i \, \Delta r_i}{\cos \theta_{bot}} \Delta\Phi_k \qquad \text{[Eq. 11]}$$

At present, analytical bottom and surface backscattering equations developed by Mackenzie [Ref. 4]

$$10 \log_{10} \mu = -27 + 10 \log (|\sin \theta_1 \sin \theta_2|) \qquad \text{[Eq. 12]}$$

and Chapman-Harris [Ref. 5],

$$10 \log_{10} \mu = 3.3 \, \beta \log \frac{\theta}{30} - 42.4 \log_{10} \beta + 2.6 \qquad \text{[Eq. 13]}$$

where

$$\beta = 158 \, (vf^{1/3})^{-0.58} \quad , \qquad \text{[Eq. 14]}$$

v is the wind speed, and f is the frequency, respectively have been implemented in the computer program. The volume backscattering strength is found by interpolating in a table of strength versus depth. Figure 2 illustrates a typical backscattering strength-depth curve. The actual unit of strength is more complicated than simply decibels and should be associated with a unit of volume, in this case, cubic yards.

Independent array response models supply the transmitting and receiving responses of the sonar in the form of tables of loss versus inclination angle at a particular azimuthal angle. Then by looping through the reverberation program numerous times, one is able to consider three dimensional beam pattern effects.

The propagation losses and travel times of the eigenrays, which are required in the reverberation calculation, are computed in CONGRATS I using the continuous gradient ray tracing technique to be described shortly.

A CONTINUOUS GRADIENT RAY TRACING TECHNIQUE

The basic assumption of CONGRATS I is that the velocity of sound in the ocean can be adequately approximated by a function of depth only, say $V(z)$. Let us also confine our attention to ray segments that do not intersect ocean boundaries. Then Snell's law

$$V(z) = C_v \frac{dr}{ds} \qquad \text{[Eq. 15]}$$

uniquely determines the coordinates (r,z) of a point on the ray segment as a function of initial position (r_a,z_a), initial direction $\left(\frac{dr}{ds}\Big|_a, \frac{dz}{ds}\Big|_a\right)$, and arc length s. The vertex velocity C_v is constant along the segment and can be expressed in terms of the initial conditions through Snell's law. Travel time t is related to s and V by

$$\frac{ds}{dt} = V(z) \qquad \text{[Eq. 16]}$$

It is well known that a ray passing from an initial depth z_a to a greater depth z_b will undergo the change in range

$$\Delta r = \int_{z_a}^{z_b} \frac{V\, dz}{\sqrt{C_v^2 - V^2}} \qquad \text{[Eq. 17]}$$

and travel time

$$\Delta t = \int_{z_a}^{z_b} \frac{C_v\, dz}{V\sqrt{C_v^2 - V^2}} \qquad \text{[Eq. 18]}$$

providing that C_v is always greater than V. When C_v equals V, the ray is horizontal and is said to vertex. It can also be shown that these integrals are convergent unless the velocity gradient $V'(z)$ vanishes at a vertexing depth.

In practice, V is known only at discrete data points (z_i, V_i), and one must evaluate Eqs. 17 and 18 numerically. Unfortunately, the number of data points is usually insufficient to expect standard numerical integration formulae to give accurate results. An alternative approach is to first fit the data with an interpolating function, and then either integrate Eqs. 17 and 18 in closed form if possible, or generate additional data points to be used in conjunction with standard numerical integration formulae. However, it is desirable to approximate the velocity-depth profile with a function that has a continuous derivative, for discontinuities in the velocity gradient often cause erroneous values of geometrical spreading loss [Ref. 6].

Before describing the particular velocity representation that is used in the CONGRATS programs, it is convenient to clarify the notation. The function $V(z)$ denotes the velocity of sound in the ocean and is defined from the ocean surface to the ocean bottom. V_i is the value of $V(z)$ evaluated at the depth z_i [Fig. 3].

The function $V_i(z)$, on the other hand, is only defined in the interval $z_i \leq z \leq z_{i+1}$. Primes of functions denote differentiation with respect to depth, while G_i is the value of $V'(z)$ evaluated at z_i. In general G_i is not known but can be estimated from the given data V_i using numerical differentiation. The quantities v_0, g_0, g_1 and g_2 are parameters. They are constant in each horizontal layer but may differ from layer to layer. Then a continuous gradient velocity approximation can be constructed as follows:

For each pair of adjacent data points i and i+1, find a four parameter analytic function $V_i(z)$ such that its derivative $V_i'(z)$ is continuous in the closed interval $z_i \leq z \leq z_{i+1}$ and satisfies the boundary conditions

$$V_i(z_i) = V_i \quad , \qquad \text{[Eq. 19]}$$

$$V_i(z_{i+1}) = V_{i+1} \quad , \qquad \text{[Eq. 20]}$$

$$V_i'(z_i) = G_i \quad , \qquad \text{[Eq. 21]}$$

and

$$V_i'(z_{i+1}) = G_{i+1} \quad . \qquad \text{[Eq. 22]}$$

Finally, set $V(z) = V_i(z)$ in the half-closed interval $z_i \leq z < z_{i+1}$.

It can be shown that parameters v_0, g_0 g_1 and g_2 can be chosen so that the function

$$V_i(z) = \left[v_0 + \Delta z \frac{g_0 + \Delta z\, g_1}{(1 + \Delta z\, g_2)^2} \right]^{-\frac{1}{2}} \quad . \qquad \text{[Eq. 23]}$$

where

$$\Delta z = z - z_i \qquad \text{[Eq. 24]}$$

satisfies the above conditions [Ref. 7]. It can also be shown that the corresponding range integral Eq. 17 and time integral Eq. 18 can be evaluated in closed form in terms of elementary transcendental functions.

There are some difficulties involved with this curve fitting method, most of which are due to computer truncation errors. All can be removed by making appropriate modifications. The method has been used extensively in CONGRATS I, and every velocity profile that was considered could be satisfactorily fitted.

A useful option in the program allows one to relax certain boundary conditions. The resulting representation still has a continuous gradient but is not forced to go through all of the data points. Instead, the condition

$$\max|V(z_i) - V_i| \leq \epsilon \qquad \text{[Eq. 25]}$$

must be satisfied, where $\epsilon \geq 0$ is a velocity tolerance to be supplied by the user. This option tends to reduce the number of functions in the form of Eq. 23 required to fit the given profile. Hence fewer integrals need to be evaluated, and a substantial saving in computer execution time is realized.

CONTINUOUS VERSUS CONSTANT GRADIENT FIT TO AN EPSTEIN PROFILE

A second option in CONGRATS I allows one to substitute the well known constant gradient technique for the continuous gradient technique. The velocity-depth profile is then approximated by straight line segments instead of by functions in the form of Eq. 23, and one can integrate the resulting ray tracing equations more easily. In fact, because of the relative simplicity of the constant gradient technique, it is the most commonly used ray tracing method. The reason we prefer the more complicated continuous gradient technique will become clear after the following example.

Figure 4 shows an Epstein velocity-depth profile which was fitted with five CONGRATS velocity functions. There were fifty original data points as indicated by plusses. The CONGRATS velocity break-points are indicated by circles and by plusses within circles. A 0.1 m/s velocity tolerance was used. That is, the maximum error in the curve fit was less than 0.1 m/s. Since the continuous gradient technique would perform only one-tenth the number of integrations required by the constant gradient technique, and a single integration uses five times more computer execution time, CONGRATS appears to be twice as fast, at least in this particular example.

When the source is placed on the channel axis at 76 m, there is a high degree of focussing as shown in Fig. 5. The CONGRATS ray diagram (on top) and the constant gradient ray diagram (on the bottom) are similar. Note, however, that the constant gradient solution is not focussed as sharply.

The corresponding propagation loss curves for a 60 m target depth are given in Fig. 6. Anomalies in the computed value of geometrical spreading loss which were caused by discontinuities in the velocity gradient, are clearly visible in the constant gradient solution. There are no such anomalies in the CONGRATS solution.

EIGENRAYS

The most important function of CONGRATS I with respect to the reverberation program CONGRATS III is to determine acoustic eigenrays, that is, those rays that join a given source (r_s, z_s) to a given target (r_t, z_t). One method of determining eigenrays which was tried and later discarded involves an iterative scheme:

a. Set $i = 1$ and choose an initial vertex velocity $C_v^{(1)}$.

b. Trace the ray with vertex velocity $C_v^{(i)}$ to the target depth z_t and denote the corresponding range by $r^{(i)}$.

c. If $|r_t - r^{(i)}|$ is sufficiently small, convergence has occurred. If $|r_t - r^{(i)}|$ is not sufficiently small, set

$$C_v^{(i+1)} = C_v^{(i)} + \frac{r_t - r^{(i)}}{\left.\frac{\partial r^{(i)}}{\partial C_v}\right|_{z = z_t}} \qquad \text{[Eq. 26]}$$

increment i, and return to step b.

This iterative scheme has two drawbacks. First of all, convergence is slow near caustics (points at which $\left.\frac{\partial r}{\partial C_v}\right|_{z = z_t}$ vanishes) unless a convergence acceleration technique is used. Secondly, the method is inefficient when many eigenrays are to be determined. For example, assume that there are 1000 targets, that each target has 5 eigenrays, and that each eigenray requires 3 iterations for convergence to occur. Then the total number of rays to be traced (15 000) becomes excessive.

An alternative approach involves a preselected set of rays. When two adjacent rays bound a target, an interpolation is performed to determine the eigenray. If the derivatives $\left.\frac{\partial r}{\partial C_v}\right|_{z = z_t}$ are known, one can use a higher order interpolation routine. Otherwise a linear interpolation can be used instead.

The interpolation technique was incorporated into CONGRATS I and was found to be as accurate as the convergence method. One of the outputs of the program is geometrical spreading loss N_{sp}, where

$$N_{sp} = 60 + 10 \log_{10} \left| \frac{C_v \sin \theta_s \sin \theta_t}{\cos^2 \theta_s} r_t \frac{\partial r_t}{\partial C_v} \right|_{z = z_t} \qquad \text{[Eq. 27]}$$

is in decibels, and θ_s and θ_t are the inclination angles at the source and target, respectively. The number 60 appearing in Eq. 27 is present because the unit of range is in kiloyards. The total propagation loss N along a ray is given by

$$N = N_{sp} + N_a + N_s + N_b \quad , \qquad \text{[Eq. 28]}$$

where N_a is the attentuation loss, N_s is the loss incurred at surface reflections, and N_b is the loss incurred at bottom reflections.

If several eigenrays arrive at the same target, the effective propagation loss N_{eff} is given by

$$N_{eff} = -10 \log_{10} \sum_j 10^{-\frac{N^{(j)}}{10}} \qquad \text{[Eq. 29]}$$

(random phase addition) or by

$$N_{eff} = -20 \log_{10} \left| \sum_j 10^{-\frac{N^{(j)}}{20}} e^{i[2\pi f t^{(j)} + \Phi^{(j)}]} \right| \quad , \qquad \text{[Eq.}$$

where $i = \sqrt{-1}$, f is the frequency in hertz, $t^{(j)}$ is the travel time in seconds, $\Phi^{(j)}$ is the phase change in radians of the j^{th} eigenray (coherent addition). Phase changes are caused by interactions of the ray with the ocean surface and bottom, and they also occur when a ray passes through a caustic curve. In the last instance, a phase change of π radians is added although the generally accepted value is $-\pi/2$ radians. The erroneous phase shift of π radians reduces the high intensities predicted by ordinary ray theory. It is used as an artifice to make reasonable predictions until one of the more sophisticated theories treating caustics can be added to the computer program.

EXAMPLES

Figures 7, 8 and 9 illustrate some of the more widely used programs in the CONGRATS series. They pertain to the Mediterranean Sea in the summer. Some of the results have been compared to measured data taken during the summer of 1970 by the Ocean Sciences Division of the Naval Underwater Systems Center. Figure 7 is a plot of sound speed as a function of depth. The warm surface temperatures cause a sharp negative gradient near the surface, which causes the energy from a near surface source to be initially directed downward as shown in Fig. 8.

The ray plot shows both bottom bounce and convergence zone rays. The convergence zone is defined by the caustic line intersecting the surface at a range of about 44 kyds. For the set of data, the predicted zones and measured zones have agreed in range to approximately 200 yards. This is a relative error of about one-half of one percent.

Figure 9 displays the level at a point as a function of time. Since the intensity at a point changes whenever a sound pulse arrives and since the travel times associated with each arrival are generally different, the curves are composed of numerous step functions. These curves were obtained by adding beam pattern information to each arrival, and then adding the resultant signals in random phase. For the relatively large pulse length of one-half second the intensity builds up quickly, remains constant until the first arrival ceases to contribute, and then decays. On the other hand, if the pulse length is sufficiently small such as 10 ms, then the dominant individual arrivals become more apparent. The computer program can also add the signals coherently if the user so desires.

In order to plot propagation loss as a function of range, a single point from the pulse shape plot is chosen as a resultant level. When random phase addition is used, the maximum level is usually chosen.

CONGRATS VALIDATION

For certain simple propagation situations, for example constant or linear sound speed profiles, the ray integrals, the spreading loss formulae, and the reverberation integrals have been evaluated analytically and compared to the results produced by the computer programs. The analytic answers and computer answers have been in excellent agreement. For the numerical integration scheme described for the reverberation calculation, the range-depth grid over which the integral is taken must be sufficiently fine. At any rate, the close agreement indicates that the mathematical equations used to model propagation and reverberation are being evaluated correctly in the computer for the circumstances examined. We are now trying to determine how well the program predicts propagation and reverberation levels measured at sea.

The propagation loss for a 25-foot target depth is shown in Fig. 10. The strengths of the various arrivals were summed using random phase addition, as shown by the dashed line, and coherent phase addition, as shown by the solid line. The predictions generally agree well with the measured data. Here the peak level is about 80 dB.

Figure 11 is similar to Fig. 10 except the target depth is now at 503 ft. Note that the maximum level has dropped about 10 dB which is also in agreement with measured data.

Figure 12 shows reverberation level as a function of time, as predicted by the CONGRATS programs. Again the predictions were good.

In addition to the in-house validation effort, a joint programme between NUSC and SACLANTCEN here at La Spezia has been developed. Two joint reports will be published, one presenting propagation loss measurements and predictions; the other comparing reverberation levels. A preliminary investigation has shown very good agreement in the propagation loss area, and good agreement in reverberation.

SUMMARY

To summarize, CONGRATS I is the fundamental ray tracing program of the CONGRATS series. It uses a continuous gradient ray tracing technique in order to reduce the problem of false caustics, a problem which often occurs when discontinuities in the velocity gradient are introduced. Eigenrays are found by interpolation rather than by iteration in order to reduce the running time of the program. Options allow the user to reduce the number of horizontal layers into which the ocean is divided, to substitute the constant gradient ray tracing technique for the continuous one, to print and plot ray data, and to use various attentuation, surface loss, and bottom loss models. Although the examples discussed pertained to oceans in which the boundaries are assumed to be horizontal, one can also input a linear segmented surface and bottom.

The propagation loss curves and pulse shape curves were supplied by CONGRATS II. There are several other programs in this series, but most are of a specific nature and would not be of general interest. The user may choose between random phase and coherent phase additions to obtain resultant intensities.

CONGRATS III computes bottom, surface, and volume reverberation as a function of time. Future plans include the addition of a program to compute echo-to-reverberation level as a function of time, and attempts to increase the efficiency of the existing reverberation program.

CONGRATS IV when completed, will allow the sound speed to vary with range as well as depth.

The existing programs have been implemented on UNIVAC 1108 computers in New London, in California, in Rome, and at other installations. It has run on General Electric and Burrough's computers also. There is an effort presently underway to program a modified version of CONGRATS on a shipboard computer. Thus CONGRATS has become a useful tool in the field of underwater acoustics.

REFERENCES

1. H. Weinberg, "CONGRATS I: Ray Plotting and Eigenray Generation", NUSL Report No. 1052, New London, Conn., 30 October 1969.

2. J.S. Cohen and L.T. Einstein, "Continuous Gradient Ray Tracing System (CONGRATS) II: Eigenray Processing Programs", NUSL Report No. 1069, New London, Conn., 5 Februarly 1970.

3. J.S. Cohen and H. Weinberg, "Continuous Gradient Ray Tracing System (CONGRATS) III:Boundary and Volume Reverberation", NUSL Report No. 4071, New London, Conn., 30 April 1971.

4. K.V. Mackenzie, "Bottom Reverberation for 530- and 1030-cps Sound in Deep Water", J.Acous.Soc.Am., Vol.33, Nov. 1961, pp. 1498-1504.

5. R.P. Chapman and J.H. Harris, "Surface Backscattering Strengths Measured with Explosive Sound Sources", J.Acous.Soc.Am., Vol.34 Oct. 1962, pp. 1592-1597.

6. M.A. Pederson, "Acoustic Intensity Anomalies Introduced by Constant Velocity Gradients", J.Acous.Soc.Am., Vol. 33, April 1961, pp. 465-474.

7. H. Weinberg, "A Continuous Gradient Curve Fitting Technique for Acoustic Ray Analysis". To be published in J.Acous.Soc.Am., 1971.

DISCUSSION

Typical times to run the CONGRATS system were given as one to two minutes for a range of 100 kyd and a flat bottom, and 10 to 15 minutes for a volume reverberation calculation, both on a UNIVAC 1108.

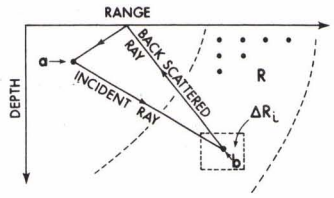

FIG. 1

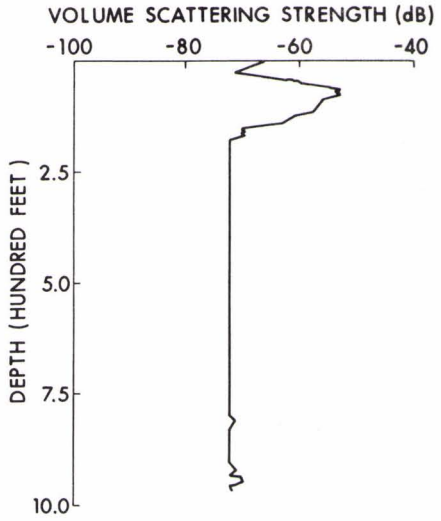

FIG. 2

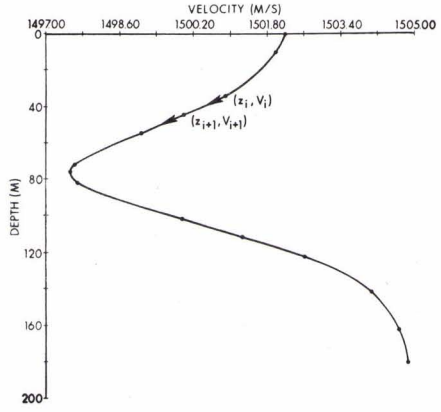

FIG. 3

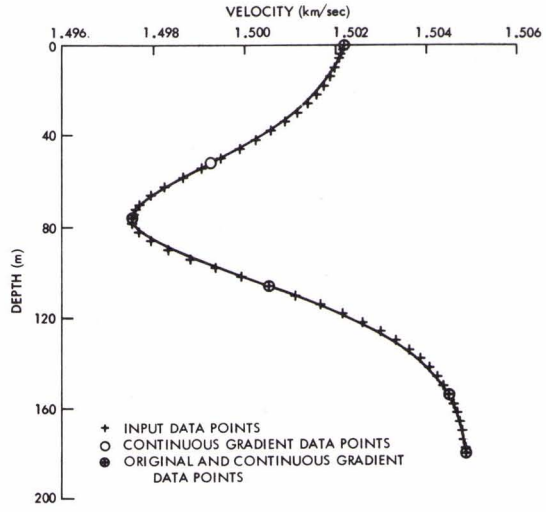

FIG. 4

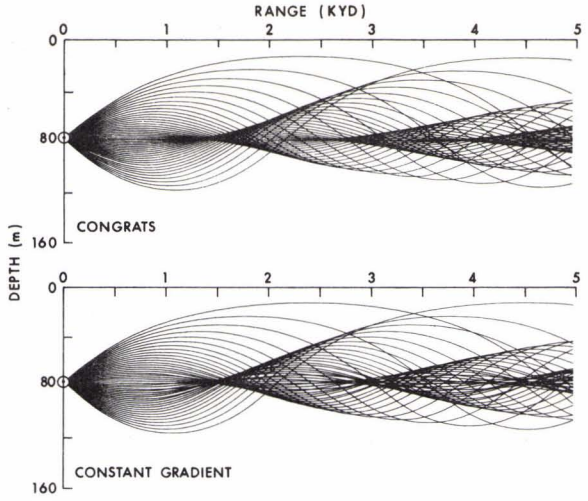

FIG. 5

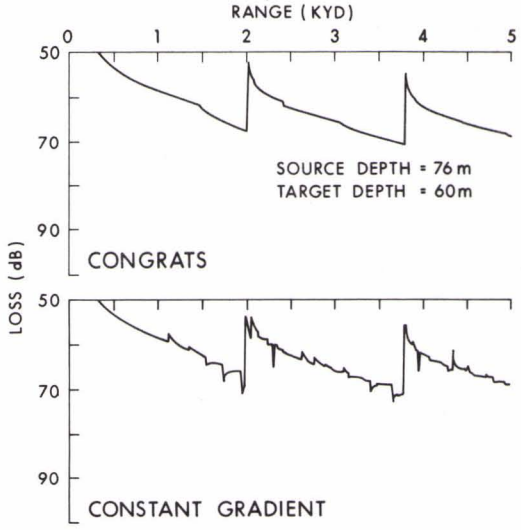

FIG. 6

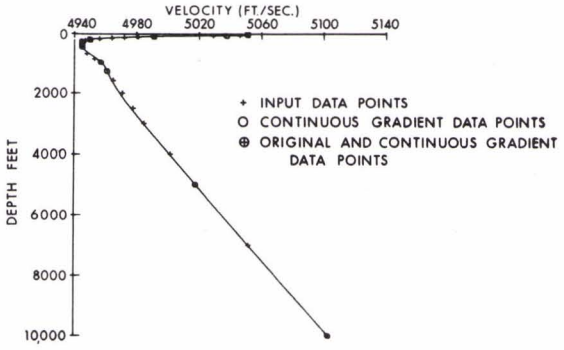

FIG. 7

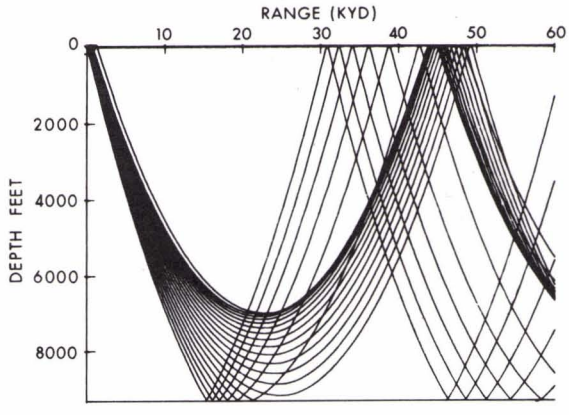

FIG. 8

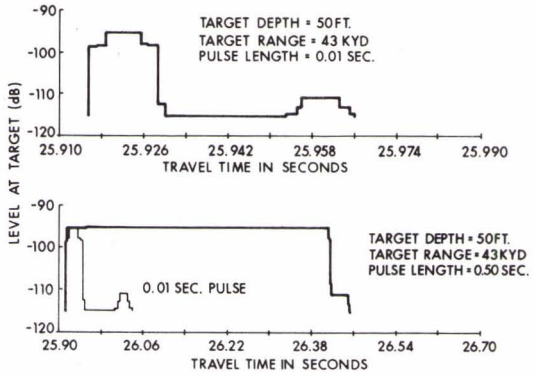

FIG. 9

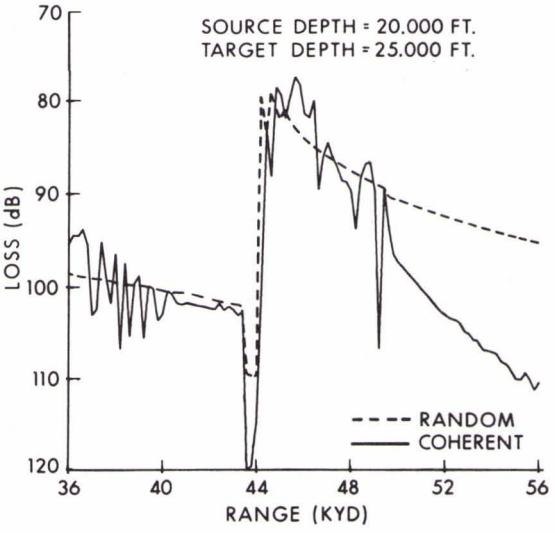

FIG. 10

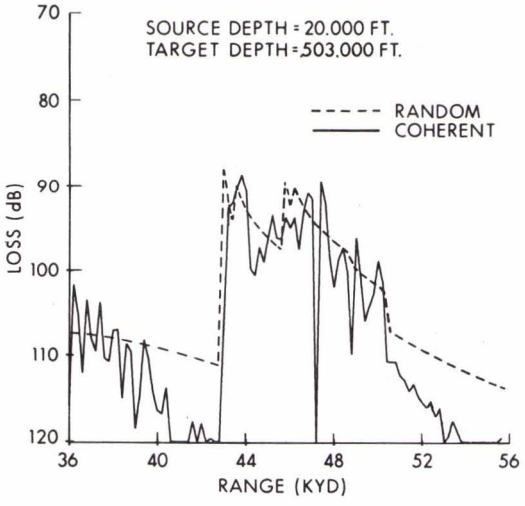

FIG. 11

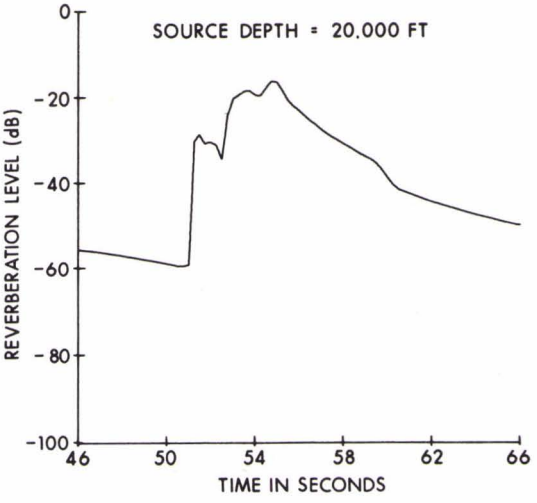

FIG. 12

INTENSITY CALCULATIONS ALONG A SINGLE RAY

by

H.R. Krol
SACLANT ASW Research Centre
La Spezia, Italy

ABSTRACT

A method is presented for the calculation of sound intensity using only one ray. The sound velocity profile is assumed to be continuous up to the second derivative and it is supposed that the ray equations are solved numerically. An example is given.

INTRODUCTION

In this paper a method is presented for the calculation of the spreading loss along a ray, using only that particular ray. (The medium is assumed to be lossless, and so the intensity is equal to the spreading loss.) It appears that the spreading loss may be expressed by two different formulae, one not usable near any point where the first derivative of the sound velocity becomes zero, the other not near a turning point of the ray. By switching from one formula to the other near these critical points, these difficulties are avoided. It will be assumed that the sound-velocity profile is a continuous, differentiable curve, but not expressible in one mathematical formula, so that the ray-differential equations have to be solved numerically.

After a short introduction, in which some basic formulae used in the paper are given, the two intensity formulae will be discussed. Finally the method is illustrated with a computer result.

For the ray path shown in Fig. 1, the basic equations, when there is no z-dependence of the sound velocity c, are [Ref. 1]

$$\frac{d}{ds}\frac{1}{c}\frac{dx}{ds} = \frac{\partial}{\partial x}\frac{1}{c} \qquad \text{[Eq. 1a]}$$

$$\frac{d}{ds}\frac{1}{c}\frac{dy}{ds} = \frac{\partial}{\partial y}\frac{1}{c} \qquad \text{[Eq. 1b]}$$

For a velocity profile dependent only on y, this reduces to

$$\frac{dx}{ds} = c \cdot A \qquad \text{(Snell's law)} \qquad \text{[Eq. 2a]}$$

$$\frac{d}{ds}\frac{1}{c}\frac{dy}{ds} = -\frac{c'}{c^2} \qquad \text{[Eq. 2b]}$$

where A is the ray constant, the prime denotes the derivative with respect to y, and ds is the curvilinear parameter along the ray. From Fig. 1, we have

$$\frac{dy}{dx} = \tan\theta \ . \qquad \text{[Eq. 3]}$$

From Eq. 3 and eliminating ds from Eq. 2 it is easy to derive

$$\frac{d^2y}{dx^2} = -\frac{Ac'}{c \cdot \cos^3\theta} \ . \qquad \text{[Eq. 4]}$$

Now for the radius of curvature ρ we have

$$\frac{1}{\rho} = \frac{\left|\frac{d^2y}{dx^2}\right|}{\left[1 + \left(\frac{dy}{dx}\right)^2\right]^{3/2}} = \left|\frac{c' \cos\theta}{c}\right| \ . \qquad \text{[Eq. 5]}$$

From

$$ds = \rho\,|d\theta| \qquad \text{[Eq. 6a]}$$

and the sign convention of Fig. 1 we arrive at

$$\left|\frac{ds}{d\theta}\right| = \left|\frac{c}{c' \cos\theta}\right| \qquad \text{[Eq. 6b]}$$

$$\frac{dx}{d\theta} = -\frac{c}{c'} \qquad \text{[Eq. 6c]}$$

$$\frac{dy}{d\theta} = -\frac{c}{c'} \tan\theta \qquad \text{[Eq. 6d]}$$

THE INTENSITY CALCULATION

The intensity calculation [Fig. 2] is based on the assumption that the energy is confined in an infinitesimally narrow bundle of rays. This implies that the intensity along a ray can be expressed in terms of that one particular ray.

$$I(x) = p\,\frac{d\Omega}{dF} = p\,\frac{2\pi \cos\theta_o\, d\theta_o}{2\pi x\, dn} \qquad \text{[Eq. 7]}$$

where Ω is the unit solid angle and F the area swept out by the wave surface normal to the rays [Ref. 1]. (In the following, the emission of the point source p will assumed to be 1). It is possible to express dn in different ways, depending on which variables are looked upon as the independent ones. For a reason that will become clear later we will assume θ_o and y to be independent. In the appendix we also give a variant with θ_o and θ being independent.

A. The First Formula

From Fig. 2 it is seen that

$$dn = -\sin\theta\, dx = -\sin\theta \frac{\partial x}{\partial \theta_o}\, d\theta_o \qquad \text{[Eq. 8]}$$

except, exactly at the turning point (x_H, y_H) where Eq. 8 is not valid;

after the turning point both dx and $\sin\theta$ change sign, abruptly. So, Eq. 7 reduces to,

$$I(x) = \frac{-\cos\theta_o}{x \sin\theta \frac{\partial x}{\partial \theta_o}} . \qquad \text{[Eq. 9]}$$

From Eq. 3 it follows that

$$x = \int_{y_o}^{y} \text{cotan}\,\theta \, dy , \qquad \text{[Eq. 10]}$$

only valid if $x < x_H$, and from this

$$\frac{\partial x}{\partial \theta_o} = \int_{y_o}^{y} - \frac{1}{\sin^2\theta} \frac{\partial \theta}{\partial \theta_o} \, dy \qquad \text{[Eq. 11]}$$
$$x < x_H$$

From Snell's law [Eq. 2a] we know that

$$c_o \cos\theta = c \cos\theta_o . \qquad \text{[Eq. 12]}$$

Partial differentiation with respect to θ_o provides

$$\frac{\partial \theta}{\partial \theta_o} = \frac{\cos\theta \sin\theta_o}{\sin\theta \cos\theta_o} . \qquad \text{[Eq. 13]}$$

(We see the advantage of taking θ_o and y as independent variables here, $\frac{\partial c}{\partial \theta_o}$ being zero.)

Substitution in Eq. 11 yields,

$$\frac{\partial x}{\partial \theta_o} = -\tan\theta_o \int_{y_o}^{y} \frac{\cos\theta}{\sin^3\theta} \, dy \qquad \text{[Eq. 14]}$$
$$x < x_H$$

With the aid of Eq. 3 this can be expressed as

$$\frac{\partial x}{\partial \theta_o} = -\tan \theta_o \int_{x_o}^{x} \frac{1}{\sin^2 \theta} \, dx \qquad x < x_H \qquad \text{[Eq. 15]}$$

Substitution of this result in Eq. 9, provides,

$$I(x) = \frac{\cos^2 \theta_o}{x \sin \theta_o \sin \theta \int_{x_o}^{x} \frac{1}{\sin^2 \theta} \, dx} \qquad x < x_H \qquad \text{[Eq. 16]}$$

B. Consideration of the First Formula

There are some interesting points to make now with regard to this formula [Eq. 16].

Firstly, it appears to be the continuous form of the formula often used in the case of the piecewise linear sound velocity profile, viz.,

$$I(x) = \frac{\cos^2 \theta_o}{x \sin \theta_o \sin \theta_n \sum_{i=1}^{n} \frac{x_i - x_{i-1}}{\sin \theta_{i-1} \sin \theta_i}} \qquad \text{[Eq. 17]}$$

where i indicates the layer number.

Secondly, Eq. 16 is not valid after a turning point ($\theta = 0$), is passed. The point $\theta = 0$ is a singular point of the integral and also the point where assumption [Eq. 8] does not hold. But the whole expression converges if we approach the turning point from the left side, as is easily proved in the case of a linear sound velocity profile. For, in this case the solution is

$$x = \frac{c_o}{g \cos \theta_o} (\sin \theta_o - \sin \theta) \qquad \text{[Eq. 18a]}$$

$$dx = \frac{-c_o}{g \cos \theta_o} \, d \sin \theta \qquad \text{[Eq. 18b]}$$

(where g is the sound velocity gradient), and substitution in Eq. 16 provides

$$I(x) = \frac{\cos^2 \theta_o}{x^2} \,. \qquad \text{[Eq. 19]}$$

This is the solution for a linear profile shown to be true also after a turning point [Ref. 1]. Let us formally extend Eq. 16 for $x > x_H$, then for this example, after substitution of Eq. 18b

$$\sin\theta \int_{x_o}^{x} \frac{1}{\sin^2\theta}\, dx = -\frac{c_o \sin\theta}{g\cos\theta_o} \left[\lim_{\theta_H \downarrow 0} \int_{\theta_o}^{\theta_H} \frac{d\sin\theta}{\sin^2\theta} + \lim_{\theta_H \uparrow 2\pi} \int_{\theta_H}^{\theta} \frac{d\sin\theta}{\sin^2\theta} \right] =$$

$$= \frac{c_o \sin\theta}{g\cos\theta_o} \left[\lim_{\theta_H \downarrow 0} \frac{1}{\sin\theta_H} - \lim_{\theta_H \uparrow 2\pi} \frac{1}{\sin\theta_H} - \frac{1}{\sin\theta_o} + \frac{1}{\sin\theta} \right] \qquad \text{[Eq. 20]}$$

The integral from x_o to x has been divided into one from x_o to x_H and another from x_H to x.

We see that the first two terms in Eq. 20 lead to $+\infty$ at both limits and in order now to satisfy Eq. 19 they have to be ignored. They appear because we pass the turning point, that point where our initial assumption [Eq. 8] did not hold. Thirdly, from a numerical point of view [Eq. 16] is no longer usable in close proximity of the turning point, because $\sin\theta$ goes to zero and the integral becomes infinite.

C. The Second Formula

By means of partial integration we can transform the last two terms of the denominator in Eq.16, viz.,

$$\sin\theta \int_{x_o}^{x} \frac{1}{\sin^2\theta}\, dx = -\sin\theta \int_{x_o}^{x} \frac{dx}{d\theta}\, d\,\mathrm{cotan}\,\theta =$$

$$= \sin\theta \left\{ \frac{c}{c'} \mathrm{cotan}\,\theta \Big|_{x_o}^{x} - \int_{x_o}^{x} \mathrm{cotan}\,\theta\, d\,\frac{c}{c'} \right\} \qquad \text{[Eq. 21a]}$$

which may be developed further, under the condition that a second derivative of the sound velocity exists, to

$$\frac{c}{c'}\cos\theta - \sin\theta \operatorname{cotan}\theta_0 \frac{c_0}{c'_0} - \sin\theta \int_{x_0}^{x} \frac{c'^2 - cc''}{c'^2}\,dx \qquad \text{[Eq. 21b]}$$

where c_0 denotes the sound-velocity at the source.
Substitution in Eq. 16, provides

$$I(x) = \frac{\cos^2\theta_0}{x \sin\theta_0 \left[\frac{c}{c'}\cos\theta - \sin\theta \operatorname{cotan}\theta_0 \frac{c_0}{c'_0} - \sin\theta \int_{x_0}^{x} \frac{c'^2 - cc''}{c'^2}dx\right]} \qquad \text{[Eq. 22]}$$

We can derive [Eq. 22] in a different way (see Appendix), from which it appears that this expression is also valid beyond the turning point. It is shown there that that derivation is in fact the more natural way of deriving [Eq. 22], and is totally independent of the turning point. But by a formal application of partial integration to Eq. 16 in a manner similar to Eq. 20 for $x > x_H$ we would obtain two extra terms in the denominator, viz.

$$\lim_{\theta_H \to 0} \frac{c}{c'} \operatorname{cotan}\theta_H - \lim_{\theta_H \to 2\pi} \frac{c}{c'} \operatorname{cotan}\theta_H \qquad \text{[Eq. 23]}$$

which both go to $+\infty$.

These two terms again express explicitly the wrong contribution due to the fact that our original assumption [Eq. 8] does not hold at the turning point, and the terms have to be ignored. It is easy to see that Eq. 22 is applicable in the proximity of the turning point; the last two terms in the denominator go to zero, but the first term remains finite.

D. Extension of First Formula beyond the Turning Point

From the fact that Eq. 22 is also valid after the turning point and the fact that Eqs. 22 and 16 are identical before the turning point, it follows that we can extend expression 16 after the turning point by writing

$$I(x) = \frac{\cos^2\theta_o}{x\left|\sin\theta_o \sin\theta \int_{x_o}^{x} \frac{1}{\sin^2\theta}\,dx\right|} \qquad \text{[Eq. 24a]}$$

where the bar in the integral means that in the neighbourhood of x_H by definition

$$\int_{x_H-\varepsilon}^{x_H+\varepsilon} \frac{1}{\sin^2\theta}\,dx = \frac{c}{c'}\cot\theta\,\Big|_{x_H-\varepsilon}^{x_H+\varepsilon} - \int_{x_H-\varepsilon}^{x_H+\varepsilon} \frac{c'^2 - cc''}{c'^2}\,dx \qquad \text{[Eq. 24b]}$$

where ε is some finite number >0 and $|c'|>0$ for $|x - x_H| < \varepsilon$.

We see that with this definition it happens that the integral of Eq. 24a changes sign after the turning point, and we get the shape as sketched in Fig. 3.

Numerical Example

Formulae 22 and 24 have been implemented in a computer program. The ray equations are converted to a set of first order equations and solved numerically, using a Kutta Merson procedure [Ref. 2].

The sound velocity profile is approximated by Cubic Spline interpolation [Ref. 3]. The advantage of this interpolation method is that a continuous second derivative of the sound velocity, is obtained. The advantage of the Kutta Merson method is that it is highly accurate, 4-th order, and that its step-size is automatically adapted to the required accuracy during the integration. With each

integration step the intensity contribution is calculated either with Eqs. 22 or 24 depending on the magnitude of c' and $\sin\theta$. For instance, if Eq. 24 is used and $\sin\theta$ decreases below a certain limit, the integral of Eq. 22 is at that point calculated by equating both denominators of Eqs. 22 and 24 and the calculation is continued with Eq. 22 until $\sin\theta$ is large enough to continue the calculation with Eq. 24.

The example in Fig. 4 illustrates the method very well. There are two points where c' equals zero and, for all the rays, there is one point where $\sin\theta$ becomes zero. The intensity peaks correspond to the caustic. They indicate the points where the denominator is zero. We also see that for the first part all the intensity curves coincide. The results there can be compared with the solution for the linear profile, formula 19.

CONCLUSION

A method has been presented for the intensity calculation in the case of a sound velocity profile which is continuous up to the second derivative. The intensity is calculated along the ray simultaneously with the numerical integration of the ray differential equations. It appears that the intensity can be expressed by two different formulae, theoretically valid everywhere, but numerically one is not usable near the turning point, and the other is not usable near points where c' is zero. By switching from one formula to the other in the computer program these difficulties can be avoided.

REFERENCES

1. C.B. Officer, "Introduction to the Theory of Sound Transmission", McGraw-Hill, 1958

2. P.M. Lukehart, "Algorithm 218 - Kutta Merson", Collections Assoc. Comp. Mac., Vol. 4, p.273, 1966.

3. C.B. Moler and L.P. Solomon, "Use of Splines and Numerical Integration in Geometrical Acoustics", J. Acoust. Soc. Am., Vol. 48, No. 3 (Pt.2), 1970.

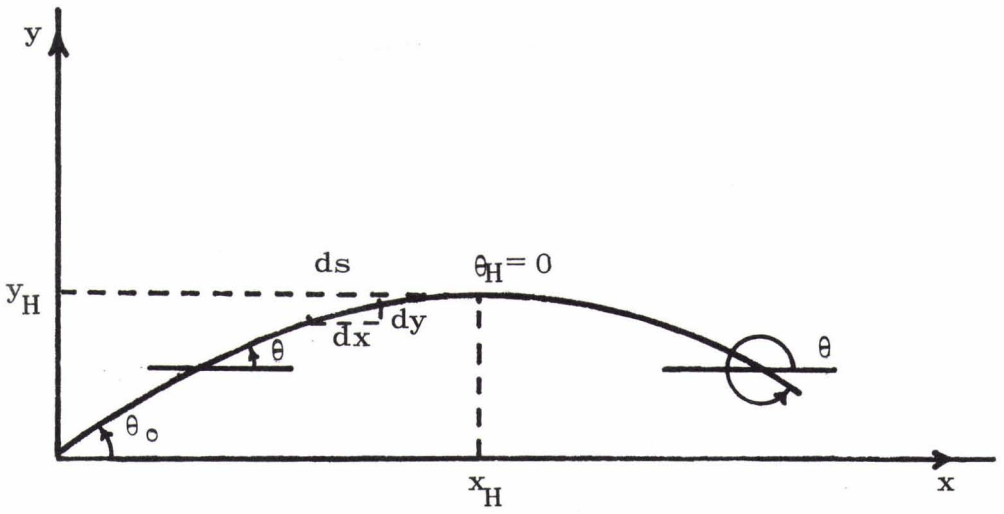

FIG. 1

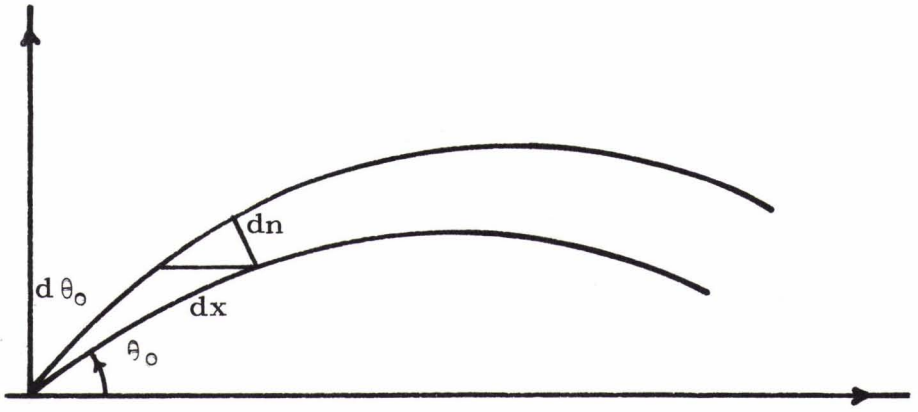

FIG. 2

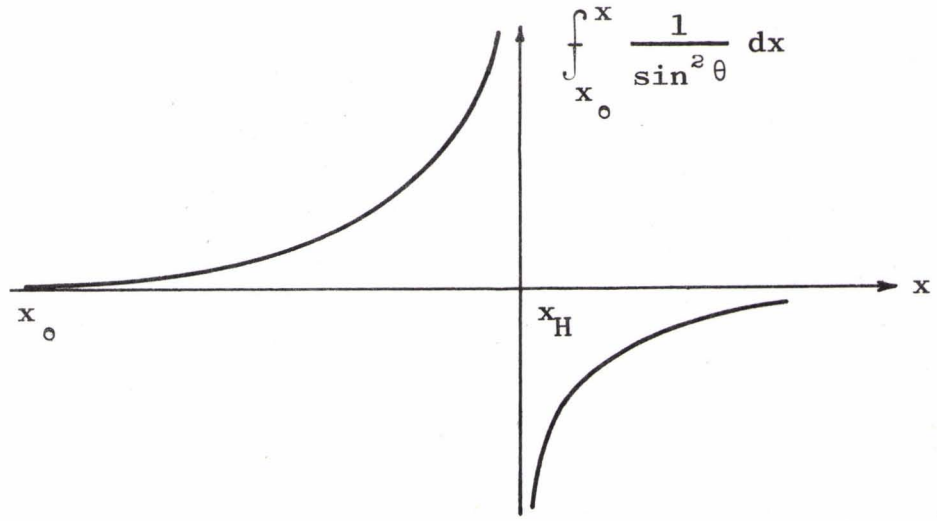
$\int_{x_0}^{x} \frac{1}{\sin^2\theta}\, dx$
x
x_0
x_H

FIG. 3

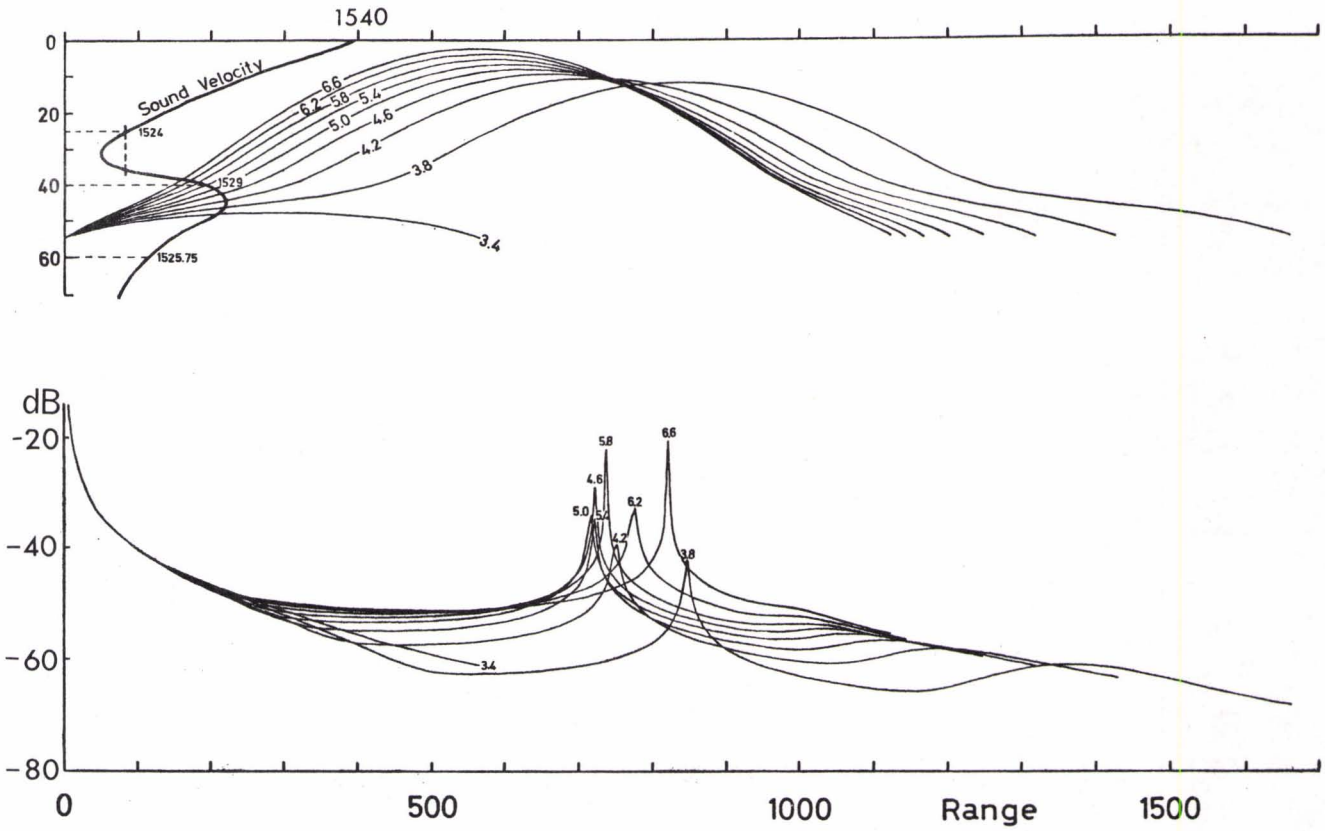
1540
0
20
40
60
Sound Velocity
1524
1529
1525.75
6.6
6.2
5.8
5.4
5.0
4.6
4.2
3.8
3.4
dB
-20
-40
-60
-80
0
500
1000
Range
1500

FIG. 4

APPENDIX A

ANOTHER DERIVATION OF THE SECOND FORMULA

Equation 22 can be derived in a different way [see Fig. A.1]. At P, the point where the intensity is required, we transform coordinates

$$n = -x \sin\theta + y \cos\theta \qquad \text{[Eq. A.1a]}$$

$$t = x \cos\theta + y \sin\theta \qquad \text{[Eq. A.1b]}$$

We now choose θ_o and θ as independent variables. Instead of Eq. 8 we develop dn as,

$$dn = \frac{\partial n}{\partial \theta_o} d\theta_o \,. \qquad \text{[Eq. A.2]}$$

This leads to

$$I(x) = \frac{\cos\theta_o}{x \frac{\partial n}{\partial \theta_o}} \qquad \text{[Eq. A.3]}$$

From Eq. A.1a it follows that

$$\frac{\partial n}{\partial \theta_o} = -\sin\theta \frac{\partial x}{\partial \theta_o} + \cos\theta \frac{\partial y}{\partial \theta_o} \,. \qquad \text{[Eq. A.4]}$$

From Eq. 6c we know that

$$x = -\int_{\theta_o}^{\theta} \frac{c}{c'} d\theta \,. \qquad \text{[Eq. A.5]}$$

Partial differentiation with respect to θ_o of Eqs. A.5 and 12 (Snell's law) respectively provides

$$\frac{\partial x}{\partial \theta_o} = -\int_{\theta_o}^{\theta} \frac{\partial[\frac{c}{c'}]}{\partial \theta_o} d\theta + \frac{c_o}{c'_o} \qquad \text{[Eq. A.6a]}$$

$$\frac{\partial y}{\partial \theta_o} = \frac{c}{c'} \tan \theta_o \qquad \text{[Eq. A.6b]}$$

Because

$$\frac{\partial[\frac{c}{c'}]}{\partial \theta_o} = \frac{d[\frac{c}{c'}]}{dy} \frac{\partial y}{\partial \theta_o} = \frac{\partial[\frac{c}{c'}]}{\partial y} \frac{\partial y}{\partial \theta_o} \qquad \text{[Eq. A.7]}$$

it follows that

$$\frac{\partial x}{\partial \theta_o} = \frac{c_o}{c'_o} + \tan \theta_o \int_{x_o}^{x} \frac{c'^2 - cc''}{c'^2} dx \ . \qquad \text{[Eq. A.8]}$$

Substitution of Eqs. A.6 and A.8 in Eq. A.4 and substitution of this result in Eq. A.3 gives Eq. 22. This derivation of Eq. 22 is the most natural, since it is independent of the turning point and, in addition, proves the extension of Eq. 16 to Eq. 24.

DISCUSSION

It was suggested that some of the problems of calculating intensity along a single ray might be avoided by the use of a second order differential equation and the consideration of energy propagation along the ray.

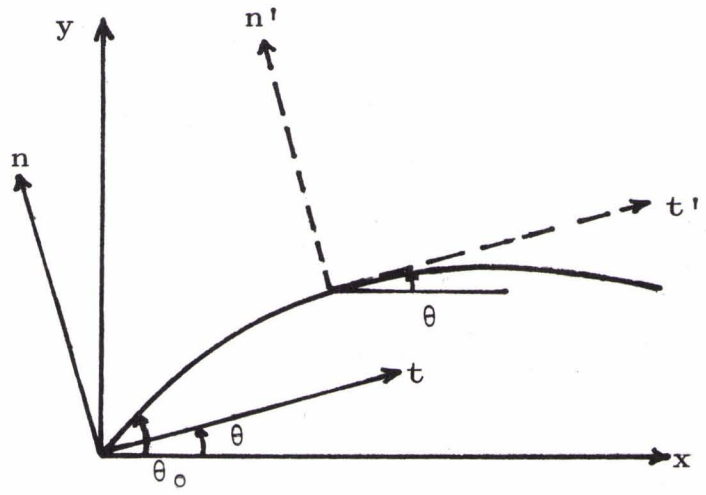

FIG. A.1

CALCULATION OF PROPAGATION LOSSES IN A MEDIUM WITH A VELOCITY PROFILE APPROXIMATED BY A NUMBER OF EPSTEIN PROFILES

by
T. Strarup
Danish Defence Research Establishment
Copenhagen, Denmark

ABSTRACT

This paper presents a digital ray-theory program, by which the ray trace, travel time and intensity can be calculated for velocity profiles approximated by a number of Epstein functions.

INTRODUCTION

In order to extract information from underwater acoustic propagation measurements the Danish Defence Research Establishment have started an investigation on calculation of propagation losses in a medium with a given sound velocity profile. The object is to calculate propagation losses with reasonable accuracy by a method which requires a limited computer capacity. In order to obtain reasonable accuracy by using relatively few approximating functions for the sound velocity profile, symmetrical Epstein profiles were chosen. In this way the profile approximation is a continuous function with a continuous first derivative and, moreover, the mathematical problems are much simplified, as will be seen in the following.

The problems related to the curve fitting procedure will not be mentioned here. At the moment the curve fits are made by means of a combined manual and digital procedure which, however, will be improved in the future at DDRE.

A SHORT DESCRIPTION OF THE PROGRAM

The first four figures show the capability of the program. Figure 1 is a plot of a velocity profile approximated by two Epstein functions which join at a depth of 40 m. Figure 2 shows the ray-trace from a transmitter placed at a depth of 5 m and with a beamwidth of 20°. The travel time at 900 m distance is shown in Fig. 3. The sign $\sim$ indicates the starting point, which corresponds to the steepest upgoing ray from the transmitter. The plot indicates four wave fronts arriving at $x = 900$ m with travel times $0.6345 < t < 0.6365$ s. Figure 4 shows the propagation losses at $x = 900$ m and at 1 kHz. They are calculated by a vectorial addition of the separate arrivals. A reflection coefficient of $r = 1$ is assumed at the surface, not in accordance with reality. However, it should be mentioned, that the program can accept an arbitrary value for r as well as an arbitrary radiation pattern from the transmitter.

In Fig. 5 is shown the mathematical expression for a symmetrical Epstein function and our definition of the ray-parameter p from Snell's law, which makes the mathematical expressions practical for both upgoing and downgoing rays.

Figures 6 and 7 show the simplicity of the mathematical formulae $x = f(z)$ and $t = f(x,z)$.

The above-mentioned formulae are valid only in the first quarter of a ray-trace period. Figure 8 shows how it is possible for an arbitrary x to transform x to a value where the formulae mentioned are valid.

An outline of the program is given in Fig. 9.

CONCLUSIONS

In a way there is no conclusion of this paper, so far. In order to obtain a conclusion, it is necessary to:

1. Compare some of our outputs with outputs from other ray-theory programs.
2. Investigate the computer capacity required by solving hard problems.
3. Finish the work concerning curve fitting.

DISCUSSION

In response to questions, the author explained the technique of fitting Epstein profiles to a given sound speed profile as first fitting the upper and lower portions, then the centre portion by an Epstein profile which preserved a continuous first derivative across the two boundaries. He found the display of depth, travel time, intensity, etc., as functions of range a convenient method of presenting the results, but had no strong feelings about this.

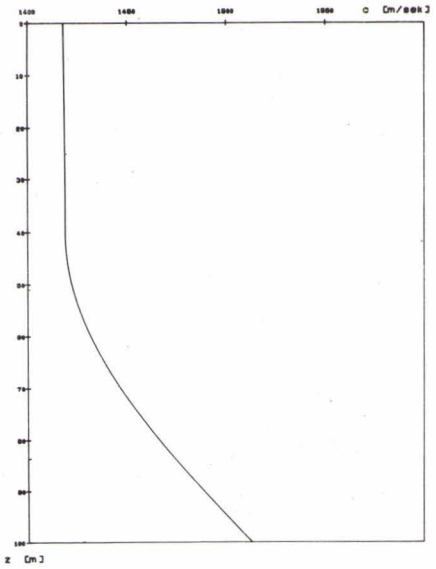

FIG. 1

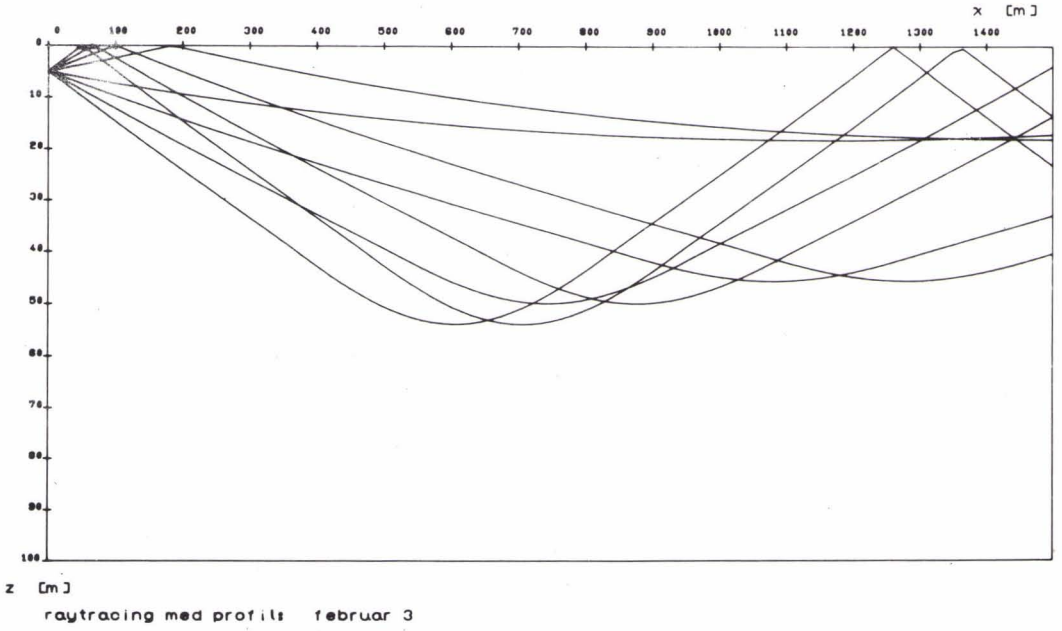

FIG. 2

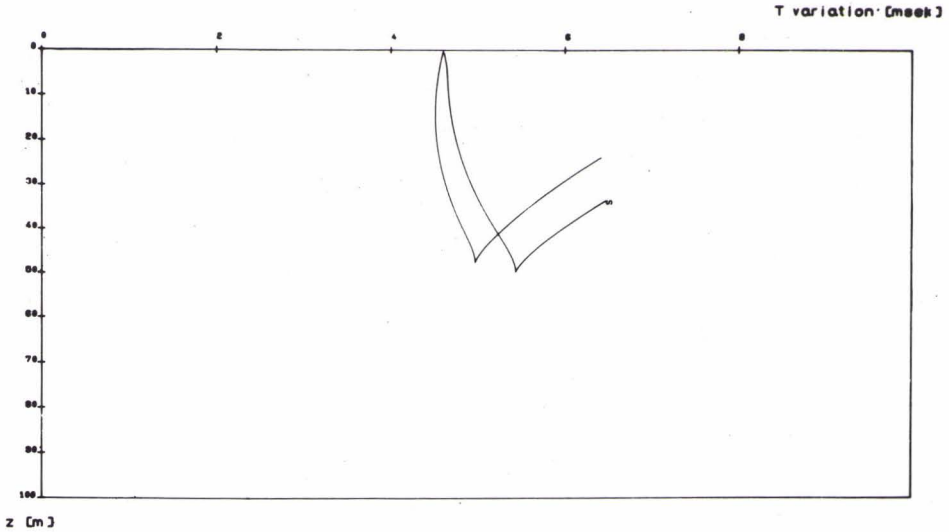

FIG. 3

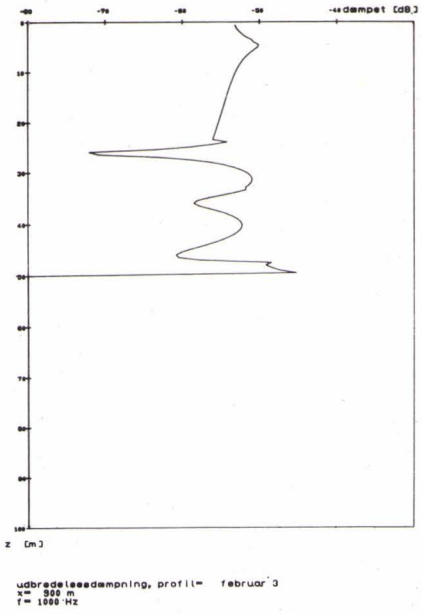

FIG. 4

The soundvelocity profile is approximated by a number of Epstein Profiles.

$$C_n(z) = \frac{1}{\sqrt{A_n \tanh^2 \frac{z - z_{c0}}{H_n} + B_n}}$$

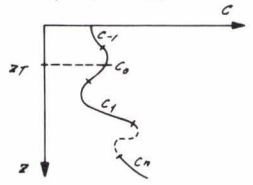

Snells law:

$$\frac{\sin\theta}{C_0} = \frac{\sin\theta_n}{C_n} = p$$

$p = \frac{\sin\theta_0}{C_0}$ for $0 < \theta_0 < \frac{\pi}{2}$ and

$p = -\frac{\sin\theta_0}{C_0}$ for $\frac{\pi}{2} < \theta_0 < \pi$

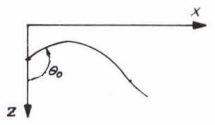

FIG. 5

$$x = p\int_{z_1}^{z} \frac{dz}{\sqrt{C(z)^{-2} - p^2}}$$

$$= p\int_{\sinh\frac{z_1 - z_0}{H}}^{\sinh\frac{z - z_0}{H}} \frac{du}{\sqrt{(A + B - p^2)u^2 + B - p^2}}$$

I: $B - p^2 > 0$ and $A + B - p^2 < 0$

$$x = \frac{pH}{b}\sin^{-1}\left(\frac{b}{a}\sinh\frac{z - z_0}{H}\right) - x_1$$

where $a = \sqrt{|B - p^2|}$ and

$b = \sqrt{|A + B - p^2|}$

II: $B - p^2 > 0$ and $A + B - p^2 > 0$

$$x = \frac{pH}{b}\sinh^{-1}\left(\frac{b}{a}\sinh\frac{z - z_0}{H}\right) - x_1$$

III: $B - p^2 < 0$ and $A + B - p^2 > 0$

$$x = \frac{pH}{b}\cosh^{-1}\left(\frac{b}{a}\sinh\frac{z - z_0}{H}\right) - x_1$$

FIG. 6

$$t = \int_{z_1}^{z} \frac{C(z)^{-2}}{\sqrt{C(z)^{-2} - p^2}}\, dz$$

$$= \frac{(A+B)}{|p|} x + \frac{pH}{|p|} \int_{\tanh\frac{z_1 - z_0}{H}}^{\tanh\frac{z-z_0}{H}} \frac{-A\, du}{\sqrt{Au^2 + B - p^2}}$$

FIG. 7

$$\underline{TI:\ A < 0}$$

$$t = \frac{A+B}{|p|} x + H\,\mathrm{sign}(p)\sqrt{|A|}\,\sin^{-1}\left(\sqrt{\frac{|A|}{|B-p^2|}}\,\tanh\frac{z-z_0}{H}\right) - t_1$$

$$\underline{TII:\ A > 0}$$

$$t = \frac{A+B}{|p|} x + H\,\mathrm{sign}(p)\sqrt{|A|}\,\sinh^{-1}\left(\sqrt{\frac{|A|}{|B-p^2|}}\,\tanh\frac{z-z_0}{H}\right) - t_1$$

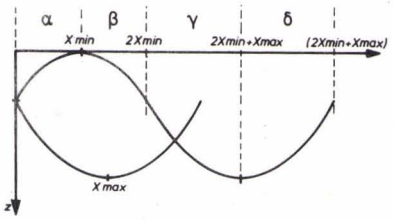

FIG. 8

Interval α :

$z(x) = \varphi(x)$

$t(x) = \psi(x)$

Interval β :

$z(x) = \varphi(2x_{min} - x)$

$t(x) = 2t_{min} - \psi(2x_{min} - x)$

Interval γ :

$z(x) = \varphi_0(x - 2x_{min})$

$t(x) = 2t_{min} + \psi_0(x - 2x_{min})$

Interval δ :

$z(x) = \varphi_0[2(x_{max} + x_{min}) - x]$

$t(x) = 2t_{min} + 2t_{max} - \psi_0[2(x_{max} + x_{min}) - x]$

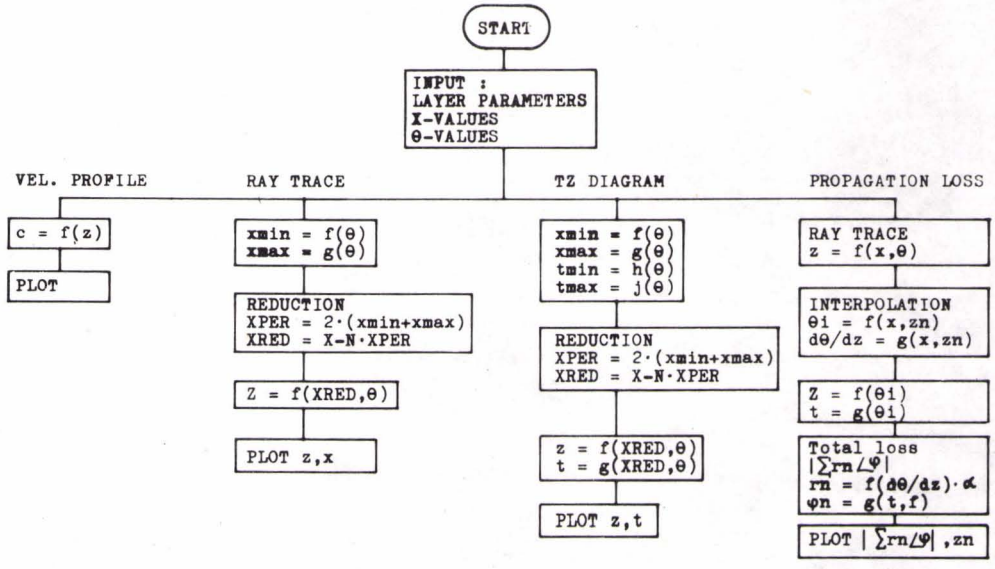

FIG. 9

OUTLINE

SENSITIVITY OF RAY THEORY TO INPUT DATA

by

J.L. Reeves
Department of the Navy
Naval Ship Systems Command
Sonar Research Directorate
Washington, D.C., U.S.

and

L.P. Solomon
Tetra Tech. Inc.
Arlington, Va., U.S.

ABSTRACT

Acoustic propagation problems which are solved using ray theory require certain input data. In particular, the source and receiver locations, sound-velocity field and bottom and surface conditions are required. Frequently, this data is known only to within certain confidence limits. Ray calculations are performed assuming that the input data is known to the required accuracy. A theory is presented which indicates the sensitivity of the calculations to small variations in the input data. The ray equation is characterized by a second-order ordinary differential equation; the intensity can be calculated along the particular ray directly. The necessity of having twice continuously differentiable velocity, surface and bottom profiles is clearly demonstrated in the theory. Specific examples are provided for specialized velocity profiles.

INTRODUCTION

The entire field of geometrical acoustics is expressed mathematically by the solutions associated with the first-order term in the

asymptotic expansion of the wave equation, where the expansion parameter is proportional to the inverse powers of the wavenumber, k. Inherent in any expansion procedure is an error analysis which will describe the range of applicability for the expansion. Ray theory provides an accurate approximation to the exact solutions of the wave equation so long as:

$$\frac{\delta \left(\frac{dc}{dz}\right)}{c/\lambda} \ll 1 \quad . \qquad \text{[Eq. 1]}$$

This expression indicates that the solution of the eikonal equation will be an excellent approximation to the wave equation if the fractional change in the velocity gradient over a wavelength is small compared with 1. It is clear that this condition will be satisfied if the frequencies are sufficiently high and, for present acoustic systems operating throughout the world, this condition is met with ease. Other problems can arise in using an approximate theory which are not themselves dependent upon the analytical techniques required to derive the theory; namely, the possible sensitivity which the theory has to errors in input data or boundary conditions. Any problem in underwater acoustic propagation requires a speed of sound curve, or velocity profile, as input. This velocity profile may be simple or complicated; the ray paths will behave accordingly. The question which must be posed and, in fact, which we have addressed ourselves to is: if there are errors in the description of the velocity profile, how will these errors affect the original solutions? Extremely simple models, which are characterized by linear differential equations, generally can be considered to have the following characteristics: small changes in the model or in the inputs will produce small changes in the results. With the more complicated models which are now available in underwater acoustics, this is not necessarily the case.

Ray theory requires the specification of a source and receiver point as well as the specification of the initial ray angle, θ_o. This angle may only be known to within certain limits. This will clearly

show up under both long and short ranges as an error in the transmission loss, phase, ray path, etc. It is our purpose to present here a simplified theory which will allow the calculation of errors due to input conditions given a technique to calculate the original "error free" solutions.

Section I will deal with various types of velocity profiles. Section II will present a technique to obtain the necessary information to generate the data analysis. Section III will develop a general model for calculating the sensitivity of the original error free model to variations in input data. Section IV will present the conclusions.

I. DISCUSSION OF VELOCITY PROFILES

Present models incorporate a number of analytical techniques for describing velocity profiles. In general, the use of certain of these functions gives rise to at least one engaging characteristic — the ray paths connected with the velocity profiles can be calculated from analytical functions. Specifically, velocity profiles have been described using the following techniques:

Constant Velocity

If the velocity is assumed to be constant, then the ray paths are straight lines. Errors could arise by assuming that the velocity is a different constant than originally specified. The time delay, or phase, will be in error, but the straight lines which are, in fact, the ray paths are dependent only upon the initial angle and source position and, therefore, are not dependent upon the numerical value which is selected. However, there can be errors introduced by incorrectly assigning values for source and receiver depths as well as initial ray angle.

Linear Velocity Profile

Linear velocity profiles lead to ray paths which are circular arcs. There are two errors which can arise in describing linear velocity profiles. They are, of course, the slope and the intercept. The ray paths will again be in error due to the error in initial ray angle and source placement. Phase arrival times will be in error.

Higher Order Velocity Profiles

Curvilinear velocity profiles can be characterized by hyperbolic cosines, parabolas and the Epstein profile, to name a few. All these profiles have a number of parameters which enable them to fit actual data; for example, the Epstein profile is a five-parameter profile each of which can be adjusted to give the best fit to actual data. Once these parameters are specified, then the ray paths are also known, since they are a function of the parameters of the velocity profile [Refs. 1 & 2].

It is clear that all the above-mentioned cases have certain difficulties associated with them. Generally, they are incapable of predicting certain variations in the velocity profile. For example, the Epstein profile has difficulty predicting surface ducts. Surface ducts are, of course, characterized by a local maximum in the velocity profile some distance beneath the surface. Another difficulty is that they are merely a best fit to the data and do not easily provide a technique for generating an error analysis.

Splines

Splines are a well known mathematical technique for generating smooth curves to fit data points. The technique is simply described by Ahlberg et al [Ref. 3]. The simplest non-trivial spline is a cubic. The technique is to assume (for example) that a cubic polynomial with unspecified coefficients would describe the curve

between two data points. Another cubic polynomial with unspecified coefficients would be employed between the next two data points. At the common data point, the function, its first and second derivatives are all required to be continuous. These conditions of continuity will be almost enough to provide a unique determination of the coefficients of the various polynomials. If there are N data points, then there would be N-1 cubic polynomials.

There are two conditions which have yet to be met and these are at the end points. Generally, it is assumed that the second derivatives outside the range of interest is zero. These two conditions will then be sufficient to determine all the coefficients. This is not a unique way of specifying the coefficients, but it will serve for purposes of example. A good property of splines is that they will allow for matching all input velocity points exactly. There is no "best fit". The drawbacks are unfortunate in that cubic polynomials lead to elliptic integrals which are not solvable in closed form.

All velocity profiles discussed already have been assumed to be functions of depth only. If it is required that the velocity structure be represented as a function of depth and range, then the only technique which is readily applicable is the spline function. The theory of two-dimensional splines is well known and understood and, in fact, is directly applicable to this problem.

II. DIFFERENTIAL EQUATIONS FOR THE MODELS

Ray Paths

A description of the ray paths comes from the solution of the eikonal equation. In fact, the ray paths are the trace of the normal to the wave front as it proceeds through the medium. Since the eikonal equation is difficult to solve, another formulation has been employed: Fermat's Principle of Least Time. This leads directly

to Euler's equation which implies that the extremals will satisfy a particular differential equation.

$$\frac{d}{dx}\left[\frac{f(x,z)\,z'}{\sqrt{1+z'^2}}\right] = \frac{\partial f}{\partial z}\sqrt{1+z'^2} \qquad \text{[Eq. 2]}$$

where $f(x,z)$ is given by:

$$f(x,z) = \frac{1}{c(x,z)} \qquad \text{[Eq. 3]}$$

where $c(x,z)$ is the velocity field.

Carrying out the indicated operations leads to:

$$z'' = \frac{1+z'^2}{f}\,(f_z - z' f_x)\ . \qquad \text{[Eq. 4]}$$

The subscript notation for partial derivatives is employed, viz.,

$$\frac{\partial f}{\partial z} = f_z, \text{ etc.}$$

The initial conditions for the path are:

$$\begin{aligned} z(0; z_o, \theta_o) &= z_o \\ z'(0; z_o, \theta_o) &= \tan\theta_o \end{aligned} \qquad \text{[Eq. 5]}$$

where z_o and θ_o are the source depth and initial ray angle, respectively. This formulation is described in detail by Solomon and Armijo [Ref. 4]. Arc length and travel time can be calculated through quadrature.

Intensity

Calculation of the intensity is, in most cases, of primary interest in acoustic propagation problems. In general, if variation in

intensity is assumed to be only due to geometrical spreading, then the intensity is given by:

$$\frac{I(x)}{I_0} = \frac{1}{x} \cdot \frac{\cos \theta_0}{\cos \theta} \cdot \frac{1}{\partial z / \partial \theta_0} \qquad \text{[Eq. 6]}$$

where x is the range and θ is the local ray angle measured with respect to the horizontal.

The difficulty in calculating the intensity is easily seen to be the calculation of the function $\partial z / \partial \theta_0$.

If the ray paths are represented by simple functions, then this derivative may be calculated directly. In general, however, the problems are many and many models approximate this function at any range by using:

$$\frac{\partial z}{\partial \theta_0} \approx \frac{\delta z}{\delta \theta_0} \qquad \text{[Eq. 7]}$$

where δz is the difference $z(x; z_0, \theta_0 + \delta\theta_0) - z(x; z_0, \theta_0)$ calculated from both ray paths at a particular range. This technique is numerically acceptable if the two rays remain in close proximity to one another and if roundoff errors are negligible. Unfortunately, neither requirement is true for either long range calculations or rays that reflect many times from the bottom. Furthermore, the technique is undesirable because it requires the calculation of an extra ray path for each ray which is traced to a neighbourhood of the receiver.

Solomon and Armijo [Ref. 4] have demonstrated that it is a simple task to calculate the intensity directly along a ray path. In order to do so, they show that it is necessary to calculate the partial derivative $\partial z / \partial \theta_0$.

They define the function:

$$\zeta(x; z_0, \theta_0) = \frac{\partial}{\partial \theta_0} z(x; z_0, \theta_0) \quad . \qquad \text{[Eq. 8]}$$

Differentiating the ray path equation with respect to the parameter θ_o and making the appropriate substitutions yields the second order linear differential equation for ζ:

$$\zeta'' = \left[\frac{2z'z''}{1+z'^2} - (1+z'^2)\frac{f_x}{f}\right]\zeta'$$

$$+ \left[\frac{1+z'^2}{f}(f_{zz} - z'f_{xz}) - z''\frac{f_z}{f}\right]\zeta \ . \qquad \text{[Eq. 9]}$$

The initial conditions for Eq. 9 are:

$$\zeta(0;z_o, \theta_o) = 0$$
$$\zeta'(0;z_o, \theta_o) = \sec^2 \theta_o \ . \qquad \text{[Eq. 10]}$$

The calculation of intensity is now reduced to the problem of solving Eq. 4 with the initial conditions of Eq. 5. The numerical solution of Eq. 4 is certainly no more difficult than tracing an additional ray and the needless approximation of Eq. 7 has been removed. The numerical procedures for solving systems of ordinary differential equations may now be applied to the simultaneous determination of both z and ζ from the differential Eqs. 4 and 9. Since both differential equations are second order, the combined problem is equivalent to a system of four first order differential equations. After employing one of the several available numerical techniques to solve this system, the intensity may be calculated anywhere along the ray path from Eqs. 6 and 8.

IV. SENSITIVITY TO INPUT DATA

Inputs

All acoustic propagation models are obliged to accept certain input data. This model assumes that mean data is provided with some estimate of error as well. For example, the input with some tolerance could be provided. The model requires, therefore,

the following input data:

1. Velocity as a function of depth (and conceivably range).
2. Input angles.
3. Source and receiver positions.
4. Bottom profile (as well as reflection coefficients).

General Theory

The ray paths are assumed to be described by:

$$z'' = \frac{(1+z'^2)}{f}\,[f_z - z' f_x] \qquad \text{[Eq. 11]}$$

where

$$f(z,x) = \frac{1}{c(z,x)} \quad . \qquad \text{[Eq. 12]}$$

Assume that the ambient solution is $z_0(x)$ and this is related to the ambient speed of sound velocity profile $f_0(z,x)$.

Further, let us assume that

$$f(z,x) = f_0(z,x)\,[1+\varepsilon(z,x)] \; . \qquad \text{[Eq. 13]}$$

The error function will be related to the error in $z_0(x)$. That is:

$$z(x) = z_0(x) + \Delta(x) \; . \qquad \text{[Eq. 14]}$$

The boundary conditions are at $x=0$

$$\begin{aligned} z &= z_0, \Delta = 0 \\ z' &= \tan\theta_0 = z_0', \; \Delta' = 0 \; . \end{aligned} \qquad \text{[Eq. 15]}$$

This is where initial angle error arrives. Clearly $z_0(x)$ satisfies

$$z_0'' = \frac{1+z_0'^2}{f_0}\,[f_{0z} - z_0' f_{0x}] \; . \qquad \text{[Eq. 16]}$$

Clearly, since $z(x)$ satisfies Eq. 11 and $z_o(x)$ satisfies Eq. 16, an equation for $\Delta(x)$ must satisfy some relationship. Substitution of Eq. 14 into Eq. 11 and making use of Eq. 16 and assuming that a linearization procedure is possible, the relationship which $\Delta(x)$ must satisfy is:

$$\Delta'' = -\Delta' \{(1 + z_o'^2) \frac{f_{ox}}{f_o} + \frac{2z_o'}{f_o} (f_{oz} - z_o' f_{ox})\} + (\varepsilon_z - z_o' \varepsilon_x)(1 + z_o'^2) . \qquad \text{[Eq. 17]}$$

A similar expansion can be provided for the intensity.

It will be recalled that ζ (and ζ_o) satisfy

$$\zeta' = [\frac{2z'z''}{1+z'^2} - (1 + z'^2) \frac{fx}{f}] \zeta' + [\frac{1+z'^2}{f} (f_{zz} - z' f_{xz}) - \frac{z'' f_z}{f}] \zeta \qquad \text{[Eq. 18]}$$

with the conditions

$$\zeta(0) = 0$$
$$\zeta'(0) = \sec^2 \theta_o \qquad \text{[Eq. 19]}$$

similarly to the perturbation expansion for $z(x)$, we will assume that $\zeta(x)$ may be written as

$$\zeta(x) = \zeta_o(x) + \varkappa(x) \qquad \text{[Eq. 20]}$$

substitution of Eqs. 20, 13 and 14, and expanding, keeping only first order terms gives rise to

$$\varkappa'' = A_o \varkappa' + B_o \varkappa + A_1 \zeta_o' + B_1 \zeta_o \qquad \text{[Eq. 21]}$$

where A_o, B_o, A_1, B_1 are given by

$$A_o = \frac{2z_o' z_o''}{1+z_o'^2} - (1 + z_o'^2) \frac{f_{ox}}{f_o} \qquad \text{[Eq. 22a]}$$

$$B_o = (1 + z_o'^2)[\frac{f_{ozz} - z_o' f_{oxz}}{f_o}] - \frac{z_o'' f_{oz}}{f_o} \qquad \text{[Eq. 22b]}$$

$$A_1 = \frac{2}{1+z_o'^2}\left[\frac{(1-z_o'^2)\,z_o''\,\Delta'}{(1+z_o'^2)} + z_o'\,\Delta''\right] - \frac{2\Delta' z_o' f_{ox}}{f_o} - \epsilon_x(1+z_o'^2)\,. \qquad \text{[Eq. 22c]}$$

$$B_1 = \epsilon_z \frac{(1+z_o'^2)}{f_o}\cdot[(2f_{oz} - z'f_{ox}) - z_o''] - \epsilon_x\, z_o'(1+z'^2)\frac{f_{oz}}{f_o} - \Delta'\left[(1+3z_o'^2)\frac{f_{oxz}}{f_o} - 2z_o'\frac{f_{ozz}}{f_o}\right] + \epsilon_{zz}[1+z_o'^2] - \epsilon_{xz}[z_o'(1+z_o'^2)] - \Delta''\frac{f_{oz}}{f_o}\,. \qquad \text{[Eq. 22d]}$$

It is clear that $\eta(x)$ satisfies an ordinary differential equation which is non-homogeneous. The non-homogeneous term or forcing function is dependent upon the ray path and its perturbations, and the speed of sound and its perturbations. It is further seen that finding exact solutions to Eq. 21 are extremely difficult. Let us now investigate certain special cases.

Special Cases

Case 1:

Assume

$$f_o = \text{constant}\,. \qquad \text{[Eq. 23]}$$

Then:

$$z_o(x) = x\tan\theta_o \qquad \text{[Eq. 24]}$$

$$\Delta(0) = \Delta'(0) = 0\,. \qquad \text{[Eq. 25]}$$

Let us further assume that there is no error in x, thus,

$$\epsilon_x = 0\,. \qquad \text{[Eq. 26]}$$

And assume that the error in depth is given by:

$$\epsilon = \alpha z\,. \qquad \text{[Eq. 27]}$$

This leads to

$$\Delta(x) = \alpha\cdot\sec^2\theta_o\frac{x^2}{2}\,. \qquad \text{[Eq. 28]}$$

The appropriate boundary conditions are at $x = 0$

$$\begin{aligned} z_o(0) &= z_o \\ z(0) &= z_o + \Delta_o \\ \Delta(0) &= \Delta_o \end{aligned} \qquad \text{[Eq. 29]}$$

The error in initial angle we represent as:

$$\begin{aligned} \theta(0) &= \theta_o + \chi \\ z_o'(0) &= \tan \theta_o \ . \end{aligned} \qquad \text{[Eq. 30]}$$

This corresponds to:

$$z'(0) = z_o'(0) + \Delta'(0) \ . \qquad \text{[Eq. 31]}$$

Further,

$$\tan(\theta_o + \chi) = \tan \theta_o + \Delta'(0), \qquad \text{[Eq. 32]}$$

which leads to:

$$\Delta'(0) = \Delta_o' = \frac{\tan \chi \, (1 - \tan^2 \theta_o)}{1 - \tan \theta_o \tan \chi} \ . \qquad \text{[Eq. 33]}$$

Thus, the correct solution for the error $\Delta(x)$ including errors in initial position and ray angle as well as velocity profile error, is given by:

$$\Delta(x) = \Delta_o + \Delta_o' x + \frac{\alpha x^2}{2} \sec^2 \theta_o \ . \qquad \text{[Eq. 34]}$$

Utilization of Eq. 21 will allow us to calculate error in calculating the intensity. Recall that

$$\zeta_o = \frac{\partial z_o}{\partial \theta_o} = x \sec^2 \theta_o \ . \qquad \text{[Eq. 35]}$$

Then,

$$\varkappa'' = 2 \sin \theta_o \sec^7 \theta_o \ . \qquad \text{[Eq. 36]}$$

The boundary conditions on $\varkappa(x)$ are:

$$\varkappa(0) = 0$$

$$\varkappa'(0) = \sec^2(\theta_o + \chi) - \sec^2\theta_o = \varkappa_o' \ . \qquad \text{[Eq. 37]}$$

Thus

$$\varkappa(x) = \varkappa_o' x + \alpha x^2 \sin\theta_o \sec^7\theta_o \ . \qquad \text{[Eq. 38]}$$

Case 2:

Assume that

$$f_o(x, z) = f_o(z) \ . \qquad \text{[Eq. 39]}$$

Then $z_o(x)$ satisfies:

$$z_o''(x) = (1 + z_o'^2)\frac{f_{oz}}{f} \ . \qquad \text{[Eq. 40]}$$

If we let $f_o(z)$ be given by

$$f_o(z) = (\alpha z)^{-1} \qquad \text{[Eq. 41]}$$

then the paths are circular arcs.

In particular, $z_o(x)$ is given by:

$$z_o^2(x) = z_o^2(0)\sec^2\theta_o - (x + z_o(0)\tan\theta_o)^2 \ . \qquad \text{[Eq. 42]}$$

The error in the ray path $\Delta(x)$ must then satisfy

$$\Delta''(x) = -\Delta'(x)[\alpha_1 + 2\alpha_2 x] + [\epsilon_z - z_o'\epsilon_x][1 + z_o'^2] \qquad \text{[Eq. 43]}$$

where,

$$a_o = z_o^2(0), \quad a_1 = -2z_o(0)\tan\theta_o, \quad a_2 = -1 \ . \qquad \text{[Eq. 44]}$$

The homogeneous solution to Eq. 43 is:

$$\Delta_H(x) = \frac{\sqrt{\pi}}{2}\frac{\Delta_H'(0)}{\alpha}\,\mathrm{erf}(\alpha x) + \Delta_H(0) \ . \qquad \text{[Eq. 45]}$$

And the total solution is given by:

$$\Delta(x) = \frac{\sqrt{\pi}}{2} \frac{\Delta'_H(0)}{\alpha} \operatorname{erf}(\alpha x) + \Delta_{particular} \ . \qquad \text{[Eq. 46]}$$

Let us assume that:

$$\varepsilon(z, x) = \varepsilon(z) \ . \qquad \text{[Eq. 47]}$$

This assumption leads to:

$$\varepsilon_x = 0 \ . \qquad \text{[Eq. 48]}$$

Furthermore, assume that

$$\varepsilon_z = \text{constant} = \beta \ . \qquad \text{[Eq. 49]}$$

The particular solution is in the form:

$$\Delta_{particular} = x^2 \sum b_n x^n \ . \qquad \text{[Eq. 50]}$$

The recursion relationship for the coefficients is:

$$b_{n+2}(n+4)(n+3) + a_1 b_{n+1}(n+3) + 2a_2 b_n (n+2) = 0 \ . \qquad \text{[Eq. 51]}$$

In particular, the first few coefficients are given:

$$b_0 = \beta \tilde{A}_0 / 2 \qquad \text{[Eq. 52a]}$$

$$b_1 = \frac{\beta[\tilde{A}_1 - a_1 \tilde{A}_0]}{6} \qquad \text{[Eq. 52b]}$$

$$b_2 = \frac{\beta \tilde{A}_2 - \frac{a_1}{2} \beta(\tilde{A}_1 - a_1 \tilde{A}_0) - 2a_2 \beta \tilde{A}_0}{12} \qquad \text{[Eq. 52c]}$$

where:

$$\begin{aligned} \tilde{A}_0 &= 4a_0 + a_1^2 \\ \tilde{A}_1 &= 4a_1 + 4a_2 a_1 \\ \tilde{A}_2 &= 4a_2(1 + a_2) \ . \end{aligned} \qquad \text{[Eq. 53]}$$

Thus, the complete solution for $\Delta(x)$ is given by:

$$\Delta(x) \frac{\sqrt{\pi}\Delta'(0)}{2\alpha} \operatorname{erf}(\alpha x) + \Delta(0) + x^2 \sum b_n x^n \ . \qquad \text{[Eq. 54]}$$

To sum up, we have solved the special case where:

$$\varepsilon(z) = \beta z \qquad \Delta(0) = \Delta_0$$
$$f_0(z) = (\alpha z)^{-1} \qquad \Delta'(0) = \frac{\chi(1 - \tan^2 \theta_0)}{1 - \chi \tan \theta_0} \ . \qquad \text{[Eq. 55]}$$

The limiting cases lead to:

$$\alpha x \to \infty: \ \Delta(x) \to \frac{\Delta'(0)}{\alpha} + \Delta(0) + x^2 \sum b_n x^n \qquad \text{[Eq. 56]}$$

$$\alpha x \to 0: \ \Delta(x) \to \Delta'(0)\, x + \Delta(0) + x^2 \sum b_n x^n \ . \qquad \text{[Eq. 57]}$$

The procedure for calculating $\varkappa(x)$ is straightforward, but rather tedious.

V. CONCLUSIONS

This model is presented as a simple procedure for attempting to understand the effects of error in input data on ray path calculations. It is quite clear that these effects are not necessarily small nor can they be considered irrelevant. It is suggested that this formulation of the acoustic propagation model has within it the seeds for a full-scale deterministic model which can then predict in a uniquely defined manner the problems and effects of errors inputs. Furthermore, this technique may be of utility in attempting to analyse a deterministic-stochastic model where the error inputs are provided in a statistical manner. It seems clear that this model would be applicable if the means of the individual inputs could be considered to be deterministic by utilizing our techniques and then using the model; a probability density function could be derived by considering the interaction of the probability functions of the input.

REFERENCES

1. M. Pedersen and D. Gordon, "Comparison of Curvilinear and Linear Profile Approximation in the Calculation of Underwater Sound Intensities by Ray Theory", J. Acoust. Soc. Am., Vol. 41, No. 2, pp 419-438, February 1967.

2. M. Pedersen and De Wayne White, "Ray Theory of the General Epstein Profile", J. Acoust. Soc. Am., Vol. 44, No. 3, pp 765-787, September 1968.

3. J.H. Ahlberg, E.N. Nilsin, and J.L. Walsh, "The Theory of Splines and their Applications", Academic Press, New York, 1967.

4. L.P. Solomon and L. Armijo, "An Intensity Differential Equation in Ray Acoustics". To be published in J. Acoust. Soc. Am., September 1971.

DISCUSSION

The second author stated that this perturbation method avoided the necessity of recalculating the ray path for each perturbation. In this way it conformed to standard perturbation techniques. In reply to a further question regarding whether the effect of perturbation was more marked in areas of low sound speed gradient, he remarked that as these methods had not been programmed yet the answer to this and similar general queries was still unknown.

SESSION 3

COMPARISON OF EXPERIMENTS WITH RAY TRACING COMPUTATIONS

Session Chairman : R. Laval

Session Secretary : J.H. Stockhausen

THEORETICAL CALCULATION OF TRANSMISSION LOSS IN THE OCEAN

by

A. Aubell
Norwegian Defence Research Establishment
Horten, Norway

SUMMARY

The topic that is dealt with in this paper is a method for computation of acoustic transmission loss by sound propagation in the ocean. The method is based on the ray theory which is used in connection with an acoustic model of the ocean, the parameters of which are approximated by mathematical expressions. On this basis formulae for ray path coordinates and intensity are developed. Some computer programs have been written to carry out the numerical calculations. Results of this mathematical method are compared with practical measurements.

INTRODUCTION

Prediction of sound transmission conditions in the sea is frequently required, be it for high sonar frequencies and short ranges as well as for the low frequencies used in long range sonar and in long range passive detection systems. To meet this requirement it is first of all necessary to construct a model of the ocean comprising all the parameters which are significant for sound propagation. This work has been concerned with the task of construcing such a model. Its parameters are expressed mathematically in order to simplify the calculations. Some approximations are thereby introduced because the ocean is too complex to be completely described by mathematical laws. There are parameters which cannot be taken into account at all.

From a transmission point of view the basic parameters of a sea area are the bathymetry and the hydrographic conditions expressed by the sound velocity distribution. The acoustic properties of the ocean bottom are also of considerable interest because transmission by reflected ray paths plays an important part in many cases. Equally important for reflected paths is the scattering effect of the corrugated sea surface. Finally, high frequency signals are considerably attenuated due to energy absorption in the water volume.

According to the points of view briefly outlined above the calculation of sound propagation and sound intensity is carried out under consideration of the following laws and parameters [Fig. 1]:

a. The law of geometric spreading formulated by the ray theory.

b. Vertical and horizontal sound velocity distributions.

c. Bottom topography.

d. Energy loss by bottom reflection dependent on frequency and angle of incidence.

e. Energy absorption in the water volume dependent on frequency.

f. Energy scattering loss by reflection from the sea surface dependent on frequency and sea state.

The effects of reverberation and short-time variation of the hydrographic conditions are ignored.

BASIC FORMULAE

At this point the basic formulae for propagation and intensity ought to be reviewed [Fig. 2]. The ray path coordinates and the intensity are expressed by the well-known formulae [Ref. 1]

$$x_i = \int_{z_i}^{z_{i+1}} \frac{dz}{\sqrt{\frac{c_m^2}{c^2(z)} - 1}} \quad , \qquad \text{[Eq. 1]}$$

where c_m = constant = $\dfrac{c(z_i)}{\cos \Phi_i}$,

and where x_i is the step in the horizontal direction taken by the ray between the depths z_i and z_{i+1} .

Sometimes the propagation time is of interest. It may be expressed by

$$t_i = \frac{\cos \Phi_i}{c(z_i)} \cdot \left(x_i + \int_{z_i}^{z_{i+1}} \sqrt{\frac{c_m^2}{c^2(z)} - 1} \; dz \right) \qquad \text{[Eq. 2]}$$

Referring to Fig. 2, if there is a source at the point $(0, z_i)$ and the intensity of the source at unit distance is P, then the intensity I at the point (x_i, z_{i+1}) may be expressed by

$$\frac{I}{P} = \frac{\cos \Phi_i}{x_i \cdot \left| \frac{\partial x_i}{\partial \Phi_i} \right| \cdot \left| \sin \Phi_{x_i} \right|} \qquad \text{[Eq. 3]}$$

In the case of a number of n layers z_i and consequently $(n-1)$ steps x_i between two depths z_1 and z_2 , Eq. 2 may be developed in the form

$$\frac{I}{P} = \frac{\cos^2 \Phi_i}{\sum_{1}^{n-1} x_i \cdot \left| \sin \Phi_1 \right| \cdot \left| \sum_{1}^{n-1} \left[x_i + \int_{z_i}^{z_{i+1}} \frac{dz}{\left(\sqrt{\frac{c_m^2}{c^2(z)} - 1} \right)^3} \right] \right| \cdot \left| \sin \Phi_2 \right|} \qquad \text{[Eq. 4]}$$

MATHEMATICAL APPROXIMATION TO SOUND VELOCITY PROFILE

Considering Eq. 1, it may be integrated if the integrand, for example, can be brought into the form

$$\frac{1}{\sqrt{A + 2Bz + Cz^2}} \quad .$$

The horizontal step x_i, the intensity and propagation time can then be expressed by fixed integrals. Here the function $c(z)$ expresses the vertical sound velocity distribution. It is not possible, in general, to describe a complete depth-velocity profile by means of a single mathematical expression. The method used here [Refs. 2 and 3], is to divide the profile into segments and to make a curvilinear approximation to each segment by means of a quadratic equation, viz.,

$$\frac{1}{c^2(z)} = A1_i\, z^2 + A2_i\, z + A3_i \quad . \qquad \text{[Eq. 5]}$$

The coefficients are valid for the segment between the levels z_i and z_{i+1} [Fig. 3]. Differentiation of Eq. 5 with respect to z gives the sound velocity gradient g_i:

$$-2\frac{g_i}{c^3(z)} = 2A1_i\, z + A2_i \qquad \text{[Eq. 6]}$$

where $g_i = \frac{dc(z)}{dz}$ at the depth z_i .

The approximation is performed in such a way that the sound velocity gradient at the levels z_i and z_{i+1} is preserved. The velocity at z_i is chosen as the third parameter. To determine the coefficients A1, A2 and A3, then, one equation of the form [Eq. 5] and two of the form [Eq. 6] are used. The velocity at the level z_{i+1} is computed and used as the known sound velocity for the next segment.

One result of this procedure is presented in Fig. 4. It shows a measured sound velocity profile and the corresponding calculated approximation. The total depth is divided into 17 layers. A maximum error of 0.50 m/s occurs at 15 m depth. For the rest of the curve the error is less than the accuracy with which the sound velocity is measured.

MATHEMATICAL APPROXIMATION TO THE BOTTOM PROFILE

Propagation of sound energy via ray paths which are reflected from the ocean floor contributes to the energy transmission between two positions. Compared with direct going paths, however, this contribution is reduced because the reflection process is associated with energy loss. The loss is a function of the frequency and of angle of incidence. In order to evaluate the influence of a reflected wave, therefore, it is important to know the slope of the bottom at the point of incidence. It is an advantage if the bottom profile can be described mathematically with sufficient accuracy, because then the slope can be found by simple differentiation of some mathematical expression.

An idea which immediately suggests itself is to divide the bottom profile into segments. Considering Fig. 5 there are 4 parameters at disposal for each segment, viz., the depths and the slopes at distances x_i and x_{i+1}. It is thus possible to use a polynomial with 4 coefficients as an approximation to the measured profile, i.e, a third degree polynomial

$$y = B1_i x^3 + B2_i x^2 + B3_i x + B4_i \quad . \qquad [Eq. 7]$$

There will be a set of coefficients belonging to each value of i. The bottom ordinates are denoted by y to avoid confusion with ray path ordinates.

The example in Fig. 6 shows a measured and the corresponding computed profile. The difference between the two curves is insignificant, i.e., it is nowhere greater than about 1 m.

BOTTOM REFLECTION LOSS

The importance of the loss caused by reflection from the bottom has been briefly mentioned earlier. The loss as a function of frequency and angle of incidence (or of grazing angle) depends on the properties of the bottom and will in general vary from one locaility to another. Thus, for example the reflectivities of rock, sand and layered sediments will differ. However, a discussion of the reflectivity as a function of bottom material is outside the scope of this paper. We will study some type of loss curve and try to approximate it by mathematical expressions. Then, at a specified frequency and angle of incidence the reflection loss can be easily found.

We may, for example, consider the loss as a function of grazing angle given in Fig. 7. It represents measured loss in the frequency band 600 Hz - 1200 Hz. A little investigation shows that two parabolas will be a very good approximation to the measured curve, as shown in Fig. 8. The equations for the parabolas are:

$$0^\circ - 40^\circ : \quad \alpha = 11.247\ \Phi^2$$
$$40^\circ - 90^\circ : \quad \alpha = -6.039\ \Phi^2 + 20.072\ \Phi - 5.590 \quad ,$$

where the grazing angle Φ is expressed in radians. Thus, for the frequency band 600 Hz - 1200 Hz and for the sea area where the loss was measured the two parabolas will give the bottom reflection loss per bounce. In an area where the type of bottom varies, several such loss functions may be used.

SURFACE SCATTERING LOSS

In the case when the sound energy is propagating upwards and makes contact with the sea surface the transmission will be influenced by the sea state. The energy will be scattered. The extent to which the scattering takes place is also dependent on the frequency. The problem is dealt with by many authors.

What we want here is a function or a set of functions expressing the surface scattering loss dependence on frequency, wave height and angle of incidence. Such data were not available at the time when this work was done. The only result that seemed to be useful was a curve theoretically computed by Marsh, Shulkin and Kneale [Ref. 4], giving the loss per surface bounce as a function of a frequency-wave height parameter. It does not express any dependence on the geometry of source and receiver. The curve, which is reproduced in Fig. 9, is used in this work although it is based on criticized assumptions. It is easy, in any case, to replace this loss function by more reliable data as soon as they are available. For practical use the curve is redrawn in Fig. 10 with a frequency scale corresponding to wave height $h = 3$ (sea state 3).

It is seen that the curve approximates a hyperbola. If the frequency is denoted by f and the loss by α_s, then the hyperbola can be expressed by

$$-f^2 + C\alpha_s^2 + 2Df + 2E\alpha_s + F = 0 \qquad \text{[Eq. 8]}$$

In Fig. 10 this expression is valid above the frequency 500 Hz. In the range 0 - 500 Hz the loss is assumed to be zero. For each value of wave height h there is a set of values of the constants C, D, E and F. For $h = 3$ ft and expression for α_s is

$$\alpha_s = -0.9375 + \sqrt{1.7226 - 3.375\ 10^{-3} f + 3.375\ 10^{-6} f^2}$$

ABSORPTION LOSS IN SEA WATER

The absorption of sound energy in sea water is dealt with by many authors. In Ref. 5, for example it is suggested that the following formula should be used for practical computations of the loss (dB/m):

$$\alpha_{abs} = \left(\frac{S\,A\,f_T\,f^2}{f_T^2 + f^2} + \frac{B\,f^2}{f_T^2}\right) \cdot (1 - 6.54\,10^{-4}\,P)\ 8.686 \qquad \text{[Eq. 9]}$$

In Eq. 9, A is constant, $2.34\ 10^{-6}$, S is salinity in parts per thousand, f_T is the temperature-dependent relaxation frequency in kHz at atmospheric pressure, $21.9\ 10^{\left(6 - \frac{1520}{T + 273}\right)}$, where T is in °C, f is the acoustic frequency in kHz, B is approximately

a constant for the viscosity mechanism, $3.38\ 10^{-6}$, and P is the pressure in kg/cm^2.

It is shown in Ref. 6 that this formula gives too small values for the attenuation at low frequencies.

The absorption problem is extensively treated in Ref. 7 where the loss is expressed by

$$\alpha_{abs} = 0.006\ f^2 + \frac{0.155\ f_r\ f^2}{f_r^{\ 2} + f^2} \qquad \text{[Eq. 10]}$$

where α_{abs} is in decibels per km, the signal frequency f is in kHz and $f_r = 1.7$ kHz. The term $0.006\ f^2$ represents the absorption of magnesium sulphate relaxation. The second term accounts for a relaxation process at 1.7 kHz. In this work the absorption loss is taken into account by using Eq. 10 and expressing the distance in metres and the frequencies in Hz, giving the absorption loss in dB/m as

$$\alpha_{abs} = 10^{-9}\ (0.006 + \frac{155\ f_r}{f_r^{\ 2} + f^2})\ f^2 \qquad \text{[Eq. 11]}$$

NUMERICAL COMPUTATION

General

Numerical computation of ray path coordinates, intensities and transmission loss is carried out by means of a system of 4 FORTAN programs. The first performs the curvilinear approximation to the measured depth-velocity profiles. The second program computes the coefficients of the third degree polynomials which are used as approximation to the bottom profile. The results of these two programs are checked before they are inserted into further calculations.

Generally, for a given number N of bottom reflections, four possible ray paths exist between a source and a receiver located at depth in the sea. In addition to the reflected paths there may be refracted paths. A third program computes the angles of emission at the source corresponding to the values of N, bathymetry and distances between source and receiver.

The fourth and main program, IRATRA, is based on the mathematical expressions dealt with earlier. Some of the variables and parameters used in the main program are obtained from the results of the preceding three programs. In addition, several other data are introduced, for example number of layers, signal frequency, wave height, horizontal variation of the sound velocity. The main program also comprises three sub-programs which, when called, produce the values of absorption, scattering and reflection losses.

The output of the main program may comprise values for the ray path coordinates, the ray angle, the propagation time, the intensity and the bathymetry between source and receiver. In addition, at each specific distance the program may sum up the amounts of energy which have propagated along all ray paths and present the result as the transmission loss for the signal frequency and sea state in question.

one of the many details of the computing precedure in IRATRA will be discussed below.

Calculation of the Ray Path Coordinates

It was shown earlier that the expression

$$\frac{1}{\sqrt{\frac{c_m^2}{c^2(z)} - 1}}$$

could be brought into the form

$$\frac{1}{\sqrt{A + 2Bz + Cz^2}}$$

by expressing $1/c^2(z)$ as $A1\,z^2 + A2\,z + A3$. It is remembered that $c_m = c_0/\cos\varphi_0$. This gives

$$\frac{c_m^2}{c^2(z)} - 1 = c_m^2\,A1\,z^2 + c_m^2\,A2\,z + c_m^2\,A3 - 1$$

from which we obtain

$$A = c_m^2\, A3 - 1$$
$$B = 0.5\, c_m^2\, A2$$
$$C \quad 2 \quad c_m^2\, A1$$

The integration

$$\int \frac{dz}{\sqrt{A + 2Bz + Cz^2}}$$

may have the following results:

$$\text{(i)} \quad \frac{1}{\sqrt{C}} \ln\left(B + Cz + \sqrt{C} \cdot \sqrt{A + 2Bz + Cz^2}\right) + K, \quad C > 0$$

$$\text{(ii)} \quad \frac{1}{\sqrt{C}} \operatorname{arsinh} \frac{B + Cz}{\sqrt{AC - B^2}} + K, \quad (AC - B^2) > 0$$

$$\text{(iii)} \quad \frac{1}{\sqrt{C}} \operatorname{arcosh} \frac{B + Cz}{\sqrt{B^2 - AC}} + K, \quad (B^2 - AC) > 0$$

$$\text{(iv)} \quad \frac{-1}{\sqrt{-C}} \arcsin \frac{B + Cz}{\sqrt{B^2 - AC}} + K, \quad C < 0$$

The program computes the coefficients A, B and C between the levels z_i and z_{i+1} for each value of c_m and selects the appropriate expression out of (i) to (iv).

COMPUTATION OF TWO TRANSMISSION LOSS CURVES

General

The transmission conditions have been studied along two different tracks some miles apart in the same sea area. Only one single measurement of bottom reflection loss by oblique incidence has been done in this area. One result of this measurement is the bottom loss function shown in Fig. 7 for the frequency band 600 - 1200 Hz. The computation has been undertaken in order to learn what result may be expected when it is based on this very limited knowledge.

It is interesting because little information on the acoustical properties of the sea floor is the situation in the majority of cases. Acoustic measurements on the tracks permit a direct comparison.

Track No.1

Along the bottom profile of track No. 1, shown in Fig. 11, the transmission loss was measured in several frequency octave bands using calibrated explosive charges which were detonated at 40 m depth. The sea state was about 3 during the time of the measurement. The hydrographic conditions are described by the sound velocities in Fig. 12, which were measured along the track. The sound velocity distributions denoted by the numbers 77, 73, 74 and 75 are valid within the distance intervals indicated in Fig. 11. Thus, a 2-dimensional sound velocity variation is taken into account. This means, however, that there is a discontinuity of the velocity by passing from one interval to another.

Computation of the transmission loss under these conditions was carried out, assuming a wave height of 3 ft. The bottom loss function in Fig. 7 was used and was supposed to be valid for all distances. Surface reflection loss and absorption loss were calculated for a frequency of 900 Hz. The result is presented in Fig. 13, curve No.2. Also a curve (No.3) was computed on the assumption of no bottom loss.

It is seen that the agreement between the measured and computed transmission loss is good. The greatest difference between the two curves, some 2.5 dB, occurs at distances 9300 yd between source and receiver. The measured increase of loss may be caused by unknown irregularities in the bottom profile.

Track No. 2

The bottom profile of track No. 2 is given in Fig. 14. Acoustic measurements were done in a similar manner to those on track No.1. Average wave height was estimated to be about 4 ft. The sound velocity varied along the track as shown in Fig. 15.

Approximations were computed for the sound velocity profiles, as shown in Fig. 16 for profile No. 1. The difference between the two curves nowhere exceeds 0.15 m/s. The measured and computed transmission loss for the frequency band 600 - 1200 Hz is presented in Fig. 17, again using the bottom loss function in Fig. 7. The computation has been done in the distance interval 10 to 40 km.

The difference between the two curves is almost constant 4.5 dB. there may be several reasons for this deviation. The surface reflection loss may be incorrect and/or the bottom reflection loss may be considerably greater than expressed by the loss function of Fig. 7. The possibility of an inaccuracy in the measurements cannot be completely disregarded.

CONCLUSION

The computing procedure described seems to be a useful tool for predicting sound transmission conditions in the sea, provided that the following parameters are known:

a. The bathymetry.
b. The vertical and horizontal sound velocity distribution.
c. The bottom reflection loss.
d. The absorption loss in the water volume.
e. The surface scattering loss.
f. The sea state.

It should be stressed, however, that the calculation is carried out on the following assumptions:

(i) The ray theory must be valid, i.e., the depth of the sea ought to be at least ten times the wave length of the sound.

(ii) The effect of reverberation is not taken into account.

(iii) The amounts of energy having propagated along the various ray paths are added at the end of their travel.

Energy addition takes place if short impulse signals are used, but it does not take place for CW or noise signals in which case the signals having travelled along different paths will interfere. Therefore, the theoretical computation indicates the transmission loss values which will be obtained by measurements using explosive charges as acoustic sources.

REFERENCES

1. C.B. Officer, "Introduction to the Theory of Sound Transmission with Application to the Ocean", McGraw-Hill, New York, 1958.

2. M.A. Pedersen, "Acoustic Intensity Anomalies Introduced by Constant Velocity Gradient", J.Acous.Soc.Am., Vol. 33, 1961, pp. 465-474.

3. K.R. Stewart, "Ray Acoustical Model of the Ocean Using a Depth/Sound-Speed Profile with a Continuous First Derivative", J.Acous.Soc.Am., Vol.38, 1965, pp. 339-347.

4. H.W. Marsh, M.Schulkin and S.G. Kneale, "Scattering of Underwater Sound by the Sea Surface", J.Acous.Soc.Am., Vol. 33, 1961, pp. 334-340

5. M. Schulkin and H.W. Marsh, "Sound Absorption in Sea Water", J.Acous.Soc.Am., Vol.34, 1962, pp. 864-865.

6. W.H. Thorp, "Deep-Ocean Sound Attenuation in the Sub-and Low-Kilocycle-per-Second Region", J.Acous.Soc.Am., Vol. 38, 1965, pp. 648-654.

7. C.C. Leroy, "Sound Attenuation between 200 and 10 000 cps Measured along Single Paths", SACLANTCEN Technical Report No.43, 1965, NATO UNCLASSIFIED

DISCUSSION

The author clarified the point that when a ray crossed the velocity discontinuity between two regions described by different velocity profiles, it was made to do so with its direction unchanged.

In answer to a question, the author acknowledged that when a ray was reflected from the bottom, only the slope of the bottom — and not the curvature — was used for determining the intensity of the reflected ray.

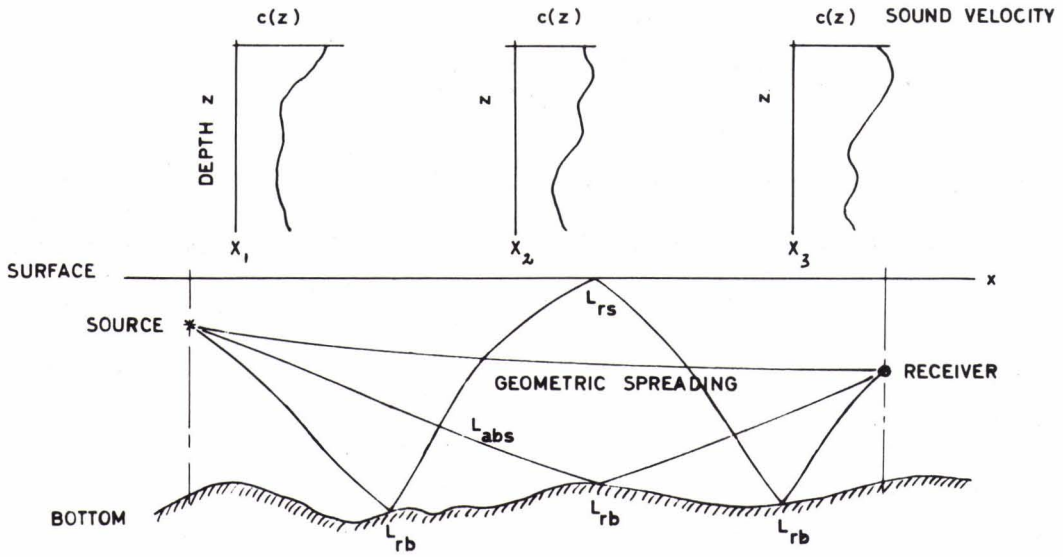

OCEAN MODEL FOR THE COMPUTATION OF TRANSMISSION LOSS

FIG. 1

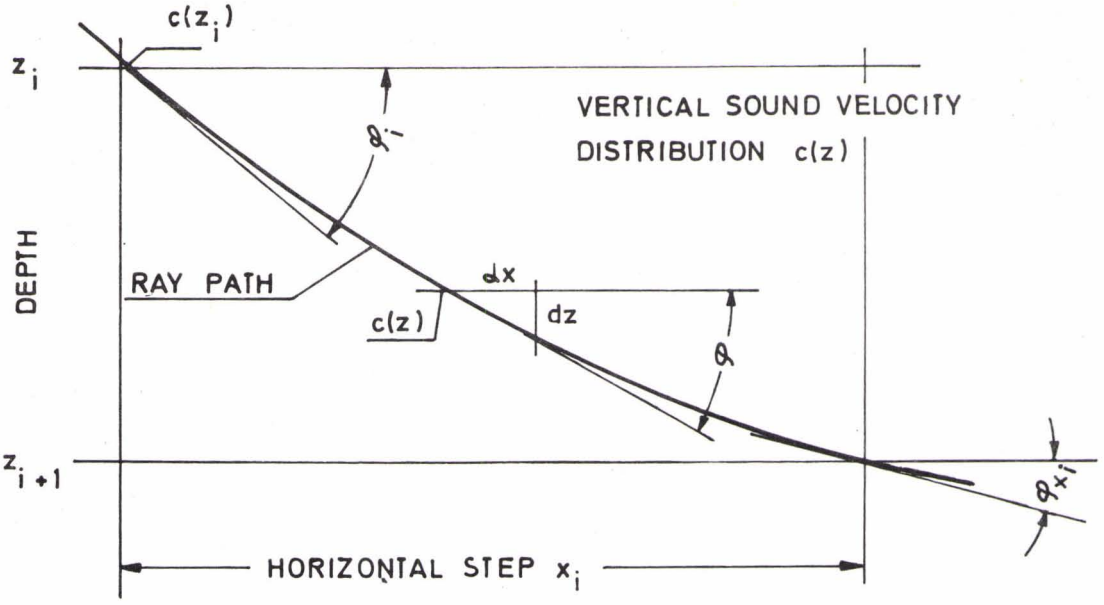

FIG. 2

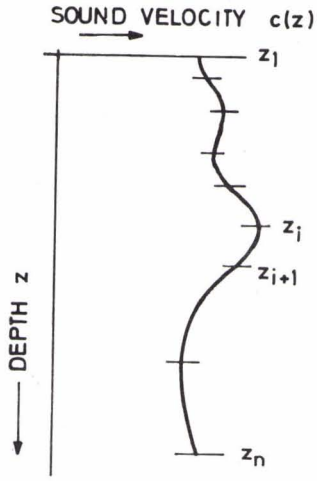

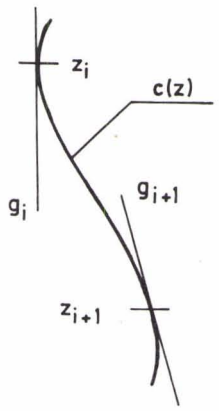

FIG. 3

DIVISION OF THE SEA DEPTH INTO LAYERS

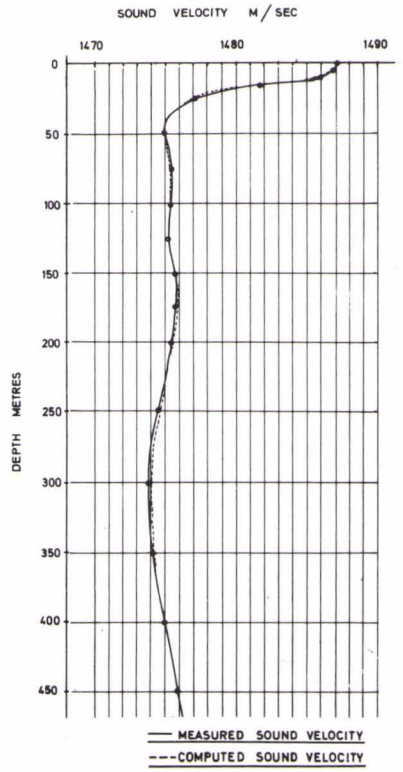

FIG. 4

FIG. 5

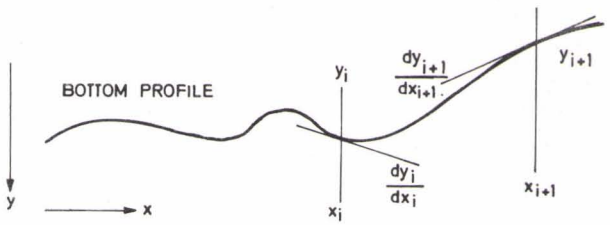

DIVISION OF BOTTOM PROFILE IN SEGMENTS

APPROXIMATION BY

$$y = B1_i \cdot x^3 + B2_i \cdot x^2 + B3_i \cdot x + B4_i$$

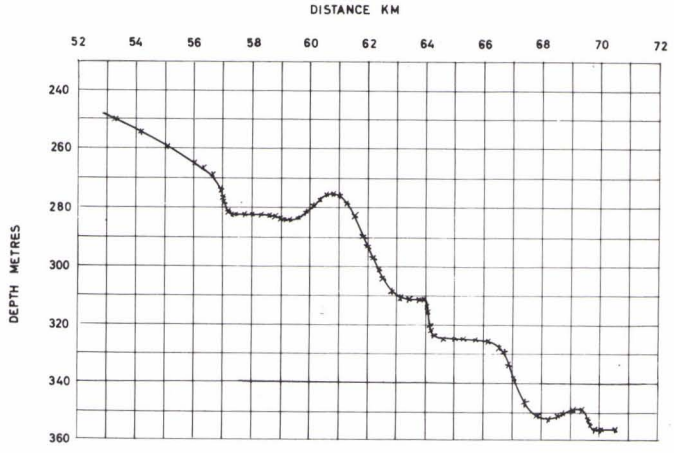

FIGURE 4.2 —— MEASURED BOTTOM PROFILE
××× COMPUTED BOTTOM PROFILE

FIG. 6

FIG. 7

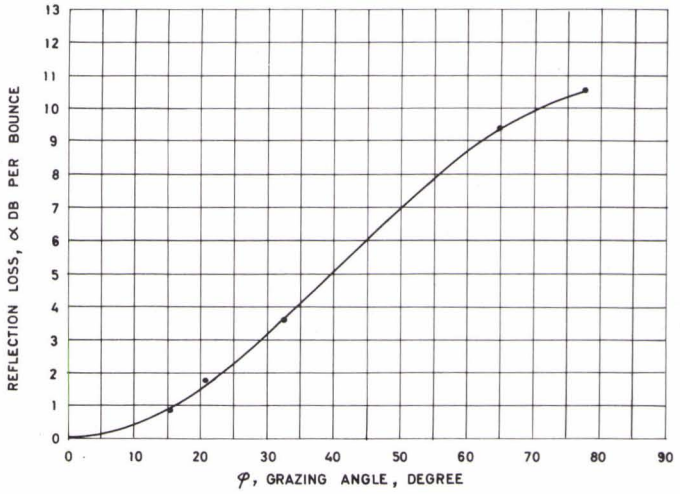

MEASURED REFLECTION LOSS, FREQUENCY BAND 600–1200 HZ

FIG. 8

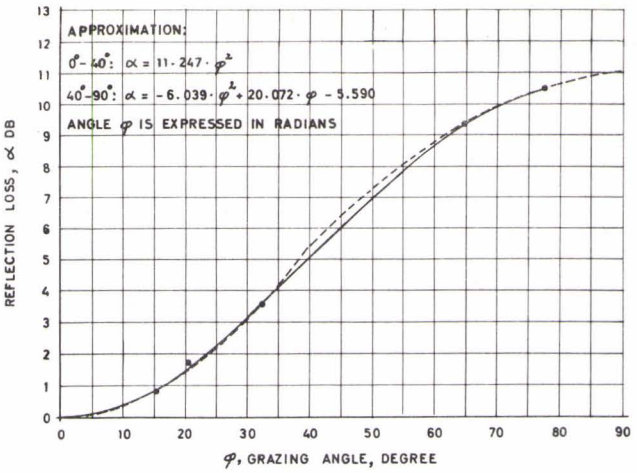

—— MEASURED REFLECTION LOSS, FREQUENCY BAND 600–1200 HZ

--- COMPUTED APPROXIMATION

FIG. 9

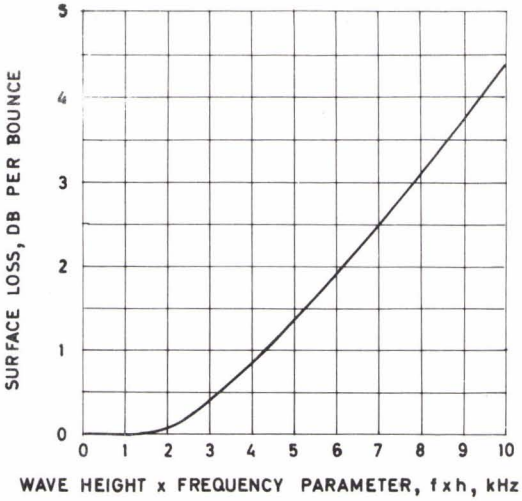

THEORETICAL SEA SURFACE SCATTERING LOSS ACCORDING TO REFERENCE (4)

FIG. 10

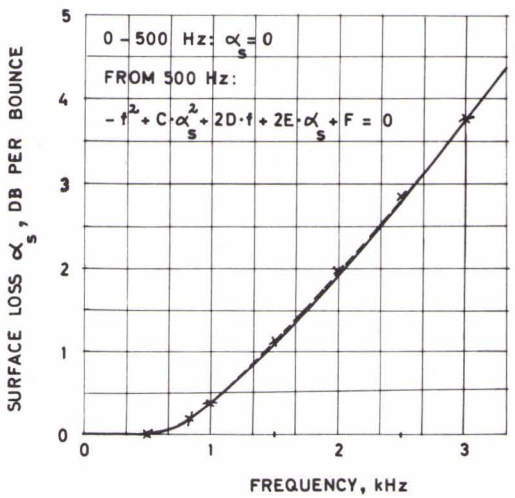

COMPUTED APPROXIMATION TO THE SURFACE LOSS FUNCTION ----

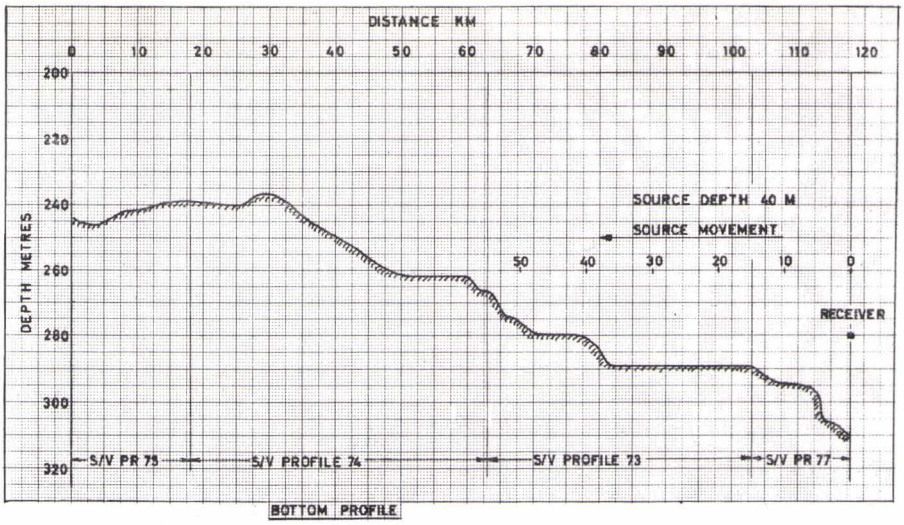

FIG. 11

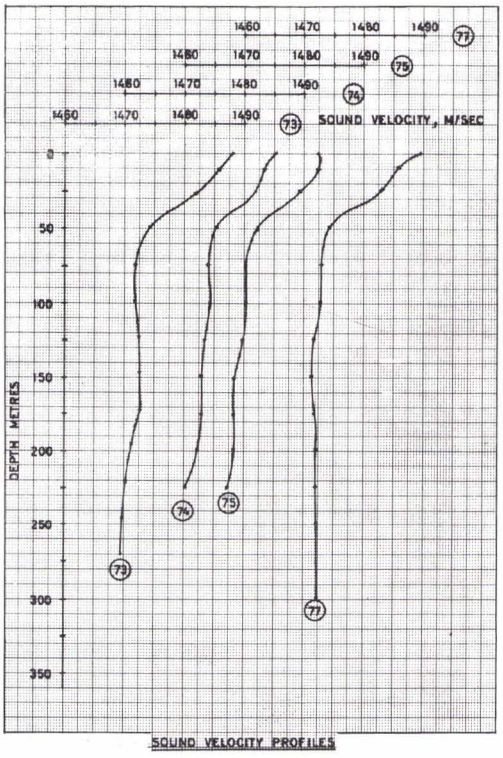

FIG. 12

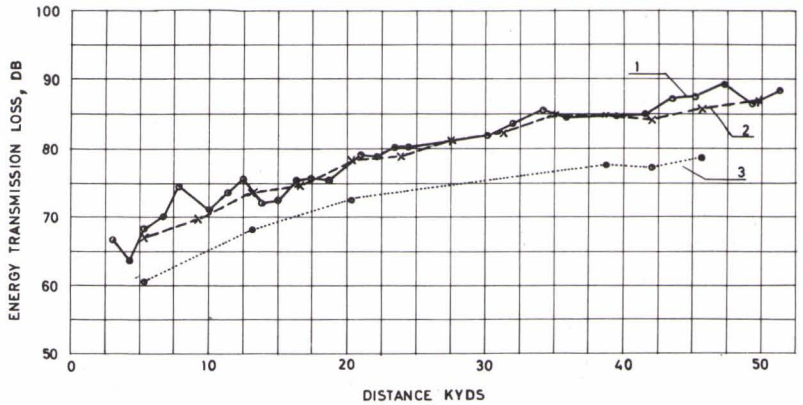

FIG. 13

CURVE 1: MEASURED TRANSMISSION LOSS, BAND 600 - 1200 HZ

CURVE 2: COMPUTED TRANSMISSION LOSS, 900 HZ, WAVE HEIGHT 3 FEET

CURVE 3: LOSS DUE TO GEOMETRIC SPREADING, ABSORPTION AND SURFACE SCATTERING, 900 HZ, WAVE HEIGHT 3 FEET

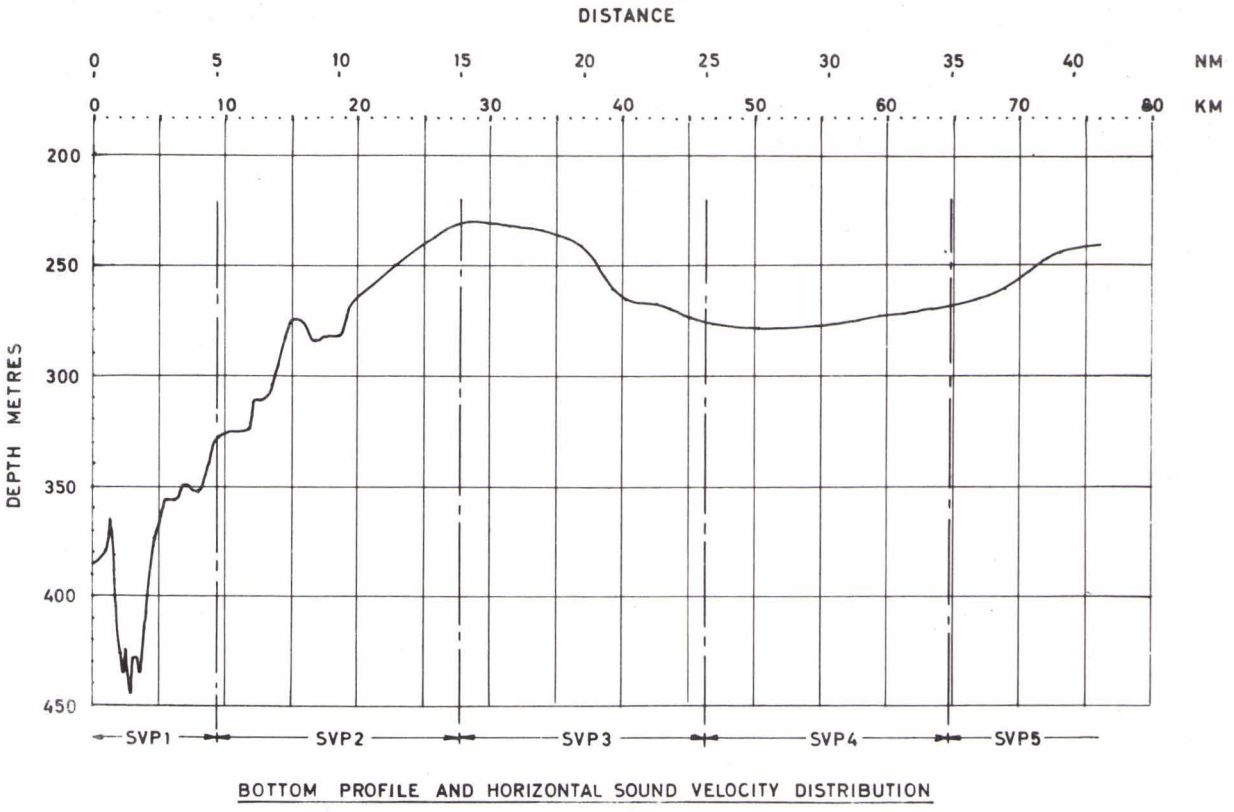

BOTTOM PROFILE AND HORIZONTAL SOUND VELOCITY DISTRIBUTION

FIG. 14

FIG. 15

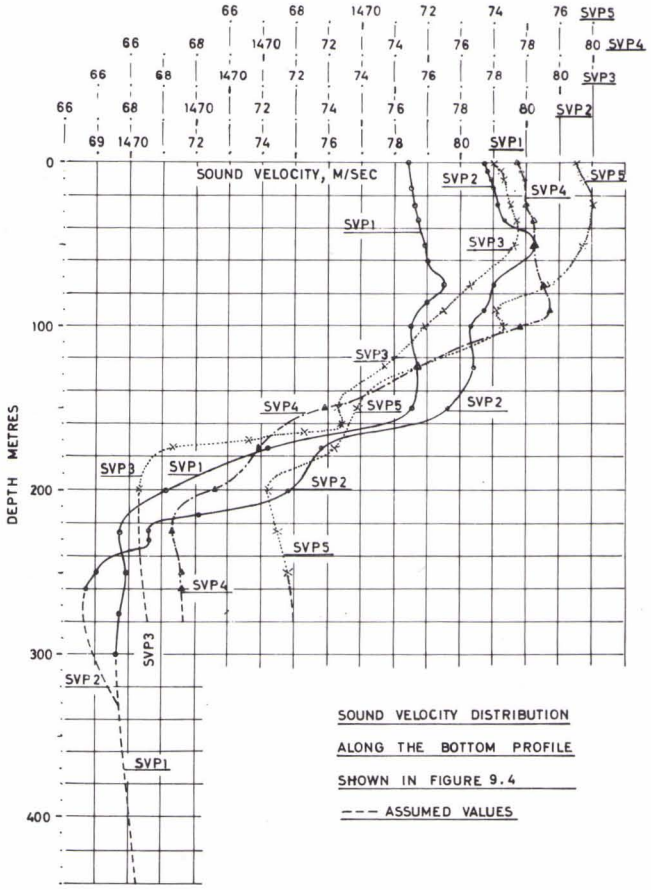

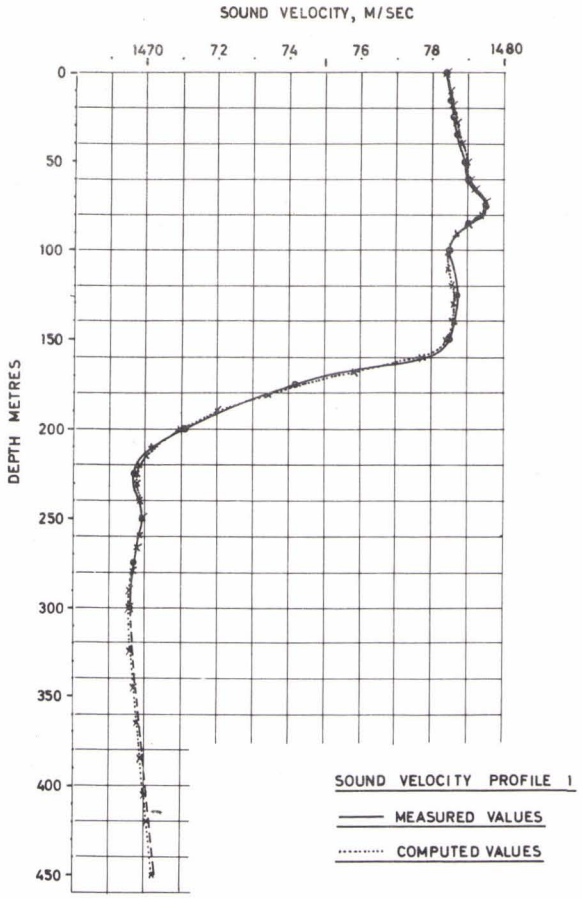

FIG. 16

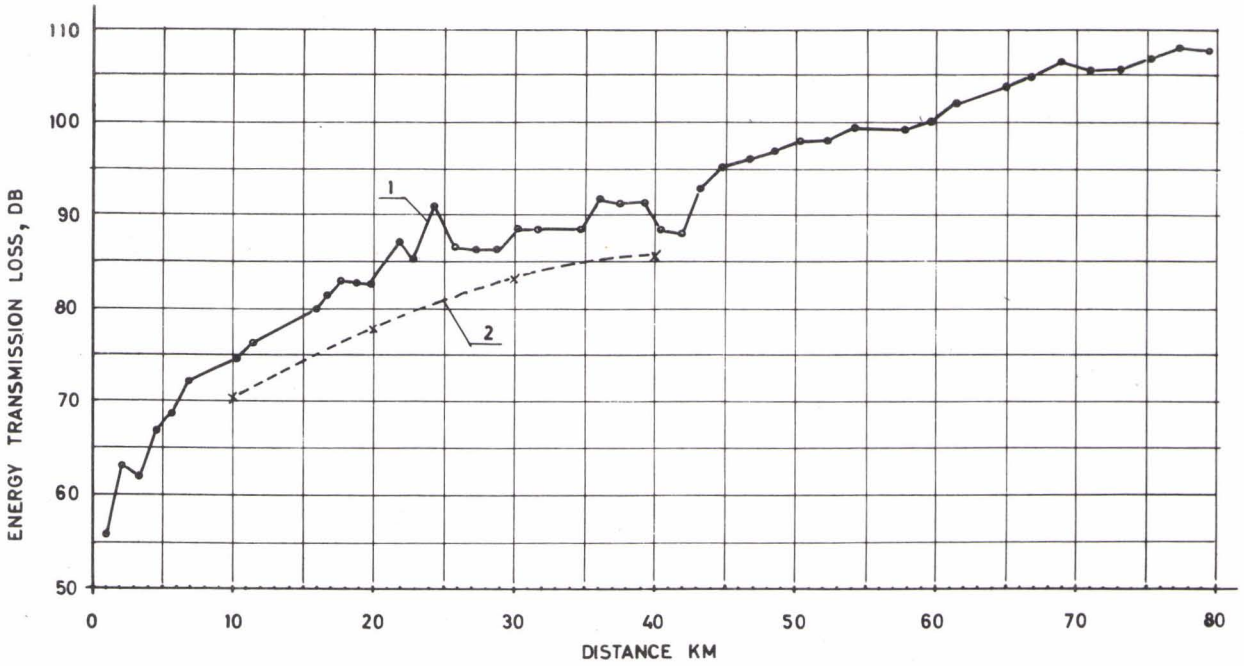

CURVE 1: MEASURED TRANSMISSION LOSS, BAND 600 - 1200 HZ

CURVE 2: COMPUTED TRANSMISSION LOSS, 900 HZ, WAVE HEIGHT 4 FEET

FIG. 17

COMPARISON OF PROPAGATION MEASUREMENTS OBTAINED USING THE MEDUSA SYSTEM WITH COMPUTER MODELLED DATA

(ABSTRACT)

by

G. Vettori and E. Cernich
SACLANT ASW Research Centre
La Spezia, Italy

Sound propagation data obtained during a sea trial in the West Ligurian Sea with SACLANTCEN's MEDUSA deep research sonar have been used to extract multipath structure and propagation loss as a function of range, for three source depths (below, above and much above critical depth). These measured propagation characteristics have been compared with those obtained from the CONGRATS computer model, developed by Messrs Einstein, Cohen and Weinberg at US NUSC, New London.

The comparison shows generally good agreement between the measurements and the model. Agreement is good in multipath delays, in individual path levels and incoherent propagation loss when the array is below the critical depth. The agreement becomes less good when the array depth is decreased. Under these conditions the measured levels of the surface refracted and reflected arrivals are often lower than those predicted by the model. The agreement is poorest in caustic regions, where the measured data never follow the sharp decrease in propagation losses that the model predicts.

DISCUSSION

See Discussion following next paper.

COMPARISON OF CONGRATS RAY TRACING PREDICTIONS WITH MEDUSA MEASUREMENTS OF REVERBERATION

(ABSTRACT)

by
B. de Raigniac and W. Bachmann
SACLANT ASW Research Centre
La Spezia, Italy

INTRODUCTION

From the user's point of view, ray tracing is just a computer procedure which is inserted into larger programs of different degrees of complexity. The following table indicates in which kind of programs this procedure is used at SACLANTCEN. It ranges from mere qualitative descriptions of the sound field to detection models.

TABLE 1

USE OF RAY TRACING PROCEDURES

1. Qualitative description of sound field
   RAY PLOT
2. Single ray descriptions
   SPREADING LOSS, TRAVEL TIME, ANGLE
3. Combined loss (coherent and incoherent), multipath
   EIGENRAYS
4. Reverberation, echo level
5. Detection model

The experimental verification of ray tracing procedures should be most significant on the level No.3 of the above table.

However — as mentioned already in Mr Vettori's presentation (see Session 3 of these Proceedings) — one can only measure a few points of the loss curve in a whole day.

In reverberation experiments (level No.4) we obtain with each ping a continuous curve covering the full interesting range [see Fig. 1]. But we have now a higher degree of uncertainty, because of the unknown behaviour of the scattering layers at long distance. But with some precautions one may well draw conclusions on the validity of the ray tracing program.

From five examples which are extensively discussed in a Technical Report* result the following tentative conclusions:

1. The curvilinear ray tracing procedure and the reverberation procedure of the CONGRATS programs (see presentation of Messrs Weinberg and Cohen in Session 2 of these Proceedings) predict reverberation levels which agree within 3 dB with measurements, as long as there are no caustics.

2. In the reverberation procedure the local scattering strength is combined with the calculated propagation loss. As both the reverberation level and the separately measured propagation loss (see presentation of Mr Vettori) agree outside of caustics with prediction, it follows that the reverberation procedure itself is correct.

3. The calculated reverberation level is always too high in caustic regions. But, as the reverberation procedure is correct it must be the propagation loss procedure (derived from ray theory) which is not valid any more in caustic regions.

4. Finally this comparison shows that it is possible to predict sound fields up to a range of 35 km on the basis of a single measurement of the sound velocity profile, volume scattering profile and wind.

---

* B. de Raigniac, W. Bachmann, and J.S. Cohen, "Comparison of Reverberation Measurements Using the MEDUSA System with Computer Modelled Data"(NU), SACLANTCEN Technical Report in preparation, NATO CONFIDENTIAL.

DISCUSSION

The discussion of the previous two papers centred on the sound speed profile used as input to the computer model. That the temperature profile was not measured for each run was not thought to be important, as evidenced by the fact that ray predictions from an average profile did not differ significantly from predictions based on an extreme profile.

It was pointed out that salinity variations could have a marked effect. (For example, when a sound channel exists, its estimated width could be in error by as much as 150 m if the salinity variations are ignored.) However, the authors were of the opinion that in their case the use of a uniform average salinity was adequate, and were supported in this view by direct sound speed measurements.

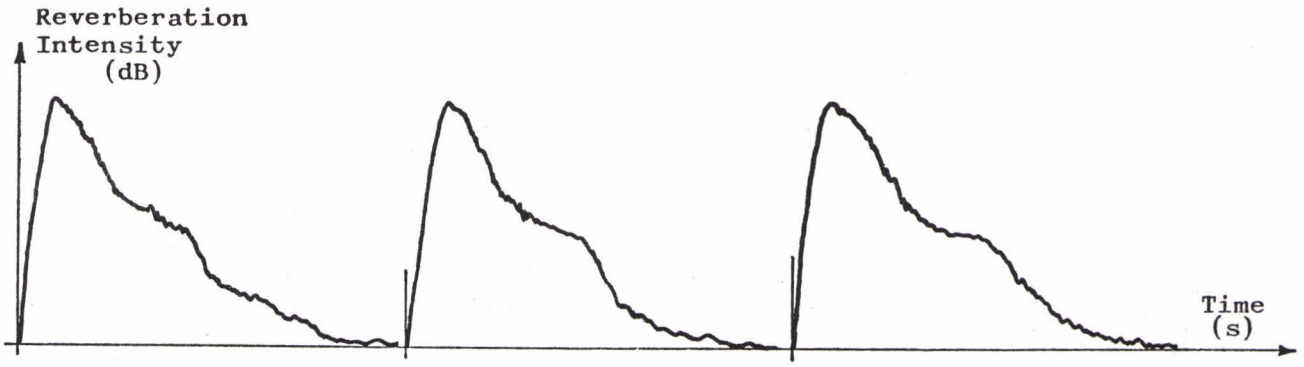

FIG. 1

COMPARISON OF RAY TRACING PREDICTIONS WITH WIDEBAND PROPAGATION MEASUREMENTS

(ABSTRACT)

by

J. Gerrebout

SACLANT ASW Research Centre

La Spezia, Italy

The paper gives an illustration of the latest methods which have been developed at SACLANTCEN for the experimental study of sound propagation in deep water. They are based on a high sampling of the sound field produced by an explosive sound source, digital recording of the received signal, processing of the data by computer programs and finally comparison of the experimental results with a theoretical model of propagation. Trials were conducted during the warming season, in a deep water area where stable oceanographic conditions were expected. Direct measurement of the sound velocity profile was made with a sound velocimeter down to 500 m, and a Nansen cast was taken to investigate the medium deeper.

To check the progressive insonification of the medium with increasing source depths, five different depths were selected from near surface down to critical depth. The receiving hydrophones were distributed on a vertical array at 20 m, 60 m, 100 m, and 600 m depth (Fig. 1 shows the experimental set-up and the sound-velocity profile). The useful frequency band of the sources extends over 10 kHz and their pulse width, 300 μs, allows a good description of the structure of the multipath to be made.

A simple one-dimensional ray-tracing program using linear segments to approximate the sound velocity profile was used to compute the various sound fields. Curves giving the time separation between

the first and successive arrivals versus range were produced for each pair of source-hydrophone depths, together with curves of the propagation loss anomaly obtained by adding incoherently all the rays arriving at the hydrophone.

From the acoustic measurements were derived general time displays of the signals as received on the hydrophones and propagation loss anomalies versus range in a series of third octave filters.

A comparison was made between predictions and experimental observations for different selected cases, with the following results. The general time evolution of the multipath structure, which is well described by the predictions at short range, correspond in the convergence zone only after the theoretical curves have been shifted by 1.5 to 2 km toward the source. (Figs. 2 and 3 show the general time series display of the arrivals as received on the 100 m hydrophone. The sources were at 27 m (Fig.2) and at 105 m depth (Fig.3) respectively. Levels have been corrected for gain settings and spherical spreading, but not for absorption.) This earlier manifestation of the convergence zone cannot be explained by the effect of the earth's curvature, which was proved to account for only a third of the discrepancy. The 90° phase shift which is characteristic of arrivals refracted at the thermocline and passing a caustic is also observed in a few cases for deep refracted arrivals (Fig. 4 is the time-series display of the arrivals received on the hydrophone at 600 m with the sources at 460 m). This confirms the presence at depth of limited caustics which have not been evidenced by the rough ray-tracing based on a smoothed velocity profile.

To be noticed is the incoherent feature of the arrivals when they have been refracted at the bottom of the thermocline, a feature which is amplified when source and receivers are lying in this region (see Fig. 3). The signal refracted, diffracted, scattered by the micro-structure inhomogeneities of the medium which are likely to be found in this region has all the characteristics of forward reverberation. Receivers which should have been in the shadow zone are insonified by the scattered sound.

The near-surface shadow zone is also penetrated by the low frequency components of the signal when the source is deep (Fig. 5 shows the time-series display with the hydrophone at 20 m and the sources at 1068 m.). Ray theory breaks down on the thermocline, which acts like a filter - the spectra of the received signal showing more and more attenuation in the high frequency domain as the range from the theoretical shadow zone limit increases.

In Fig. 6 the propagation loss anomaly (which is the propagation loss, less spherical spreading loss, less absorption) is shown as predicted (top left) and as measured in third-octave filters for a 27 m source depth and the hydrophone at 100 m. Fig. 7 is the same as the previous figure, except that the source depth is now 105 m. The measured propagation loss anomalies are in good agreement with the mean theoretical predictions except when the receivers, lying in the shadow zone, are insonified by scattered or diffracted sound. If the convergence gains predicted for the convergence zone have been observed the agreement is limited to the mean value, the high intensification on the caustics being missed.

In conclusion, one-dimensional ray-tracing programs using linearly segmented sound-velocity profiles allow a good interpretation of the experimental results and their accuracy is high enough for general operational predictions. However, they cannot take into consideration all the aspects of propagation such as diffraction and reverberation, and their domain of application should be limited to geographical areas recognized as oceanographically stable.

DISCUSSION

The author said that he had evaluated the curved earth modification while trying to explain the error in the position of the convergence zone, but that it was able to account for only about one third of the discrepancy.

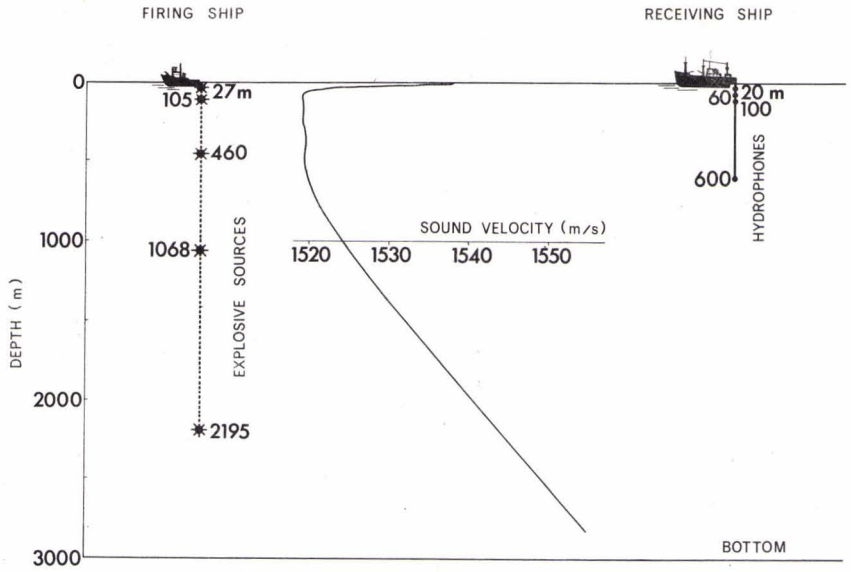
FIRING SHIP
RECEIVING SHIP
0
1000
2000
3000
DEPTH (m)
105
27m
460
1068
2195
EXPLOSIVE SOURCES
60
20 m
100
600
HYDROPHONES
SOUND VELOCITY (m/s)
1520
1530
1540
1550
BOTTOM

FIG. 1

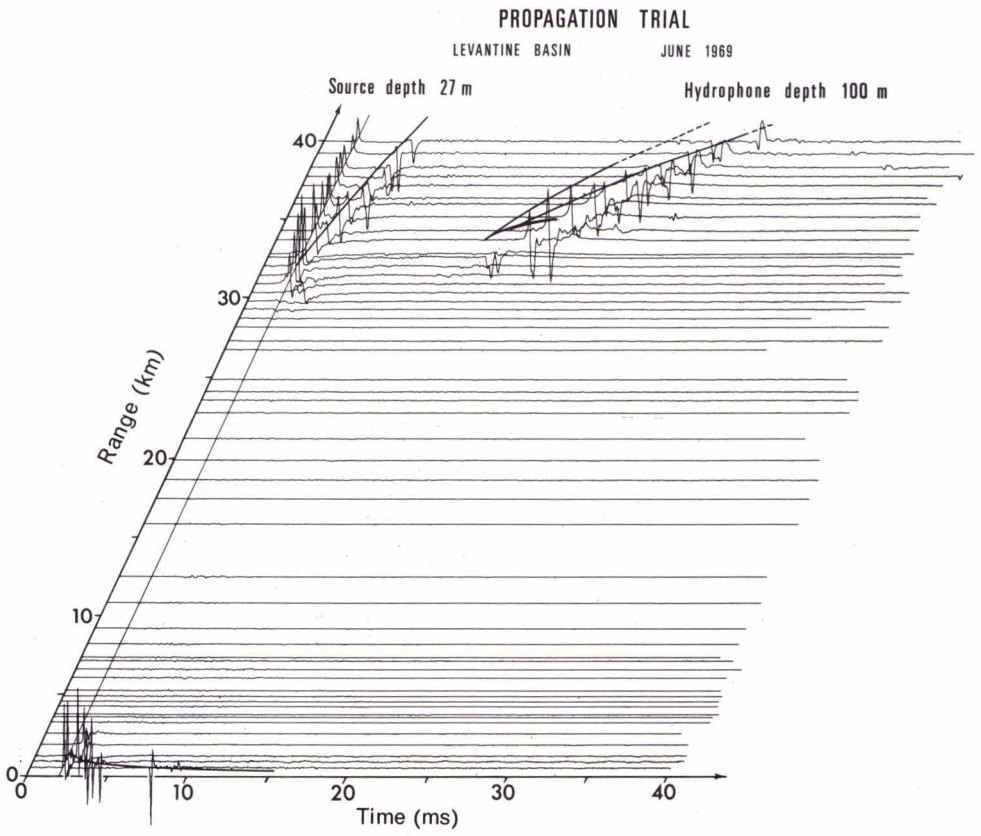
PROPAGATION TRIAL
LEVANTINE BASIN
JUNE 1969
Source depth 27 m
Hydrophone depth 100 m
Range (km)
0
10
20
30
40
Time (ms)

FIG. 2

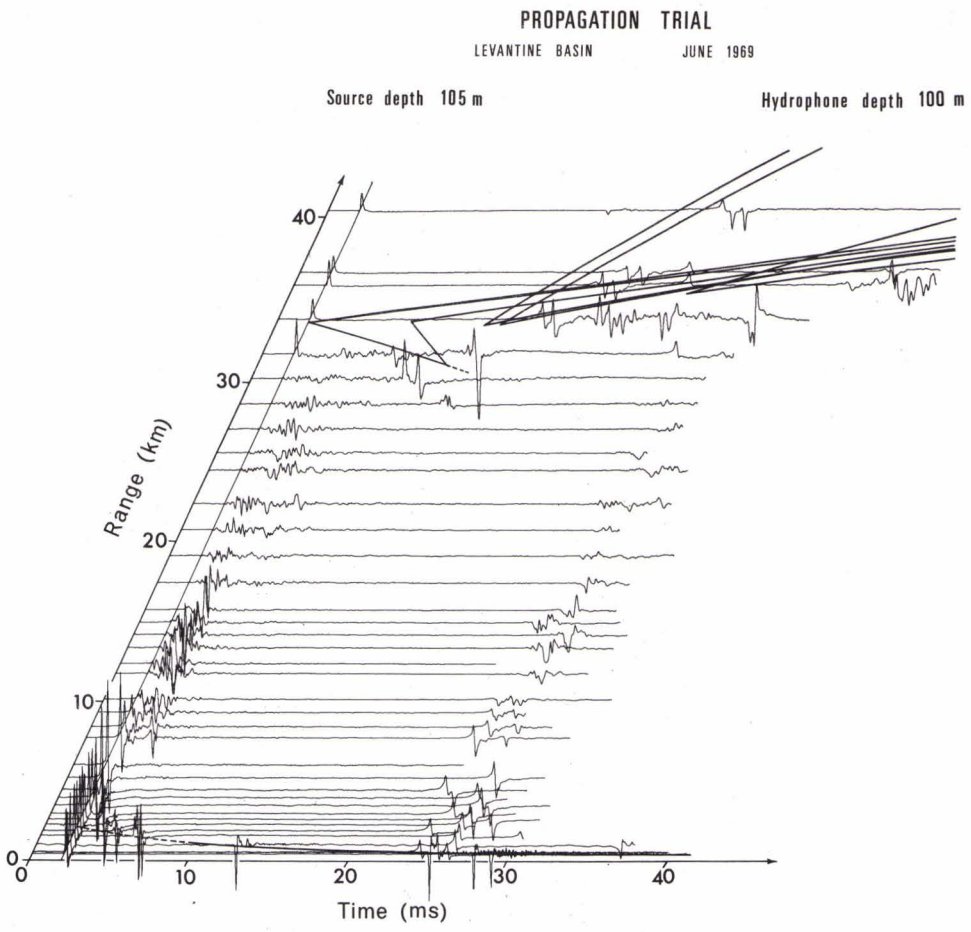
PROPAGATION TRIAL
LEVANTINE BASIN JUNE 1969
Source depth 105 m
Hydrophone depth 100 m
Range (km)
0
10
20
30
40
Time (ms)

FIG. 3

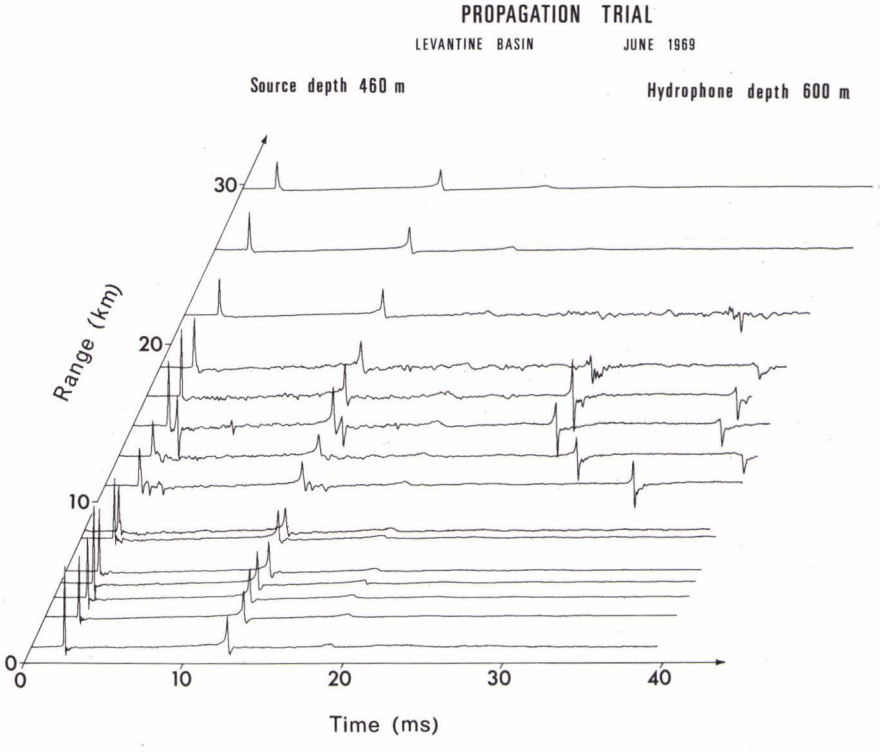
PROPAGATION TRIAL
LEVANTINE BASIN JUNE 1969
Source depth 460 m
Hydrophone depth 600 m
Range (km)
0
10
20
30
40
Time (ms)

FIG. 4

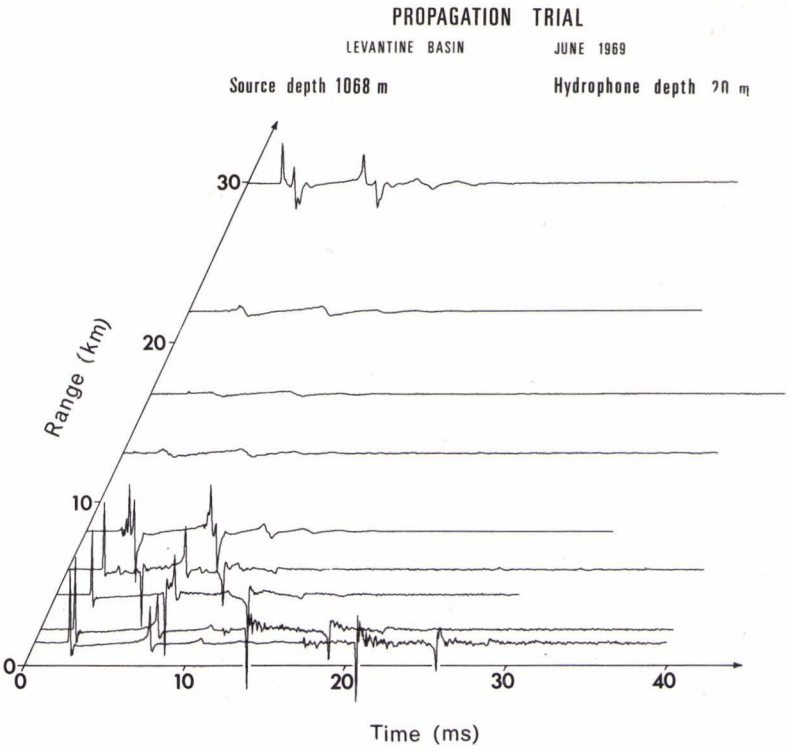
PROPAGATION TRIAL
LEVANTINE BASIN
JUNE 1969
Source depth 1068 m
Hydrophone depth 20 m
Range (km)
30
20
10
0
0
10
20
30
40
Time (ms)

FIG. 5

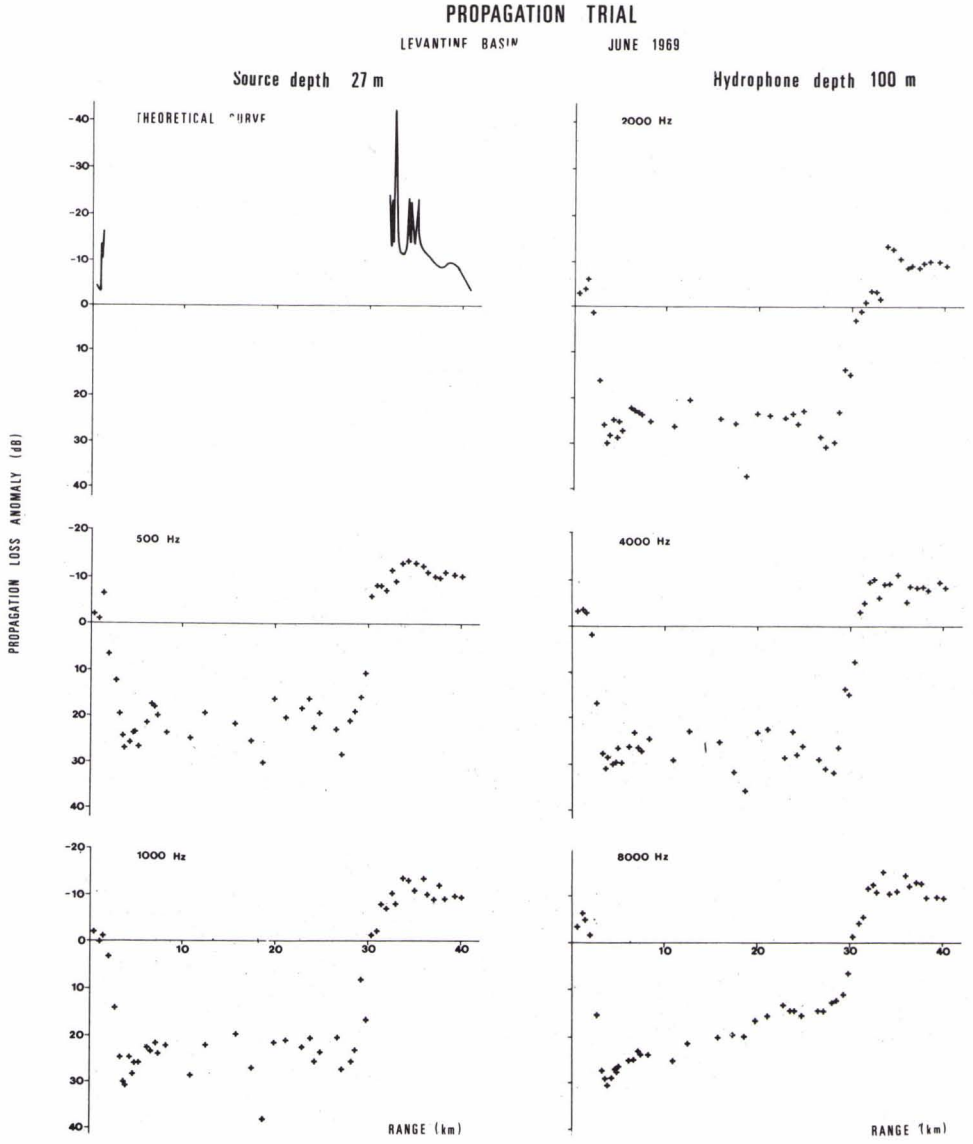
PROPAGATION TRIAL
LEVANTINE BASIN
JUNE 1969
Source depth 27 m
Hydrophone depth 100 m
THEORETICAL CURVE
2000 Hz
500 Hz
4000 Hz
1000 Hz
8000 Hz
PROPAGATION LOSS ANOMALY (dB)
RANGE (km)
RANGE (km)

FIG. 6

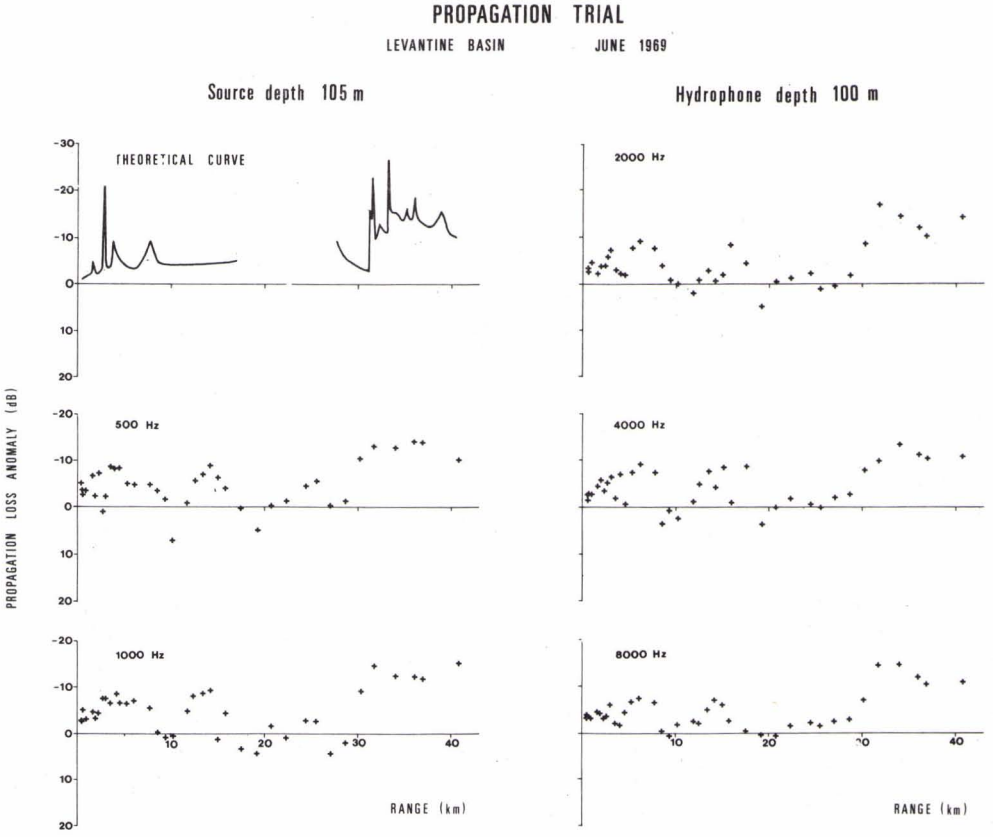
PROPAGATION TRIAL
LEVANTINE BASIN
JUNE 1969
Source depth 105 m
Hydrophone depth 100 m
THEORETICAL CURVE
2000 Hz
500 Hz
4000 Hz
1000 Hz
8000 Hz
PROPAGATION LOSS ANOMALY (dB)
RANGE (km)
RANGE (km)

FIG. 7

GEOMETRICAL PROPERTIES OF UNDERWATER SOUND PROPAGATION

by

A.T. Jaques, M.M. Coate and T.L. Goodin
U.S. Naval Ordnance Laboratory
Silver Spring, Maryland, U.S.

ABSTRACT

During the past several years, the U.S. Naval Ordnance Laboratory has made a study of the geometrical properties of propagation of sound in the ocean. Measurements have been made at sea under controlled conditions by use of a deep-draft, stable receiving platform known as SPAR. Positions of the source ship and the receiving platform were precisely known by the use of electromagnetic positioning equipment. Reference positions thus obtained were compared with positions determined by acoustic means. Propagation paths investigated have included surface channel, near-surface refracted paths, bottom reflected paths, and combinations of bottom and surface reflected paths. Corrections for refraction were made by a laboratory ray trace program. This program, which uses a linear segmented velocity profile, has provisions for double precision calculations of the ray path, corrections for a sloping bottom and corrections for the curvature of the earth. The program has been successfully run both on an IBM-7090 computer and a CDC-6400 computer.

INTRODUCTION

The work I will describe has to do with a study of the geometry of underwater sound propagation as contrasted to intensity studies. Of course, the two are closely rleated. This study has been based largely on full-scale, at-sea measurements in which a stable, sea-going platform known as SPAR has been used. Since refraction is fundamental to this problem, ray tracing has been an important part of this work.

First, I will describe the ray trace program, particularly characteristics and features which are associated with the geometrical parameters. Next, I will describe briefly the experimental setup used for the at-sea measurements, and finally I will give some typical examples and results of the work.

LABORATORY RAY TRACE EQUIPMENT AND PROGRAM

The ray tracing program to be described here was originally coded in FORTRAN II by the U.S. Naval Oceanographic Office [Ref. 1] following the general pattern established by the Canadian Pacific Naval Laboratory [Ref. 2]. In 1964 the program was converted by NOL to run in FORTRAN IV on the IBM-7090 and later that year a plotting option was added. In 1967, a subroutine was added to correct the sound velocity profile for curvature of the earth, and at the same time, double precision computations were incorporated. Just recently the program has been adapted to and is being run on the CDC-6400. The program can also be run on the UNIVAC 1108.

The basic equations used in the ray trace program are (of course) based on Snell's law:

$$V_0 \cos\theta_1 = V_1 \cos\theta_0 \ ,$$

where V_0 and θ_0 are the initial velocity and inclination of the ray to the horizontal and V_1 and θ_1 are taken at some other point on the ray. The parameter* θ is taken as positive for downward angles and negative for upward angles. A linear

---

* θ and D/E are used interchangeably in this paper.

segmented sound velocity profile is used. Thus, the ray traverses an arc of a circle in each region of constant velocity gradient.

Curvature of the earth corrections are based on the formulations given by Watson [Ref. 3] at the Admiralty Research Laboratory in the U.K. This correction takes the form of a transformation of the sound velocity profile as follows:

$$z' = r_0 \ln [(r_0 - z)/r_0]$$

and

$$c' = c \exp (z'/r_0) \quad ,$$

where z and c are the original depth, velocity coordinates, z' and c' are the transformed coordinates, and r_0 is the radius of the earth at the sea surface. The program also takes into account the variation of the radius of the earth with latitude.

GENERAL PROGRAM CHARACTERISTICS AND SPECIAL FEATURES

The program has the following features:

a. A maximum of 40 depth-velocity coordinates (straight-line segments) may be used to represent the sound velocity profile.

b. As the ray progresses in the horizontal range, the sound velocity profile may be changed as many as twenty times.

c. Corrections for the curvature of the earth are optional. If corrections for curvature are chosen, the latitude associated with the sound velocity profile is inserted. If corrections for curvature are not chosen, a flat earth is assumed.

d. The independent operating parameter is the initial angle θ_0 at the source. Both upward and downward angles between ± 90 degrees, exclusive, are accepted.

e. Individual rays are terminated when they have reached some pre-set value of the horizontal range.

f. Reflections from both the ocean surface and the bottom, either flat or sloping, are permitted. A maximum of 100 regions of different bottom slopes are allowed for one ray field. Bottom slopes are represented by straight line segments.

g. The program includes an optional feature in which a tape is generated from which the ray field is plotted on a CalComp Plotter. Up to 1000 points are plotted which represents one individual ray. Also, sound velocity profiles are plotted with 40 points per profile permitted. Typical CalComp plots are depicted in Figs. 1, 2 and 3. Figure 1 shows both a profile relating to a flat earth and the same profile corrected for the curvature of the earth. Figure 2 shows a typical ray plot for a flat bottom and no corrections for earth curvature. The ray field, shown in Figure 3, relates to a uniform sloping bottom and includes corrections for earth curvature. (These are all plotted automatically by CalComp.)

i. Computation in either single or double precision are optional.

RAY PATH GEOMETRY

Before showing a sample printout, it is instructive to depict the ray path geometry and to define certain quantities. The geometry associated with the acoustic ray is shown in Fig. 4.

A sample printout is shown in Fig. 5. Note that when the ray becomes horizontal or changes direction (upgoing to downgoing, or vice versa) because of reflection at a boundary or because of refraction, all entries except the D/E angle are repeated.

SAMPLE RAY TRACE RESULTS

The next series of figures are sample runs which show the effect of a slight change in the sound velocity profile on ray path geometry for both bottom reflected and convergence zone propagation paths. The change in profile is just that induced by curved earth corrections. Thus, the results to be presented can be looked upon as the effect of curved earth corrections or the effect of an uncertainty in the velocity profile from any cause. (I will tie these and some experimental results together later.)

Figure 6, the first figure of this series, shows (on the left) a typical sound velocity profile for the Pacific Ocean. The profile shown relates to the original or uncorrected profile. The profile corrected for earth curvature is too little different to be resolved with the plotting scale used here. Instead, since the corrected profile is characterized by a slight increase in the deep-water sound velocity gradient (between channel axis and bottom), gradient values are shown instead. The gradient denoted by "g" relates to the uncorrected or reference profile and the gradient denoted by "g'" relates to the corrected or altered profile. Note that the difference in the gradients is only about one-fourth ft/s per 1000 ft.

An explanation of the plot on the right is as follows: Two sets of ray tracing runs were made -- one for the original profile and one for the corrected profile. From each set, the range at which the ray reached the surface for the same initial D/E angle was noted. Differences in range were taken and plotted as a function of range. This is the plot shown. The short ranges are associated with large depression angles and the long ranges, bottom bounce leading into convergence zone paths, are associated with shallow depression angles. Thus, a very slight change in profile causes a considerable change in the range at which the ray returns to the surface. For the bottom reflected path, the more severe gradient (g'), or the the correction for earth curvature, causes the range to be greater. This effect is highly range dependent, becoming as large as 1500 yds at about 55 kyd. In contrast, for convergence zone propagation, the more severe gradient, or the correction for earth curvature, causes the range to be less by about 500 yards.

The absolute difference in velocity at 18 000 ft is about +5 ft/s relative to the profile shown. If the entire profile is displaced by 5 ft/s, the difference in range is less than 15 yd for all bottom bounce ranges and 35 yd at the convergence zone.

Figures 7, 8 and 9 show the nature of this effect for profiles typical of the Caribbean, the Norwegian, and the Mediterranean Seas, respectively. In all cases the change in the deep-water gradient as affected by corrections for curved earth was from one-fourth to one-third ft/s per 1000 ft and has comparable effects on the ray geometry as for the Pacific profile. However, the effect within the convergence zone itself varies widely from area to area.

The next figure, presented in similar fashion, shows the effect of a small change in the sound velocity profile on the travel time. This has to do, of course, with our ability to measure ranges acoustically from travel times. As before, both bottom reflected and convergence zone propagation paths are included. In this case, however, the difference in range is plotted as a function of range using the same travel time as the independent analytical parameter. Figure 10 shows these results for the Pacific profile. (This profile is the same as shown previously for the Pacific Ocean.) Note that with travel time as a constraint, the change in range caused by a change in profile is considerably less than that for the data just shown. In contrast to the previous case, for both bottom reflected and convergence zone propagation, the more severe gradient, or corrections for earth curvature, causes an increase in range. In this case, however, a fixed displacement in the sound velocity profile of 5 ft/s caused a greater difference in the ranges than the effect of a change in the gradient — a difference of about 50 yd throughout the range. Since the other areas gave similar results, they are not repeated here. I will say more later concerning the significance of the sound velocity gradient as it relates to ray tracing accuracies.

AT-SEA MEASUREMENTS AND RESULTS

In order to provide some overall check on our knowledge of the geometrical properties of underwater sound propagation, the U.S. Naval Ordnance Laboratory has been engaged in an at-sea measurements program for this purpose. Ray tracing, of course, is an important part of this problem.

Measurements have been made under controlled conditions by use of a deep-draft, stable receiving platform known as SPAR [Ref. 4] (Seagoing Platform for Acoustic Research). An oceanographic vessel has served as a source platform. The experimental arrangement is depicted in Fig. 11.

Receiving arrays, rigidly fixed to the hull of SPAR, consist of both horizontal and vertical lines comprising 14 hydrophones, thus providing for the measurement of both azimuth and depression-elevation angles. The accuracy in reading either the azimuth or D/E angle is believed to be better than 0.1 degree. LORAN equipment, both A and C, is used for the geographical position of SPAR. A single-dimension RAYDIST system provides a reference as "true" range between SPAR and the source ship. A radio link is used for the measurement of acoustic travel times and for communication between operating units. Thus, reference or "true" positions were compared with positions determined by acoustic means. Propagation paths investigated have included surface channel, near-surface refracted paths, bottom reflected paths, and combinations of bottom and surface-reflected paths. Corrections for refraction were made by the laboratory ray trace program just described. On-site oceanographic data included bathythermographs, sea surface temperature measurements, precision depth recorded data, and direct-reading velocimeter data (throughout the water column) when available. Some typical experimental results relating to various propagation paths follow.

NEAR-SURFACE PROPAGATION PATHS

The purpose of this experiment was to determine the accuracy of acoustic ranges from travel time measurements for near-surface propagation paths. This accuracy, of course, is directly related to the accuracy of the assignment of the mean horizontal velocity — a sound velocity and ray trace problem.

The propagation paths referred to are shown in Fig. 12. For this type of propagation, the ray travels by repeated upward refractions and successive surface reflections. A simplified sketch of the experimental setup is shown in Fig. 13. The reference or true range was measured by a single-dimension RAYDIST. The error in the reference range was estimated to be 15 ft, independent of range. (This error is comprised of a RAYDIST interpolation error and the uncertainty in the position of the underwater projector.) The error associated with the measurement of the acoustic travel time was estimated to be about 1 ms, the source of which was in the reading of the timing record. Thus, the experimental error expressed in terms of the mean horizontal velocity was estimated to be about 3 ft/s for a source-receiver separation of 6 miles and was progressively less at longer ranges. (This quantity is also referred to as the true or reference MHV.)

In determining the MHV from sound velocity data, referred to as the acoustic MHV, sound velocity data were obtained from readings of temperature, salinity and depth. Water temperatures were read on station from standard 900-foot bathythermograms, salinity values were taken from tables published by the U.S. Naval Oceanographic Data Center for that area and season. Figure 14 gives estimates of the error in determining these input quantities. Using Wilson's tables to convert to sound velocity, the total error in the determination of sound velocities, from which the profile was constructed, was estimated to be about 3 ft/s and random in nature.

Acoustic mean horizontal velocities were obtained by use of the ray trace program described previously. For channel propagation, mean horizontal velocities are plotted as a function of channel

depth in Fig. 15. Experimental results, expressed as the difference between the acoustic MHV and the reference MHV are presented in Fig. 16. The dashed curve gives the estimated error in the measurements themselves. Channel depths varied from 60 to 190 ft over the six days of measurements. The results show no significant difference between the acoustic MHV and the reference MHV based on an independent electromagnetic distance measurement. The small random differences observed, about 4 or 5 ft/s (0.1%) could be attributed to measurements errors alone. In terms of range, Fig. 17, the difference between the acoustic range and the reference range for a source-receiver separation of 12 miles, was about 15 yd, random in nature and with a mean error of substantially zero.

BOTTOM-REFLECTED PROPAGATION PATH

The purpose of this at-sea measurement was to determine the accuracy of predicting the horizontal range at which bottom-reflected sound reaches the surface from a knowledge of bottom slope, the depression angle at the source, and the sound velocity profile. Results of this experiment are shown in Fig. 18. Single-dimension RAYDIST ranges were used as the reference or true range. In this case, the acoustic range is obtained from the product of the measured travel time and the mean slant velocity derived from ray tracing. The ray tracing employed here included double precision computations and corrections for earth curvature. Note, however, the rather large error in the acoustic range -- about 1000 yd in 30 000 yd. Although not conclusive, the results suggest an error in determining the deep-water sound velocity gradient. A change in the deep-water gradient of about 2 ft/s per 1000 ft (0.016 to 0.018, for example) will remove this error. As indicated this profile was constructed from on-site bathythermograph data down to 900 ft and historical data below 900 ft. In both cases, sound velocity values were derived from temperature data using Wilson's equations [Ref. 5]. For this bottom bounce propagation path, the difference between the reference range and a range based on travel times and mean slant velocities obtained from ray tracing was less than about 20 yd out to 38 kyd. This is within the experimental error.

Wilson's equations relate sound velocity to temperature, salinity, and pressure (not depth). These results suggest that the measured pressure effect or the conversion from pressure to depth may be slightly in error. The relationship between depth and pressure is

$$p = \bar{\rho} g h \quad ,$$

where p is the pressure, $\bar{\rho}$ is the mean density of the water column from the surface to the depth considered, g is the acceleration of gravity, and h is the depth. Errors in assigning correct values to ρ and g can result in a cumulative type error in depth which causes and error in the sound velocity gradient.

The final example of at-sea measurements has to do with the measurement of bottom topography, both slope and roughness from refraction-corrected travel time differences between various multipaths [Ref. 6]. The geometry associated with this measurement technique is depicted in Fig. 19. For this work explosive charges were used for a sound source. The regional slope, α, is given by the equation shown at the bottom of the figure. Input quantities required are water depth at the receiver (SPAR), the horizontal distance between source and receiver (from RAYDIST), source and receiver depths, and certain time differences. The time differences denoted by the primes in the equation are time differences corrected for refraction effects. These corrections are made by the ray tracing program previously described by obtaining an effective mean slant velocity appropriate to any two propagation paths. By judicious choice of the experimental parameters, the extent of the bottom over which the slope is measured can be controlled. This method has the advantage of yielding bottom slope characteristics which result from sound energy reflected at the bottom at oblique angles of incidence. Thus, the reflection process is that which is associated with an effective bottom reflecting area (Fresnel zone configuration) comparable to that which exists for sonar applications.

SUMMARY AND RECOMMENDATIONS

As concerns the geometry of propagation, based on our work to date, the following comments and recommentations are made:

a. For precision ray tracing, curved earth corrections are necessary, particularly at ranges greater than about 20 kyd.

b. The principal deficiency is believed to be in the accuracy of the sound velocity profile and not in the ray trace program itself.

c. For near-surface propagation paths, the sound velocity is known sufficiently accurately.

d. The critical input quantity is the sound velocity gradient, not the absolute value of the sound velocity itself. That is, a fixed or systematic error (such as a calibration error) is not as serious as a depth dependent error.

e. It is recommended that equipment be designed and built which will directly read the sound velocity gradient as a function of depth. It would be advantageous to measure the sound velocity gradient directly, and as a function of depth.

f. Additional comparisons should be made between direct-reading velocimeter data and values derived from temperature, salinity, and depth.

g. Finally, I feel that the only meaningful evaluation of a ray trace program and the input data to this program is by full-scale, at-sea experiments.

REFERENCES

1. T.L. Goodin, "A FORTAN IV Ray Tracing Program", U.S. Naval Ordnance Laboratory, NOLTR 70-74, 1 May 1970.

2. Dosso, Lokken, Maunsell and Greenhouse, "Ray Tracing with an LGP-30: Multiple Velocity Profiles, Multiple Bottom Profiles, Bottom and Surface Reflections, Travel Time", Pacific Naval Laboratory, British Columbia, March 1960

3. A.G.D. Watson, "The Effect of the Earth's Sphericity in the Propagation of Sound in the Sea", Admiralty Research Laboratory, Teddington, Report ARL/N29/L, December 1958.

4. U.S. Naval Ordnance Laboratory, Brochure entitled "SPAR as a Research Vessel".

5. W.D. Wilson, "Equation for the Speed of Sound in Sea Water", J.Acous.Soc.Am., Vol.32, 1960, p.1357.

6. A.T. Jaques, "Determination of Bottom Slope and Roughness from Travel Time Differences", U.S. Naval Ordnance Laboratory Report NOLTR 67-100, 6 September 1967.

DISCUSSION

The author said that the expansion of the program to double-precision was not a necessary modification.

The question was asked whether the incorporation of the curved-earth correction by modifying the velocity profile was an expression of latitude-dependent gravity effects. Spofford answered that the modification was by a coordinate transformation, the effect of which could be incorporated in the velocity profile.

FIG. 1

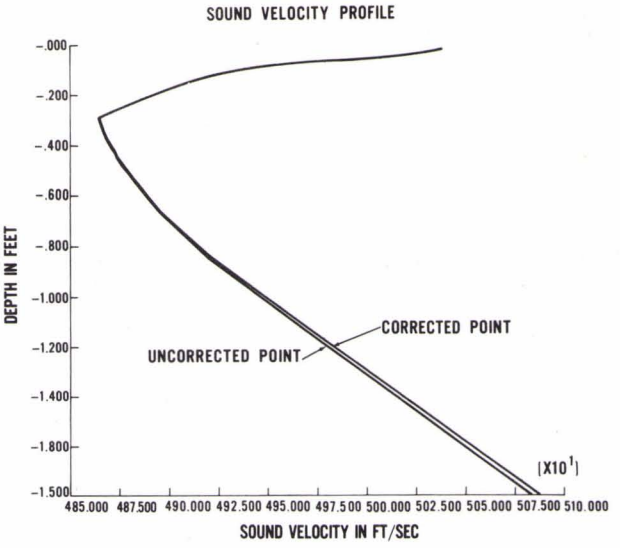

A PLOT OF BOTH THE INPUT VELOCITY PROFILE, AND THE PROFILE CORRECTED FOR EARTH CURVATURE

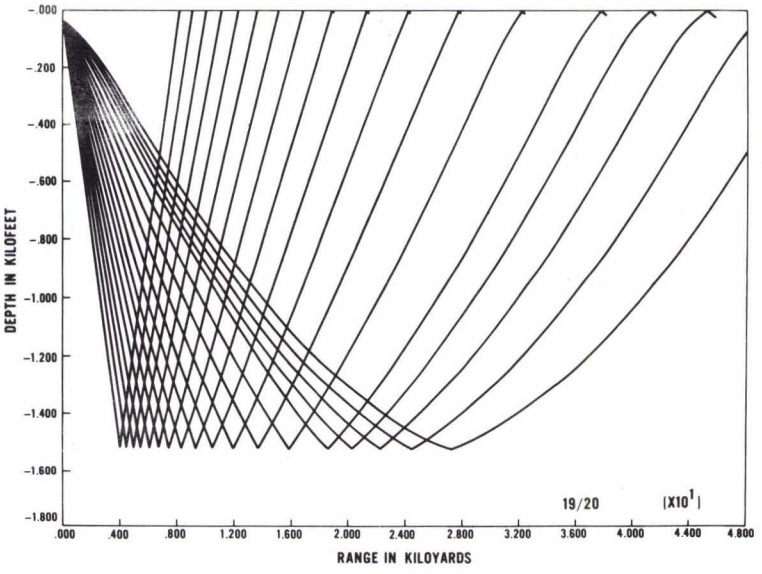

FIG. 2

A RAY FIELD PLOT WITH A FLAT BOTTOM AND NO EARTH CURVATURE CORRECTIONS

FIG. 3

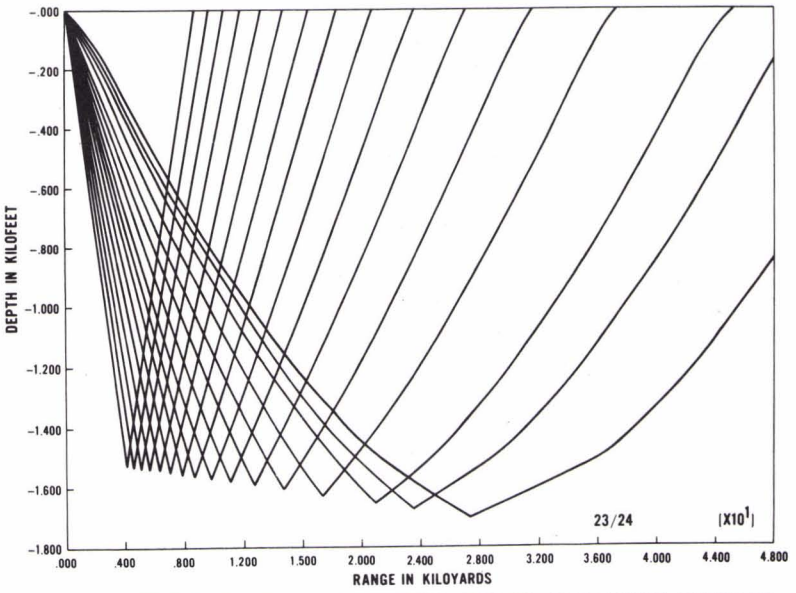

A RAY FIELD PLOT WITH A SLOPING BOTTOM - CORRECTIONS FOR EARTH CURVATURE

RAY PATH GEOMETRY

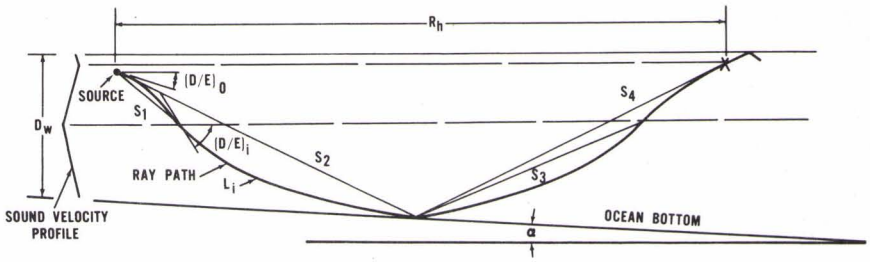

FIG. 4

D_w – WATER DEPTH AT SOURCE
R_h – HORIZONTAL RANGE
D/E – DEPRESSION-ELEVATION ANGLE
T – TRAVEL TIME ALONG THE RAY
L – PATH LENGTH ALONG THE RAY
R_S – SLANT RANGE
MHV – MEAN HORIZONTAL VELOCITY DEFINED BY R_h/T
MRV – MEAN RAY VELOCITY DEFINED BY L/T
MSV – MEAN SLANT VELOCITY DEFINED BY R_S/T
α – BOTTOM SLOPE

SAMPLE PRINTOUT

DOUBLE PRECISION COMPUTATIONS
CORRECTIONS FOR CURVATURE OF THE EARTH

WATER DEPTH AT SOURCE: 15,222 FT (2537 FMS) BOTTOM SLOPE: 0.025 (1.4 DEG.) $(D/E)_0$ = 50.50 DEG
SOURCE DEPTH; 100 FT

DEPTH (FT)	SOUND VELOCITY (FT/SEC)	D/E (DEG)	HORIZONTAL RANGE R_h (FT)	TIME T (SEC)	PATH LENGTH L (FT)	SLANT RANGE R_S (FT)	MHV (FT SEC)	MRV (FT SEC)	MSV (FT SEC)
100.00	5037.02	50.50	0.	0.	0.	0.	0.	0.	0.
150.00	5035.54	50.51	41.2	0.0129	64.8	64.8	3202.99	5036.28	5036.28
=									
=									
2400.14	4879.06	51.97	1835.6	0.5959	2942.9	2942.8	3080.50	4938.78	4938.62
=									
=									
12,003.44	4982.86	51.01	9428.1	3.0888	15,185.2	15,184.9	3052.37	4916.26	4916.16
=									
=									
15,299.26	5040.78	50.46	12,122.2	3.9381	19,442.0	19,441.3	3078.15	4936.85	4936.67
15,299.26	5040.78	−47.64	12,122.2	3.9381	19,442.0	19,441.3	3078.15	4936.85	4936.67
=									
=									
2400.14	4879.06	−49.29	23,567.3	7.4165	36,613.0	23,567.3	3162.54	4936.73	3177.71

NOTE: 56 DEPTH ENTRIES

FIG. 5

WAKE AREA

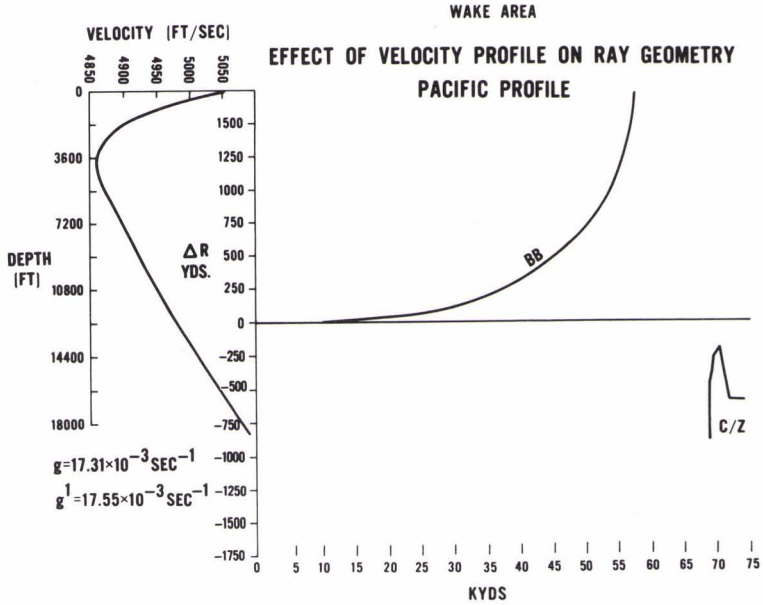

FIG. 6

EFFECT OF VELOCITY PROFILE ON RAY GEOMETRY
PACIFIC PROFILE

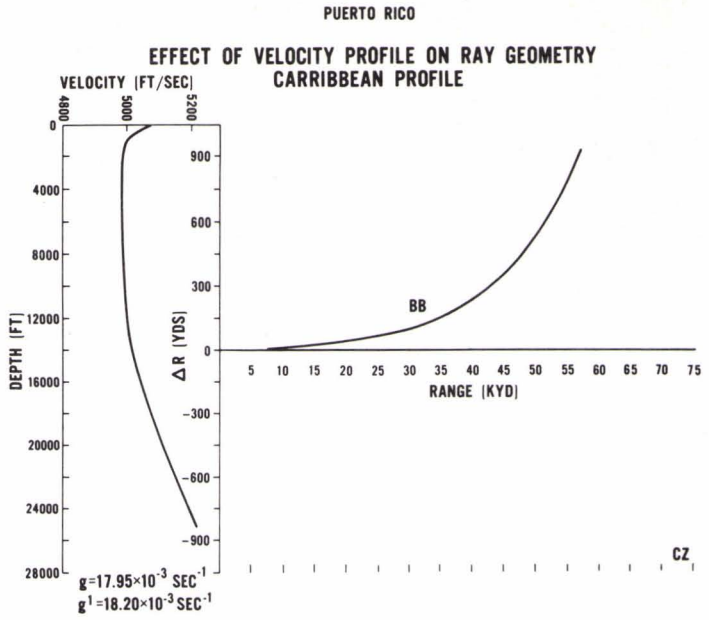

FIG. 7

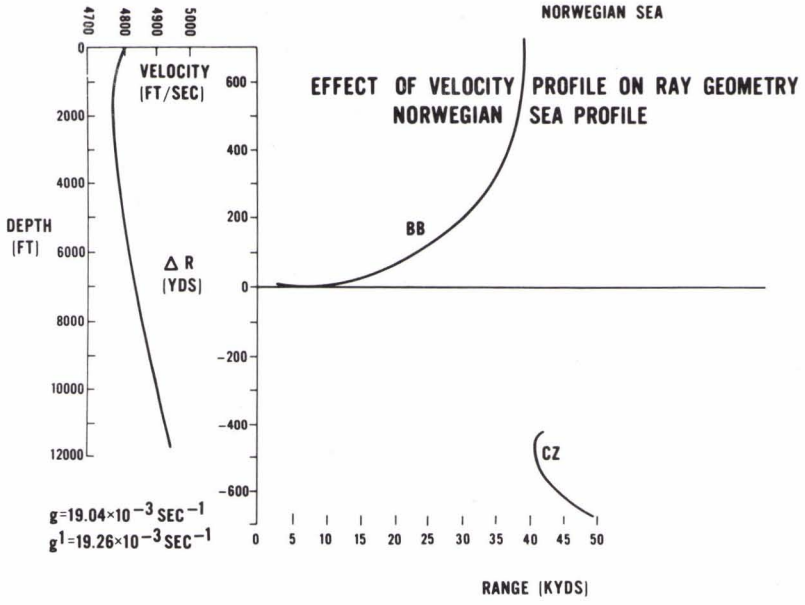

FIG. 8

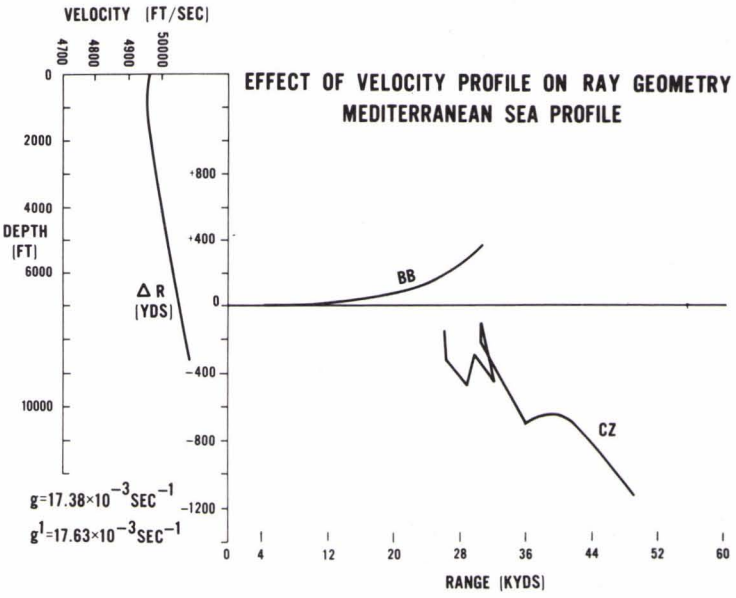

FIG. 9

FIG. 10

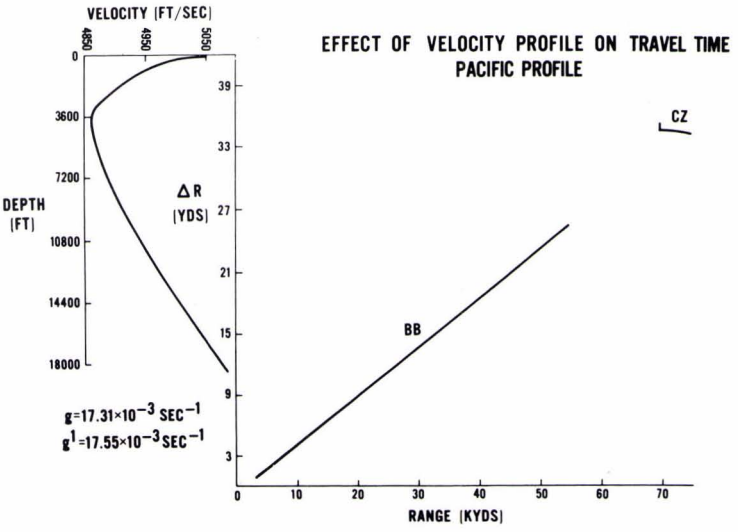

FIG. 11

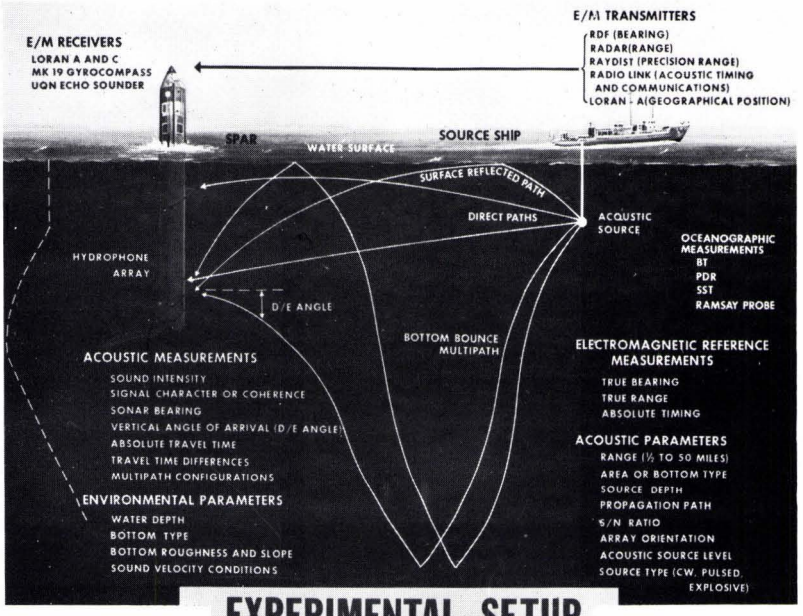

EXPERIMENTAL SETUP

FIG. 12

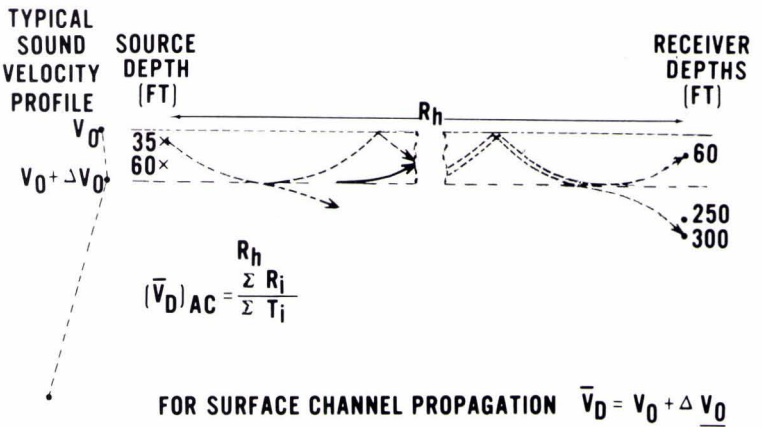

NEAR-SURFACE ACOUSTIC PROPAGATION PATHS

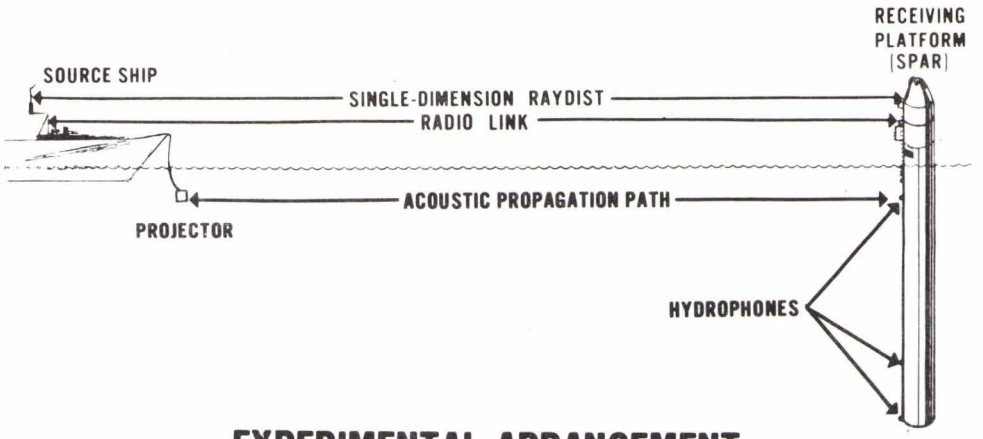

FIG. 13

EXPERIMENTAL ARRANGEMENT

ESTIMATE OF ERROR IN THE DETERMINATION
OF
THE SOUND VELOCITY

$V = f(T, S, D)$

WHERE T = TEMPERATURE
S = SALINITY
D = DEPTH

1) TEMPERATURE READING FROM BT: ± 1 FT/SEC (± 0.2 to 0.3°F)
2) SALINITY VALUES FROM TABLES: ± 2.5 FT/SEC (± 0.5 PPM)
3) DEPTH ERROR: 0.0 FT/SEC

TOTAL ERROR : ± 3 FT/SEC

FIG. 14

COMPUTED MEAN HORIZONTAL VELOCITY
CHANNEL PROPAGATION
(FROM RAY TRACE)

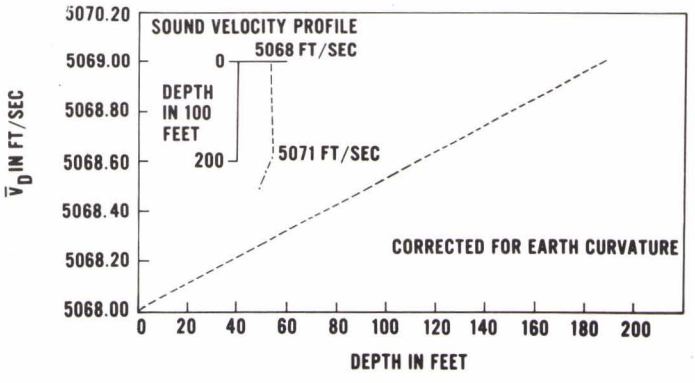

FIG. 15

COMPOSITE PLOT
SURFACE CHANNEL PROPAGATION

SOURCE DEPTH : 35 FEET
RECEIVER DEPTH: 60 FEET
CHANNEL DEPTH : 60 TO 190 FEET

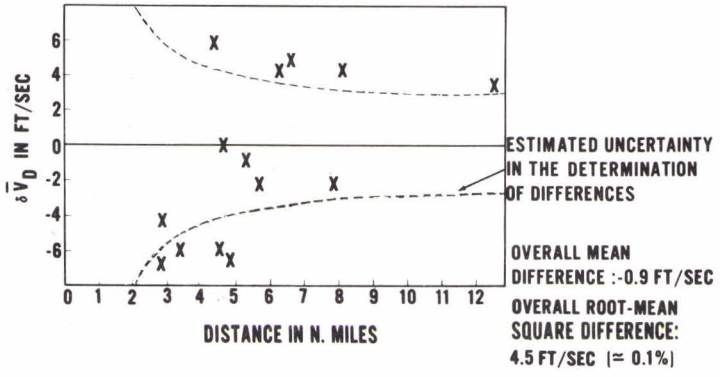

FIG. 16

ACTIVE RANGE ERROR
SURFACE CHANNEL PROPAGATION
REFERENCE RANGE: SINGLE-DIMENSION RAYDIST

FIG. 17

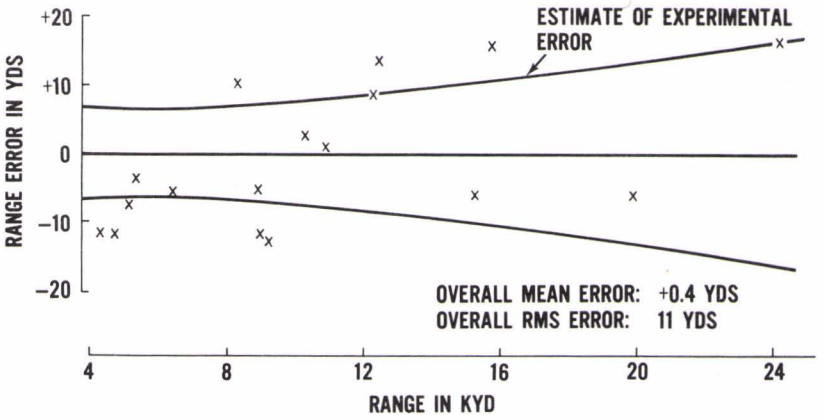

COMPARISON OF BOTTOM BOUNCE ACOUSTIC VS E/M RANGES

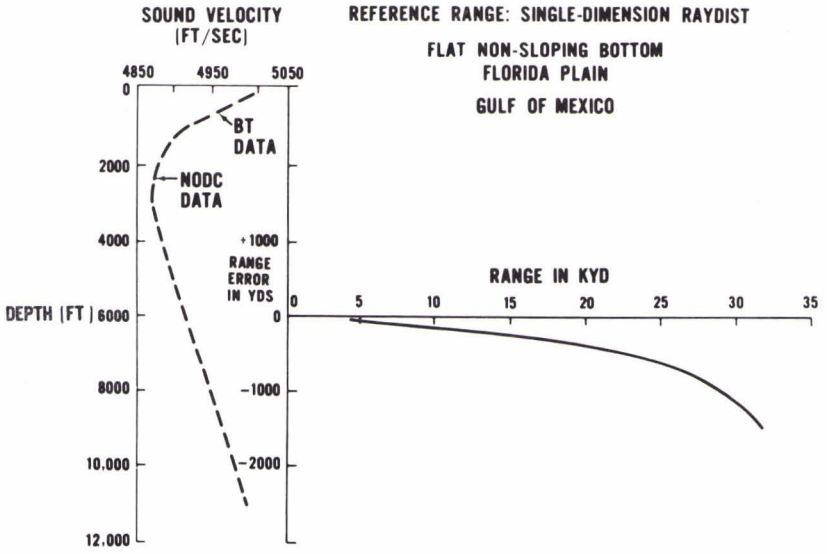

FIG. 18

BOTTOM SLOPE MEASUREMENTS FROM TRAVEL TIME DIFFERENCES CORRECTED FOR REFRACTION

FIG. 19

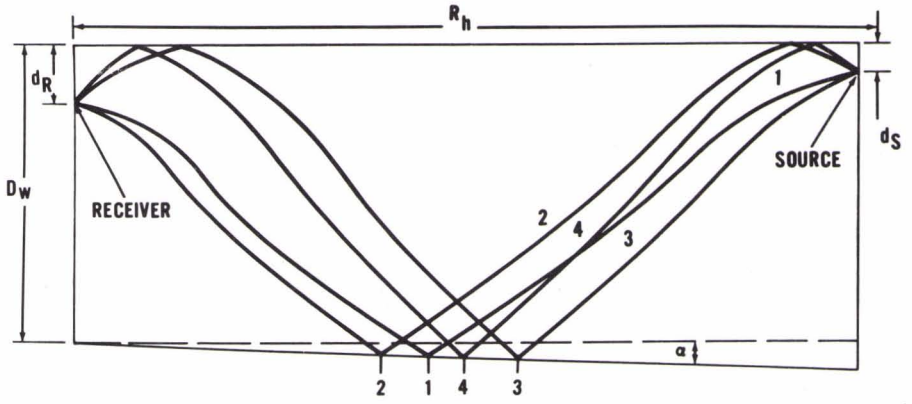

$$\text{TAN } \alpha = \frac{D_w}{R_h}\left\{\frac{d_S}{d_R}\left[\frac{(\Delta^1 T_{4-1} + \Delta^1 T_{3-2})}{(\Delta^1 T_{4-1} - \Delta^1 T_{3-2})}\right] - 1\right\}$$

EXPERIMENTAL DATA ON THE REFRACTION OF UNDERWATER EXPLOSION PULSES

by

R.M. Barash and J.A. Goertner
Naval Ordnance Laboratory
White Oak, Silver Spring, Maryland, U.S.

There are several reasons why a researcher in underwater acoustics might be interested in the use of explosion pulses as sources. The most generally recognized reason is that explosions are convenient and powerful sources of broad-spectrum sound energy. Usually, however, the received signals are filtered for analysis — for example, through one-octave or one-third octave band filters — to correspond to the characteristics of a sonar application of interest.

By contrast, the Underwater Explosions Division of the Naval Ordnance Laboratory, as well as some other groups, has direct interest in the propagation of underwater explosion pulses as such. For our purposes, we make broadband recording of the received pulses. Generally, the lower limit of the recorded frequency spectrum is practically zero; the upper limit varies from about 20 kHz, in the case of an FM recording on magnetic tape, to more the 100 kHz, for a film record of an oscilloscope trace.

With recordings of this type there are additional reasons why explosion pulses are useful sources for propagation experiments. There are kinds of information that usually show up clearly in our pulse records, but which might not be so easily or clearly obtainable, or perhaps not be obtainable at all, from sinusoidal sources or from narrow-band recordings of pressure pulses. The types of information we refer to are amplitudes, arrival times, arrival angles, and phase shifts, particularly if the received signal consists of two or more arrivals which overlap in time. Broadband explosion pulse recordings can give

enlightening answers to crucial questions concerning the validity of ray theory.

We will present some significant examples of results from U.S. experiments on the refraction of underwater explosion shock waves. In particular, we will show data that may be useful in evaluating the criteria for the conditions under which ray theory is considered valid. We shall confine our presentation mainly to a description of the data. An accompanying paper by Mr Blatstein, also of NOL, will describe a theoretical treatment of pulses under conditions for which ray tracing is not valid [see Session 4 of these Proceedings].

We will begin by describing an underwater explosion pressure pulse under non-refractive conditions; that is, in water of uniform sound velocity and of indefinite extent [Ref. 1]. Figure 1 shows a typical recording of pressure vs time measured at some distance from an underwater explosion. At the instant the shock wave pressure has subsided, there are additional smaller pulses emitted from the oscillating gas bubble that was formed by the explosion, but we shall not be concerned with these later pulses here. The exponentially-decaying shock wave pulse is described by the first equation in Fig. 1,

$$p(t) = p_m e^{-t/\theta}$$

where: $p(t)$ = the pressure above hydrostatic

p_m = the peak pressure above hydrostatic

θ = the exponential decay constant; i.e., the time at which the pressure has fallen to $1/e$ of the peak pressure.

The values of the parameters p_m and θ depend on the explosive composition, on the size of the explosive charge, and on the distance at which the pulse is observed. From many experiments, and by use of appropriate scaling laws, researchers have determined that the values of p_m and θ are given by the simple formulae shown here. W is the weight of the explosive charge, and R is the radial distance from the charge to the point of observation. The quantity $(W^{1/3}/R)$ is required by scaling considerations. K_p and K_θ are constants which depend on the charge composition.

In the expression for p_m, the exponent 1.13 requires an explanation. If, instead, we had an exponent of only 1, then the expression would represent a case in which there were no losses, but only geometrical spreading. The pressure would be equal to $K_p^{1/3}$, which is a reference pressure at unit distance, divided by R, which accounts for spherical spreading. But in the case of an explosion pulse there are significant losses. As the shock wave propagates, a substantial amount of energy is dissipated at the shock front. At larger distances, when the pressure has become small enough that the pulse can be considered an acoustic rather than a finite amplitude pulse, there are absorptive losses — the same type of frequency-dependent attentuation that is familiar in acoustics. It turns out that the combined losses of both types can be adequately described over a rather wide range of distances by using this equation with an exponent of 1.13. In the equation for the time constant, θ, the small negative exponent indicates that the decay time increases slightly as the pulse propagates. This occurs because each portion of the pulse propagates at a slightly different velocity depending on its own finite value of pressure.

This, then, is an explosion pulse in isovelocity water of infinite extent. What about a pulse reflected at the water surface? This is illustrated at the left in Fig. 2. The top pulse is a direct pulse. Just below it is a pulse arriving at the same point, but along a surface-reflected path. This pulse is inverted because its phase has been shifted by π radians. Its arrival time is later, and its amplitude is smaller, because of the longer travel path. At the receiver the two arrivals are superimposed to give the resultant pulse shown at the bottom. The reflected pulse may be large enough to reduce the resulting pressure to a negative value, as indicated by the dashed curve. But water cannot sustain this tension, and so it cavitates. Hence, we observe only the solid-line pulse, which usually goes no lower than about zero absolute pressure.

On the right side of this figure is an example of a bottom-reflected explosion pulse. Various degrees of phase shift are possible. When a non-sinusoidal pulse is shifted by a phase angle which is independent of frequency, the pulse form is necessarily distorted [Ref. 2].

With this background, let us consider refraction effects. The two pioneering U.S. experiments on the refraction of underwater explosion pulses were done with small scale simulations of oceanic conditions. The University of New Hampshire used a laboratory tank and set up an artificial thermal gradient. The Woods Hole Oceanographic Institution used a flooded quarry having a summer thermal structure very similar to that of the upper few hundred metres of the ocean. We will show data from the Woods Hole quarry experiment [Ref. 3]. Figure 3 shows a representative sound velocity profile and ray diagram from this experiment. TNT charges were placed at a few different depths and pressure gauges were placed at many positions throughout this ray pattern. In the upper half of Fig. 4 we see the most interesting portion of the ray diagram. The dots indicate gauge positions; corresponding pulse recordings are shown in the lower part of the figure.

This was an exploratory experiment that revealed marked differences in the charcter of pressure pulses observed in different regions of the pressure field. Look first at the closest two ranges, the first two columns of pulses. The undistorted character of these pulses is consistent with the corresponding portion of the ray diagram above. There is slight bending of the rays in this region but nothing severe. However, if we look at the right half of the ray diagram, we can see three features of interest: first, a region of highly divergent rays, perhaps a shadow region; second, just below it, a caustic region; and third, just below that, a region of intersecting ray groups.

Let us look at the pressure pulses recorded at these positions, starting with the highest amplitude pulse about half way down the fourth column. This was evidently recorded at a caustic. Above the caustic pulse are pulses in which the initial abrupt rise in pressure is very small. This is followed by a slow rise in pressure, to a value that is generally not so great as in isovelocity water. These pulses have the appearance of having had the high frequency energy removed while the low frequency energy is retained. These are shadow zone pulses. Now, looking at the pulses below the caustic pulse, we see that these appear to have two peaks. This is consistent with the corresponding portion of the ray diagram which shows two intersecting groups of rays. In this region we would expect to receive, at any

given point, more than one signal, each one travelling over a different path and arriving at a generally different time.

Figure 4b repeats on a larger scale the lower portion of the previous figure. The solid-line pulses are the recorded ones; the dashed lines indicate the pulses that would have been recorded at these same positions if the water had had uniform sound velocity. Thus, the effect of refraction is shown by the difference between each recorded solid-line pulse and its reference isovelocity pulse.

Looking again at the first two columns of pulses, those associated with the region containing slightly bent rays, we see that the pulses are relatively undistorted, with amplitudes only slightly affected by refraction. The cutoff in the top pulse of the first column, the top two pulses in the second column, and so on, are due simply to surface-reflected arrivals.

Now let us look again at the pulses recorded in the right half of the ray diagram. Note the high amplitude caustic pulse about half way down the fourth column. The peak pressures recorded at caustics throughout this experiment were up to four times as great as would have been expected at the same points in isovelocity water. Above the caustic pulse we see the shadow zone pulses and how they compare with the corresponding unrefracted pulses. Below the caustic we see the effect of multiple arrivals on the shape of the pressure pulse.

The characteristics of pressure pulses at caustics, and in the regions just above and below, is of sufficient interest that the Naval Ordnance Laboratory later performed a similar experiment, also in a quarry, but with a large number of very finely spaced gauges placed at the caustic on each shot [Ref.4].

Figure 5 shows a ray diagram for the NOL quarry experiment. The velocity profile was very similar to the Woods Hole profile, but it was smoother, and therefore, the ray diagram showed a smoother and better defined caustic. A vertical array of gauges, with a spacing interval of only inches, was placed at positions such as illustrated in Fig. 5. A typical set of pulse recordings is shown at the right.

Although these pulses are not positioned according to actual relative arrival times, this information is available from the original recordings. The upper pulses were recorded in the caustic regions. We found that peak pressure amplification due to refraction varied from 3.5 for the larger charges — 50 lbs — to about 6 for the smallest charges we used — 1/8 lb. The pulses shown here, from an 8-lb charge, exhibit a pressure amplification of about 5.

The pulses recorded just below the caustic region exhibit two arrivals. Because the time of each arrival is so clearly defined on each record, the calculated and observed arrival times can be clearly compared, and the angle of arrival of each of the two wave fronts can be determined. As for amplitudes, the jump in pressure from each of the two arrivals can be measured separately and compared with theoretical predictions.

How does the peak pressure, that is, the maximum pressure in the pulse, vary with gauge depth around the caustic? Figure 6 summarizes the data for all the 1/8-lb shots fired at a source depth of 35 feet and measured at a horizontal distance of 190 ft from the explosion. These three curves are plotted as a function of gauge depth relative to the depth at which the highest pressure was observed. The middle curve shows the pressure factor, the factor by which refraction has increased the peak pressure in the pulse relative to the value for isovelocity water. The maximum is 6; it falls off to half that amount about one foot into the double-arrival region, plotted toward the right, more rapidly in the shadow zone, plotted toward the left. Conventional ray tracing, used without correction, predicts infinite pressure at the caustic. Data such as presented here can be quite useful in evaluating the limitations of ray theory and the validity of other approaches.

In regions of moderate refractive convergence and divergence, the pressure at the peak of the exponential pulse is predicted well by the use of ray tracing, taken together with a straightforward modification to account for the 1.13 exponent in the equation for peak pressure vs distance. The conventional ray-tracing prediction of infinite amplitude at the caustic does not occur in reality, and we have instead the finite pressure amplification indicated by the rounded peak on this middle curve. In the shadow zone, represented by the left slope of this curve, conventional ray tracing predicts

zero pressure. The actual pressures observed in this region are those contributed by the low frequency components of the pulse, as is evident from the pulse shapes; this is also consistent with the consideration that conventional ray tracing is a high frequency approximation. A method for use in the caustic and shadow regions is described in Mr. Blatstein's paper.

The top curve in Fig. 6 shows the energy factor. This is the factor by which the energy flux density in the pulse has been increased by refraction, relative to its magnitude in isovelocity water. Here the maximum is 9. The lowest curve, which represents the impulse factor, is quite interesting. By impulse we mean the impulse per unit area carried by the pulse across the gauge point. It is measured as the integral of pressure with respect to time in the pulse, or the area under the pressure vs time curve. There is no noticeable peak in impulse with variation of gauge location through the caustic. Refraction appears to have no significant effect on impulse. It is observed that at a caustic, where peak pressure is increased because of refraction, the decay constant decreases in a compensating manner, so that the impulse remains unaffected.

The final experiment we will describe is an ocean experiment, also by the Naval Ordnance Laboratory [Ref. 5]. Figure 7 shows the sound velocity profile and the pertinent rays from the ray diagram. One pound, eight pound and 900 pound charges were fired in the Sargasso Sea at depths including 1000 feet. At the convergence zone 33 n.mi away, pressure pulses were recorded from a 200-ft long vertical array of 100 hydrophones which spanned the depth of the caustic.

Figure 8 shows a series of pulse records from one 900-lb shot. Although all time scales are the same, the records are not positioned to show time relationships among different gauge locations. Such information is obtainable, however, from the original recordings. Each record shown here consists of both a direct and a reflected pulse, the second being inverted because of phase shift upon reflection at the water surface. Reflected pulses are, of course, also subject to refractive effects. The symmetry of direct and reflected signals in each of the upper records is due to the fact that the hydrophone string was suspended, by intention and good fortune, from the point at which the caustic intersected the surface. Thus, on this particular shot, it

turned out that the direct pulses are in the double-arrival region associated with the direct caustic, and the reflected pulses are in the shadow region associated with the reflected caustic. The top record was obtained 2 ft below the surface, just at about the caustic point; here there is almost complete mutual cancellation. As we look down the string of records, we see that the direct pulse and the reflected pulse become more and more separated in time. We also see that the double arrivals on the direct pulse become more distinct and that the time difference between them also increases. As for the inverted shadow-zone pulse, it becomes weaker and less sharp.

In the oceanic convergence zone experiment, the highest pressure amplification that we observed at the caustic was about 12.

The pulse shapes contain much information, and some useful inferences can be made from them. For example, Fig. 9 shows several pulses from NOL's quarry and convergence zone experiments [Ref. 6]. The solid lines represent the observed pulses, all recorded in double-arrival regions adjacent to caustics. The dashed curves are calculated pulses, constructed to test a theory regarding phase shift. The hypothesis was that the first arrival is undistorted, while the second undergoes a phase shift of $\pi/2$ as it passes through the caustic. From this comparison of pulse shapes, it was concluded that the data are consistent with the hypothesis. It would not have been possible to perform such an analysis if the source had been a continuous sinusoidal signal. In the case of a sinusoidal wave, two arrivals with different amplitudes, different travel times, and different phases, would blend into a single sinusoidal signal at the receiver. No type of processing can extract from such a record information on the amplitude and phase of each of the contributing signals. With an explosion pulse, however, various anlytical techniques can be devised, and this was an example of one.

As a final example of the usefulness of explosive sources in studying acoustic refraction, we will present some frequency spectra of recorded explosion pulses. Figure 10 shows three pulses recorded from a 900-lb shot during NOL's oceanic convergence experiment [Ref. 5].

To the right of each pulse is the corresponding energy spectrum calculated digitally from the broadband pulse record. The pulses are arranged here in order of increasing depth. The top one is from the shadow zone, the middle one from the caustic region, and the bottom one was recorded in the double-arrival region. Remember that we are not including bubble pulses, which would contribute much more low frequency energy than shown here.

Let us look first at the middle record, the pulse from the caustic region. It is basically an exponentially decaying pulse. The energy spectral density, as expected, decreases as frequency increases.

Now let us consider the pulse at the top, the shadow zone pulse. At low frequency, the energy density is as great as it is for the caustic pulse, but much of the higher frequency energy is missing. Incidentally, the lobe at 4 to 5 kHz is simply attributable to the spurious ringing seen on the record, which was due to resonance in the hydrophone mounting.

Finally, let us consider the pulse at the bottom, which contains two arrivals. The presence of these two steep features on the pulse, separated by a time interval of almost one ms, gives rise to a periodic pattern in the energy spectrum. The spectrum exhibits deep notches at integral multiples of the reciprocal of this time interval.

This has important implications. We recall that as the point of observation moves from the caustic through the double-arrival region, the time difference between the two arrivals increases. The energy spectra of these pulses will exhibit corresponding changes in the spacing and positions of the notches and peaks. Thus, if one is interested in reception in some particular narrow frequency band, a slight shift in receiver position might shift the periodic pattern in the spectrum by enough to make a 10 dB to 20 dB change in the received energy.

If the source were a continuous sinusoidal signal, this variation in received energy could simply be described as constructive and destructive interference. The received signal would be a sinusoidal

wave, from which the characteristics of the two interfering waves could not be extracted. But by using an explosive source, and by analysing digitally as we have shown here, we determine the received energy as a function of frequency over a broad spectrum, but we can also gain an understanding of how the pattern of the spectral curve is related to particular features which are directly observable in the recorded pulse.

We have described some of the experimental data on refraction of underwater explosion pulses. We have shown pressure pulses recorded at shadow zones, caustics, single-arrival and double-arrival regions. In particular, we have shown how the recorded pulses provide information on pressure amplification, arrival time, arrival angle, and phase shift, for each arrival in a double-arrival pulse. And we have indicated how data of this type can be especially useful in understanding the refractive propagation of underwater acoustic waves.

REFERENCES

1. R.H. Cole, "Underwater Explosions", Princeton University Press, N.J., 1948; also published by Dover Publications, Inc., New York, 1965.

2. A.B. Arons and D.R. Yennie, "Phase Distortion of Acoustic Pulses Obliquely Reflected from a Medium of Higher Sound Velocity", J.Acoust.Soc.Am., Vol. 22, 1955, pp. 231-237.

3. R.R. Brockhurst, J. Bruce, and A.B. Arons, "Refraction of Underwater Explosion Shock Waves by a Strong Velocity Gradient", J.Acoust.Soc.Am., Vol. 33, 1961, pp. 452-456.

4. R.M. Barash, and J.A. Goertner, "Refraction of Underwater Explosion Shock Waves: Pressure Histories Measured at Caustics in a Flooded Quarry", Naval Ordnance Laboratory Technical Report 67-9. April 1967.

5. R. Thrun, "Refraction of Underwater Explosion Shock Waves: Sargasso Sea Measurements", Naval Ordnance Laboratory Technical Report 71-102.

6. R.M. Barash, "Evidence of Phase Shift at Caustics", J.Acoust.Soc.Am., Vol. 43, Feb. 1968, pp. 378-380 (L), and "Reply to 'Comments on Evidence of Phase Shift at Caustics'", J.Acoust.Soc.Am., Vol. 44, Aug. 1968, pp. 643-644 (L).

DISCUSSION

When asked to what range the $(\frac{W^{1/3}}{R})^{1.13}$ could be used in peak pressure calculations, the second author replied that measurements with relatively refraction-free vertical paths indicated that the expression was still valid at $\frac{W^{1/3}}{R} = 2.5 \times 10^{-5}$ lb$^{1/3}$ ft^{-1}, provided also that $R \leq 20\,000$ ft

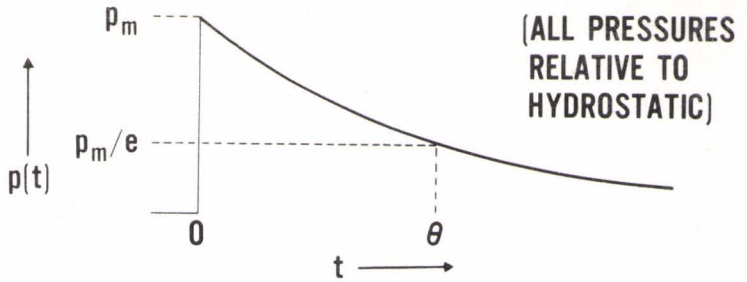

FIG. 1

$$p(t) = p_m e^{-t/\theta}$$

$$\text{WHERE} \quad p_m = K_p \left(\frac{W^{1/3}}{R}\right)^{1.13}$$

$$\text{AND} \quad \theta = K_\theta W^{1/3} \left(\frac{W^{1/3}}{R}\right)^{-0.22}$$

EXPLOSION PULSE IN ISOVELOCITY WATER

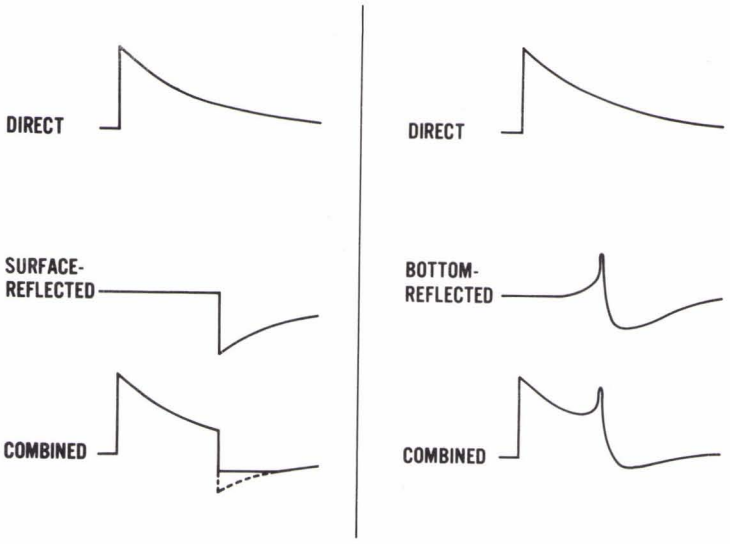

FIG. 2

REFLECTED PULSES

WHOI QUARRY EXPERIMENT

FIG. 3

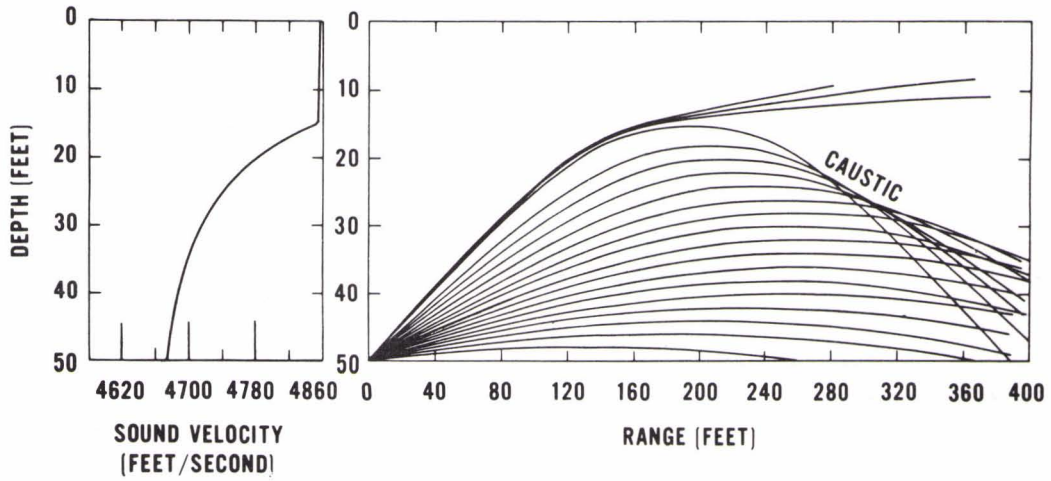

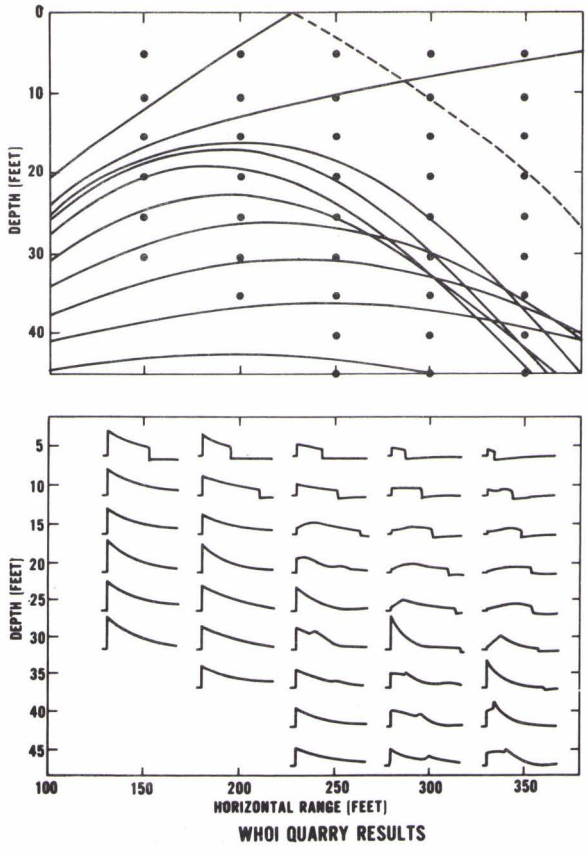
DEPTH (FEET)
0
10
20
30
40
DEPTH (FEET)
5
10
15
20
25
30
35
40
45
100
150
200
250
300
350
HORIZONTAL RANGE (FEET)
WHOI QUARRY RESULTS

FIG. 4

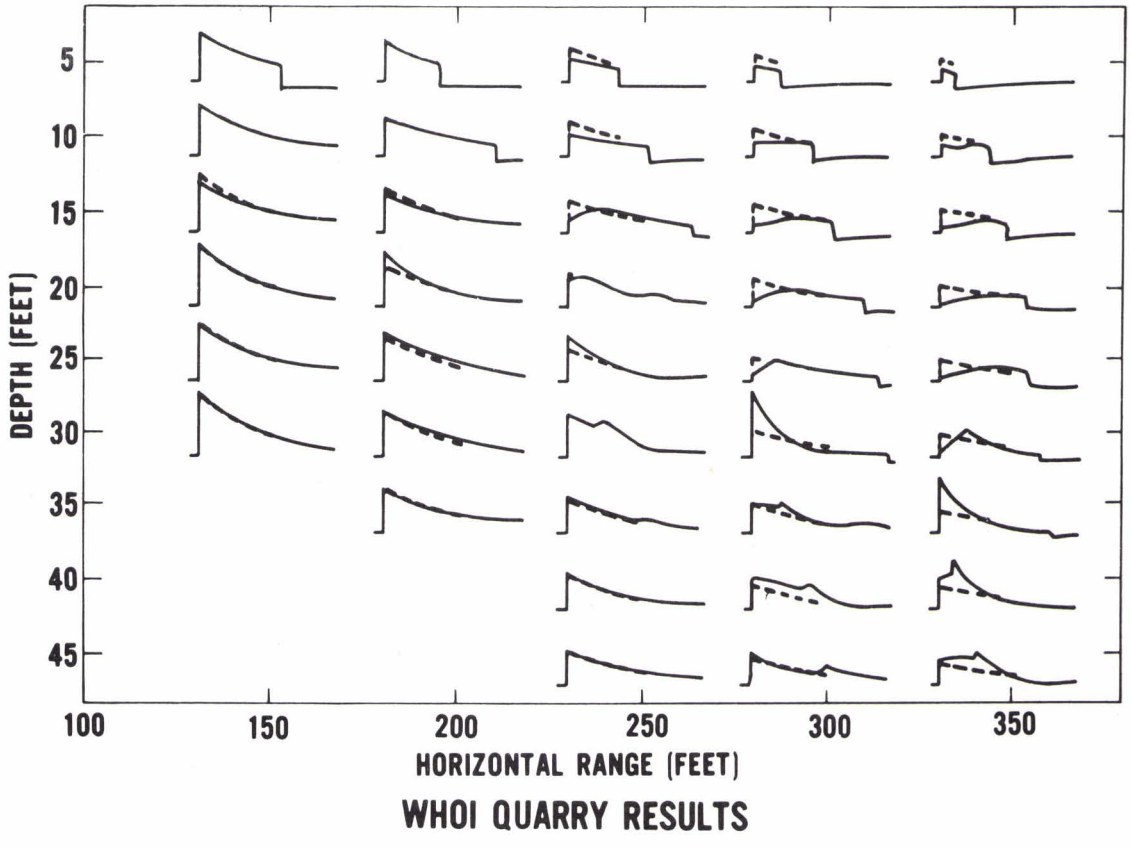
DEPTH (FEET)
5
10
15
20
25
30
35
40
45
100
150
200
250
300
350
HORIZONTAL RANGE (FEET)
WHOI QUARRY RESULTS

FIG. 4(b)

FIG. 5

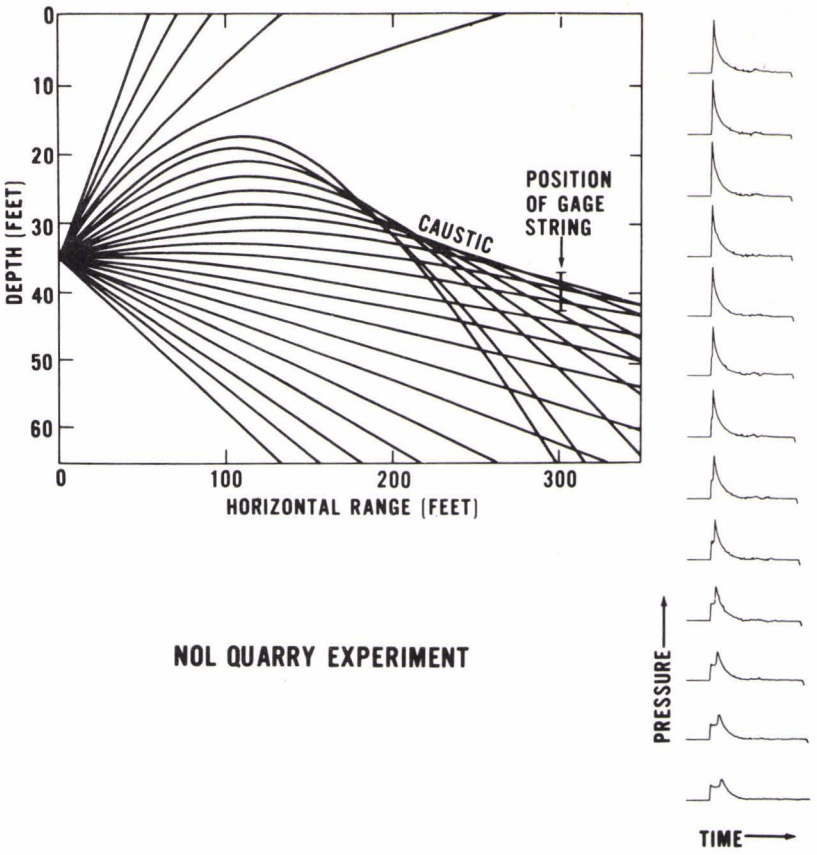

NOL QUARRY EXPERIMENT

NOL QUARRY RESULTS

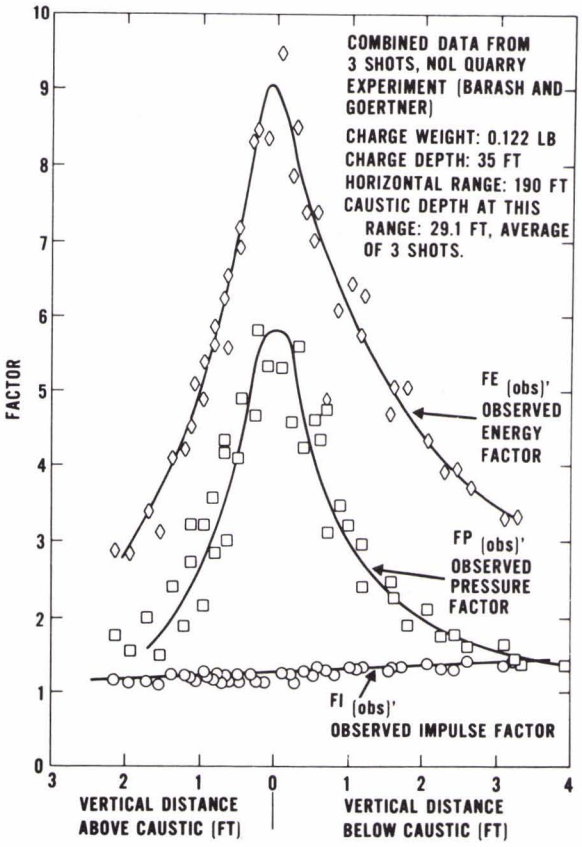

FIG. 6

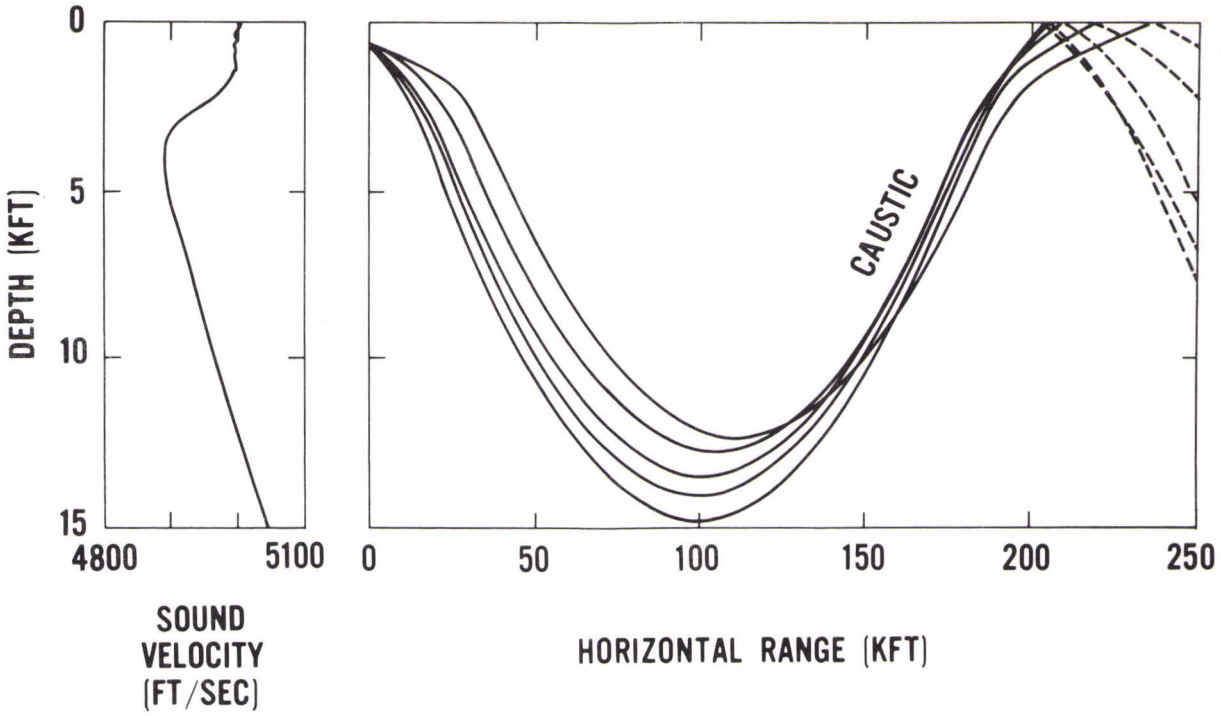

NOL CONVERGENCE ZONE EXPERIMENT

FIG. 7

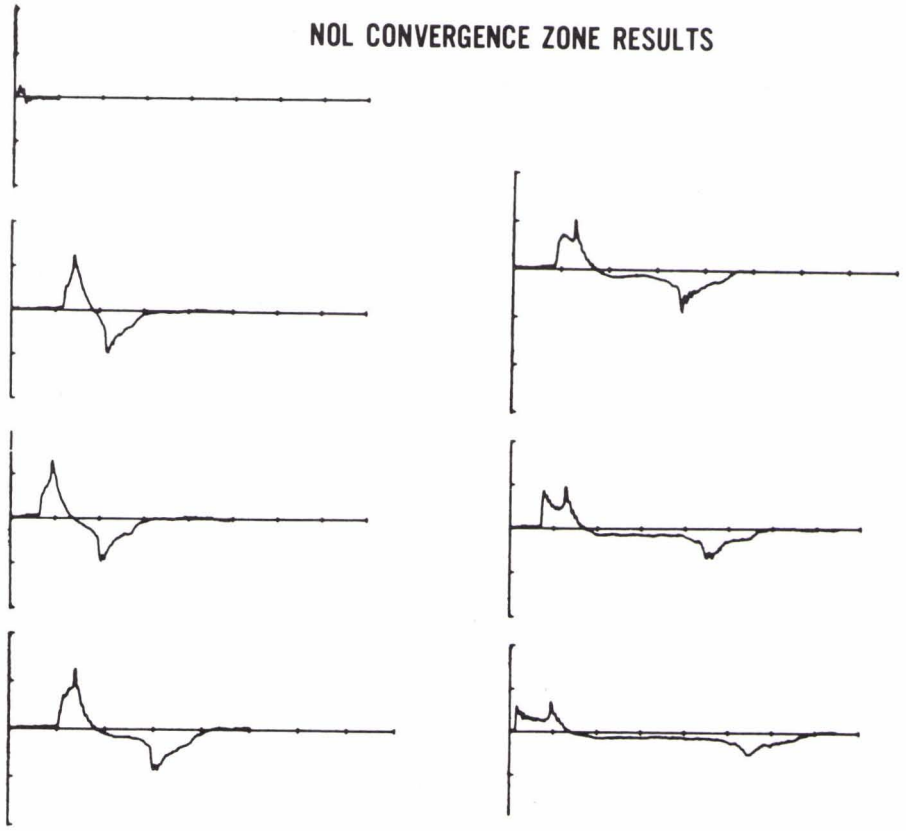

FIG. 8

RECORDED PULSES COMPARED WITH PHASE SHIFT CALCULATIONS

FIG. 9

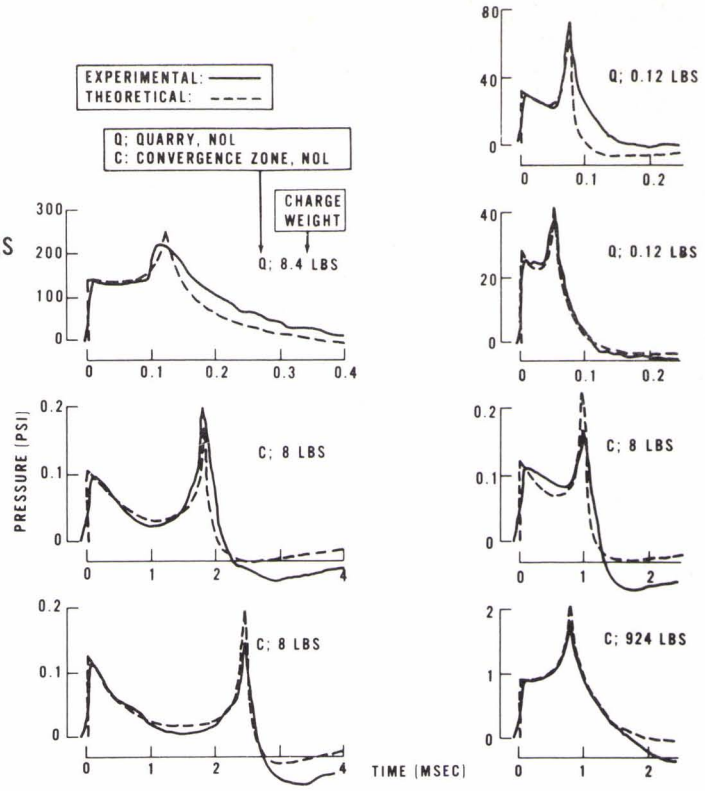

ENERGY SPECTRA OF REFRACTED PULSES

FIG. 10

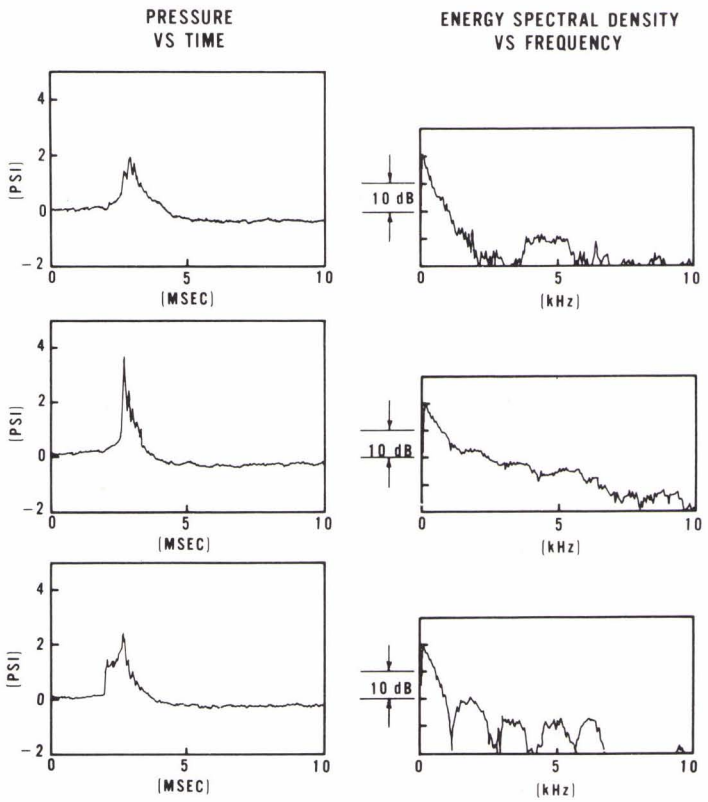

AN EXPERIMENTAL VERIFICATION OF A GEOMETRIC ACOUSTIC APPROXIMATION

by

M.J. Daintith
Admiralty Underwater Weapons Establishment
Portland, Dorset, U.K.

This paper sets out to show that a very simple ray treatment may be used to give a surprisingly good estimate of a sound field, even in conditions where the criteria for the use of geometric acoustics are apparently not fulfilled.

Experimental Arrangement [Fig.1]

A hollow thin-walled air-filled steel cylinder was immersed in water with its axis horizontal. Its dimensions were 4 ft long by 1 ft diameter by 0.05" wall thickness. The ends were capped to make it watertight. The cylinder could be rotated about a vertical axis through its centre, while in a horizontally-travelling continuous plane wave sinusoidal acoustic field. Three frequencies, 4.8 kHz, 10 kHz and 19.2 kHz, were used.

To investigate the field round the cylinder a probe hydrophone was mounted on a bracket as shown in Fig. 1, its position with respect to the cylinder being determined by the dimensions x and y. Both x and y could be varied. For each position of the probe hydrophone a response curve was plotted by rotating the cylinder through an angle γ about the vertical axis; $\gamma = 0$ corresponding to the situation in which the axis of the cylinder was parallel to the incident wavefront.

A selection of the amplitude/azimuthal angle plots for a number of combinations of x and y, and for each of the three frequencies, is shown in Fig. 2 (dashed lines).

Theory

At the lowest frequency the cylinder is only 4 wavelengths long by 1 wavelength diameter. This is in the intractable region where neither the small nor the large wavelength approximations apply. Although an exact wave-theoretical solution is known for a cylinder of infinite length, it was feared that this series solution might be only slowly convergent, and as simplicity was a prime requirement an attempt was made to use a crude ray theory.

Simplifying assumptions were necessary, viz:

(a) That the cylinder is of infinite length.

(b) That on reflection at the cylinder wall the phase change appropriate to a small pencil of incident energy could be calculated as that which would be obtained on reflection from a plane parallel thin sheet of steel of a plane wave at the same angle of incidence.

(c) That any ray is reflected specularly at the surface.

(d) That shear waves in the cylinder wall may be neglected.

In these circumstances it is easily shown that the sound field at the hydrophone will arise from the coherent addition of the intensities associated with the incident ray and a unique reflected ray arriving at the hydrophone.

Denote the radius of the cylinder by a, and the wall thickness by δ. The hydrophone position will be given by the polar coordinates r, Φ referred to the cylinder [in Fig. 1 $r^2 = (x+6)^2 + y^2$; $\tan \Phi = y/(x+6)$]. Let the wavelengths in water and in steel be λ and λ_1 respectively, the corresponding densities being ρ_1 and ρ_2. The problem is now essentially a simple but somewhat tedious exercise in coordinate geometry.

The first step is to compute an auxiliary angle ψ from the transcendental equation

$$\sin(2\psi - \Phi) = (a/r) \sin \psi \qquad \text{[Eq. 1]}$$

(ψ is in fact the cylindrical angular coordinate defining the position of the point of specular reflection). It should be noted that this angle is independent of the azimuthal angle γ.

We now compute separately the amplitude and phase of the reflected intensity at the hydrophone.

If the incident amplitude is 1 and the reflected amplitude A, we assume that A^2 = ratio of the cross-section of a pencil of rays before reflection to the cross-section of the same pencil at the hydrophone. The result is that

$$A^2 = \frac{(a/r) \cos \psi}{(a/r) \cos 2\psi + 2 \operatorname{cosec} \psi \sin(\Phi - \psi)} . \qquad \text{[Eq. 2]}$$

It will be noted that A never exceeds 1 (since the reflected pencil always diverges). As $r \to a$, $A \to 1$, as we should expect. For $r >> a$, $A^2 \to (a/r) \cos(\Phi/2)$; this is exactly the result obtained by the Fresnel zone approach. The amplitude A is independent of γ.

The relative phase of the reflected ray has two components. The first arises from the path difference to the hydrophone. This turns out to be

$$\Delta = 2r \cot \psi \cos \psi \sin(\Phi - \psi) \cos \gamma . \qquad \text{[Eq. 3]}$$

The second phase change is that due to specular reflection. Assuming Rayleigh reflection for stratified three media (water, steel, air), the reflected ray suffers a change of phase ε, but is unaltered in amplitude. The complete expression for this change of phase assumes a different form according to whether the critical angle is or is not

exceeded. However, in the circumstances considered, where $2\pi\delta/\lambda \ll 1$, it can be shown that the approximation

$$\tan(\varepsilon/2) = \frac{\sec\gamma \sec\psi}{2\pi} \frac{\rho_1}{\rho_2} \frac{\lambda}{\delta} \qquad \text{[Eq. 4]}$$

holds throughout the complete range. It will be noted that for this thin sheet the value of λ_1 (i.e. a knowledge of the speed of sound in steel) is irrelevant.

Expressions 1 to 4 are easily calculable, and the results are plotted in Fig. 2. The amplitude scale has been normalized so that the free-field response of the hydrophone is unity, and it should be noted that this is a linear scale.

Discussion of Results

Considering the crudeness of the theory the agreement with experiment is, in general, gratifying, particularly in view of the fact that there are no fitted parameters in the theory. It is not easy to ascertain, indeed, whether the differences observed arise from the deficiencies of the theory or the inevitable errors in the experimental measurements. Two sources of error are, for example, the disturbance of the sound field by the bracket/hydrophone combination (the hydrophone was a cylinder approximately $\frac{1}{2}" \times \frac{1}{4}"$), and the difficulty of ensuring accuracy in maintaining the exact geometry (which can have a large effect on the phase relationships).

There is some suggestion that some of the unpredicted oscillations of the experimental results about the theoretical curve may arise from multipath effects, perhaps arising from shear wave stimulation, in that the positions of peaks and nulls correspond to paths in the steel having the appropriate time delays. The amplitudes of these oscillations are, however, slight in general, suggesting that these secondary effects are reasonably insignificant.

CONCLUSION

It is concluded that even in limiting conditions an extremely crude theory may give a surprisingly accurate answer. It is difficult to lay down criteria for the validity of such approaches, but when combined with an experimental validation they may be very useful.

DISCUSSION

The author acknowledged that his predictions might have been improved by incorporating phase shifts and delays as treated for example by Brekhovskikh, and also creeping rays; but that his work was done quite some time ago, predicated on simplicity, and without the benefit of a computer, and that the results were quite encouraging as they were.

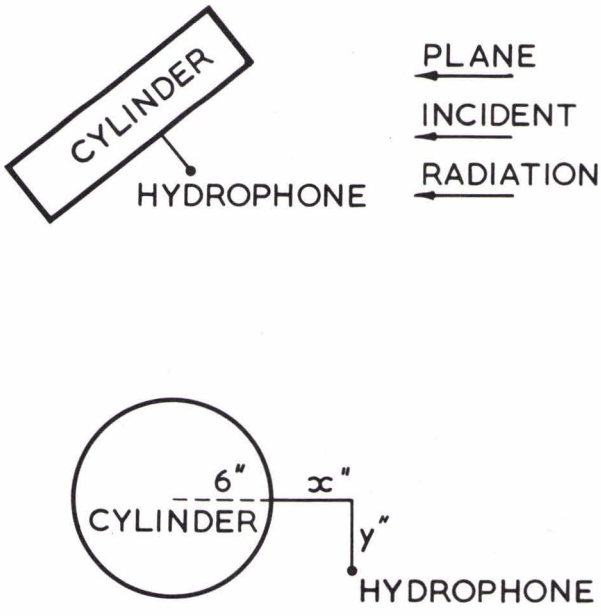

EXPERIMENTAL ARRANGEMENT

FIG. 1

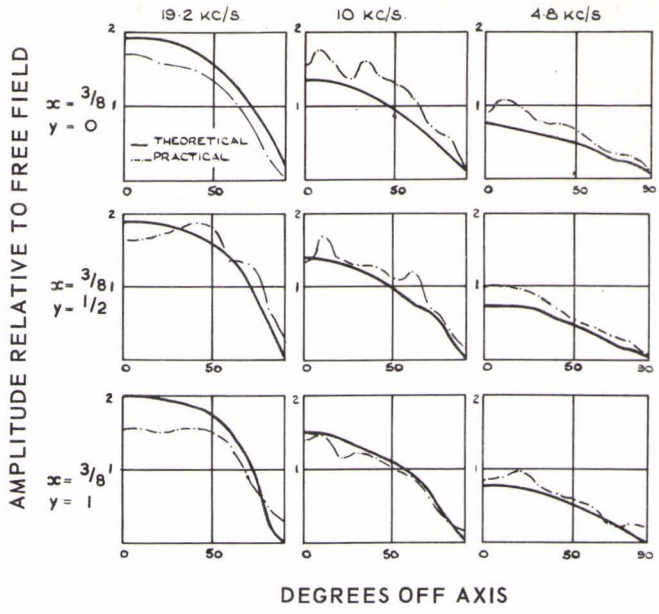

FIG. 2a

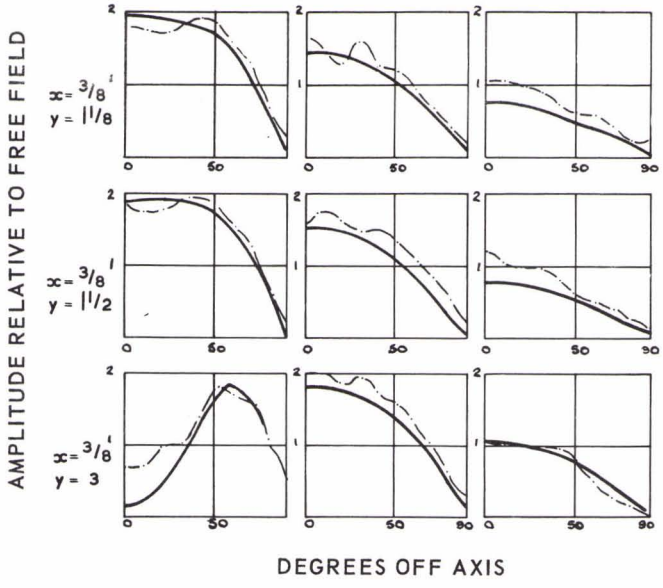

FIG. 2b

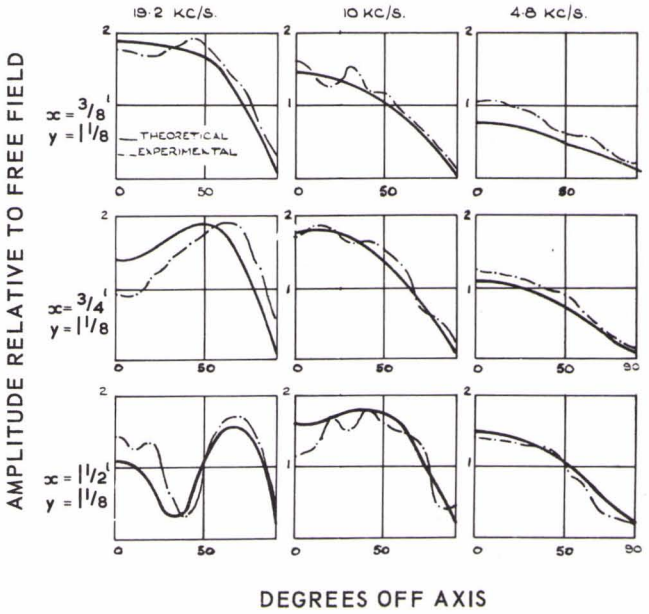

FIG. 2c

INITIAL DISTRIBUTION

MINISTRIES OF DEFENCE	Copies
MOD Belgium	5
DND Canada	10
CHOD Denmark	8
MOD France	8
MOD Germany	15
MOD Greece	11
MOD Italy	10
MOD Netherlands	12
CHOD Norway	10
MOD Portugal	5
MOD Turkey	5
MOD U.K.	20
SECDEF U.S.	68

NATO AUTHORITIES	Copies
Defence Planning Committee	3
NAMILCOM	2
SACLANT	10
SACLANTREPEUR	1
CINCWESTLANT	1
COMSTRIKFLTLANT	1
COMIBERLANT	1
CINCEASTLANT	1
COMSUBACLANT	1
COMOCEANLANT	1
COMCANLANT	1
COMMAIREASTLANT	1
COMNORLANT	1
COMSUBEASTLANT	1
COMSTANAVFORLANT	1
SACEUR	3
CINCNORTH	1
CINCSOUTH	1
COMNAVSOUTH	1
COMSTRIKFORSOUTH	1
COMEDCENT	1
COMSUBMED	1
COMMARAIRMED	1
COMTWOATAF	1
CINCHAN	1

SCNR FOR SACLANT	Copies
SCNR Belgium	1
SCNR Canada	1
SCNR Denmark	1
SCNR Germany	1
SCNR Greece	1
SCNR Italy	1
SCNR Netherlands	1
SCNR Norway	1
SCNR Turkey	1
SCNR U.K.	1
SCNR U.S.	2

NATIONAL LIAISON OFFICERS	Copies
NLO Italy	1
NLO Portugal	1
NLO U.K.	1
NLO U.S.	1

NLR TO SACLANT	Copies
NLR Belgium	1
NLR Canada	1
NLR Denmark	1
NLR Germany	1
NLR Greece	1
NLR Italy	1
NLR Norway	1
NLR Portugal	1
NLR Turkey	1
ESRO/ELDO Doc Service	1